Speciation of the Sulfuric Acid-Ferric Sulfate-Ferrous Sulfate-Water System and its Application to Chalcopyrite Leaching Kinetics up to 150 ℃

by

Guikuan Yue

B. Eng., Henan University, 2005

M. Eng., Institute of Process Engineering, Chinese Academy of Sciences, 2008

A THESIS SUBMITTED IN PARTIAL FULFILLMENT OF
THE REQUIREMENTS FOR THE DEGREE OF

DOCTOR OF PHILOSOPHY

in

THE FACULTY OF GRADUATE AND POSTDOCTORAL STUDIES

(Materials Engineering)

THE UNIVERSITY OF BRITISH COLUMBIA

(Vancouver)

March 2015

Abstract

Hydrometallurgical oxidation methods are increasingly being considered for the extraction of Cu from chalcopyrite. However, the kinetics of cathodic ferric ion reduction are poorly understood. This thesis investigates the kinetics of cathodic ferric ion reduction on chalcopyrite and its influence on the leaching process in acidic iron sulfate solution, with an emphasis first placed on the development of a speciation model for the H_2SO_4-$Fe_2(SO_4)_3$-$FeSO_4$-H_2O system from 25 ℃-150 ℃.

Speciation results show that most Fe(III) is distributed as complexes or precipitates and the free Fe^{3+} accounts for only a minor percentage (up to 5.2% of total ferric) whereas a large amount of Fe(II) exists in the form of free Fe^{2+}. The Nernst equation was used to study the redox potential of Fe^{3+}/Fe^{2+} couple. The speciation model explains the change of redox potential with temperature for all nominal Fe^{3+}/Fe^{2+} ratios. This model was validated by reliable prediction of measured redox potential, comparison of previously published results of ferric solubility, together with an analysis of the calculated pH and ionic strength.

A novel expression was also developed to predict the redox potential of the ferric/ferrous couple. It seems that the redox potential can be easily and accurately determined only based on the variables of temperature and nominal Fe^{3+}/Fe^{2+} ratio.

The calculated free Fe^{3+} concentration allowed for a detailed investigation of the reduction kinetics of ferric ion on chalcopyrite by cathodic potentiodynamic polarization. The exchange current densities of the Fe^{3+}/Fe^{2+} couple are on the order of 10^{-7}-10^{-5} A/cm^2 in the range of 25–150 ℃, substantially less than that on platinum. Calculated rate constants can be well described by the Arrhenius equation. The transfer coefficient increases linearly with temperature (rather than being constant).

The importance of the cathodic ferric ion reduction reaction on the overall leaching process is progressively increased when increasing the nominal Fe^{3+}/Fe^{2+} ratio and temperature. Leaching is under anodic control when the nominal Fe^{3+}/Fe^{2+} ratio is around 1:1, whereas at higher nominal Fe^{3+}/Fe^{2+} ratios and temperatures it is under mixed control.

These findings provide the basis for mechanistic analyses and attendant optimization studies of industrial leaching processes of chalcopyrite and other sulfide minerals.

Preface

Financial support for this work was provided by SNC Lavalin, Glencore, HudBay and the Natural Sciences and Engineering Research Council of Canada (NSERC). The journal papers and conference presentations listed below have been prepared from the research work presented in the dissertation. I am the primary contributor to all of them and was responsible for conducting the research, preparing and analyzing the results, and writing the manuscripts. The contributing co-authors are as follows: Dr. Edouard Asselin (supervisor) extensively helped with all the aspects of the research work; Dr. Liming Zhao is gratefully acknowledged for her help with programming and numerical methods to solve the non-linear equations (Fortran code by Brent's method), in order to obtain the species distribution of the model results; Dr. Oscar G. Olvera helped measure the redox potentials at 25-90 ℃, which is used in Chapter 5. Chapters 5 and 6 are based on journal paper "1". Chapters 7 and 8 are based on journal paper "2".

Journal Papers

1. **Guikuan Yue***, Liming Zhao, Oscar G. Olvera, Edouard Asselin. Speciation of the H_2SO_4-$Fe_2(SO_4)_3$-$FeSO_4$-H_2O System and Development of an Expression to Predict the Redox Potential of the Fe^{3+}/Fe^{2+} Couple up to 150 ℃. ***Hydrometallurgy*, 2014, Volumes 147-148, Pages 196-209**.
2. **Guikuan Yue***, Edouard Asselin. Kinetics of Ferric Ion Reduction on Chalcopyrite and its Influence on Leaching up to 150 ℃. ***Electrochimica Acta,* 2014, Volume 146, Pages 307–321**.

Conference Presentations with Proceeding

1. **Guikuan Yue***, Edouard Asselin. Reduction Kinetics of Fe(III) on Chalcopyrite up to 110 ℃. In M.J. Collins, D. Filippou, J.R. Harlamovs, E. Peek (Eds.), *42nd Annual Hydrometallurgy Meeting, Pressure Hydrometallurgy 2012* (pp. 241-255), September 30-October 3, 2012. Niagara Falls, ON: Canadian Institute of Mining, Metallurgy and Petroleum. (***Conference paper & Oral presentation***)
2. **Guikuan Yue***, Edouard Asselin. Fundamental Reduction Kinetics of Fe(III) on Chalcopyrite Surface. In M. Free, M. Moats, G. Houlachi, E. Asselin, A. Allanore, J. Yurko, & S. Wang (Eds.), *TMS (The Minerals, Metals & Materials Society) 2012 Annual Meeting, Electrometallurgy 2012* (pp. 183-198), March 11-15, 2012. Orlando, FL: John Wiley & Sons, Inc. (***Conference paper & Oral presentation***)

Conference Presentations

1. **Guikuan Yue***, Edouard Asselin. Analysis of Chalcopyrite Leaching Behavior by Mixed Potential Theory in Acidic Iron Sulfate Solution from 25 ℃ to 150 ℃. *The 6th International Conference on Hydrometallurgy*, Beijing, China, October 16-19, 2014. (***Poster presentation***)
2. **Guikuan Yue***, Edouard Asselin. Speciation of Acidic Iron Sulfate Solutions and its Application to the Study of the Reduction Kinetics of Fe(III) on Chalcopyrite up to 150 ℃. *Hydrometallurgy 2014*, Victoria, British Columbia, June 22-25, 2014. (***Poster presentation***)
3. **Guikuan Yue***, Edouard Asselin. Speciation of the H_2SO_4-$Fe_2(SO_4)_3$-$FeSO_4$-H_2O System and its Application to Chalcopyrite Leaching from 25 ℃ to 150 ℃. *CQU-UBC Research Workshop on Materials Science and Engineering*, Chongqing, China, May 13-15, 2014. (***Oral presentation***)

4. **Guikuan Yue***, Edouard Asselin. Fundamental Reduction Kinetics of Fe(III) or O_2 on Chalcopyrite Surface. *23rd Canadian Materials Science Conference*, Kelowna, British Columbia, June 22-24, 2011. (***Oral presentation***)

Table of Contents

List of Tables

List of Figures

Acknowledgements

First of all, I would like to express my sincere gratitude to my supervisor, Dr. Edouard Asselin, for his continuous support, kind guidance and encouragement during this project. The numerous critical discussions that he gave almost every day significantly accelerate my research. Without his help this work would not have been possible.

I would also like to thank my thesis committee members, Dr. Xiaotao Bi, Dr. Akram Alfantazi and Dr. Daan Maijer, for their great comments and input about my research. I also wish to express my thanks to Dr. David Dreisinger and Dr. Marek Pawlik for their great advice, suggestions and comments at my Final Oral Defence. I would like to especially thank Dr. Vladimiros Papangelakis for reviewing my thesis and providing valuable feedback. Colleagues such as Dr. Hamidreza Zebardast, Dr. Berend Wassink are also acknowledged for their helpful discussions.

I gratefully acknowledge the financial support of SNC Lavalin, Glencore, HudBay and the Natural Sciences and Engineering Research Council of Canada (NSERC).

I wish to thank the Department of Earth, Ocean and Atmospheric Sciences at the University of British Columbia (EOAS) for providing the mineral samples. I also wish to thank Ms. E. Czech and Dr. Mati Raudsepp from EOAS, for obtaining the XRD data featured in this work.

Special thanks to all colleagues and officemates in the Department of Materials Engineering at the University of British Columbia for providing a friendly environment that was always a pleasure to work in.

Finally, the author would like to thank his wife, Lirun Zhao, and other family members for their exceptional patience, understanding, support and encouragement, which enabled this work to be carried to completion.

Dedication

To my beloved family

1 Introduction

1.1 General Information on the Copper Extraction Industry

Copper is widely used by human beings and is produced all over the world. Due to its high electrical conductivity, thermal conductivity and corrosion resistance (the most exploited properties), in conjunction with its excellent formability and joinability, copper has been employed in diverse applications, either in metallic form or alloys [1]. The present section aims to briefly describe and discuss the principal methods by which it is obtained.

There are three major sources of copper: copper-iron-sulfide and copper sulfide minerals (most common), such as chalcopyrite ($CuFeS_2$) and chalcocite (Cu_2S); oxidized minerals (carbonates, oxides, hydroxy-silicates, sulfates); copper and copper alloy scrap [1]. Among the minerals, chalcopyrite is the most abundant copper mineral in nature, accounting for about 70% of known copper reserves in the world [2].

Depending on the mineralogy and grade of the deposit, different extraction routes are required to produce copper [1]. About 80% of the world's copper-from-ore (~18 million tonnes per year) is produced by concentration/smelting/refining of copper-iron-sulfide ores ($CuFeS_2$). The main processes of the flowsheet for extracting copper from this kind of ore are shown in Figure 1-1. The other 20% is hydrometallurgically produced by heap leaching/solvent extraction/electrowinning of mainly copper oxide, and chalcocite ores (Figure 1-2). This technology dominates in Chile. Copper production from recycled used objects is about 10 or 15% of mine production.

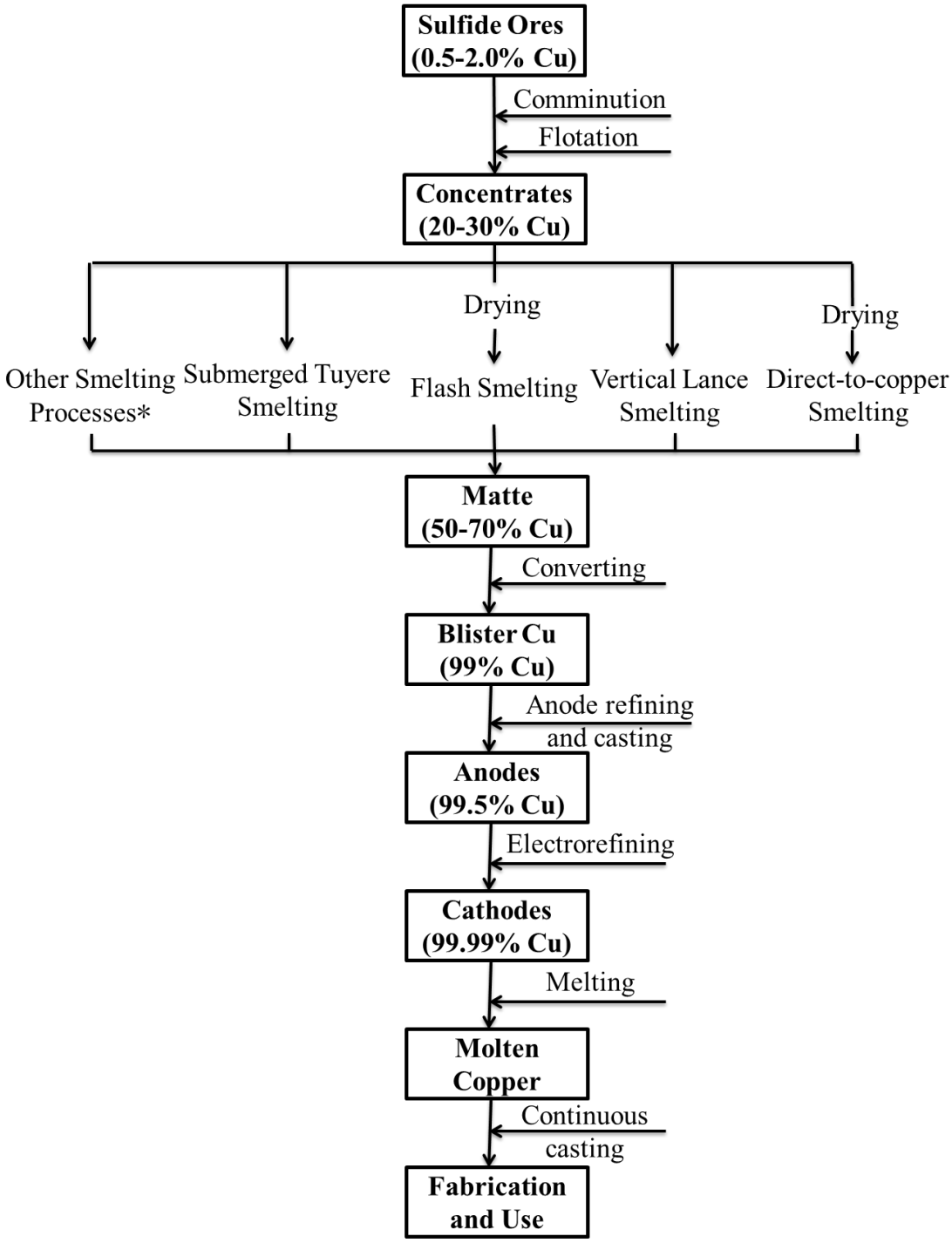

Figure 1-1 Main processes for extracting copper from sulfide ores [1].

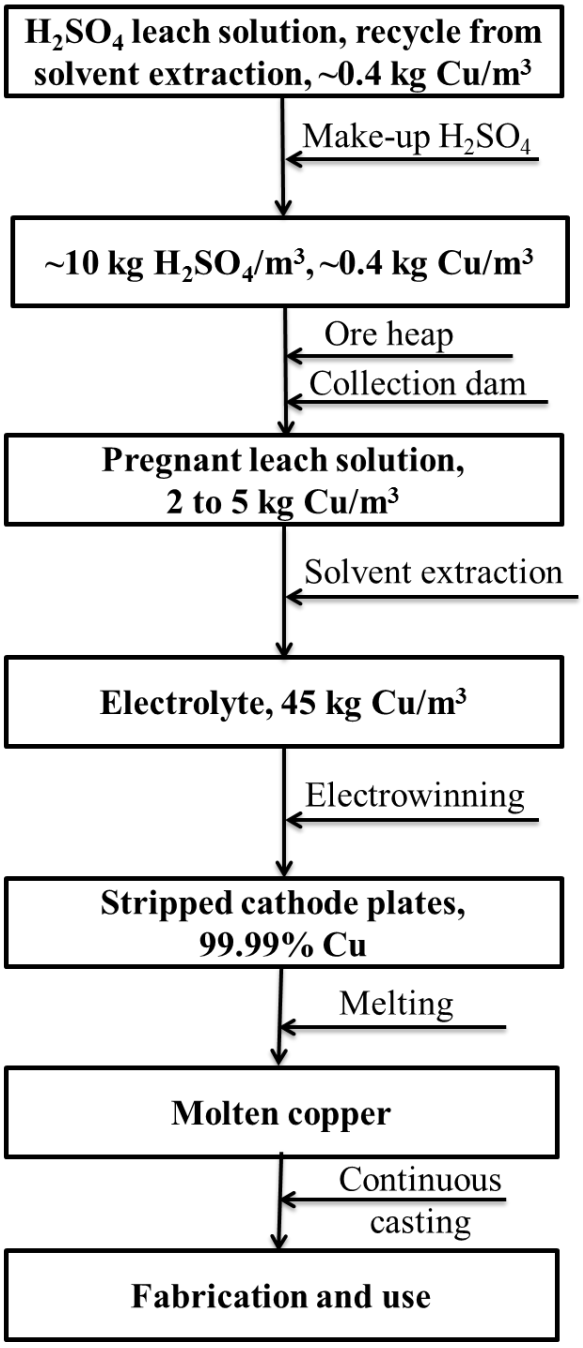

Figure 1-2 Flowsheet for leaching oxide and Cu_2S ores. The dissolved Cu is recovered by solvent extraction purification/strengthening and then electrowinning. Leaching accounts for ~20% of primary (from ore) copper production [1].

The traditional pyrometallurgical flowsheet remains the dominant existing industrial process. The main drawbacks for pyrometallurgical treatment of chalcopyrite include high capital costs associated with smelting, the limited ability of smelters to handle growing concentrations of As and Sb, and emissions of SO_2. The hydrometallurgical method to extract copper from minerals, with leach/solvent extraction/electro-winning operations, is only applied to treat oxide or Cu_2S ores. Sulfuric acid is almost always used as the leaching lixiviant. Copper production by this method is steadily increasing as more mines begin to leach all or some of their ore and treat lower-grade materials, some of which were previously considered to be waste [1].

Finally, it should be emphasized that according to the data published by Schlesinger et al. [1], due to the small equipment and infrastructure requirements, the total direct plus indirect costs of producing electrowon copper cathodes from oxide and chalcocite ores (including mining) by heap leach/solvent extraction/electrowinning ($1-$2 per kg of copper) are considerably lower than those for producing electrorefined copper from ore by conventional mining/concentration/smelting/refining (in the range of $3-$6 per kg of copper). This is the reason why leaching is being rapidly adopted around the world, especially in Chile. Please note that the cost data were obtained during early 2011 and are expressed in 2011 USA dollars. Unfortunately, as the world's largest source of copper, chalcopyrite ore cannot yet be economically processed by heap leach/solvent extraction/electrowinning, and it must usually be treated by conventional concentration/smelting/refining, regardless of the cost.

1.2 Analysis and Discussion on Hydrometallurgical Treatment of Chalcopyrite in Acidic Iron Sulfate Solution

Obviously, the above brief analysis of copper extraction technology strongly supports the concept that it is important to develop a hydrometallurgical process as an alternative to smelting to treat chalcopyrite, the most abundant copper mineral in nature, in view of the commercial and technological importance of this sulfide ore.

The challenge for process development of chalcopyrite leaching is to dissolve copper quickly and completely with, preferably, a high yield of elemental sulfur. Although in the past several decades enormous efforts have been continuing to seek a deeper understanding of the kinetics and mechanisms involved in the proposed hydrometallurgical leaching systems, due to various technical obstacles or economic concerns, few have yet been successfully commercialized and can achieve sustained commercial production above a demonstration plant scale. Indeed, as stated by Schlesinger et al. [1], development of commercially viable technologies for the hydrometallurgical processing of chalcopyrite remains the holy grail of copper metallurgy, in spite of the fact that a lot of progress in technological advances for modern smelters has been made to tackle the problems faced by the conventional pyrometallurgical treatment.

Activity in this area has steadily increased recently due to some inherent advantages associated with hydrometallurgical processing, such as the possibility of treating low-grade ores (increasingly more abundant in the case of copper) and easier control of waste, with the attendant benefits to the environment [3]. Unfortunately, chalcopyrite is highly refractory under most hydrometallurgical conditions, owing to the formation of an anodic passivation layer on the chalcopyrite surface that renders the process kinetics very slow. Most of the currently proposed

processes are based on sulfuric acid with ferric ions and/or dissolved oxygen as oxidants (the most important hydrometallurgical oxidants) at elevated temperatures. Sulfuric acid is preferred over all other leaching reagents in terms of cost, environmental friendliness, and ease of its regeneration during electro-winning. Additionally, acidic iron sulfate solution can easily be combined with conventional SX-EW methods. Some of these processes have been piloted or demonstrated in attempts to implement these technologies on an industrial scale, such as Activox [4], Nenatech [5], Dynatec [6], AAC/UBC [7], Total Pressure Oxidation [8], CESL [9] and Galvanox [10]. Table 1-1 summarizes the general operating parameters for those processes.

Table 1-1 Typical industrial leaching processes (including the general operating parameters) for $CuFeS_2$ based on sulfuric acid.

Process	Temperature	Pressure	Leaching Solution
Galvanox	60-80℃	Atmospheric conditions, sparging oxygen and/or air	H_2SO_4+Ferric+Ferrous+Pyrite Pure sulphate medium
Activox	90-110℃	Oxygen partial pressure 700-1000 kPa	H_2SO_4+Fe/Cu/Cl Fine grinding/high oxygen pressure
MIM/Highlands Albion (Nenatech)	60-90℃	Atmospheric pressure, sparging oxygen or air	H_2SO_4+Ferric+Ferrous+Lignosol Atmospheric ferric leaching
AAC/UBC	150℃	Oxygen partial pressure 400-750 kPa	H_2SO_4+Ferric/Ferrous/Cuppric+ Quebracho/lignosulfonate/OPD
Dynatec	150℃	Oxygen partial pressure 400-750 kPa	H_2SO_4+Ferric/Ferrous+Coal Low grade coal used as an additive
Total Pressure Oxidation	220℃	Oxygen partial pressure 345-2068.5 kPa	H_2SO_4/Water Extreme conditions of T and P
CESL	150℃	Oxygen partial pressure 345-1735 kPa	H_2SO_4+Cu+Cl(HCl) Chloride catalyzed in the autoclave

The dissolution of semiconducting chalcopyrite in oxidizing acidic iron sulfate solution can be regarded as an electrochemical corrosion process, with cathodic reduction of the soluble oxidant (ferric regenerated by dissolved oxygen) and anodic oxidation of chalcopyrite. Therefore, the application of electrochemical techniques is also ideal to research the mechanism and rate-determining steps of the anodic and cathodic reactions involved in the leaching process. According to the published literature, there is considerable evidence that, for the oxidation of

sulfide minerals such as PbS, ZnS, CuS and Cu_2S in acid solutions and possibly for $CuFeS_2$ as well, the dissolved Fe^{3+}/Fe^{2+} couple plays an important catalytic role in accelerating the leaching rate with oxygen as an oxidant [1,11]. Hence, it is generally believed that oxygen plays a central role in the regeneration of Fe^{3+}, and the Fe(III)/Fe(II) redox couple acts in a catalytic manner in these reactions [1,11]. Figure 1-3 is a schematic diagram of the relationship indicating the roles of ferric, oxygen and chalcopyrite in the leaching system: chalcopyrite is oxidized by Fe^{3+} to release copper from the minerals into solution as Cu^{2+}; the produced Fe^{2+} (from either Fe^{3+} reduction or $CuFeS_2$ dissolution) is re-oxidized by dissolved O_2 to generate Fe^{3+} (as a surrogate oxidant).

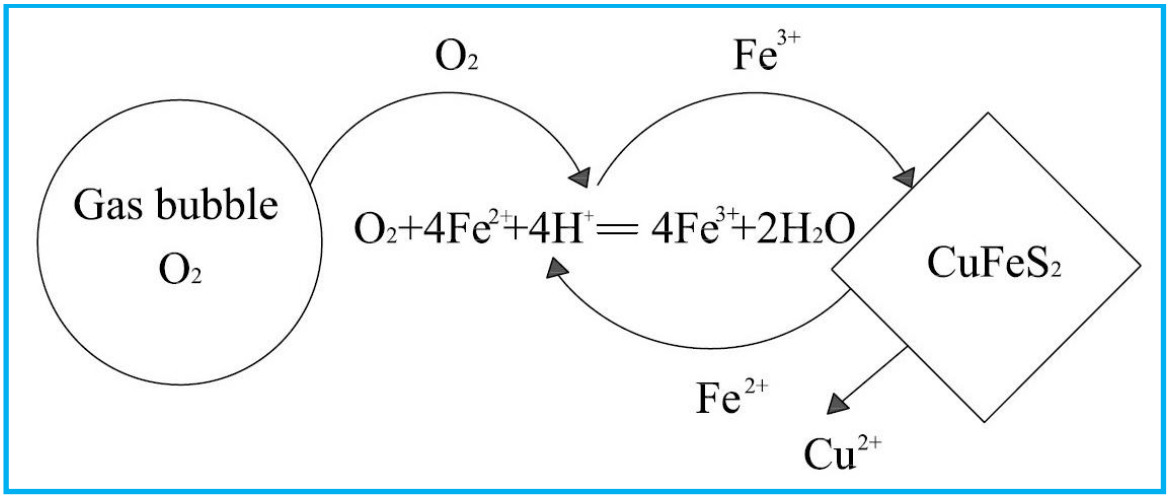

Figure 1-3 Schematic diagram of the relationship indicating the roles of ferric, oxygen and chalcopyrite in the leaching system.

In order to promote the development and application of the hydrometallurgical technologies to treat chalcopyrite on a commercial scale, basic studies that elucidate the chemical

and electrochemical aspects governing leaching (i.e. establish the rate-determining step for each leaching system) should be taken into account, and remain topics of ongoing research.

Most of the chemical or electrochemical research has traditionally focused on the oxidative processes [12-18] or cathode reduction reactions of chalcopyrite itself [19-22]. However, the cathodic reduction of oxidants (ferric ions or dissolved molecular oxygen), as the most important cathodic process in these systems, are also of great significance due to the fact that they can affect the overall leaching rate of the process and the actual reduction behavior of ferric ions is vital to obtain the true leaching rate, as predicted by mixed potential theory [23, 24]. Figure 1-4 presents a conceptual diagram to show the hypothetical polarization curves for the anodic and cathodic reactions superimposed on one another [23]. A sulfide mineral under leaching conditions is presumed to give up electrons to an oxidant, and hence the potential of the mineral is governed by the electrochemical kinetics of both the anodic process (oxidation of the mineral) and the cathodic process (reduction of the oxidant). At the intersection point of the anodic and cathodic curves, the electrochemical leaching rate is determined, along with the mixed potential. The mixed potential cannot be higher than the reversible potential of the oxidant that is actually collecting electrons from the surface, nor can it be lower than the potential below which the mineral is stable thermodynamically. As seen in Figure 1-4, each individual polarization curve (A: anodic; C: cathodic) has three distinct stages: 1, 2, and 3. Stage 1 represents the equilibrium (steady state) region where the particular electrode reaction is mostly reversible and the potential obeys Nernst Equation. The potential in this region should be related to the current in a linear fashion, and hence kinetics should depend on conduction through the electrode and the electrolyte. Stage 2 is known as the Tafel region, where the potential is directly dependent on the logarithm of the current and the process is under activation control. Stage 3 represents the

limiting current region where diffusion of the reactant or the product species controls the reaction singly or jointly. Partial and general kinetic expressions for all the nine situations can be derived from the position of the intersection point with respect to the stage of individual half-cell reactions of a leaching process [23, 24].

Taking various possible combinations between A1-A3 and C1-C3, there can be a total of 9 possible situations for the intersection points of the anodic oxidation branch and cathodic reduction branch. Clearly, the overall leaching rate can also be affected by the cathodic reduction reaction. A detailed analysis of the behavior of cathodic ferric ion reduction on chalcopyrite is required in order to better understand the factors affecting the leaching process.

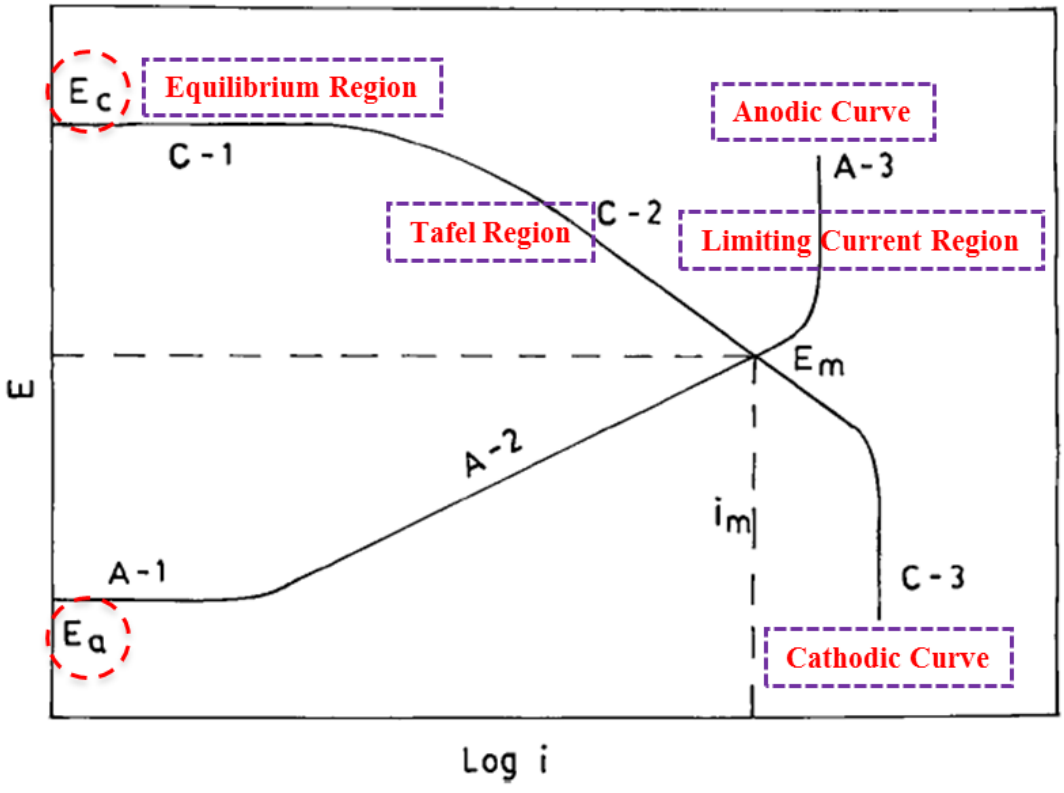

Figure 1-4 Hypothetical polarization curves for the anodic and cathodic reactions superimposed on one another.

Nevertheless, the ferric reduction behavior on chalcopyrite has hardly been investigated, and very few data are available about the reduction processes in leaching systems. Some research has shown that the Fe^{3+}/Fe^{2+} couple (indeed most redox couples) is much less reversible on corroding or polarized chalcopyrite than on pyrite, platinum or freshly polished chalcopyrite [25-27]. The formation of a passive film slows transport of ions from $CuFeS_2$ to the solution, slows electron transfer to oxidants such as Fe^{3+} and slows the supply of holes to the solid-solution interface. Compared with the I_3^-/I^- and Cu^{2+}/Cu^+ redox couples, the rate of electron transfer between the Fe^{3+}/Fe^{2+} couple and the surface of $CuFeS_2$ is slower [25, 26] and it follows that the slow kinetics for ferric reduction on a polarized $CuFeS_2$ surface is a contributing factor for $CuFeS_2$ passivation [27]. Some investigators have assumed that it is the cathodic half-cell reaction (i.e. ferric reduction) that limits the overall rate of leaching [28]. These limited studies are typically performed at lower temperatures, and it is generally accepted that the reaction rate of the ferric/ferrous couple on chalcopyrite is much slower than that on platinum or pyrite, for example [25, 26]. However, there is a lack of published reports describing just how slow the reduction rate of ferric ions may be (not to mention a comprehensive study and comparison of reduction kinetics at different temperatures), and to what extent the cathodic reaction can influence the overall leaching reaction.

In order to study the reduction behavior of ferric ions and further obtain its influence on the leaching rate, true ferric ion concentration/activity in the leaching solution is required. In addition, despite the fact that ferric ion plays a central role in the oxidation of chalcopyrite, it has been reported that the reversible/redox potential of the Fe^{3+}/Fe^{2+} couple, determined by the Fe^{3+}/Fe^{2+} concentration ratio, also has a predominant effect on chalcopyrite leaching and passivation behavior [13, 29-32]. For example, Kametani and Aoki (1985) found that ferric

concentration had little effect on the oxidation rate of chalcopyrite and copper extraction was mainly controlled by the redox potential of the solution (a function of the Fe^{3+}/Fe^{2+} ratio) [29]. It is clear that a more efficient leaching process, therefore, requires an understanding of the factors affecting the true redox potential in leaching solutions. However, due to the fact that ferric and ferrous ions readily form complexes (charged cations and anions, neutral species, as well as precipitates at higher temperatures) in acidic iron sulfate solutions [33-45], and thus limiting the concentration of ferric and ferrous ions, to date it has been difficult to accurately invoke the Nernst equation. This equation requires the concentrations of free ferric and ferrous ions in the acidic iron sulfate solution. Similarly, this information is required to obtain the redox potential of acidic iron sulphate solutions [33, 34, 37], and to apply other basic electrochemical kinetic equations (Butler-Volmer equation and its extensions). Accurate speciation of this system is thus essential to obtain information relevant to the mechanism of industrial leaching processes. For example, the Nernst equation can be used to distinguish which half reaction, cathodic or anodic, may govern the overall reaction rate [23, 24, 46-50], by comparing the relative polarization degrees of the anodic and cathodic reactions using mixed potential theory.

Moreover, although it is generally accepted that ferric ion is an effective oxidant for chalcopyrite leaching, and increased $FeSO_4$ concentration substantially decreases the leaching rate (and the mixed potential) [12], Hiroyoshi et al [51-53] have observed that some chalcopyrite samples were more effectively leached in ferrous sulfate solution than in ferric sulfate solution. This raises some concerns about the role of ferrous during ferric leaching of chalcopyrite. Speciation analysis of the acidic iron sulfate system can help explain this discrepancy.

In addition, during the oxidation of chalcopyrite, there are a number of solution species that can interact by forming complexes that may exert influence on the overall process. Dutrizac

et al (1969) [54] and Hirato et al (1987) [12] have shown that chalcopyrite's leaching rate is strongly affected by ferric ion concentration only at concentrations less than 0.01 or 0.1 M; at higher concentrations the effect is negligible. Hirato et al attributed this to the variation of Fe^{3+} and/or $FeHSO_4^{2+}$ concentrations, according to the species distribution analysis for acidic ferric sulfate solution. A similar trend was observed by Crundwell (1987) [55], who found that the dissolution rate of sphalerite in acidic ferric sulfate solutions was proportional to the sum of the concentrations of the Fe^{3+} and $FeHSO_4^{2+}$ species. Although $FeSO_4^{+}$ was the dominant species present under the leaching conditions, it was inactive as an inner-sphere complex. Clearly, the leaching kinetics at higher ferric concentration may be related to the distribution of iron species in solution.

Therefore, based on the above analyses, solution speciation is required to better understand and determine the factors affecting industrial leaching processes, so as to establish the optimum conditions and improve the leaching rates for copper recovery. However, although several studies have examined the speciation of the quaternary acidic iron sulfate system as a function of the initial amounts of iron, acidity, and temperature [33-38], to the knowledge of the present author, most of these are limited to lower concentrations and temperatures. There are very few published data pertaining to a systematic study on the speciation of the H_2SO_4-$Fe_2(SO_4)_3$-$FeSO_4$-H_2O system, especially at higher concentrations and temperatures where most of the chalcopyrite hydrometallurgical processes operate. Moreover, ferric is a very common oxidant for many other metal sulfide leaching systems, thus its distribution in sulfate solutions is also of general importance.

1.3 Scope of the Present Study and Thesis Organization

This work is first to explore the possibility of establishing aqueous speciation diagrams of the quaternary acidic iron sulfate system under conditions most relevant to the hydrometallurgical industry, thereby obtaining more detailed information about the electrolytes involved. These speciation results can further provide the data that can enable one to systematically investigate the kinetics of the cathodic ferric ion reduction reaction on chalcopyrite in industrially relevant leaching systems at different temperatures from 25℃ to 150℃. This kinetics investigation aims to determine the temperature dependence of the fundamental electrochemical kinetic parameters, such as exchange current density, transfer coefficient and rate constant. The obtained information will finally be employed to shed light on the mechanism of industrial chalcopyrite leaching processes, i.e. by using mixed potential theory to obtain detailed information about which of the cathodic or anodic reactions may, in principle, govern the overall reaction rate [23, 24, 46-50]. The present study yields detailed information about the electrochemical processes involved and enables a deeper understanding of the kinetics and mechanisms in industrially significant leaching conditions relevant to such processes as Activox, Nenatech, Dynatec, AAC/UBC, Total Pressure Oxidation, CESL and Galvanox.

In the following chapter (Chapter 2) various important topics and results found in the literature, which are highly related to the present project, will be summarized and discussed. Chapter 3 will present the objectives of this study. The methodology involved, including experimental procedures for the electrochemical and analytical methods, will be provided in Chapter 4. Chapter 5 discusses the development of a thermodynamic model to simulate the speciation of the quaternary sulfuric acid-ferric sulfate-ferrous sulfate-water system and so as to quantify the concentrations of the main species included in the solution through a wide range of

solution compositions and temperatures (25 ℃-150 ℃). Chapter 6 presents how to calculate the redox potential of the Fe^{3+}/Fe^{2+} couple based on the speciation results obtained previously. It also presents a novel expression to predict the redox potential of the Fe^{3+}/Fe^{2+} couple in the above-mentioned quaternary acidic iron sulfate electrolyte (which is widely used in the hydrometallurgical industry for the leaching of minerals and mineral concentrates) up to 150 ℃ (**Application 1**). The kinetics of ferric ion reduction on chalcopyrite (including the temperature dependence of the exchange current density, transfer coefficient and rate constant) and its influence on the overall chalcopyrite leaching reaction will be presented in Chapter 7 (**Application 2**) and Chapter 8 (**Application 3**), respectively. Finally, Chapter 9 presents the conclusions, industrial applications and recommendations for future work in this area.

The present work contributes to the research on aqueous speciation of acidic iron sulfate solutions, prediction of redox potential of the Fe^{3+}/Fe^{2+} couple in acidic iron sulfate solutions, the reduction kinetics of the Fe^{3+}/Fe^{2+} couple in general and in particular on the surface of chalcopyrite, as well as the mechanistic analysis in industrial leaching processes of chalcopyrite and other sulfide minerals. It is believed that these findings can enable better understanding of the critical factors to make the proposed chalcopyrite leaching process an economic proposition, and eventually reach full commercial acceptance.

2 Literature Review

From the **Introduction**, it can be seen that very few studies about the reduction kinetics of ferric and oxygen on chalcopyrite have been published. Nevertheless, the following subjects, previously discussed in the literature, will be presented: the oxidation of chalcopyrite and cathodic reduction of chalcopyrite itself, the chemical or electrochemical reduction of ferric or oxygen on chalcopyrite, rotating disc electrode studies of chalcopyrite and other related sulfide minerals, electrochemical impedance spectroscopy studies of chalcopyrite, and, high temperature electrochemistry of both chalcopyrite and ferric/oxygen reduction.

2.1 Oxidation of Chalcopyrite and Cathodic Reduction of Chalcopyrite Itself

To date, much effort has been devoted to understanding the kinetics and mechanisms of the oxidation processes or the cathodic reduction reactions of chalcopyrite itself, in order to develop possible hydrometallurgical leaching processes. In this section, a brief introduction on oxidation of chalcopyrite and cathodic reduction of chalcopyrite will be given.

2.1.1 Chemical or Electrochemical Oxidation of Chalcopyrite in Sulfuric Acid

Among the several factors determining choice and effectiveness, leaching reagents are usually assessed in terms of dissolution power, price, and environmental friendliness. In the search for suitable and sustainable alternative leaching reagents, attention has been refocused on the use of easily available and cheap reagents like sulfuric acid. Sulfuric acid has been used for a very long time for sulfide ore leaching, and ways of improving its effectiveness have been investigated by various researchers. For the oxidation of chalcopyrite in sulfuric acid, ferric ions and dissolved oxygen are the most often used oxidants. These processes involve the oxidation of chalcopyrite to elemental sulphur, sulphate or other oxysulfur anions, and can be regarded as an

electrochemical reaction with the cathodic reduction of the oxidant and the anodic oxidation of chalcopyrite. These studies have shown that the poor leaching kinetics are a result of anodic passivation.

2.1.1.1 Thermodynamics and Stoichiometry of Chalcopyrite Dissolution

The thermodynamics of the dissolution process may be discussed on the basis of Eh-pH diagrams [56]. According to the following diagram (Figure 2-1), a pH lower than 4 and an oxidizing redox potential higher than +0.4V is required to dissolve copper from chalcopyrite. These conditions are achieved using oxidizing agents, the most common being ferric ion as a sulphate or chloride. It may be noticed that information on the kinetics and mechanism of the possible reactions is not provided by this kind of diagram. Chalcopyrite dissolves in the presence of ferric ion according to the following reactions [3]:

$$CuFeS_2 + 4Fe^{3+} = Cu^{2+} + 5Fe^{2+} + 2S^o \quad (2\text{-}1)$$

$$CuFeS_2 + 4Fe^{3+} + 3O_2 + 2H_2O = Cu^{2+} + 5Fe^{2+} + 2H_2SO_4 \quad (2\text{-}2)$$

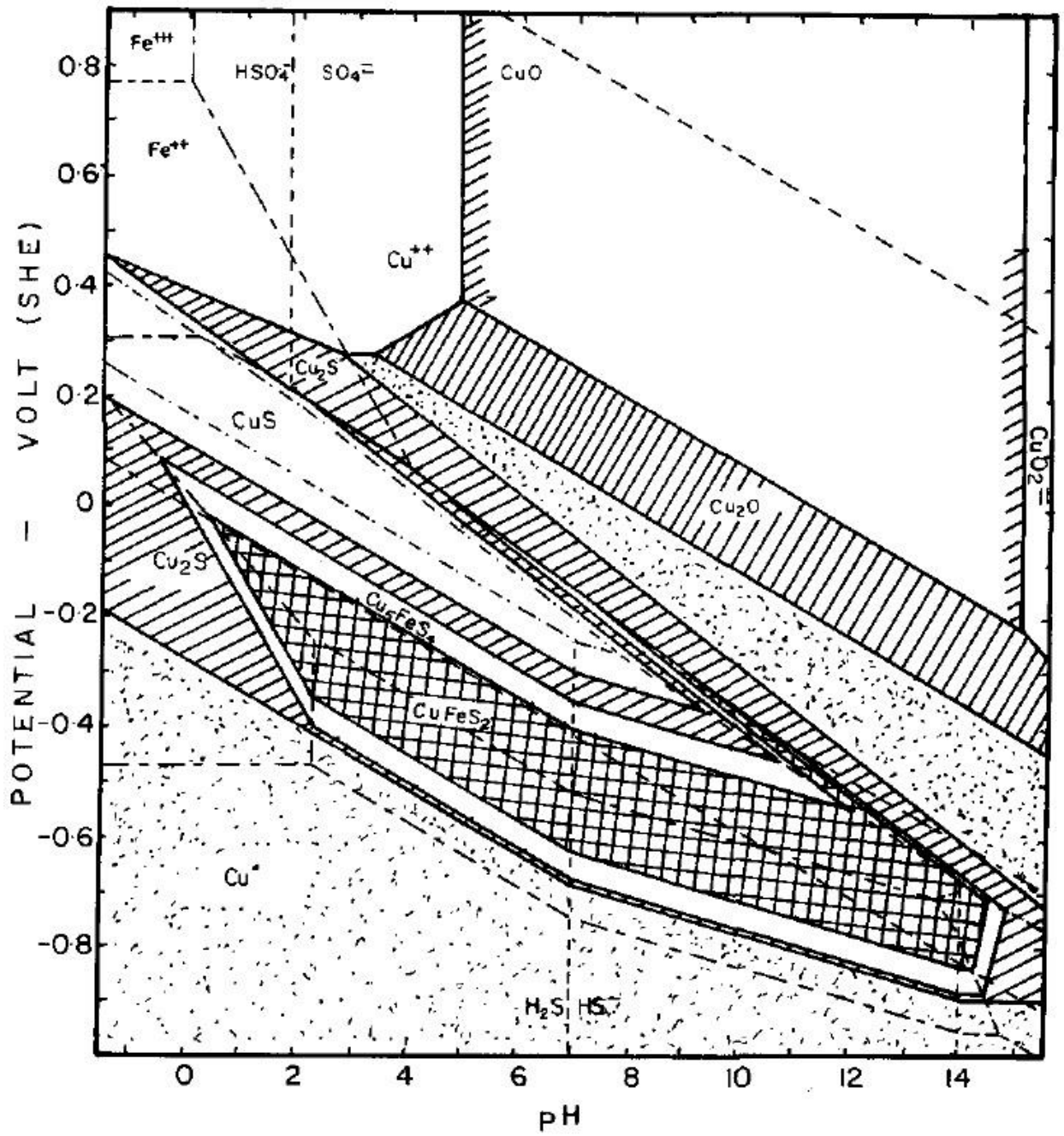

Figure 2-1 Eh-pH diagram of the Cu-Fe-S-H_2O system at 25°C: all solutes at 0.1 M activity except Cu^{2+} = 0.01 M. All reactions are reversible [56].

2.1.1.2 Chemical Leaching of Chalcopyrite-Roles of Ferric/Ferrous and Redox Potential

Ferric ions are very commonly used in the leaching process of chalcopyrite and other metal sulfides, and widely regarded as an oxidant. Thus, ferric distribution in acid iron sulfate solutions is of major importance. However, it has been reported that increasing the concentration of ferric does not consequently result in a corresponding increase in the leaching rate [12]. In addition, during the oxidation of the chalcopyrite, there are a number of solution species that can interact by forming complexes that may exert influence on the overall process. And, it has been suggested by different authors that the leaching rate of chalcopyrite is strongly affected by redox potential of the solution determined by the ferric/ferrous ratio [29], ferrous concentration [51-53], or low ferric ion concentrations [12]. Thus, this raises some concerns about the real role of ferric, ferrous and the ratio of ferric to ferrous during the ferric leaching of chalcopyrite, which can facilitate the study of ferric reduction kinetics.

Here we take some typical results published in previous studies into account to introduce this question in detail in acidic iron sulfate leaching solutions.

Suspension potential control

The oxidation rate of chalcopyrite is expected to be dependent on the potential difference between the surface of the suspended particles and the solution. However, it is not possible to measure directly or to control the potential difference, which makes it difficult to compare directly leaching reactions and the electrode processes. A way of conducting the experiments with a constant redox potential in the solution to overcome the problem was reported by Kametani and Aoki [29]. This potential is referred to as the suspension potential. Suspension potential (Pt vs SCE, in the presence of Fe^{3+}/Fe^{2+}) in 1 mol/dm^3 sulfuric acid solution at 90℃ was maintained constant in the range 0.54 to 0.89 V (vs SHE). The oxidation appeared to be

under surface reaction control. Ferric concentration had little effect on the oxidation rate of chalcopyrite and the copper extraction was mainly controlled by the redox potential of the solution, as a function of the ferric/ferrous ratio. Chalcopyrite in the concentrate was oxidized to form elemental sulfur over the entire suspension potential range.

Ferrous-promoted leaching

It is generally accepted that ferric ions, as an oxidant, are effective for leaching chalcopyrite but that ferrous ions contribute to leaching only in that, after oxidation, they represent a source of ferric ions. However, Hiroyoshi et al [51] found some chalcopyrite samples were more effectively leached in ferrous sulfate solution than in ferric sulfate solution. It was suggested that ferrous ions enhance the following reaction:

$$CuFeS_2 + O_2 + 4H^+ = Cu^{2+} + Fe^{2+} + 2S^0 + 2H_2O \quad (2\text{-}3)$$

The amount of extracted copper increased markedly with increasing ferrous sulfate addition and with decreasing pH. When the leach solution was sparged with nitrogen, the amount of copper extracted was negligible even with ferrous sulfate.

A reaction model was proposed [52] and the model considers the leaching in two steps: (1) reduction of chalcopyrite to Cu_2S by ferrous ions in the presence of cupric ions and (2) oxidation of the Cu_2S to cupric ions and elemental sulfur by dissolved oxygen and/or by ferric ions. Further research [53] also obtained similar results and shows that in the presence of high concentrations of cupric ions, the chalcopyrite oxidation was enhanced by high concentrations of ferrous ions and copper extraction was mainly controlled by the concentration ratio of ferrous to ferric ions or the redox potential of the solutions.

Leaching in acidic ferric sulfate solution

Leaching of chalcopyrite by Hirato et al [12] showed parabolic-like kinetics during the initial stage, and then linear kinetics over the extended period in acidic ferric sulfate. Leaching was chemically controlled, with apparent activation energy in the range of 76.8-87.7 kJ mol^{-1}. The leaching rate increased with an increase in $Fe_2(SO_4)_3$ concentration up to 0.1 mol dm^{-3}, but a further increase had little effect on the leaching rate. Both the leaching rate and the mixed potential decreased with an increased $FeSO_4$ concentration.

Córdoba et al [13] reported the effect of redox potential (or Fe^{3+}/Fe^{2+} ratio) on chalcopyrite leaching in a Fe^{3+}/Fe^{2+} sulphate solution at pH 1.8 at temperatures of 35°C and 68°C. The redox potential range used was 497-797 mV (vs SHE) and it was found to be a key factor. A high potential at the onset of leaching provoked rapid passivation due to rapid precipitation of ferric ion as jarosite. They hypothesized that although ferric ion is responsible for the oxidation of chalcopyrite, ferrous ion has an important role in that it controls precipitation and nucleation of jarosites, which ultimately cause passivation. Chalcopyrite dissolves through the intermediate formation of covellite, CuS, which is later oxidized by ferric ion to release Cu^{2+} ions. The elemental sulphur that formed during chalcopyrite leaching was porous and did not form a passivating layer on the chalcopyrite surface. Further research by Córdoba et al [14] showed the the role of pH in the chalcopyrite leaching with ferric sulphate was found to be exclusively related to control of ferric species hydrolysis rather than oxidation of sulphide. The absence of oxygen in the leaching medium remarkably slows down chalcopyrite dissolution. Oxygen plays a key role in the regeneration of ferric ion as the oxidizing agent of the sulphide.

Vilcáez et al [32] reported that the oxidation of ferrous ion by oxygen did not take place in the absence of sulfides such as Cu_2S and CuS. Leaching was insensitive to the addition of ferric

ion above about 0.01 M because ferrous ion released during the initial leaching stages did not suffice to reduce the initial ORP to values below 450 mV, where chalcopyrite leaching has been proven to be enhanced. If lower amounts of additional ferric ion were employed, the amount of ferrous ion released by ferric ion attack of chalcopyrite sufficed to reduce the initial ORP to values below a critical value (450 mV) such that the leaching of chalcopyrite was enhanced. The possibility of chalcopyrite being directly leached by ferric ion at high ORP values, and indirectly through the formation of intermediates at low ORP values, was supported by this work.

Leaching of chalcopyrite ore using sulphuric acid containing oxygen and iron(III) in PVC columns was reported by Antonijević and Bogdanović [57] and it was also shown that iron(III) concentration had no important influence on the copper leaching rate.

Summary

The above results would suggest that the observed leaching kinetics may be alternatively due to the ferric/ferrous ratio, ferrous concentration, or ferric ion concentration. Hence, it is necessary to study the reason for this discrepancy to clarify this controversial issue, and speciation analysis of the acidic iron sulfate solution can definitely facilitate this research.

2.1.1.3 Electrochemical Oxidation of Chalcopyrite

The fundamentals of chalcopyrite leaching have been extensively studied through electrochemical techniques, since it is thought to be essentially an electrochemical mechanism that takes place at the mineral-solution interface. Munoz et al [58] studied acid ferric sulfate leaching of chalcopyrite (1.0M H_2SO_4, 0.25 M $Fe_2(SO_4)_3$, 90℃) using mono-sized particles in a well stirred reactor at ambient pressure and dilute solid phase concentration in order to obtain fundamental details of the reaction kinetics. The electrochemical reaction of chalcopyrite conforms to the stoichiometry of Reaction 2-1.

The chief function of the acid appears to be to prevent the hydrolysis of ferric. The rate limiting step is found to be the transport of electrons through the elemental sulfur layer. The reaction rate was independent of $Fe^{3+,}$ Fe^{2+}, Cu^{2+} and H_2SO_4 concentrations. Experimental activation energy was 20 kcal/mol (83.68 kJ/mol) and is approximately the same as the apparent activation energy for the electron transfer through elemental sulfur, 23 kcal/mol (96.23 kJ/mol), reported in the literature.

Potentiodynamic polarization/Linear potential sweeps

Most of electrochemical studies have used relatively fast linear potential sweeps. Warren et al [15] studied electrochemical oxidation of $CuFeS_2$ in 1.0 M H_2SO_4 using massive electrodes (approximately cubic, 1.0 cm on each side) by potentiodynamic polarization. Chalcopyrite samples obtained from six different localities often produced polarization curves that differed slightly from each other, which could be due to a difference in crystal orientation, impurities, changing surface area, etc (Figure 2-2). The overall shape of the polarization curves was generally the same, consisting of: dissolution, passive and transpassive regions. Although none of the samples exhibited the classical behavior of passivating metals, a portion of the anodic polarization curve exists where the current does not increase with increasing potential. This portion will be referred to as the "passive" region.

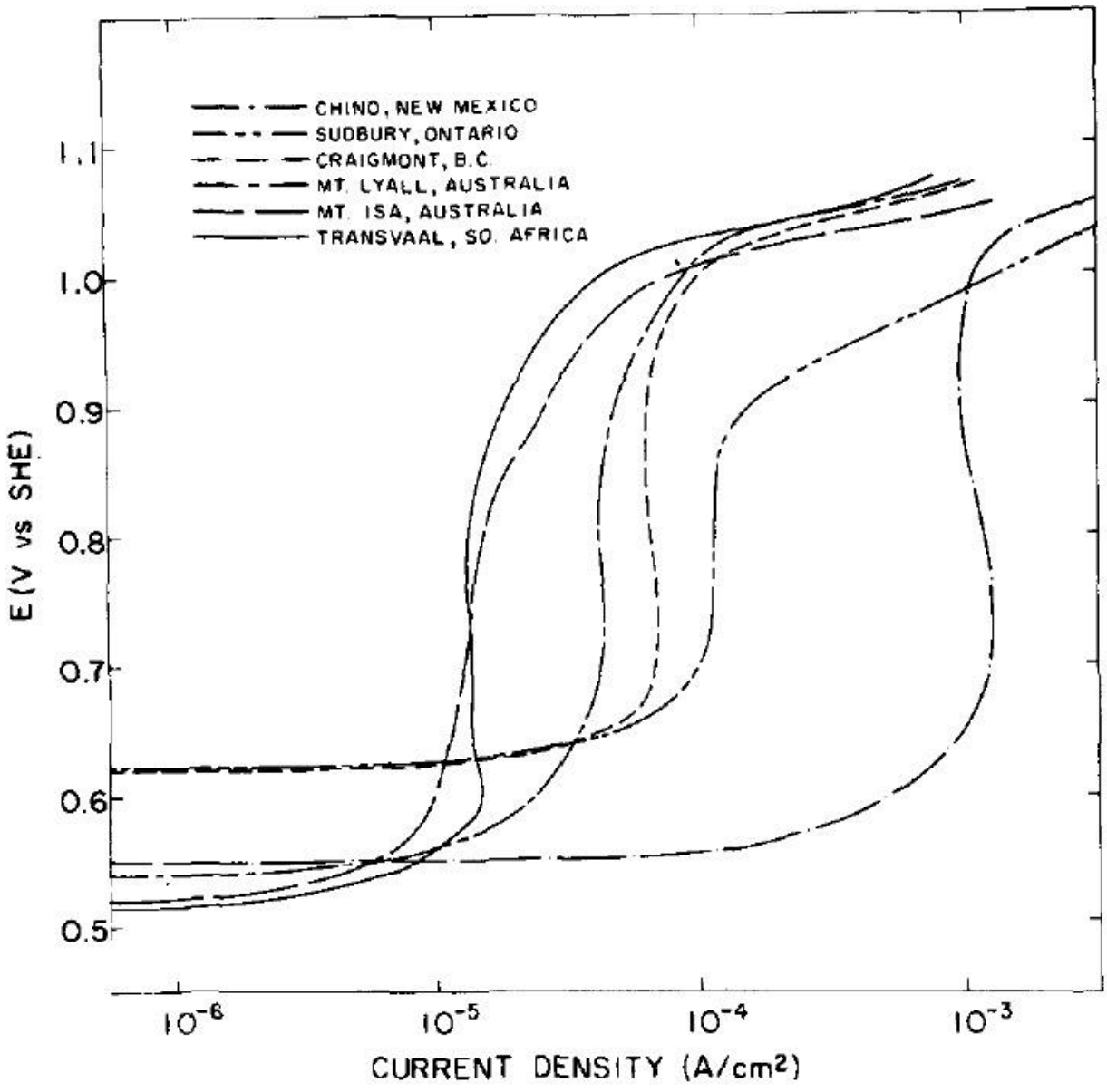

Figure 2-2 Anodic polarization curves for $CuFeS_2$ from 6 different locations in 1 M H_2SO_4, 30 mV/min, 25 ℃ [15].

Slower scanning rates shifted the curves to lower currents but did not cause the current to decrease drastically as would be expected (Figure 2-3). The presence of this current plateau was attributed to the formation of a thin layer of a defective copper sulfide intermediate as well as sulfur on the surface.

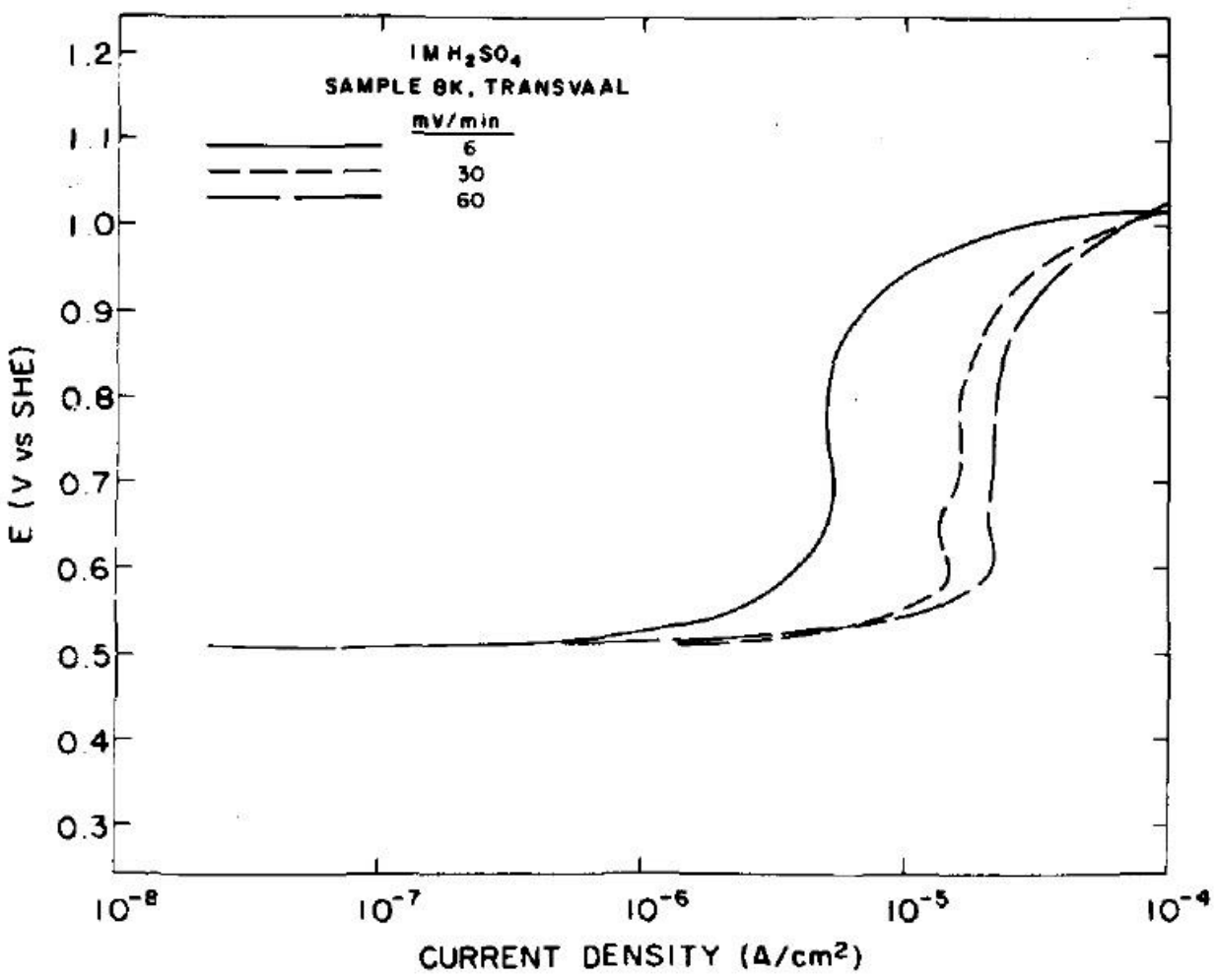

Figure 2-3 Effect of scanning rate on the anodic polarization curve of Transvaal $CuFeS_2$ in 1 M H_2SO_4, 25 ℃ [15].

Additions of cupric ion up to 50 g/L had little or no effect on the polarization curve (Figure 2-4). Ferrous additions, on the other hand, greatly affect the curves (Figure 2-5). The observed increase of the current in the passive region was directly related to the initial Fe^{2+} concentration. This is attributed to an additional competing oxidation reaction of the ferrous to ferric ion at the $CuFeS_2$ surface. This result confirms the electron conducting character of the surface products.

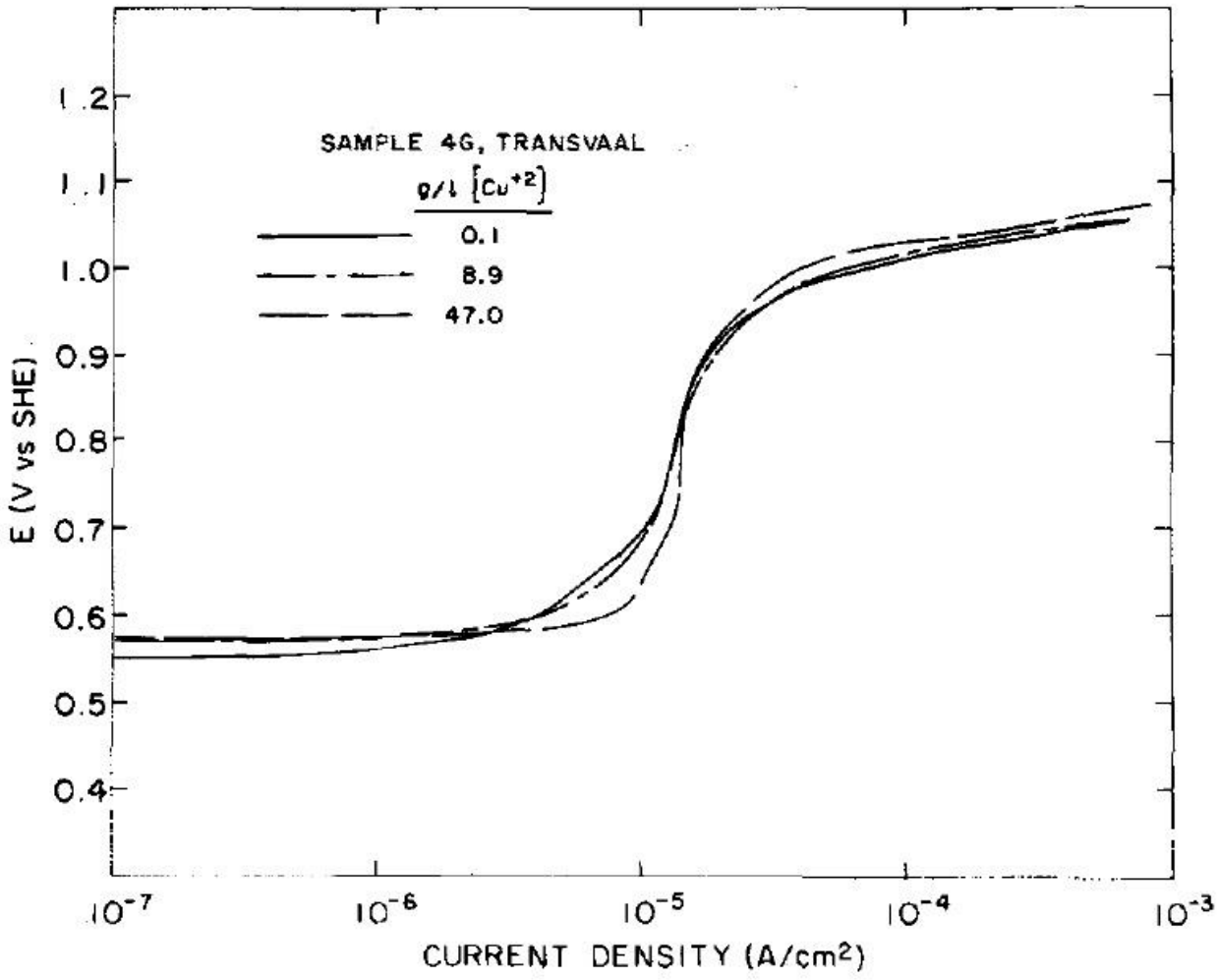

Figure 2-4 Effect of cupric ion on the anodic polarization curve of Transvaal $CuFeS_2$ in 1 M H_2SO_4, 40 mV/min, 25 ℃. [Fe^{2+}] was held constant at 0.04 g/1 [15].

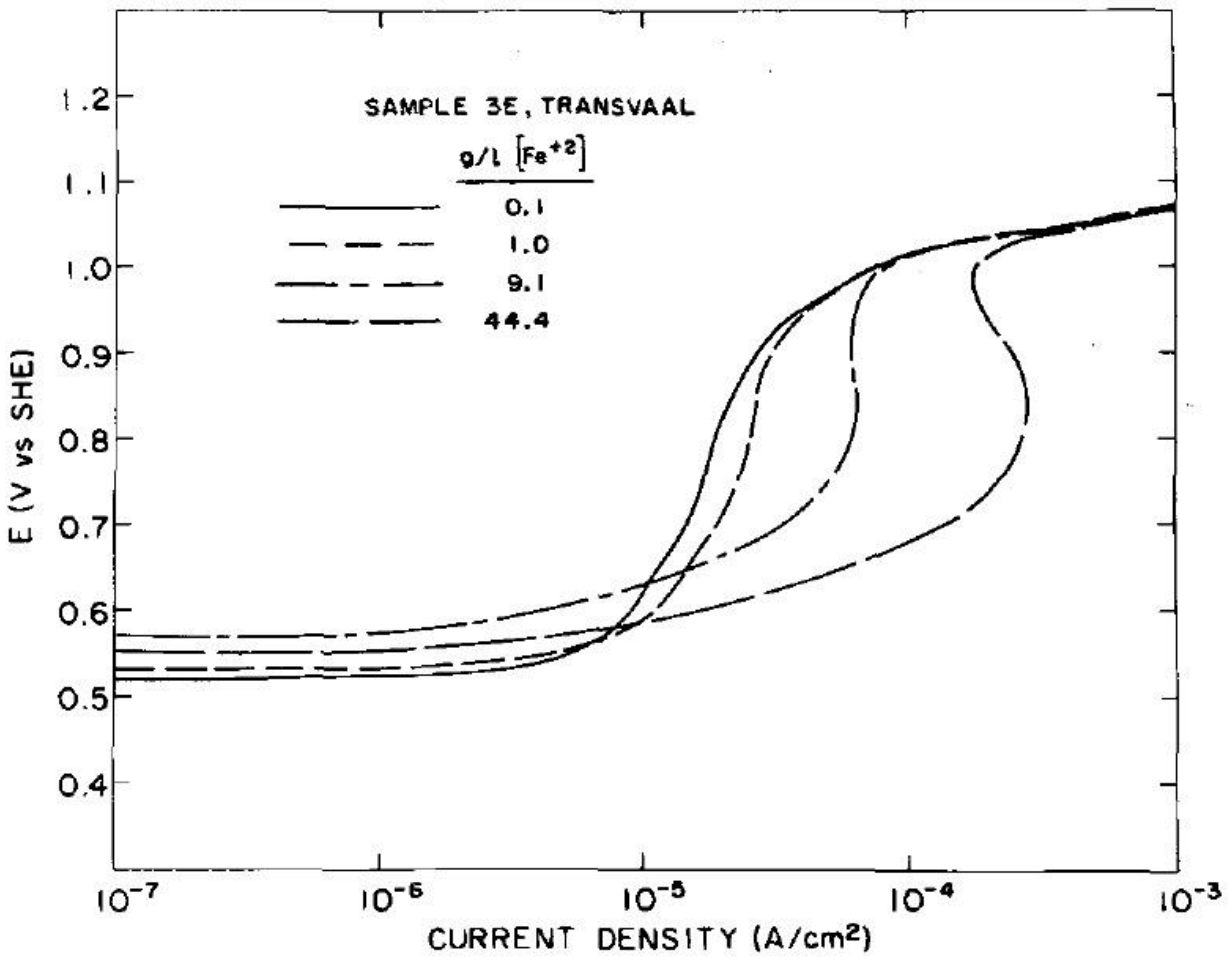

Figure 2-5 Effect of ferrous ion on the anodic polarization curve of Transvaal $CuFeS_2$ in 1 M H_2SO_4, 40 mV/min, 25 ℃. [Cu^{2+}] was held constant at 0.90 g/l [15].

Anodic dissolution of n- and p-type chalcopyrite was studied in both acidic sulphate (0.3 mol dm^{-3} H_2SO_4) and acidic chloride (0.3 mol dm^{-3} HCl) media under conditions relevant to chemical leaching, i.e., at temperatures > 70℃ and over the potential region 0.44-0.84 V vs SHE by McMillan et al [26]. Analysis in both systems indicated the formation of a surface layer, a solid electrolyte interphase (SEI), which slowed the rate of electron transfer. The higher Tafel slopes and anomalous Arrhenius behaviour obtained in H_2SO_4 suggested the surface layer formed in that medium was different from that produced in HCl electrolyte.

Tshilombo et al [27] studied the kinetics of the half-reactions involved in the oxidation of $CuFeS_2$ (potential range 0.44-0.84 V vs SHE) by potentiodynamic polarization techniques in sulfuric acid. Anodic characteristics showed that $CuFeS_2$ passivation was more severe in the potential range 0.69-0.89 V (vs SHE) at 25℃. However, there was no evidence of $CuFeS_2$ passivation at higher temperatures (45 and 65℃). Cu was preferentially dissolved from $CuFeS_2$ at lower potentials and high temperatures at a ratio of copper to iron of about 3:2.

Parker et al [59] used gold plating of chalcopyrite surfaces to stimulate surface enhancement of Raman scattering, thereby detecting oxidation products undetectable using normal Raman spectroscopy. In situ spectroscopic investigations during potentiodynamic scanning revealed that the oxidation product was amorphous, ubiquitous over the surface and showed some evidence of the commencement of S-S bonding in the transpassive potential region. The product was not characteristic of polysulfides or polythionates, indicative of an aging metal-deficient remnant sulfide lattice based on low frequency and the broad nature of the ν_{SS} bands on the oxidised surfaces.

Ghahremaninezhad et al [16] studied the dissolution of chalcopyrite electrodes in 0.5M sulfuric acid by means of potentiodynamic, EIS and Mott-Schottky techniques. A sequence of chalcopyrite dissolution and surface layer formation was proposed under different potential regions from open circuit potential (around 415 mV vs SHE) to higher positive potentials. EIS studies at open circuit potential proved the existence of a thin surface layer on the electrode. This layer was stable up to 100 mV and was assumed to be $Cu_{1-x}Fe_{1-y}S_2$. Increasing the potential through the range of 100-300 mV results in the partial dissolution of previously formed layer and the formation of a second layer ($Cu_{1-x-z}S_2$). Both of the layers showed the characteristics of passive layers at low potentiodynamic scan rate (0.05 mVs^{-1}) while at high scan rates they acted

like pseudo-passive layers. However, in the potential range of 300-420 mV, both of these surface layers dissolved and active dissolution of the electrode started. Further increase in potential caused the formation of a CuS layer which hindered the dissolution rate of the electrode. The formation of CuS was concomitant with $Fe_2(SO_4)_3$ formation and the latter may have acted as a nucleation precursor for jarosite at higher potentials (around 1.4 V vs SHE). Jarosite precipitation on the electrode surface hindered the dissolution of chalcopyrite at higher potentials. Different equivalent electrochemical circuits were modeled and compared to experimental results to support the proposed sequence of chalcopyrite dissolution and surface layer formation.

Potentiostatic polarization

It is found that potentiodynamic polarization curves with fast linear potential sweeps in acidic ferric/ferrous sulphate media at atmospheric pressure in the vast literature that exists cannot be used to faithfully predict important operational parameters. These parameters include the range of potentials most appropriate to leach the mineral and the potential for the onset of passivation (in order to avoid exceeding it). However, Viramontes-Gamboa et al [60, 61] found that potentiostatic anodic curves display true active-passive behavior with a passivation potential very well defined and close to the one observed in leaching tests. They show that the passive window is much smaller than predicted by potentiodynamic sweeps, such that the transpassive region is easily reached within the working range of the Fe^{3+}/Fe^{2+} redox couple.

The oxidative leaching rate of chalcopyrite by ferric ions or by dissolved oxygen in sulfuric acid solutions is known to be faster at low redox potentials but slower at potentials above a critical value, due to the passivation of the mineral. However, most conventional electrochemical studies on the anodic dissolution of chalcopyrite in sulfuric acid solutions have disagreed with the results of leaching studies, i.e., they have reported monotonic increases in the

steady-state anodic current with potential. A study by Hiroyoshi et al [17] shows that active-passive behavior occurs only when cupric and ferrous ions coexist (conditions of anodic polarization curves in 0.1 kmol m^{-3} sulfuric acid with stirring at 298 K in a nitrogen-sparged solution). The current in the active region (at potentials lower than about 0.65V vs SHE) was larger than the current observed without cupric and/or ferrous ions, indicating that the coexistence of these ions (0.1 kmol m^{-3}) causes activation rather than passivation. Hiroyoshi et al [31] also investigated the effects of solution composition on the optimum redox potential by potentiostatic curves using a $CuFeS_2$ electrode at 298 K. Anodic-polarization curves of the $CuFeS_2$ electrode showed that there was a current peak on the curves in the presence of Cu^{2+} and Fe^{2+}, corresponding to the maximum leaching rate. The redox potential of the peak increased markedly with increasing Cu^{2+} concentration, while it was less dependent on the H_2SO_4 and Fe^{2+} concentrations. An empirical equation for the optimum redox potential for $CuFeS_2$ leaching was proposed:

$$E\text{op}=E_A=0.691+0.030 \log [Cu^{2+}] + 0.013\log [Fe^{2+}] \quad (2\text{-}4)$$

where Eop is the optimum redox potential for $CuFeS_2$ leaching and E_A is the "rest potential of $CuFeS_2$" dipped in the leaching solutions.

Galvanostatic polarization

Galvanostatic curves (potential vs time) show two regions: a transient state that is related to anodic film formation; and a steady state represented by a leveling off of potential, corresponding to the condition where the corrosion current is equal to the applied current, resulting in a film thickness of constant value. Research by Sequeira and Santos [62] focused on the study of the anodic film formation on chalcopyrite in the transient time-dependent region (generally data between 0.7 and 0.9 V vs SHE) in sulphuric acid at 25℃. Two passivation sub-

regions were observed: the first at lower potentials, shows a slope greater than the second, which occurs at higher potentials. Both followed the Sato-Cohen (logarithmic) model for the growth of anodic passive films. Cupric ion concentration up to 10 g/L had little or no effect on the anodic dissolution. Addition of ferrous ion up to 1.0 g/L had no effect, but for higher concentrations, over 5 g/L, galvanostatic curves show a plateau value at approximately 0.7 V vs SHE, due to the preferred oxidation reaction of ferrous ion at the chalcopyrite surface.

Carbon paste electrode

An interesting aspect of the published electrochemical studies concerning chalcopyrite is an apparent lack of reproducibility. Chalcopyrite electrodes supported on epoxy resin present low reproducibility, low resolution and a tendency to fracture. In addition, the physical properties of these electrodes are very different from the properties of the mineral on which the process of mineral leaching is performed. For this reason it is not possible to conduct systematic electrochemical studies on this kind of electrode. One alternative is the use of electrodes made of fine particles of the mineral mixed with graphite and a conducting/non-conducting binding material. Lázaro et al [63] have shown that a mixture of pulverized chalcopyrite with graphite and a non-conducting binder (silicon oil) permits electrochemical studies to be performed similar to those with massive mineral electrodes. This has the added advantage of an excellent reproducibility, due to the absence of problems, associated with polishing deficiencies, fracture, and a lack of homogeneity, presented by the larger mineral electrodes. It is thus expected that the electrochemical data would more accurately reflect the mechanisms that occur during an industrial leaching process. The carbon paste electrode has been further employed to study the electrochemical oxidation or reduction processes of chalcopyrite to identify the proposed intermediates such as chalcocite, covellite and bornite [19, 64, 65].

Rotating electrode (RDE and RRDE)

Some of the research by electrochemical techniques has been directed at anodic dissolution in a potential region that is now called the anodic ‘‘prewave’’ which represents the initial stages of oxidation of chalcopyrite. Nevertheless, the reactions involved in this potential region and the mechanism of dissolution are still not resolved. The RDE and RRDE technique provide a means of evaluating the possibility of this reaction because its main feature is its ability to detect very low concentrations of soluble species. The versatility of the RRDE technique allows for independent control of potential and current of the ring and disk and this permits the detection on the ring of the soluble species generated during the dissolution of the mineral disk.

Biegler and Swift [66] studied the anodic behaviour of chalcopyrite (connected with Beckman rotating assembly) in 1M acids (H_2SO_4 and HCl) at 25℃. Voltammograms with a fresh surface showed a small prewave (from the rest potential around 0.4 V vs SHE to 0.85 V/0.95 V) attributed to a surface oxidation process, followed by a region of active dissolution characterized by a steeply rising anodic current (potential 1V and above). No intermediate solid products were detectable on the electrode surface. Surface reaction involved the selective dissolution of iron. There was no indication that the semiconducting nature of chalcopyrite determined its anodic behaviour. A further study [18] showed that the small anodic prewave takes place at around 0.52-0.62V vs SHE. The main anodic reaction, with complete dissolution of copper and iron, occurs at more positive potentials. The prewave is not a consequence of atmospheric oxidation during surface preparation and represents a surface oxidation of chalcopyrite to form a thin passivating film. The prewave reaction is identified with the initial phase of the oxidative dissolution of chalcopyrite. These results indicate a prewave reaction with Fe^{2+} and Cu^{2+} dissolving at the ratio 4:1 and a solid product of stoichiometry $Cu_{0.7}S_2$:

$$CuFeS_2 \rightarrow 0.75CuS + 0.25Cu^{2+} + Fe^{2+} + 1.25S + 2.5e^- \quad (2\text{-}5)$$

Anodic dissolution of chalcopyrite in acidic solutions has also been studied using cyclic voltammetry with RDE and RRDE at 298 K by Holliday and Richmond [67]. In the studies on chalcopyrite RDEs, an anodic prewave is observed between +0.44 V and +0.64 V (vs SHE) on the first scan of the electrode. The prewave reaction forms a passive surface layer that inhibits further reaction. RRDE studies show that the prewave reaction results in only partial dissolution of chalcopyrite, with iron being more readily leached from the mineral than copper.

Investigation of the products formed during the initial stages of chalcopyrite dissolution using an RRDE by Lazaro and Nicol [68] provided evidence that the mineral undergoes a non-oxidative dissolution process under freely dissolving conditions in dilute sulfuric acid solutions at 60℃ and in the absence of oxidant. This process involves the formation of soluble copper(II) ions and a soluble sulfur species which is presumably H_2S. The dissolution of chalcopyrite under oxidative conditions involves the formation of copper(II) and iron(II) ions together with detectable amounts of a soluble sulfur species (Ring–disk data suggested that this species was thiosulfate).

Bulk solution potential/Mineral potentials

A number of recent publications have focused on the use of redox (or platinum electrode) potentials to monitor the rate of reduction of iron(III) and also as a means of controlling the rate of oxidation of the mineral by controlling the redox potential. It has been tacitly or inadvertently assumed in these studies that the potential (the so-called E_H) of an inert electrode such as platinum in the bulk solution is identical to that experienced by the oxidizing mineral surface (mixed potential). However, this is not the case. Measurements of the potentials of pyrite, arsenopyrite and chalcopyrite rotating disk electrodes in acid sulfate solutions containing iron(III)

and iron(II) at 25℃ with pH 1.5 demonstrated that the potential measured in the bulk of the solution can only be approximated to that at the surface of the minerals under conditions of relatively high concentrations of iron(II) (5g/L ferric+5g/L ferrous) [69]. The results of the so-called E_H-stat experiments, in which the bulk E_H is controlled by the electrochemical or chemical oxidation of iron(II), should be used with caution if used to derive mechanistic information.

2.1.2 Chemical or Electrochemical Reduction of Chalcopyrite Itself in Sulfuric Acid

The difficult separation of copper and iron atoms in chalcopyrite by conventional hydrometallurgical procedures has encouraged the proposal of alternative processing routes. These processes consist of the reduction of chalcopyrite, in order to extract the iron from its crystal structure, forming alternate copper sulfides, which are more susceptible to oxidative leaching. Thermodynamic data, summarized in the form of Eh-pH diagrams, predict that the reduction products of chalcopyrite in acid solutions could include hydrogen sulphide and ferrous ion together with the solid phases bornite, chalcocite and elemental copper, formed in this order with decreasing potential. The stability boundaries between these phases are all below the reversible hydrogen potential, which means that their actual formation will depend on kinetic factors, in particular the over-potential for hydrogen evolution. Hydrometallurgical treatments with different reducing agents have been shown to produce copper sulfides with low iron content. Actually, one of the greatest challenges is to determine the optimum reducing agent, medium and temperature, which allow the efficient removal of the iron.

Chalcopyrite electrodes were cathodically reduced typically in 2 M H_2SO_4 at 20℃ by Biegler and Swift [20]. At current densities below 10 mA cm^{-2} chalcocite was generally formed (in some runs closely related to djurleite, $Cu_{1.97}S$; calculated standard potential for the reactions forming chalcocite and djurleite from chalcopyrite were -0.138 V and -0.144 V respectively, vs

SHE) and at higher currents (larger than 10 mA cm^{-2}) the solid product contained elemental copper (calculated standard potential is -0.269 V). The other reduction products were H_2S and Fe^{2+}. The decreased current efficiency, measured in terms of the Fe^{2+} produced, was attributed to evolution of hydrogen. Further study [21] using cathodic linear sweep cyclic voltammetry (from 0 V to -0.4 V) with a freshly-polished chalcopyrite electrode (connected with Beckman rotating assembly) shows a narrow cathodic peak (prewave, at -0.1 V) preceding the main voltammetric wave for reduction to chalcocite. The possible identity of the product phase is suggested according to a general electrode reaction:

$$CuFeS_2 + (4-2z)H^+ + (2x+2y-2z)e \rightarrow Cu_xFe_yS_z + (1-x)Cu^{2+} + (1-y)Fe^{2+} + (2-z)H_2S \qquad (2\text{-}6)$$

which represents a cathodic process when x + y > z. Possible products which fulfill this condition include the copper-iron sulphides bornite (Cu_5FeS_4), haycockite ($Cu_4Fe_5S_8$), mooihoekite ($Cu_9Fe_9S_{16}$) and talnakhite ($Cu_9Fe_8S_{16}$), and the several copper sulphides known to exist in the composition range $Cu_{1.1}S$ to Cu_2S.

Research by Arce and Gonzâlez [19] in sulfuric acid solutions at 298 K using carbon paste electrodes has shown that the reduction product of chalcopyrite is chalcocite and bornite is not the formed intermediary species. Transient products preceding chalcocite formation during chalcopyrite reduction were also characterized in 1.7 M H_2SO_4 using carbon paste electrodes [22]. Several potential intervals could be identified: from $0.115 \geq E_{cat} \geq -0.085$ V vs SHE, an intermediate copper sulfide is formed whose composition is between those of chalcopyrite and bornite, such as talnakhite. The reduction of this product occurs slowly, giving bornite at potentials less than −0.085 V. In the applied potential region $-0.085 \geq E_{cat} > -0.185$ V, the bornite gradually decomposes causing the incomplete conversion to chalcocite. In the potential interval

$-0.185 > E_{cat} \geq -0.285$ V, energetic conditions are large enough to allow the immediate decomposition of bornite, forming chalcocite in a more quantitative manner.

2.1.3 Other Oxidation or Reduction Systems/Methods for Chalcopyrite

In addition to the above-mentioned systems and methods, over the years a host of other innovative copper hydrometallurgical processes and methods have been proposed to improve the dissolution rate of chalcopyrite at moderate temperature and/or pressure. These processes and methods are silver-catalyzed chalcopyrite leaching [70, 71], nano-sized silica as an additive to modify the mineral surface [72], galvanic interactions with manganese dioxide and other sulfide minerals (FeS_2) [28, 73, 74], electro-assisted reduction of chalcopyrite to chalcocite by transient reactive monatomic hydrogen species produced on an aluminum cathode [75], hydrogen peroxide as a stronger oxidant to accelerate the reaction kinetics [76, 77], sodium chloride-sulfate [78-80], pure chloride systems such as ferric chloride or cupric chloride [81-84], ammoniacal solution [85], in-situ generated ferric sulfate solution by a mixture of O_2 and SO_2 [86], perchloric acid [87], acid sodium nitrate [88], alkaline solution [89-92], NaCl solution under differential stress [93], sulfidation of chalcopyrite by gaseous sulfur at moderate temperatures to transform its mineralogy to various simple sulfides (such as CuS and FeS_2) which can be leached more easily than chalcopyrite [94-96].

Details about these proposed ways to treat chalcopyrite and its mechanism to enhance the leaching rate could be found in the cited literature. Any proposal for an economically viable hydrometallurgical process for the treatment of chalcopyrite should take into account basic studies that elucidate the chemical and electrochemical aspects governing leaching.

2.2 Chemical or Electrochemical Reduction of Ferric or Oxygen on Chalcopyrite

2.2.1 Reduction of Ferric or Oxygen on Chalcopyrite

Chemical or electrochemical studies of chalcopyrite have generally placed emphasis on understanding the mechanisms of the oxidative processes or reduction reactions of chalcopyrite. However, the reduction of ferric ions or dissolved molecular oxygen is the most important cathodic process in these systems. Cathodic reduction of ferric ions or dissolved oxygen on $CuFeS_2$ is of great significance since the true leaching rate can be predicted based on the mixed potential theory, i.e., by combining the cathodic and anodic branches of the half-cell reactions. Their position can affect the overall leaching rate of the process. Its kinetics, as is usual with corrosion systems, can be examined by electrochemical techniques.

Four electrochemical processes, anodic oxidation of chalcopyrite itself ($CuFeS_2 \rightarrow Cu^{2+}$ + $Fe2^{+}$ + 2S + $4e^{-}$), anodic oxidation of iron(II) on the corroding chalcopyrite, cathodic reduction of Fe^{3+} or oxygen at the corroding chalcopyrite surface and cathodic reduction of chalcopyrite itself due to the presence of a strong reducing agent, can contribute currents during the leaching of chalcopyrite. Thus, it is important to examine the electrochemistry of each of these processes separately, if possible, to obtain the actual reduction behavior of ferric ions or dissolved molecular oxygen.

Research by Parker et al [25] showed that oxidative dissolution of chalcopyrite is controlled by the formation of an unstable, metal-deficient polysulfide film, which is a semi-conductor, on the chalcopyrite surface. This film slows transport of ions from $CuFeS_2$ to the solution, slows electron transfer to oxidants such as Fe^{3+} and slows the supply of holes to the solid-solution interface. The Fe^{3+}/Fe^{2+} couple, indeed most redox couples, are much less

reversible on corroding chalcopyrite than on pyrite. Values of i_c and i_a on pyrite were always higher than 20 mA/cm^2 but on corroding chalcopyrite, values were often well less than 1 mA/cm^2. The sulfur film that forms on corroding chalcopyrite does not account for the electrochemical or kinetic aspects of chalcopyrite leaching. Faster oxidation of chalcopyrite can be achieved by addition to the solution of fast electron acceptors (Cu^{2+}, I_2, Br_2) under conditions such that a high corrosion potential is achieved. Results from McMillan et al [26] also show that the Fe^{3+}/Fe^{2+} couple is much less reversible on corroding chalcopyrite than the Cu^{2+}/Cu^{+} and I_3^-/I^- redox couples in general. Cu^{2+}/Cu^{+} and I^-/I_3^- species can interact with the chalcopyrite reaction surface to allow facile electron transfer to occur. Fe^{3+}/Fe^{2+} species indeed passivate the surface towards electron transfer.

Tshilombo et al [27] studied the kinetics of the half-reactions involved in the oxidation of $CuFeS_2$ (potential range 0.44-0.84V vs SHE) by potentiodynamic polarization techniques in sulfuric acid. Cathodic characteristics also showed that the passive layers formed at 25℃ and high potentials strongly inhibit ferric reduction on polarized $CuFeS_2$ surfaces. The Tafel slopes for the reduction of ferric ions after polarization of the $CuFeS_2$ surface ranged between 0.15 and 0.22 V/decade. These high values of Tafel slopes clearly indicate that the polysulphide layer inhibits the transport of electrons. It follows that the slow kinetics for the ferric reduction on polarized $CuFeS_2$ surface is a contributing factor for $CuFeS_2$ passivation. Dixon et al have even assumed that it is the cathodic half-cell reaction (i.e. ferric reduction) that limits the overall leaching rate of chalcopyrite in acidic iron sulfate solution [28].

More attention should been paid to these issues in order to obtain detailed information on the characteristics of ferric ion or oxygen reduction on chalcopyrite, such as kinetic and mechanistic data.

2.2.2 Reduction of Ferric or Oxygen on Other Sulfide Minerals/Passive Electrodes

Although very few studies are available about the cathodic reduction of ferric ions and/or oxygen on chalcopyrite, there are some published reports related to the reduction kinetics of ferric or oxygen on other sulfide minerals or electrodes.

2.2.2.1 Pyrite

The dissolution of pyrite is an oxidation-reduction reaction, as the pyrite is oxidized and the Fe^{3+} ions and/or O_2 are reduced on the pyrite surface. Pyrite can be readily dissolved at fairly anodic potentials in sulfuric acid solutions.

The electro-reduction of oxygen was studied at rotating electrodes of pyrite by Biegler [97, 98]. In oxygen-saturated 1 M acid solutions (H_2SO_4, HCl, $HClO_4$), the Tafel slopes and exchange currents were of the order of 130 mV and 10^{-11} A cm^{-2}, respectively. The results at low pH indicated that the first electron transfer step to form O_2^- is rate-determining. At low rotation speeds, linear sweep voltammograms reached a limiting current corresponding to 4-electron reduction of oxygen to water. The dependence of current on rotation speed, potential and surface roughness was analyzed in terms of a mechanism involving kinetic control of peroxide reduction and diffusion control of its escape into the solution bulk. Further study showed that Pyrite specimens from different sources and with different semiconducting properties show some degree of variation in detailed shapes of voltammograms, Tafel slopes and their electrocatalytic activities for oxygen reduction. The kinetic data are shown in Table 2-1. There was no obvious correlation between kinetic parameters for oxygen reduction and the semiconductive nature of the pyrite.

Table 2-1 Kinetic data for oxygen reduction on pyrite electrodes [98].

Sample no.	Electrical type	In 0.1 M $HClO_4$		In 1 M H_2SO_4	
		$-(\partial E/\partial \log i)$/ mV	Current at 0.1 V vs. SCE/μA cm^{-2}	$-(\partial E/\partial \log i)$/ mV	Current at 0.1 V vs. SCE/μA cm^{-2}
1	n-type semi.	121	50	130	41
2	n-type semi.	148	186	117	338
3	n-type metallic	125	46	128	56
4	n-type metallic	135	46	129	71
5	n-type metallic	141	29	131	35
6	p-type semi.	154	51	123	78
7	p-type semi.	145	40	158	73
8	p-type semi.	159	142	118	123

Holmes and Crundwell [99] studied the kinetics of the reduction half-reaction of pyrite in H_2SO_4 in the presence of Fe^{3+} and/or dissolved oxygen. The current density due to oxidation and reduction of dissolved iron at the pyrite surface was described and the measured Tafel slope, given by $2.303RT/(\alpha_{Fe}\ F)$ was close to 0.12 V/decade, which yields a value of 0.51 for α_{Fe}. The current density due to the reduction of oxygen at the pyrite surface was also obtained and the measured Tafel slope was 0.115 V/decade, which gives a value of 0.53 for α_{O2}.

Rimstidt and Vaughan [100] found during the overall oxidation process of pyrite the reaction at the cathodic sites is the rate-determining step for the overall process. The reduction of Fe^{3+} ions and/or O_2 involved in the pyrite dissolution process were investigated by steady-state voltammetry using three pyrite materials in sulfuric acid [101]. Tafel slope and the apparent

transfer coefficient for all of the reactions show that the oxidative dissolution of pyrite and the reduction of Fe^{3+} ions and O_2 were governed by charge transfer processes for all the pyrite samples studied. Pyrite oxidation in chloride solutions (0.5 M HCl+4.5 M NaCl) at 25℃ with cyclic voltammetry [102] indicated the reaction is controlled by the diffusion of ferric ions or electrons through the passive film.

2.2.2.2 Kinetics of Ferric/Ferrous Reaction on Passive Electrodes

Overpotential measurements for the Fe^{3+}/Fe^{2+} couple on passive Ni, Fe, Ti, Fe-Cr alloy and stainless steel were carried out [103-105] and Tafel lines were generally obtained with exchange currents between 10^{-8} and 10^{-5} amp/cm^2. Compared to the oxide-free electrodes (e.g. Pt), the exchange current is substantially smaller on passive electrodes, and the sum of the apparent anodic and cathodic transfer coefficients is significantly less than unity. The main difference in the kinetics (aside from difference of the exchange current) is in the apparent transfer coefficient for the anodic reaction. The results show that a potential drop exists within the passive film. The potential drop across the film increases linearly with the total applied potential. This dependence leads to an apparent transfer coefficient for the anodic reaction that is substantially less than what is expected for the oxidation of Fe^{2+}.

2.3 Rotating Disc Electrode Studies of Chalcopyrite and Other Related Sulfide Minerals under Leaching Conditions

As mentioned in **Section 2.1.1.3**, RDE and RRDE techniques have been used to study the oxidation of chalcopyrite, especially in a potential region that is now called the anodic ‘‘prewave’’ which represents the initial stages of oxidation of chalcopyrite. Besides the anodic

‘‘prewave’’ studies of chalcopyrite, there are some other interesting RDE reports about the leaching of chalcopyrite or other sulfide minerals under leaching conditions [54, 106,107].

Dutrizac et al [54] also studied the dissolution kinetics of chalcopyrite in acidic ferric sulfate solutions from 50℃ to 94℃. To avoid the complications of impurities and an indefinite surface area, they used synthetic chalcopyrite that was pressed into disks. The leaching rate decreased with time, according to a parabolic rate law. This result was attributed to a thickening film of elemental sulfur on the surface, which retarded the reaction. An activation energy of 17.3 kcal/mol (72.38 kJ/mol) was determined. The reaction was found to be independent of pH, rotation speed and ferric concentration above a very low level (0.01 M) but sharply dependent on ferrous concentration. It followed that the rate-determining step was the diffusion of ferrous ions away from the surface (through the S^o film in this case). When the ferric concentration was less than 0.01 M, the leaching rate was probably controlled through a mechanism involving the diffusion of ferric sulfate through the sulfur layer.

Sintered disks of synthetic chalcopyrite were also prepared with known amounts of various sulfide impurities to study the effect of the second phase on the rate of chalcopyrite dissolution [106]. The disks were leached in 0.1 M Fe^{3+}-0.1 M H_2SO_4 solutions at 80℃ and were rotated at 200 rpm. Chalcopyrite-cubanite mixtures behave almost additively; chalcopyrite-bornite mixtures dissolve slightly more rapidly than would be expected from their additive rates. The presence of pyrite, molybdenite or stibnite (which reacts to form pyrite) accelerates the chalcopyrite dissolution rate; the presence of galena retards its dissolution. High-iron sphalerite slightly retards the chalcopyrite dissolution but low-iron sphalerites behave erratically. These results are consistent with a galvanic corrosion mechanism except for the observed effects of molybdenite.

Thomas, using rotating sintered disks of synthetic chalcocite, found that the dissolution rate was linearly dependent on ferric up to about 0.1 M (at 95 rpm and 25℃), and then appeared to level off somewhat [107]. A similar dependence of dissolution rate upon rotation speed was found. These findings, together with an activation energy of 5 kcal/mol (20.92 kJ/mol), were taken as an indication of a process controlled by mass transport of reagents across the boundary layer.

2.4 Electrochemical Impedance Spectroscopy Studies of Chalcopyrite

The chalcopyrite electrode/electrolyte interface can be studied by EIS, in order to obtain more insight into the leaching process. Very few papers related to the dissolution of chalcopyrite electrodes have been published

2.4.1 Sulfuric Acid

Ghahremaninezhad et al [16] explored the dissolution of a massive chalcopyrite electrode in 0.5 M sulfuric acid at 25℃ by means of potentiodynamic, EIS and Mott-Schottky techniques. EIS studies at open circuit potential (around 415 mV vs SHE) proved the existence of a thin surface layer on the electrode. Different equivalent electrochemical circuits were modeled and compared to experimental results to support the proposed sequence of chalcopyrite dissolution and surface layer formation at different potential regions.

A study by Hiroyoshi et al [17] shows that active-passive behavior occurs only when cupric and ferrous ions coexist, based on anodic polarization curves in 0.1 kmol m^{-3} sulfuric acid with stirring at 298 K in nitrogen. The current in the active region (at potentials lower than about 0.65V vs SHE) was larger than the current observed without cupric and/or ferrous ions, indicating that the coexistence of these ions (0.1 kmol m^{-3}) causes activation rather than

passivation. AC impedance spectra indicated that a high-resistance passive layer grows on the chalcopyrite surface without cupric and/or ferrous ions, and that coexistence of these ions causes the formation of another product layer and inhibits the passive layer growth in the active region. A reaction model, assuming the formation of intermediate Cu_2S in the active region, was suggested to account for the active-passive behavior of chalcopyrite.

2.4.2 Alkaline Solution

EIS results in an alkaline solution [90] for different oxidation potentials reveal the oxidation of chalcopyrite produces a modification of the electrode surface: for values lower than 0.64 V vs SHE a Randles equivalent circuit can be used, but the Nyquist plots present a change when the applied potential is higher than 0.64 V vs SHE and a surface layer model must be used. This change gives rise to a modification of the charge transfer resistance and the diffusion coefficient of charge carriers across the interlayer electrode/electrolyte resistance. This behaviour was attributed to the initial formation of a layer of Fe_2O_3 and an inner layer of CuO and Fe_2O_3, which conferred an irregular and non-homogeneous surface to the electrode.

2.4.3 Sulfuric Acid plus Iron Sulfate

The corrosion rate of chalcopyrite was studied at various temperatures (25℃-65℃) and concentrations of acid in sulfuric acid containing only 5 g/L ferric (no ferrous) using EIS. The corrosion rate increased with temperature and decreased with the acid concentration [60].

EIS has also been used to investigate the influence of the ferric-ferrous couple on a passivated chalcopyrite electrode in sulfuric acid at 25℃ [108]. In the presence of the ferric-ferrous couple, the double-layer resistance, as a characteristic quantity for the charge transfer step of an electrochemical reaction which indicates its inherent speed, shows a large decrease. It was found that ferric reduction on chalcopyrite is faster than the chalcopyrite oxidation reaction

itself. This result indicates the electronic conduction of the passive film is relatively high, and the passive dissolution of chalcopyrite is mass transport controlled by the passive film, which is consistent with the above-mentioned studies from McMillan et al [26].

2.5 High Temperature Electrochemistry of Chalcopyrite Electrode and Ferric/Oxygen Reduction Reaction

Many of the proposed leaching processes for chalcopyrite are operated under pressure oxidation conditions, primarily because fast leaching kinetics can be achieved at the elevated temperatures employed in an autoclave. However, although a large number of important studies have been carried out to understand the mechanisms involved and the key parameters that limit the leaching kinetics, and lots of publications have suggested the electrochemical nature of the oxidation leaching process, except for the very few results reported by Jones and Lázaro [46, 109,110], the majority are limited to low temperatures below 90℃.

According to recent reviews about the high temperature and high pressure (HTHP) electrochemical studies [111, 112], although in recent years significant developments have been made, HTHP electrochemistry remains a relatively unexplored field of research and the relative lack of experimental data is ascribed to the various technical obstacles. In the case of mineral electrochemistry, the major drawback seems to be the mineral electrode preparation and reproducibility of results, which are highly dependent on the nature of the mineral. Furthermore, there are only a few reports of mineral electrochemistry at high temperature and pressure [113].

2.5.1 Sulfuric Acid

Anodic oxidation studies by Jones and Peters [109] using potentiostatic polarization in 0.1M $HClO_4$ or H_2SO_4 solutions at temperatures from 7℃ to 175℃ show that at low

temperatures (up to about 85℃) the polarization curves in the two acids are very similar but at higher temperatures the reactivity of chalcopyrite suddenly drops in H_2SO_4, whereas in $HClO_4$ it continues to increase steadily with temperature. The current obtained at low potentials (up to around 800 mV vs SHE) is time-dependent whereas it is time-independent at the higher potentials. The time dependence of the current in the low current region is indicative of a rate-controlling diffusion process, such as metals out to the surface, and in the high current region where the current is time-independent it is possible that the formation of holes is rate-determining.

Jones [46] reported that for chalcopyrite leaching in ferric sulfate solutions from 20℃ to 175℃ an electrochemical mechanism is operative. Mixed potential measurements at 90℃ indicate that the reaction is under mixed control, and that both anodic and cathodic reactions are quite irreversible, according to the relative position of the mixed potential, the Nernst potentials of the anodic and cathodic reactions having been calculated with some simple assumptions. Small additions, up to 0.05 M ferrous in a 0.2 M H_2SO_4+1 M $Fe_2(SO_4)_3$ at 90℃ had little effect, but thereafter a substantial drop in mixed potential was observed. The mixed potential of chalcopyrite is responsive to ferric and ferrous concentration in sulfate solutions.

Lázaro and Jeffrey reported a study of the pressure acid leaching of chalcopyrite using a chalcopyrite rotating disc electrode at 150℃ in a 0.2 M H_2SO_4 solution containing ferric or oxygen [110]. All the potentials measured by a platinum electrode were always higher than those obtained using a chalcopyrite electrode under the same conditions. It is interesting to note that either with platinum or chalcopyrite, the potential of an acid solution in the presence of O_2 is lower than that of a platinum electrode in a 0.1 M iron(III) solution. Even though there is Fe^{2+} being produced through reduction of Fe^{3+} and oxidation of $CuFeS_2$, it is not a high enough

concentration to produce a significant change in potential during the measurement time of the experiment. Mixed potential measurements and anodic behavior of chalcopyrite at 150℃ indicate that pressure acid leaching in a solution containing 0.1 M iron(III) will occur quite rapidly. In comparison, when using 120 psi partial pressure of oxygen, the mixed potential is in the so-called "prewave" region, and hence slow leaching would be expected.

2.5.2 Reduction of Ferric or Oxygen on Other Electrodes at High Temperatures

Apart from those directly relevant to chalcopyrite, there are other interesting HTHP reports relating to ferric or oxygen reduction. Clouser et al [114] investigated the temperature dependence of Tafel slope and apparent transfer coefficient for oxygen reduction on platinum by RDE in concentrated H_3PO_4 over a wide range of temperatures (25-250℃). The observed Tafel slopes were essentially independent of temperature over the 25-250℃ range, and were quite different from the values expected from theory. The apparent transfer coefficient for the oxygen reduction has been found to be approximately proportional to temperature rather than independent of temperature. Cathodic reduction of oxygen was also studied on gold [113] in ammonium chloride solutions by RDE over the temperature range of 30-150℃. The rate of oxygen reduction increases with increasing temperature and pressure. Electrochemical studies by Liu and Nicol [115] demonstrated that the effective oxidant for gold pressure leaching using Au-RDE in acidic sulfate solution containing various concentrations of chloride ions is ferric and not dissolved oxygen. The equilibrium solubility of gold increases with increasing temperature, chloride concentration and iron(III)/iron(II) ratio. The role of oxygen was largely confined to that of maintaining a high ratio of Fe(III) to Fe(II).

2.6 Summary

Obviously, based on this literature review, most of the published papers are about the above-noted oxidation of chalcopyrite and cathodic reduction of chalcopyrite itself. Even within these studies, most are under a single low temperature and in a discrete range of solution concentration, and it is difficult to compare among the studies.

In addition, the cathodic reduction kinetics of ferric and oxygen on chalcopyrite has hardly been studied, and research on RDE, EIS, as well as high temperature electrochemistry of chalcopyrite and ferric/oxygen reduction on minerals is almost non-existent, not to mention a comprehensive study and comparison of reduction kinetics at different temperatures.

3 Objectives

The overall objective of this investigation is to determine chalcopyrite leaching mechanisms in acidic iron sulfate solutions-by far the most adopted leaching media.

Although various methods and systems have been used to investigate chalcopyrite leaching, most of the published literature has placed emphasis on understanding the mechanisms of the oxidative processes or reduction reactions of chalcopyrite itself at low temperatures, and very few data are available about the reduction processes in leaching systems. However, the cathodic reduction of ferric ions on $CuFeS_2$ is also of great significance because actual reduction behavior of ferric ions is vital to obtain the true leaching rate.

In view of the preceding discussion, the specific objectives of this thesis are set out as follows:

(1) Develop a thermodynamic model to simulate the speciation of the quaternary H_2SO_4-$Fe_2(SO_4)_3$-$FeSO_4$-H_2O solutions in order to quantify the concentrations of the main species (including Fe^{3+} and Fe^{2+}) in the solution from 25 ℃ to 150 ℃.

(2) Develop an expression to predict the redox potentials of the Fe^{3+}/Fe^{2+} couple in the above-noted solutions under different temperatures, via Nernst equation based on the concentrations of free ferric and ferrous ions determined by the speciation results. The results will also indicate how the real Fe^{3+}/Fe^{2+} ratios will change with temperature.

(3) Investigate the reduction kinetics of ferric ion on chalcopyrite by cathodic potentiodynamic polarization at elevated temperatures relevant to existing industrial processes, in order to determine temperature dependence of kinetics parameters such as exchange current density, transfer coefficient and rate constant. These parameters can be useful quantities for determining the mechanism of an electrochemical reaction. The free ferric ion concentration

previously obtained from the speciation results of the thermodynamic model, together with the calculated redox potentials of the Fe^{3+}/Fe^{2+} couple, will be employed to analyze the electrochemical experimental curves and so as to obtain the kinetic parameters.

(4) Based on the obtained reversible potentials of the Fe^{3+}/Fe^{2+} couple (calculated from the speciation results) and the measured mixed potentials, as well as the calculated reversible potentials of possible anodic reactions, the mechanism involved in the chalcopyrite leaching system are further analyzed by mixed potential theory to obtain detailed information about which of the cathodic or anodic reactions may, in principle, govern the overall reaction rate [23, 24, 46-50]. The analysis of control scenario for the electrochemical processes involved can also be used to clarify to what extent the cathodic reaction can influence the overall leaching reaction.

For the first time, to the author's knowledge, a reliable thermodynamic model is developed to simulate the speciation of the quaternary H_2SO_4–$Fe_2(SO_4)_3$–$FeSO_4$–H_2O system through a wide range of solution compositions and temperatures (25 ℃-150 ℃), and is used to propose a novel equation to predict the redox potential of the ferric/ferrous couple; the kinetics of ferric ion reduction on chalcopyrite was quantified and its influence on the leaching was determined over a wide range of temperature. The findings of the present thesis are an original contribution to the current knowledge of chalcopyrite leaching in acidic iron sulfate media.

4 Methodology and Experimental Procedure

4.1 Measurement of the Redox Potential of the Quaternary Acidic Iron Sulfate System from 25 ℃ to 150 ℃

Experimental work to measure the redox potential of the quaternary acidic iron sulfate system was carried out at temperatures ranging from 25 ℃ to 150 ℃.

4.1.1 Electrode Preparation

According to several publications on the redox behavior of the ferric-ferrous couple in H_2SO_4 on Pt [116-118], the kinetic parameters such as exchange current density (about 1.1 A/cm^2) and rate constant (10^{-2}-10^{-3} cm/s), are relatively large at or near room temperature. The reaction can be considered reversible or highly quasi-reversible according to the literature [119]. In addition, one would expect kinetics to increase with temperature thus preserving the reversibility of the reaction. For this reason Pt has been widely employed for the measurement of reversible potentials in the H_2SO_4-$Fe_2(SO_4)_3$-$FeSO_4$-H_2O system over a wide range of temperatures, such as room temperature [30, 31, 53, 69], 78 ℃ [55], 90 ℃ [33], and 150 ℃ [110].

The platinum wire used in this investigation for the redox potential measurement was purchased from Sigma-Aldrich. The diameter was 0.5 mm and it had a purity of 99.9% (mass percentage). The electrical contact between the Pt electrode and a copper wire lead (enameled copper wire was used for the experiments in the autoclave) was made with silver conductive epoxy (MG Chemicals) for the experiments conducted at or below 90 ℃ and Silvertech PT-1 Silver-filled Epoxy (Materion Corporation) for the experiments performed in the autoclave. The whole assembly was protected from the solution by mounting it in epoxy resins (832HT-375ML from MG Chemicals) along with an appropriate fitting, leaving only one part of the platinum

electrode exposed to the solution. Before each test, the Pt working electrode was activated in a 0.1M H_2SO_4 solution according to a published method [120].

4.1.2 Electrolyte Preparation

In the present study, the overall composition of the solutions was determined based on the operating conditions described for the above-mentioned industrial leaching chalcopyrite processes. The largest ferric concentration was limited to 0.18 mol/kg, because much of the dissolved ferric could precipitate in the quaternary system, especially at higher temperatures.

Deionized water, sulfuric acid (H_2SO_4, 95.0-98.0%, Fisher Scientific Canada), Iron(III) sulfate pentahydrate ($Fe_2(SO_4)_3$•$5H_2O$, 97%, Acros), Iron (II) sulfate heptahydrate ($FeSO_4$•$7H_2O$, 99+% for analysis ACS, Acros) were used to prepare the desired electrolyte. Prior to each test, fresh solution was prepared, with the concentration of H_2SO_4 and ferric ion being 0.31 mol/kg and 0.18 mol/kg, respectively. The ferrous ion concentration was set by the various nominal molar ratios of ferric to ferrous (1:1, 10:1, 100:1, 1000:1). The solution was prepared by first dissolving 16.80 mL H_2SO_4 (transferred by pipette) in deionized water. Then, 45.22g $Fe_2(SO_4)_3$•$5H_2O$ and the corresponding amount of $FeSO_4$•$7H_2O$ were balanced and dissolved in the sulfuric acid solution.

The choice of the particular sulfuric acid concentration is due to the fact that it is an appropriate concentration for chalcopyrite leaching and is widely used in industrial leaching processes. Please note that typically the initial sulfuric acid concentration employed in the previously mentioned industrial leaching processes is in the range of 5-60 g/L. Depending on the operating temperature and leaching products (elemental sulfur or sulfate), acid can be consumed or produced due to the ferric hydrolysis reaction. Also, at 150 ℃, a relatively lower acid concentration can facilitate the formation of Fe_2O_3, which is the preferred iron precipitate.

Furthermore, at low temperatures (≤110°C), such a concentration results in an initial pH lower than 2, which prevents iron precipitation from taking place in the systems considered in this work.

According to Dutrizac (1980) [121], there may be small colloidal particles generated (which are associated with the formation of small iron polymers generated by iron hydroxyl complexes). However, in the present studied solutions, the pH is typically lower than 1 for all conditions (as shown in **Section 5.3.4.3**), which does not facilitate the formation of iron hydroxyl complexes and iron hydroxides. Even if formed, thermodynamically these polymers or colloids should eventually transform to stable precipitates such as FeOOH and Fe_2O_3. Therefore, we believe that there should be little or no influence exerted by the formation of colloids on the speciation model in the present work.

4.1.3 Electrochemical Measurements at 25 ℃, 70 ℃ and 90 ℃

Electrochemical experiments were carried out using a standard three-electrode cell with a thermostated water jacket. The counter electrode (CE) was graphite and the prepared Pt electrode served as the working electrode (WE). A saturated Ag/AgCl electrode (saturated with KCl, Accumet* Glass Body, Fisher Scientific) was used as a reference electrode (RE). All potentials have been converted from Ag/AgCl to the standard hydrogen electrode (SHE). All further potentials in this study are quoted with respect to the SHE at 25 ℃ unless otherwise stated. Details of the corrections used for the measured potential are discussed below. The RE was connected to a Luggin capillary to minimize IR drop. The cell solution was slowly heated to the predetermined temperature by the circulating water from a Cole-Parmer Polystat Heated Circulating Bath with Analog Control, and kept at the constant temperature with an accuracy

±1 ℃. Prior to use, the CE was immersed in ethanol for degreasing, rinsed with deionized water, and finally dried with cool air.

The test solution was deaerated by sparging high-purity N_2 prior to- and throughout the electrochemical experiments at a constant flow rate to eliminate the effect of dissolved oxygen. This was done to ensure that no confounding effects from dissolved oxygen existed. The cell off-gas, after passing through an Allihn condenser, was passed through deionized water and finally discharged to a fumehood. The open circuit potentials (OCP) of the samples were recorded to yield a steady-state potential (as the redox potential).

Electrochemical measurements were performed using a Potentiostat/Galvanostat VersaSTAT 3F Electrochemical System with an optional frequency response analyzer contained in a single unit, controlled by the VersaStudio electrochemistry software package (Princeton Applied Research).

4.1.4 Electrochemical Measurements at 110 ℃ and 150 ℃

A 5100 low pressure reactor from the Parr Instrument Company, with a 600 mL glass cylinder and 4848 reactor controller, was used for the electrochemical experiments at 110 ℃ and 150 ℃. A Pt-Nb electrode from Cortest Inc. was used as a CE and the prepared Pt electrode was used as the WE. The Pt-Nb electrode is relatively inert and can be used for high temperature high pressure electrochemistry experiments because Nb oxides are extremely insoluble in most conditions and actually thicken under polarization. This electrode was used for convenience. An external pressure balanced Ag/AgCl RE (EPBRE) with a double-porous junction filled with 0.1 mol/kg KCl (Cortest Inc.) was used and it was maintained at room temperature. All potentials measured against Cortest's external Ag/AgCl electrode filled with 0.1 mol/kg KCl have been converted to the SHE at 25 ℃, as shown in the following section. The cooling loops and the

magnetic drives were removed from the three port holes in the head of the 5100 Reactor in order to provide the space necessary for the WE, CE and RE, which were installed in the head by Swagelok 316 stainless steel fittings.

Prior to use, the CE was immersed in ethanol for degreasing, rinsed with deionized water, and finally dried with cool air. The test solution was deaerated by sparging high-purity N_2 prior to the electrochemical experiments at a constant flow rate for 40 min to eliminate the effect of dissolved oxygen. The autoclave was then heated to 110℃ or 150℃. The OCP of the samples were recorded until a steady-state potential was achieved. The external RE used is a commercial high temperature high pressure (HTHP) reference electrode. Such electrodes have been widely used for potential measurements in a significant number of HTHP electrochemical experiments [122-124]. Very stable potentials were achieved during the experiments and no drift was found within the experimental duration (typically one experiment lasted about 2 hours). The OCP experiments for redox potential took approximately 15 minutes. In general, the redox potential measurements were very stable and their values varied to within ±3mV. The potential drift resulting from thermal diffusion (the Soret effect) can be neglected for this kind of RE [125].

The double junction design of the EPBRE can effectively prevent the contamination of the internal reference solution. Herein a brief explanation of the RE is provided for clarity. Figure 4-1 shows the schematic diagram of the EPBRE (Also shown in appendix A, Figure A-5). In this design, the Ag/AgCl electrode itself is maintained at ambient temperature and communication with the high temperature zone is made via a non-isothermal electrolyte bridge. So, there is a temperature gradient along the bridge between the Ag/AgCl RE outside the autoclave and the high temperature zone at the operating temperature inside the autoclave. As demonstrated in the cited literature (see in the following section for the potential correction part), the potential drop

resulting from such a temperature difference (including the thermo-electrical effects in the metallic components, temperature influence on the electrochemical half-cell potentials, thermal liquid junction potential and the concentrations changes by thermal diffusion of the solute along the temperature gradient), is discussed in detail. Based on some reasonable assumptions, such as neglecting the thermo-electrical effects in the metallic components and the Soret effect, the influence of the temperature gradient on the measured potential is thus included in the term $E_{\text{correction}}$ in Eq. (4-1) as shown in the following section.

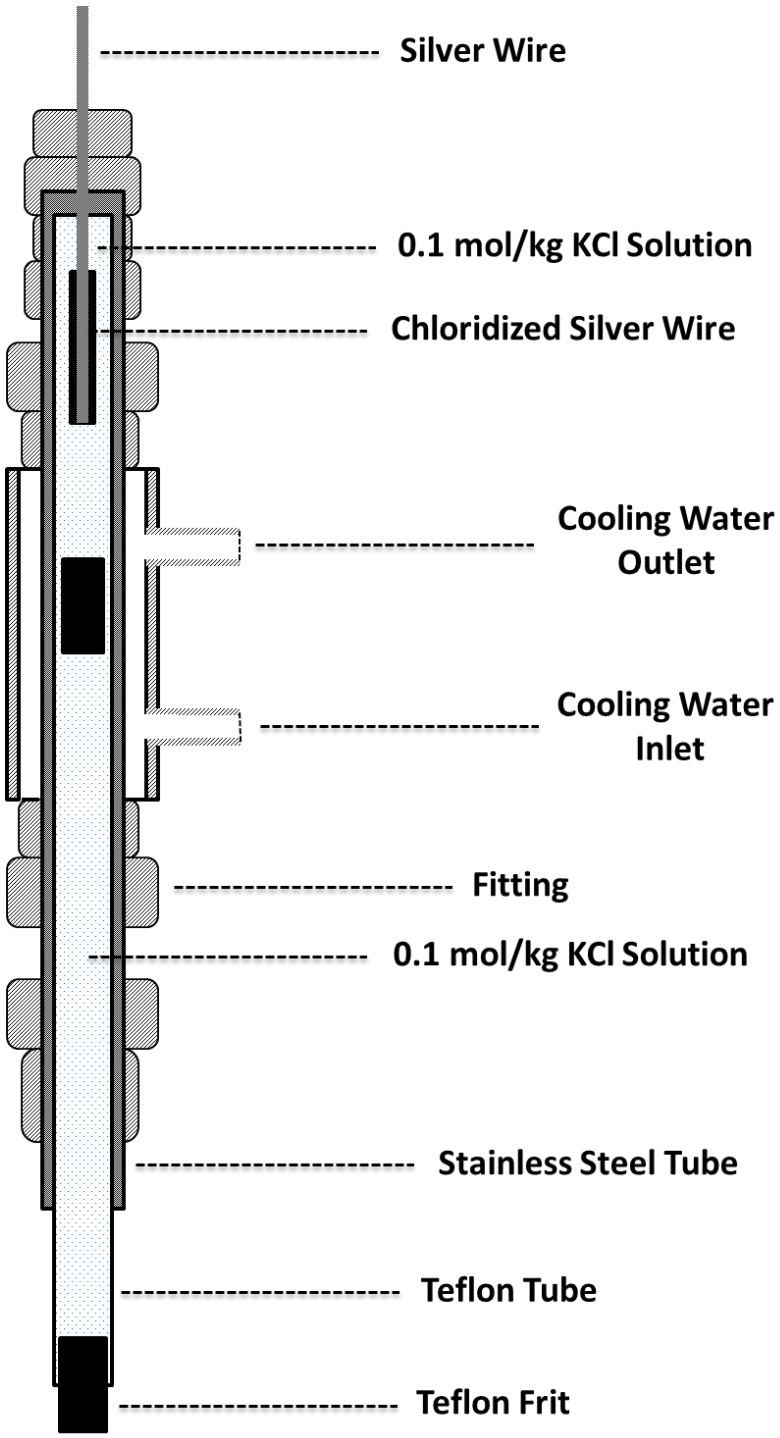

Figure 4-1 Schematic diagram of Ag/AgCl external pressure balanced reference electrode with double porous junction.

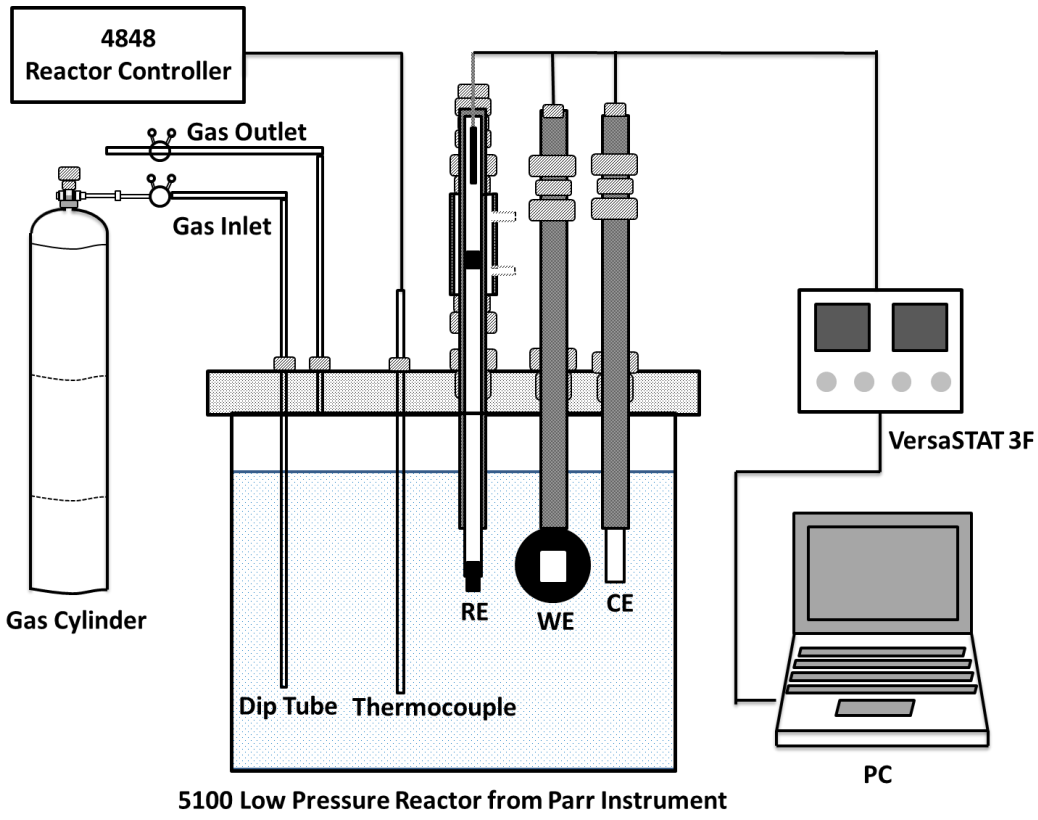

Figure 4-2 Schematic diagram of the apparatus for high temperature high pressure electrochemical tests by using the EPBRE.

Figure 4-2 is a detailed schematic diagram of the setup used in this study. All the experiments were carried out in a high temperature high pressure autoclave (Please see appendix A, Figures A-1 to A-5).

4.1.5 Correction of the Measured Potentials to SHE at 25 ℃

In the present study, it is assumed that the SHE potential is a function of temperature and is zero only at 25 ℃ (Traditionally, the SHE potential is 0 at any temperature by definition). All of the potentials reported herein are thus with respect to the SHE at 25 ℃. We prefer this definition

as the SHE is not in fact 0 at elevated temperature (a potential can be measured between a SHE at 25 ℃ and one at 100 ℃, for example).

At 110 ℃ and 150 ℃, all electrode potentials have been converted to SHE at a particular temperature according to the following relationship [125-127]:

$$E_{SHE}\,(T) = E_{obs} + E_{correction} = E_{obs} + E_{Ag/AgCl}\,(T) - \Delta E_{th} \quad (4\text{-}1)$$

where E_{SHE} (T) is the potential of a WE in the autoclave versus the SHE at the operating temperature T; E_{obs} is the observed potential of a WE in the autoclave versus the external Ag/AgCl RE filled with 0.1 mol/kg KCl; $E_{correction}$ is a potential correction value; $E_{Ag/AgCl}$ (T) is the isothermal potential of the Ag/AgCl electrode versus the SHE at the operating temperature T; ΔE_{th} is the measured potential difference of the thermal cell between an internal and an external RE connected by a cooled salt bridge.

The E_{SHE} (T) was further corrected and referred to the SHE at 25 ℃ by the following equation:

$$E_{SHE}\,(25\,℃) = E_{SHE}\,(T) + \Delta E_{SHE} \quad (4\text{-}2)$$

where E_{SHE} (25°C) is the potential with respect to a SHE at 25°C; ΔE_{SHE} is the potential difference of the SHE thermal cell at T and 25°C. ΔE_{SHE} data were computed by applying the above-mentioned Criss-Cobble method, with the values being 43.9 mV at 110 ℃ and 54.2 mV at 150 ℃.

Details about the conversion of the measured potentials to the two SHE scales can be found in Ref. [125-127]. As an example of the correction for the experiments in the autoclave, when measuring the redox potential of the Fe(II)-Fe(III)-H_2SO_4 solutions at [H_2SO_4] = 0.31 mol/kg and [Fe^{3+}]total = 0.18 mol/kg with the nominal Fe^{3+}/Fe^{2+} ratio of 10:1 at 110 ℃, the E_{obs} = 515.57 mV and $E_{correction}$ = 209 mV as published in Ref. [125], and hence E_{SHE} (T) = 724.57

mV at 110 ℃ according to Eq. (4-1). Then, by using Eq. (4-2), with ΔE_{SHE} being 43.9 mV at 110 ℃, the E_{SHE} (25 ℃) at 110 ℃ is 768.47 mV with respect to a SHE at 25 ℃.

A similar method was employed to convert the potentials measured using the Ag/AgCl electrode (saturated with KCl) at 70 ℃ and 90 ℃ to the SHE at 25 ℃. At these two temperatures, the $E_{Ag/AgCl}$ (T) was obtained from the literature [128]. Since ΔE_{th} values are highly related to temperature difference and relatively independent of different chloride-containing alkaline and neutral solutions with various concentrations, as reported by Bosch et al (2003) [125], ΔE_{th} was determined by the data published in the literature for 0.1 mol/kg KCl solution, with the values of about 15 mV at 70 ℃ and 20 mV at 90 ℃, respectively. This assumption is reasonable and it was verified by measuring the potential for an acid iron sulfate solution with the Cortest external Ag/AgCl RE filled with 0.1 mol/kg KCl. ΔE_{SHE} was also calculated, with a value of 26.7 mV at 70 ℃ and 36.1 mV at 90 ℃. It should be noted that the thermodynamic data of H_2 used to calculate the ΔE_{SHE} were obtained from the literature [129,130].

As an example of correction for the tests at 70 ℃ and 90 ℃, when measuring the redox potential of the Fe(II)-Fe(III)-H_2SO_4 solutions at [H_2SO_4] = 0.31 mol/kg and [Fe^{3+}]total = 0.18 mol/kg with the nominal Fe^{3+}/Fe^{2+} ratio of 100:1 at 70 ℃, the E_{obs} = 671.4 mV, $E_{Ag/AgCl}$ (T) = 148.8 mV as published in Ref. [128] and ΔE_{th} = 15 mV, and hence E_{SHE} (T) = 805.2 mV at 70 ℃ according to Eq. (4-1). Then, by using Eq. (4-2), with ΔE_{SHE} being 26.7 mV at 70 ℃, the E_{SHE} (25 ℃) at 70 ℃ is 831.9 mV with respect to a SHE at 25 ℃.

The diffusion potential between the test solution and the internal KCl solution in the reference electrode (also known as the isothermal liquid junction potential), can be evaluated by Henderson's equation for dilute solutions [119] or Harper's method for more concentrated systems [131]. However, insufficient data are available on the properties (transport number or

ionic mobility) of dissolved species included in the present model to accurately predict the liquid junction potentials. In addition, calculations for similar systems (KCl solution in contact with sulfate solution) indicate that the isothermal liquid junction potentials at room temperature are very small, typically no more than several mV [132, 133]. Therefore, it is believed that this potential probably plays a minor role and it was ignored in the calculations in the present work. This assumption is approximately correct, because the experimental results in this work were in good agreement with those calculated by the developed thermodynamic model.

4.2 Measurement of the Cathodic Potentiodynamic Polarization Curves

Experimental work to study reduction kinetics of ferric on chalcopyrite in the quaternary acidic iron sulfate system was carried out at temperatures ranging from 25 to 150 ℃.

4.2.1 Electrode Preparation

The chalcopyrite used in this investigation was obtained as massive mineral samples from the Creighton Mine (Sudbury, Ontario). The quantitative phase analysis of the chalcopyrite ore was determined using the Rietveld method and X-ray powder diffraction data, and the result is shown in Table 4-1. The material is of high quality, with a purity of 97.5% (mass percentage) and few impurities. To gather this data, the sample was reduced to fine powder to the optimum grain-size range for X-ray analysis (< 10 μm) by grinding in ethanol in a vibratory McCrone Micronising Mill for 7 minutes. Step-scan X-ray powder-diffraction data were collected over a range 3-80 °2θ with CoKa radiation on a Bruker D8 Focus Bragg-Brentano diffractometer equipped with an Fe monochromator foil, 0.6 mm (0.3 °) divergence slit, incident- and diffracted-beam Soller slits and a LynxEye detector. The long fine-focus Co X-ray tube was operated at 35 kV and 40 mA, using a take-off angle of 6 °. The X-ray diffractogram was analyzed using the

International Centre for Diffraction Database PDF-4 and Search-Match software by Siemens (Bruker). X-ray powder-diffraction data of the sample were refined with Rietveld program Topas 4.2 (Bruker AXS).

Further analysis results of the ore by multi-element ICP (4 acid digestion, 30 package) and Au analysis (fire assay) are shown in Table 4-2. Please note that the ICP analysis's focus is on the Ag and Au contents, and that the Cu and Fe amount were above the detection limit and therefore unreliable.

Massive electrodes were prepared by cutting the bulk chalcopyrite into approximately cubic shaped pieces with an area of 1 cm^2 exposed to the solution. The electrical contact between a copper wire (enameled copper wire was used for the experiments in the autoclave) and the sample was made at the back of the sample with silver conductive epoxy (MG Chemicals) for the experiments at or below 90 ℃ and Silvertech PT-1 Silver-filled Epoxy (Materion Corporation) for the experiments performed in the autoclave. The whole assembly was protected from the solution by mounting it in epoxy resins (Cold Cure for 25 ℃, 832HT-375ML from MG Chemicals for 70-110 ℃, Duralco 4460 from Cotronics for 150 ℃) along with an appropriate fitting, leaving only one face of the electrode exposed to the solution. Before each test, working electrodes were mechanically polished with no. 1200 SiC paper (LECO) so as to begin each experiment with a fresh surface. The surface was examined under an Optical Microscope (OM) before each experiment to verify that no inclusion/significant cracks or voids existed.

Table 4-1 Results of quantitative phase analysis of the chalcopyrite used in this study (wt.%).

Mineral	Ideal Formula	Sample "Chalcopyrite"
Chalcopyrite	$CuFeS_2$	97.5
Pyrrhotite	$Fe_{1-x}S$	1.7
Mackinawite ?	Fe_9S_8	0.8
Total		100.0

Table 4-2 Chemical analysis (ICP-OES, 4 Acid Digestion) and Au analysis (Fire Assay). Results for elements with concentrations lower than 10 ppm are not presented.

Method	FA	ICPM	ICPM	ICPM	ICPM	ICPM	ICPM	ICPM	ICPM	ICPM	ICPM
Element	Au	Ag	Cd	Co	Cu	Fe	Mn	Ni	Pb	Sb	Zn
Unit	g/mt	ppm	ppm	ppm	%	%	ppm	ppm	ppm	ppm	ppm
Sample	0.88-2.49	77.3-78.3	100.5-106.5	14-40	28-29	22.6-23.36	65-193	16-535	396-442	10-16	2036-2223

4.2.2 Electrolyte Preparation

The electrolyte used in this section is the same as that of **Section 4.1.2.**

4.2.3 Electrochemical Measurements at 25 ℃, 70 ℃ and 90 ℃

Electrochemical experiments were carried out using a standard three-electrode cell with a thermostated water jacket. The counter electrode (CE) was graphite and the prepared chalcopyrite electrode served as the working electrode (WE). A saturated mercury/mercury (I) sulfate electrode (MSE, saturated with potassium sulfate, London Scientifics) was used as a reference electrode (RE) for the tests at 25 ℃. At 70 ℃ and 90 ℃, a saturated Ag/AgCl electrode (saturated with KCl, Accumet* Glass Body, Fisher Scientific) was employed as a RE. All potentials have been converted to the standard hydrogen electrode (SHE). All further potentials in this study are quoted with respect to the SHE at 25 ℃ unless otherwise stated. Details of the corrections used for the measured potential have been discussed previously. The RE was connected to a Luggin capillary to minimize IR drop. The cell solution was slowly heated to the predetermined temperature by circulating water from a Cole-Parmer Polystat Heated Circulating Bath with analog control, and kept at the constant temperature with an accuracy ±1 ℃.

Prior to use, the WE and CE were immersed in ethanol for degreasing, rinsed with deionized water, and finally dried with cool air. The WE was immersed in the solution for around 30 minutes to stabilize the potential before starting the measurements in order to ensure reproducibility. The test solution was deaerated by sparging high-purity N_2 prior to- and throughout the electrochemical experiments at a constant flow rate to eliminate the effect of dissolved oxygen. The cell off-gas, after passing through an Allihn condenser, was passed through deionized water and finally discharged to a fumehood. The open circuit potentials (OCP) of the samples were first recorded for 30 min to yield a steady-state potential, and then the

cathodic potentiodynamic polarization curves (CPC) were obtained by changing the electrode potential from OCP to -700 mV (versus OCP) at a scanning rate of 0.5 mV/s.

The exchange current density, i_0, was obtained from the curves using the intersection of the cathodic linear extrapolation and the reversible potential of the ferric/ferrous couple.

4.2.4 Electrochemical Measurements at 110 ℃ and 150 ℃

The experimental setup is similar to that used for the redox potential measurements, as shown in **Section4.1.4**. The difference is that the prepared chalcopyrite electrode was used as the WE in this section.

Prior to use, the WE and CE were immersed in ethanol for degreasing, rinsed with deionized water, and finally dried with cool air. The test solution was deaerated by sparging high-purity N_2 prior to the electrochemical experiments at a constant flow rate for 40 min to eliminate the effect of dissolved oxygen. The autoclave was then heated to 110 ℃ or 150 ℃. The OCP of the samples were recorded when a steady-state potential was achieved, and then CPC tests were performed in the same way as those at 25-90 ℃.

4.2.5 Correction of the Measured Potentials to SHE at 25 ℃

The correction method used in this section is the same as that of **Section 4.1.5**.

4.3 Scanning Electron Microscope Study

The surface morphology and elemental composition of the prepared chalcopyrite electrode was examined via a scanning electron microscope (SEM, Hitachi S-2300) coupled with EDX (Silicon Lithium Detector from Advanced Analysis Technologies).

As clearly shown in Figure 4-3, the surface distribution of S, Fe and Cu elements are quite uniform for the chalcopyrite electrode prepared in the present study. In Figure 4-4, it is shown

that the electrode sample displays a strong peak for sulfur, and relatively weak peaks of iron and copper. Table 4-3 presents the elemental components of the electrode sample clearly (the raw data was from the EDX data as shown in Figure 4-4). It should be noted that EDX only measures elemental concentrations near the surface of the electrode and therefore does not constitute a true chemical analysis of the mineral.

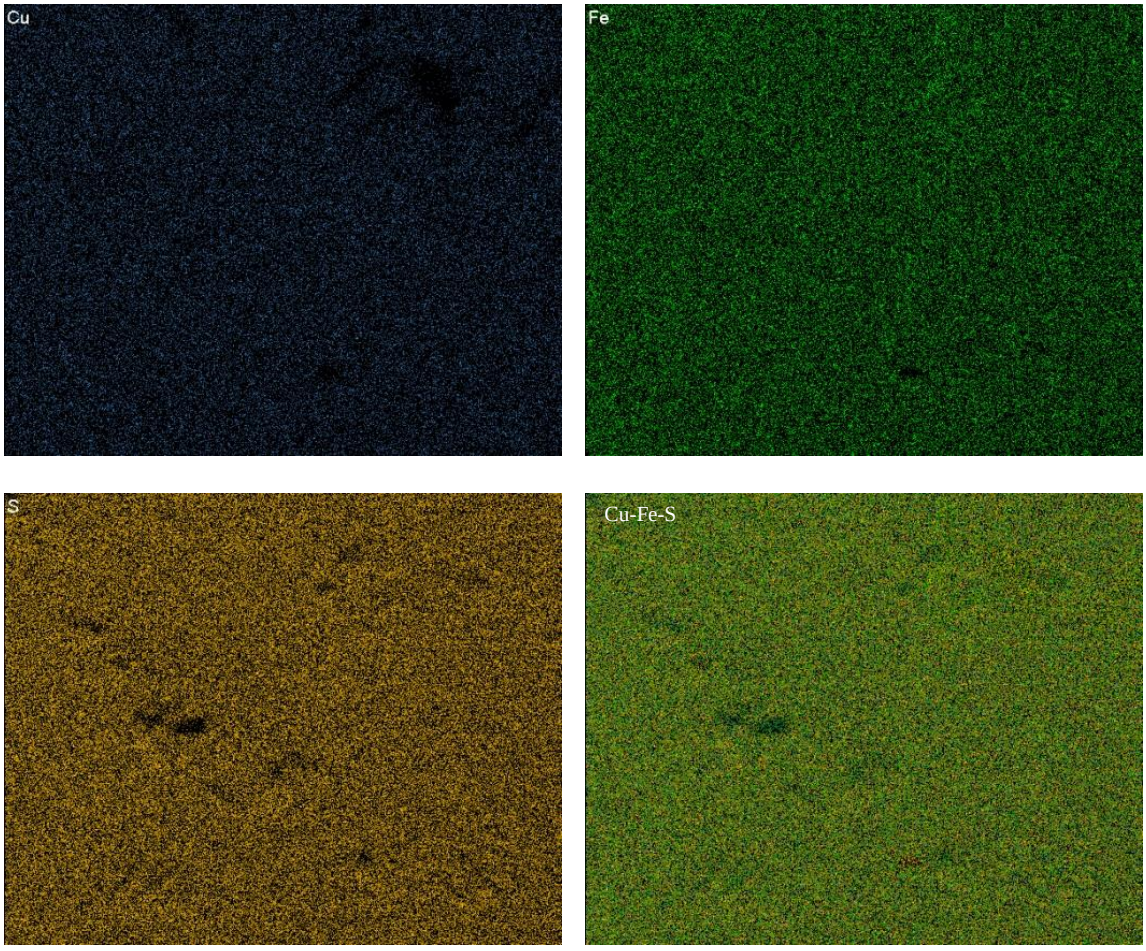

Figure 4-3 SEM-EDX analysis results of the prepared chalcopyrite electrode surface. The magnification is 300X.

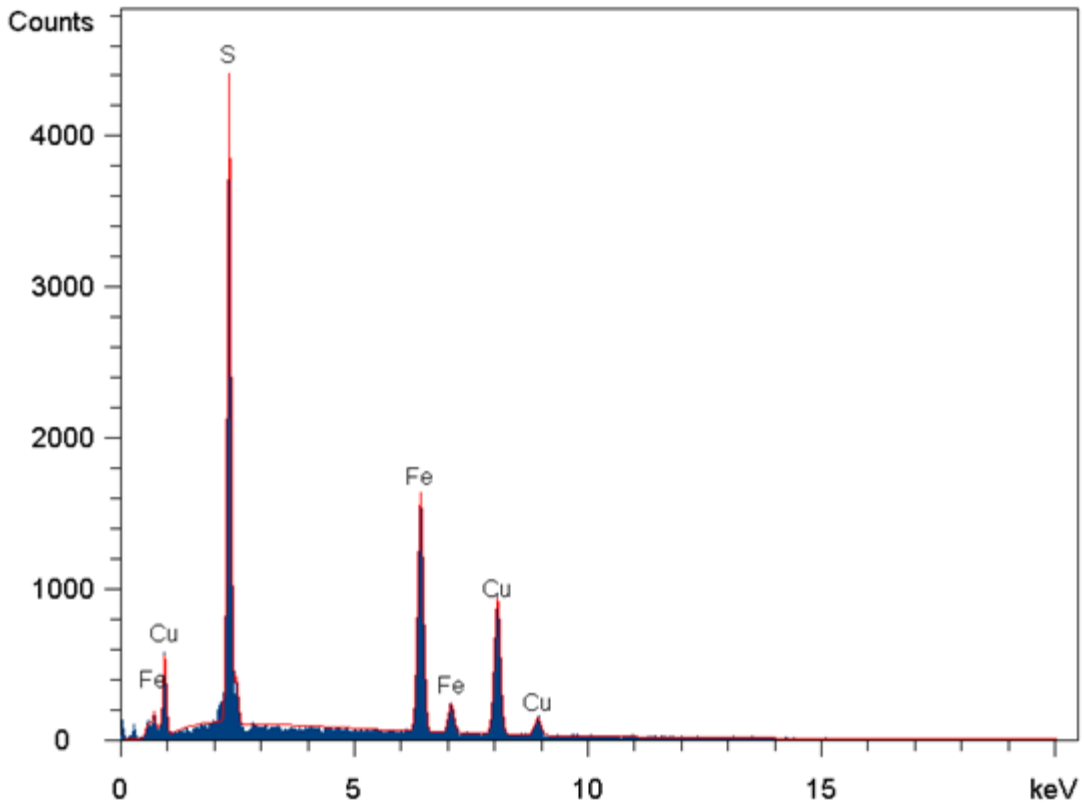

Figure 4-4 EDX spectra of the prepared chalcopyrite electrode.

Table 4-3 Components of the prepared chalcopyrite electrode in this study (wt.%).

Element	Concentration	Theoretical Concentration of $CuFeS_2$
Sulfur	28.88 wt%	34.92 wt%
Iron	32.53 wt%	30.52 wt%
Copper	38.59 wt%	34.56 wt%
Totals	100.00%	100.00%

4.4 Optical Microscope Study

In order to characterize the surface morphology variation of the chalcopyrite electrode before and after electrochemical experiments, a Nikon MA200 microscope coupled with NIS Elements F3.0 Software was used.

5 Development of a Thermodynamic Model to Simulate the Speciation of the Quaternary Sulfuric Acid-Ferric Sulfate-Ferrous Sulfate-Water System

5.1 Introduction

As discussed in the Introduction, most of the previous speciation studies on the acidic iron sulfate system are limited to lower temperatures and/or dilute solutions. Hence, the work in the present Chapter was initiated to explore the possibility of establishing aqueous speciation diagrams for the quaternary acidic iron sulfate system at higher temperatures and solute concentrations, thereby obtaining more detailed information about the acidic iron sulfate electrolytes involved and further providing the data that can enable one to predict the redox potential of the Fe^{3+}/Fe^{2+} couple and study the kinetics of the cathodic reduction reactions on chalcopyrite in industrially relevant leaching systems, at different temperatures from 25 ℃ to 150 ℃. Herein the main species involved (including H^+, Fe^{2+}, Fe^{3+}, SO_4^{2-}, HSO_4^-, $FeHSO_4^+$, $FeSO_4^\circ$, $FeHSO_4^{2+}$, $Fe(SO_4)_2^-$, $FeSO_4^+$, Fe_2O_3 and H_2O) were first investigated, and their thermodynamic data are collected and critically reviewed for the calculation of activity coefficients and equilibrium constants involved in the model. The speciation for the quaternary acidic iron sulfate system is investigated as a function of the initial amounts of iron, acidity, nominal Fe^{3+}/Fe^{2+} ratio and temperature. The model results are finally validated, by comparing with experimental data by the present author and results published by other authors. An analysis of the calculated pH and ionic strength provide additional justification for the model. This information will be used in further investigations of the electrochemical reduction kinetics of the

Fe^{3+}/Fe^{2+} couple on chalcopyrite as well as to shed light on the mechanism of chalcopyrite leaching, as shown in the following Chapters.

5.2 Model Development

When iron sulfates are present in sulfuric acid solution they are distributed as soluble species such as simple cations, neutral or charged complexes, as well as precipitates such as Fe_2O_3, which forms at high temperatures. Because of the lack of thermodynamic data and analytical techniques for in-situ measurement of ions and ionic complexes at high temperature, chemical modeling is a very useful tool to predict and understand the behavior of complex aqueous processing systems, provided that reliable models exist with acceptable predictive power based on the limited available experimental data [134].

However, modeling the speciation in the H_2SO_4-$Fe_2(SO_4)_3$-$FeSO_4$-H_2O system at the temperature and concentration of interest requires reliable values of the thermodynamic properties for all species existing in the system. These properties include the standard Gibbs free energy of species to calculate the equilibrium constants, and the activity coefficients of species as a function of solution composition and temperature, to describe the non-ideal thermodynamic behavior.

5.2.1 Activity Coefficient Model-B-dot Equation

The activity coefficients for ions can be estimated by using different models such as the Debye-Hückel equation and its extensions, the B-dot, Pitzer, electrolyte NRTL, Bromley-Zaemaitis and the mixed solvent electrolyte (MSE) models. These models have been employed in hydrometallurgical applications, and reviewed by several authors [134-136].

In the present work, the B-dot activity coefficient model was applied. This model has been used to evaluate the activity coefficients of dissolved species in similar aqueous sulfuric

acid/metal sulfate systems and has given reasonable predictions through a limited range of temperature and solution composition [35, 134]. It was proposed by Helgeson [137, 138], and is valid for aqueous electrolyte solutions with moderate ionic strengths up to I = 1 molal in a range of 0-300 ℃ [139]:

$$\log \gamma_i = -\frac{A_\gamma z_i^2 \sqrt{I}}{1 + \mathring{a}_i B_\gamma \sqrt{I}} + \dot{B} I \qquad (5\text{-}1)$$

where $\mathring{a}_i$ (Å) is the hard-core diameter of species i, z_i is the ionic charge of species i, A_γ ($kg^{0.5}$ $mol^{-0.5}$) and B_γ ($kg^{0.5}$ $mol^{-0.5}$ cm^{-1}) are Debye-Hückel parameters depending only on the dielectric constant, density and temperature, I (mol kg^{-1}) is the effective (or real/true) ionic strength of the solution, and $\dot{B}$ (kg mol^{-1}) is the characteristic B-dot parameter whose value depends only on the temperature. A_γ, B_γ, and $\dot{B}$ values were selected from the above literature [137, 138]. This equation is a modification of the classic Debye-Hückel model which is valid for electrostatic (long-range) binary interactions between cations and anions. The term *"$\dot{B}I$"* represents a correction for short-range interactions between dissolved species-other than electrostatic ones.

The only two species-specific parameters are the z_i and hard-core parameter $\mathring{a}_i$. The $\mathring{a}$ values for H^+ (9Å), Fe^{2+} (6Å), Fe^{3+} (9Å), HSO_4^- (4.5Å) and SO_4^{2-} (4Å) were taken from literature [140,141]. For other species that were not included in the literature, estimates were assigned according to a method published in the literature. For example, $\mathring{a}$ was given a value of 4.0 Å for monovalent ions like $FeSO_4^+$, $Fe(SO_4)_2^-$ and $FeHSO_4^+$, and 4.5 Å for divalent ions like $FeHSO_4^{2+}$ [134].

In the case of polar neutral species, the activity coefficients were assigned a value of unity according to the literature [139, 142]. Actually, given that the z_i is zero for neutral species, even

when calculating the activity coefficients for the neutral species by the B-dot equation (using the corresponding $\dot{B}$ and I values in the present studied solutions), the values are almost always unity.

In the systems considered in the present work, only concentrations that are similar to those found in hydrometallurgical processing of chalcopyrite were used, and the real ionic strength of the solution was generally lower than 0.85 molal (see the results in Figure 5-9). These considerations justify the use of the B-dot model. The use of the above-mentioned alternative models may have better described the non-ideal behavior of the ionic solutions examined herein, however, these models usually require a large amount of theoretical or experimental data (such as mean activity coefficient, osmotic coefficient and solubility) in order to obtain numerous interaction parameters by regression, which can be further used to calculate the activity coefficients. Such data are usually unavailable, especially at elevated concentrations and temperatures.

5.2.2 Collection and Calculation of Thermodynamic Data and Equilibrium Constants

Standard molar Gibbs free energy of the reaction products and reactants are required to obtain the equilibrium constant of a reaction. Thermodynamic data for all of the species that may exist in the specific system were collected and critically assessed to calculate the equilibrium constants at different temperatures.

Table 5-1 and Table 5-2 present the main species and their corresponding thermodynamic data, formation reactions and thermodynamic equilibrium constants at various temperatures. The equilibrium constants for the main species in the range of 25-35 ℃ were taken from the literature [34, 36], while equilibrium constants at 70-150 ℃ were calculated by the Criss-Cobble method. This set of species and data was found to be the best to accurately predict the experimental results. Detailed information will be given in the following discussion.

Table 5-1 Thermodynamic data at 25 ℃ and equilibrium (standard formation) constants for the main species in aqueous Fe(II)-Fe(III)-H_2SO_4 solutions in the range of 25-35 ℃. The reference state for aqueous species is infinite dilution (Data given are for 25 ℃, 1 atm and standard state).

Species	$\Delta G°$ (kJ/mol)	$S°$ (J/mol K)	Species and Formation Reactions	Log $K_f°$ 25°C	Log $K_f°$ 35°C
H^+	0.00	0.00			
SO_4^{2-}	-744.63	20.10			
HSO_4^-	-756.01	131.80	$H^+ + SO_4^{2-} \leftrightarrow HSO_4^-$	1.98	2.12
Fe^{2+}	-91.20	-107.10			
$FeHSO_4^+$	-841.99	134.19	$Fe^{2+} + H^+ + SO_4^{2-} \leftrightarrow FeHSO_4^+$	1.08	1.42
$FeSO_4°$	-848.67	3.26	$Fe^{2+} + SO_4^{2-} \leftrightarrow FeSO_4°$	2.25	2.33
Fe^{3+}	-16.70	-280.30			
$FeHSO_4^{2+}$	-775.48	34.97	$Fe^{3+} + H^+ + SO_4^{2-} \leftrightarrow FeHSO_4^{2+}$	2.48	2.90
$FeSO_4^+$	-784.38	-5.93	$Fe^{3+} + SO_4^{2-} \leftrightarrow FeSO_4^+$	4.04	4.34
$Fe(SO_4)_2^-$	-1524.60	423.16	$Fe^{3+} + 2SO_4^{2-} \leftrightarrow Fe(SO_4)_2^-$	5.38	6.33
Fe_2O_3	-742.20	87.40	$2Fe^{3+} + 3H_2O \leftrightarrow Fe_2O_3 + 6H^+$		
H_2O	-237.178	69.91			

a. The thermodynamic data ($\Delta G°$ and $S°$) for H^+, Fe^{2+}, Fe^{3+}, SO_4^{2-}, HSO_4^-, Fe_2O_3 and H_2O, and the equilibrium constants for HSO_4^- and the five iron complexes at 25 ℃ and 35 ℃ were taken from the literature [34, 36, 129].

b. The ΔG° and S° of the iron complexes were estimated by the present work. See text for details.

c. The heat capacity parameters (Kelley equation coefficients) of Fe_2O_3 and H_2O used to calculate the equilibrium constants of Fe_2O_3 were taken from HSC 7.1 [143].

Kelley equation: $C_p(T) = A + B*10^{-3}*T + C*10^{5}*T^{-2} + D*10^{-6}*T^{2}$ (J/mol*K).

For Fe_2O_3: A=143.566, B=-36.323, C=-31.433, D=71.792.

For H_2O: A=186.884, B=-464.247, C=-19.565, D=548.631.

5.2.2.1 Species Involved in This System

It is well-known that iron forms complexes in H_2SO_4 solutions [33-38]. The important equilibrium reactions in such a system could include: the association of SO_4^{2-} and H^+ to give rise to HSO_4^-; formation of complexes between iron ions and SO_4^{2-} or HSO_4^-; reaction of iron ions with water to form hydroxyl complexes and protons. Here the most important iron species published in previous studies are taken into account to study the speciation and distribution of ferrous and ferric species involved in H_2SO_4 solutions as a function of temperature, iron and acid concentration, and the nominal Fe^{3+}/Fe^{2+} ratio.

The pH value of the acidic iron sulfate solution used in chalcopyrite leaching is usually below 2, because higher pH will lead to the formation of iron hydroxyl complexes and even iron precipitates. Speciation calculations indicate that iron hydroxide complexes always play a minor role in these solutions where pH is below 2. As a result, at the high acidities of interest (pH generally less than 2.0), hydroxide (OH^-) ions have not been taken into account herein under equilibrium conditions. Consequently, iron hydroxyl complexes were excluded in the present study.

The changes in the activity of water participating in the chemical reactions are negligible compared to its concentration, and were thus also ignored.

It has been reported that at low pH the concentration of $Fe(SO_4)_2^-$ was consistently found to be negligible [33, 37]. In addition, a declining trend was found regarding the temperature dependence of $Fe(SO_4)_2^-$ concentration from about 50 ℃. At around 70 ℃ it is almost non-existent [36]. Furthermore, Dry and Bryson (1988) also reported that the inclusion of $Fe(SO_4)_2^-$ resulted in poor predictions of redox potential [33]. It was also found in this work that poor solution potential prediction resulted from the inclusion of $Fe(SO_4)_2^-$, especially at temperatures above 70 ℃. Particularly, from 90 ℃ to 150 ℃, at lower nominal Fe^{3+}/Fe^{2+} ratios such as 1:1 and 10:1, the potential difference between the model result with the inclusion of $Fe(SO_4)_2^-$ and that by experiments ranges from 20 mV to even 100 mV. Thus in the present study, $Fe(SO_4)_2^-$ was considered only at 25 ℃ and 70 ℃, and was not considered at higher temperatures.

$FeH(SO_4)_2^\circ$ was also not considered because the inclusion of this species always gave a poor fit to the measured experimental data. This complex was reported by Casas et al [35] and no other authors have reported evidence of the existence of this species. Hence, it is possible that $FeH(SO_4)_2^\circ$ is not a stable species under the conditions of temperature and acidity studied in the present acid iron sulfate solutions.

Fe_2O_3 was included in the model at 150 ℃ according to reports from the literature, which will be discussed in detail in the following sections. From 25 ℃ to 110 ℃, as discussed later, there were almost no precipitates formed during the experiments under the conditions in the present work, and consequently they were excluded in the model through this temperature range.

It should be emphasized that many discrepancies have been reported in the literature among authors regarding which complexes should be included in the speciation model for the H_2SO_4-$FeSO_4$-$Fe_2(SO_4)_3$-H_2O system to provide the best results, especially at higher temperature and/or concentration. The criterion for selecting or rejecting different species in this model was

based on whether the model calculated redox potentials agreed with those measured by experiments (typically the difference between the calculated potentials from the model and measured potentials at lower temperatures was lower than 5-10 mV and at higher temperatures it was lower than about 20 mV). The most important species reported in previous studies for the thermodynamics of this system were considered.

5.2.2.2 Thermodynamic Data and Equilibrium Constants at High Temperature

After the selection of the possible species, the next step was to collect their thermodynamic data and calculate the equilibrium constants at different temperatures. For many aqueous reactions, there is a lack of equilibrium constants for high temperatures. In most cases, even if available, a big variation often exists among different reports. The Criss-Cobble method [144, 145] and the Helgeson-Kirkham-Flowers (HKF) model [146, 147] are two methods commonly used to calculate the standard Gibbs free energies for a single ionic species at elevated temperature based on thermodynamic data available at room temperature. The Criss-Cobble method has been extensively used in calculating temperature-dependent thermodynamic properties for aqueous ions below 200 ℃ since Criss and Cobble proposed an ion entropy correspondence principle in 1964. This method was selected in the present calculation. For solid and liquid species, this can be achieved with knowledge of the standard Gibbs free energy of formation at 298.15 K and the heat capacity. The heat capacity parameters (Kelley equation coefficients) of Fe_2O_3 and H_2O were taken from HSC 7.1 [143], and ΔG° and S° data for Fe_2O_3 and H_2O at higher temperature were calculated by the Kelley equation.

The thermodynamic data at 298.15 K (ΔG° and S°) for H^+, Fe^{2+}, Fe^{3+}, SO_4^{2-}, HSO_4^-, Fe_2O_3 and H_2O, and the equilibrium constants for HSO_4^- and the five iron complexes at 25 ℃ and 35 ℃ were taken from the literature [34, 36, 129].

Thermodynamic data for the five iron complexes have been reported, and were reviewed and summarized by several reports [33, 38, 129, 135] based on the previous studies and thermodynamic databases. There are differences among these studies with respect to the reported values for the thermodynamic properties. In addition, although there are some reported ways to calculate the ΔS° of some species of interest, such as $Fe(SO_4)_2^-$ [148], no reliable reports of the ΔG° and S° of $FeHSO_4^{2+}$ and $FeHSO_4^+$, as well as S° of $Fe(SO_4)_2^-$ at 298.15 K could be found in the literature. For the sake of maintaining internal consistency, the thermodynamic data of all the species partaking in these ferrous and ferric equilibria are based on the values reported by Stipp (1990) [34] who studied and examined these data. The ΔG° of the five iron complexes were calculated from the equilibrium constants at 25°C: first, the ΔG° of the formation reaction was calculated using the equation $\Delta G^\circ = -2.303RT\text{Log}\ K_f^\circ$; then, the ΔG° of the single iron complex was estimated based on the calculated ΔG° of the formation reaction and the known available ΔG° for the remaining individual species.

As to S° for the five iron complexes, first by using the equilibrium constants at 25 ℃ and 35 ℃ [34, 36], the enthalpy change ΔH° of the formation reactions were calculated based on the van't Hoff equation. Then, the entropy change ΔS° of the formation reactions were calculated according to the equation $\Delta G^\circ = \Delta H^\circ - T\ \Delta S^\circ$. Finally, the S° for the single iron complex was estimated based on the calculated entropy change ΔS° of the formation reaction and the known S° for the remaining single species in the formation reaction.

It should be noted that the calculated ΔG° and S° values of the iron complexes in the present work are a little different from those published in the above noted sources, however, they are generally in reasonable agreement with each other.

Prior to calculating the speciation, to obtain the equilibrium constants for HSO_4^- and the five iron complexes at 70 ℃-150 ℃, models based on the Lewis formulation of the Criss-Cobble correspondence principle [149] were used to predict ΔG° of the main species in the solution at the temperatures of interest. In addition, because there is a lack of thermodynamic data at high temperatures in the literature for neutral species $FeSO_4^\circ$, the average molal ionic heat capacity at high temperatures was estimated by using the average heat capacity constants of simple cations and simple anions. It was found that this method gave very reasonable equilibrium constant estimations (The model-predicted redox potentials agree very well with those measured by experiments). The calculated equilibrium constants at 70 ℃–150 ℃ are listed in Table 5-2.

Table 5-2 Calculated equilibrium (standard formation) constants for the main species in aqueous Fe(II)-Fe(III)-H_2SO_4 solutions in the range of 70-150 ℃.

Species and Formation Reactions	Log K_f° 70°C	Log K_f° 90°C	Log K_f° 110°C	Log K_f° 150°C
$H^+ + SO_4^{2-} \leftrightarrow HSO_4^-$	2.64	2.96	3.31	4.05
$Fe^{2+} + H^+ + SO_4^{2-} \leftrightarrow FeHSO_4^+$	2.52	3.09	3.62	4.61
$Fe^{2+} + SO_4^{2-} \leftrightarrow FeSO_4^\circ$	2.63	2.80	2.98	3.35
$Fe^{3+} + 2SO_4^{2-} \leftrightarrow Fe(SO_4)_2^-$	7.48	9.07	10.54	13.16
$Fe^{3+} + H^+ + SO_4^{2-} \leftrightarrow FeHSO_4^{2+}$	4.22	4.89	5.50	6.61
$Fe^{3+} + SO_4^{2-} \leftrightarrow FeSO_4^+$	5.37	5.92	6.46	7.52
$2Fe^{3+} + 3H_2O \leftrightarrow Fe_2O_3 + 6H^+$	2.54	3.63	4.59	6.21

It is clearly seen in Figure 5-1 that the equilibrium constants for HSO_4^- and the five iron complexes increase with increasing temperature. That is, these complexes become more stable as temperature is increased.

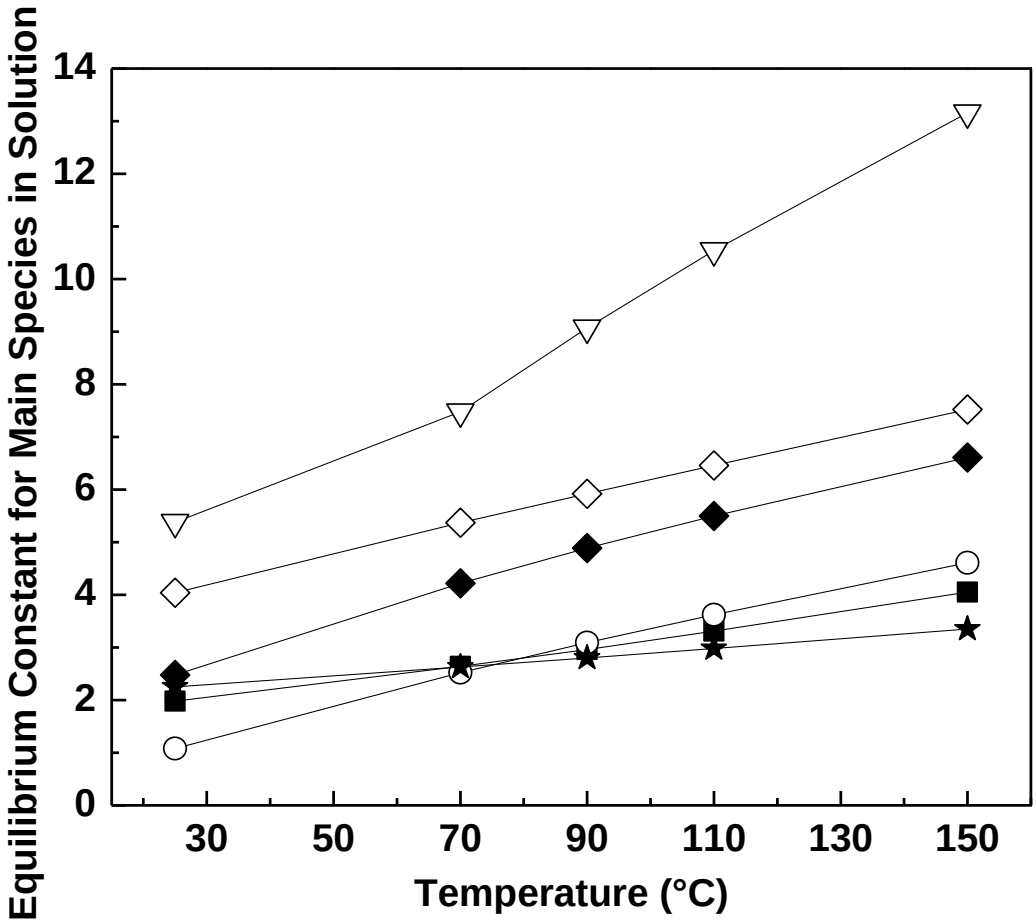

(HSO_4^- ■; $FeHSO_4^+$ ○; $FeSO_4$ °★; $FeHSO_4^{2+}$ ◆; $Fe(SO_4)_2^-$ ▽; $FeSO_4^+$ ◇)

Figure 5-1 Equilibrium (standard formation) constants used in the present study for the main species in aqueous Fe(II)-Fe(III)-H_2SO_4 solutions in the temperature range of 25-150 ℃.

5.2.3 Calculation of Models in the Solution

Chemical equilibrium equations (7 in total shown in the Table 5-2) based on the above formation reactions (including the equations of activity coefficient and ionic strength), and additional component mass balance equations in terms of Fe^{2+}, Fe^{3+} and SO_4^{2-}, as well as the electroneutrality equation (the solution must remain electrically neutral and a charge balance equation must be able to be written), were obtained and these non-linear equations were solved in a Fortran code employing Brent's method [150]. Molal concentrations were used in order to exclude the density changes with temperature, thus allowing a comparison of solute concentrations at different temperatures. Each set of the equations (with a specific solution composition at any temperature) was solved with high accuracy and excellent convergence was obtained. Basically, the convergence criteria used in the present work is that the error for each of the equations (please note that each equation was transferred in the form of f(x)=0 when solving each set of equations; the error here thus means the difference between the left hand side and the right hand side of each equation) is smaller than 10^{-8}. Using this method, high accuracy and excellent convergence was obtained. The actual error was typically smaller than 10^{-15} for each equation. A Fortran code sample for the calculation at 150 ℃, together with the calculated concentrations of all species in aqueous Fe(II)-Fe(III)-H_2SO_4 solutions in the range of 25-150 ℃ according to the developed speciation model with nominal Fe^{3+}/Fe^{2+} ratio of 10:1, are shown in Appendix B.

Commercial chemical modeling software were not used in this study (such as OLI, EQ3NR, EQ3/6, and WATEQ), as their internal databases are not currently adequate to model this quaternary system (a modification of the species involved under different temperatures is

required in order to fit the experimental data). Hence, it was more convenient to do the calculation of the thermodynamic model by the proposed Fortran code.

5.3 Results and Discussion

5.3.1 Speciation Results Calculated at 25 ℃ and 70 ℃

The results of the aqueous speciation calculation (expressed as a percentage of the total ferric or ferrous) for Fe(II)-Fe(III)-H_2SO_4 solutions with different nominal Fe^{3+}/Fe^{2+} ratios at 25 ℃ and 70 ℃ are presented in Figure 5-2 and Figure 5-3. Please note that throughout this thesis, nominal Fe^{3+}/Fe^{2+} ratio means the ratio of total Fe(III) to total Fe(II) added to the electrochemical cell or autoclave. $FeSO_4^+$ is the predominant species for Fe(III) (71.9%-76.2% at 25 ℃ and 61.1%-71.5% at 70 ℃), followed by the $Fe(SO_4)_2^-$ species (22.9%-16.9% at 25 ℃ and 35.8%-23.7% at 70 ℃). The remaining Fe(III) is distributed as free ferric and $FeHSO_4^{2+}$. The percentage of the free ferric is ~3.8%-5.2% at 25 ℃, and 0.5%-1.0% at 70 ℃.

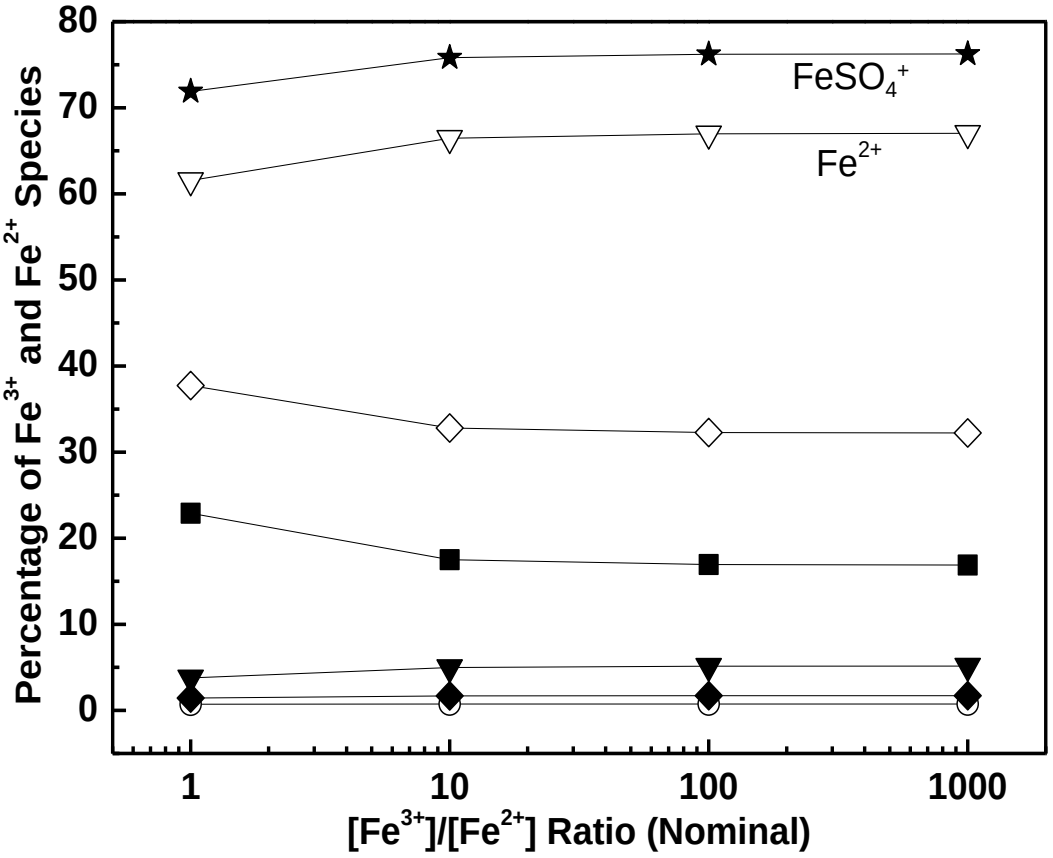

(Fe^{2+} ▽; $FeHSO_4^+$ ○; $FeSO_4$ ◇; Fe^{3+} ▼; $FeHSO_4^{2+}$ ◆; $Fe(SO_4)_2^-$ ■; $FeSO_4^+$ ★)

Figure 5-2 Calculated aqueous speciation diagram of the main ferric and ferrous species in the Fe(II)-Fe(III)-H_2SO_4 solutions at $[H_2SO_4]$ = 0.31 mol/kg and $[Fe^{3+}]_{total}$ = 0.18 mol/kg with different nominal Fe^{3+}/Fe^{2+} ratios at 25 ℃. Please note that the sum of the percentage values of Fe(II) species (unfilled symbols) is 100%, which is also the case for the Fe(III) species (filled symbols).

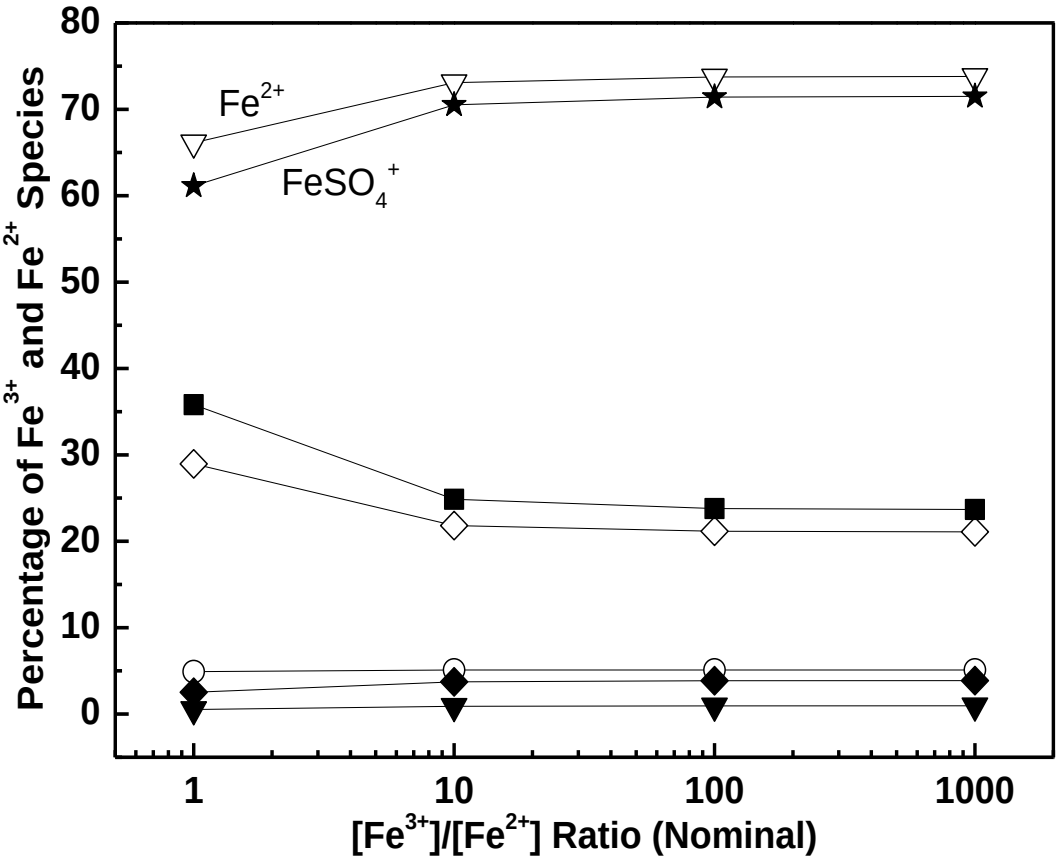

(Fe^{2+} ▽; $FeHSO_4^+$ ○; $FeSO_4$ °◇; Fe^{3+} ▼; $FeHSO_4^{2+}$ ◆; $Fe(SO_4)_2^-$ ■; $FeSO_4^+$ ★)

Figure 5-3 Calculated aqueous speciation diagram of the main ferric and ferrous species in the Fe(II)-Fe(III)-H_2SO_4 solutions at [H_2SO_4] = 0.31 mol/kg and $[Fe^{3+}]_{total}$ = 0.18 mol/kg with different nominal Fe^{3+}/Fe^{2+} ratios at 70 ℃. Please note that the sum of the percentage values of Fe(II) species (unfilled symbols) is 100%, which is also the case for the Fe(III) species (filled symbols).

Free ferrous ions account for the largest percentage of the total ferrous (61.5%-67.0% at 25 ℃ and 66.1%-73.8% at 70 ℃), followed by $FeSO_4$ °(37.7%-32.2% at 25 ℃ and 29.0%-21.1% at 70 ℃), and $FeHSO_4^+$. The speciation results regarding iron (II) in the present work agree very well with those published by Sahoo et al in 2012 [151]. In addition, the fact that free ferrous ions

are the most abundant iron (II) species is in agreement with the previously published results at low temperatures from 25 ℃ to 55 ℃ [35, 36], although the solution conditions and species used in these models are a little different.

With the exception of $FeSO_4^\circ$ and $Fe(SO_4)_2^-$, the percentages of all other Fe-sulfate complexes increase with an increase in the nominal Fe^{3+}/Fe^{2+} ratio from 1:1 to 1000:1 at both 25 ℃ and 70 ℃. At the same time, it was found that the concentration of free ferric (on the order of 10^{-3} mol kg^{-1}) slightly increases with increasing nominal Fe^{3+}/Fe^{2+} ratios, whereas the concentration of free ferrous decreases significantly from the order of 10^{-1} mol kg^{-1} to the order of 10^{-4} mol kg^{-1} (Please note that the concentration of each species can be calculated by using the total amount of Fe(II) or Fe(III) multiplied by the corresponding percentage, and the total amount of Fe(II) decreases when increasing the nominal Fe^{3+}/Fe^{2+} ratio).

Under the same nominal Fe^{3+}/Fe^{2+} ratios, increasing the temperature from 25 ℃ to 70 ℃ results in an increase of the amount of $FeHSO_4^{2+}$, $Fe(SO_4)_2^-$, free ferrous and $FeHSO_4^+$, but a decrease in the percentage of free ferric, $FeSO_4^+$, and $FeSO_4^\circ$.

5.3.2 Speciation Results Calculated at 90 ℃ and 110 ℃

Figure 5-4 and Figure 5-5 show the calculated results of the aqueous speciation of the ferric and ferrous species for Fe(II)-Fe(III)-H_2SO_4 solutions with different nominal Fe^{3+}/Fe^{2+} ratios at 90 ℃ and 110 ℃, respectively. It is found that $FeSO_4^+$ remains the predominant species of Fe(III), with a proportion larger than 90% under all of the conditions (ranging from about 93.0% to 96.2%). Free ferric ion and $FeHSO_4^{2+}$ only account for a minor percentage. In fact, free ferric is the least abundant species with values of 0.3%-0.6% at 90 ℃, and 0.2%-0.4% at 110 ℃, respectively.

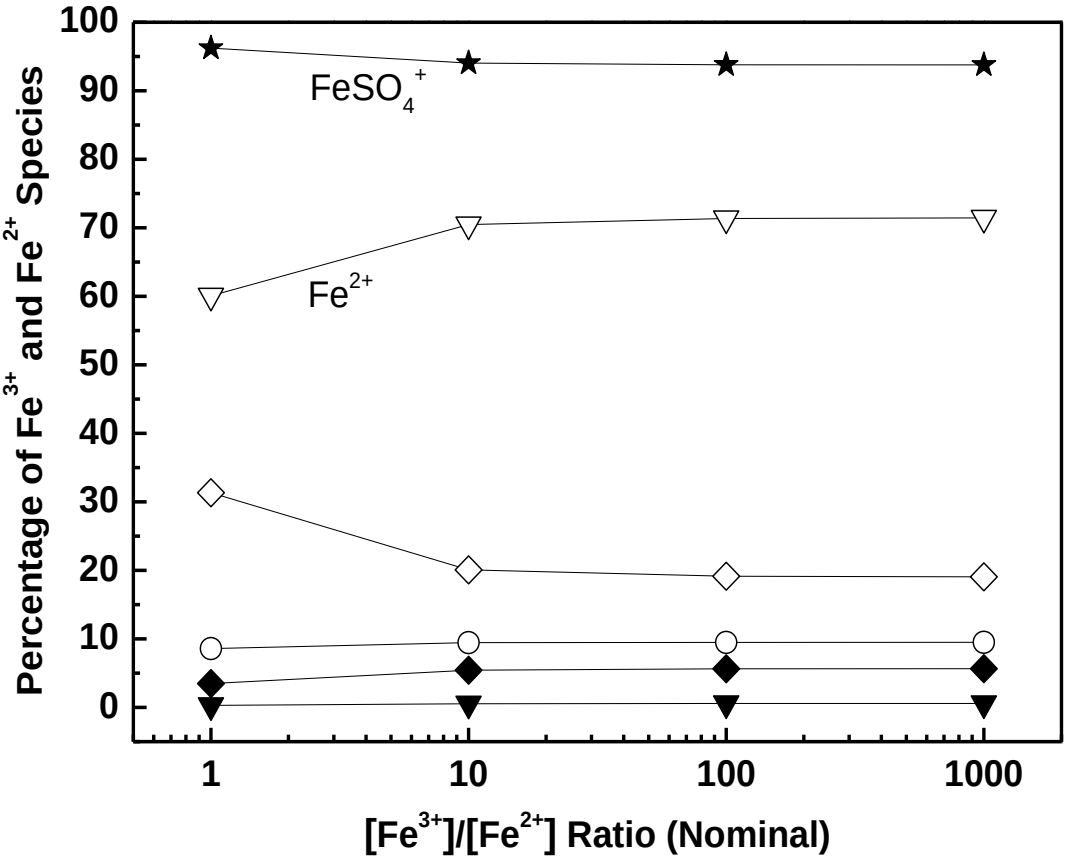

(Fe^{2+} ▽; $FeHSO_4^+$ ○; $FeSO_4$ °◇; Fe^{3+} ▼; $FeHSO_4^{2+}$ ◆; $FeSO_4^+$ ★)

Figure 5-4 Calculated aqueous speciation diagram of the main ferric and ferrous species in the Fe(II)-Fe(III)-H_2SO_4 solutions at $[H_2SO_4]$ = 0.31 mol/kg and $[Fe^{3+}]_{total}$ = 0.18 mol/kg with different nominal Fe^{3+}/Fe^{2+} ratios at 90 ℃. Please note that the sum of the percentage values of Fe(II) species (unfilled symbols) is 100%, which is also the case for the Fe(III) species (filled symbols).

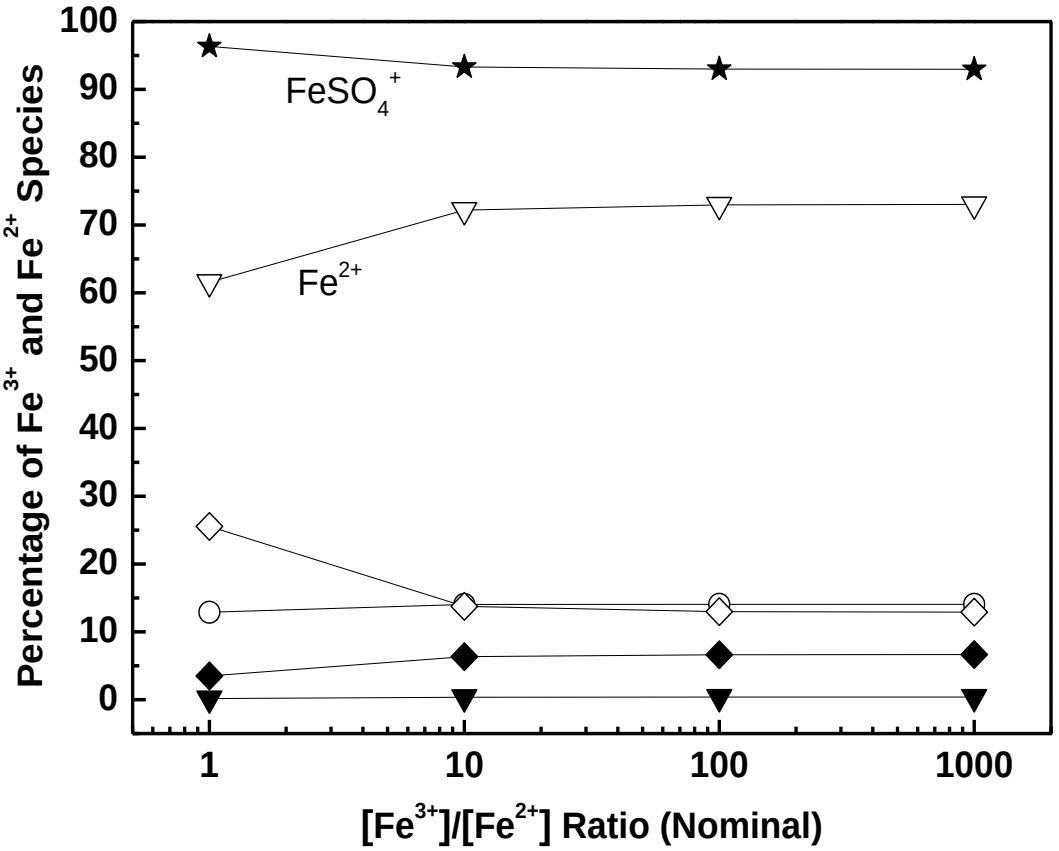

(Fe^{2+} ▽; $FeHSO_4^+$ ○; $FeSO_4$ ° ◇; Fe^{3+} ▼; $FeHSO_4^{2+}$ ◆; $FeSO_4^+$ ★)

Figure 5-5 Calculated aqueous speciation diagram of the main ferric and ferrous species in the Fe(II)-Fe(III)-H_2SO_4 solutions at $[H_2SO_4]$ = 0.31 mol/kg and $[Fe^{3+}]_{total}$ = 0.18 mol/kg with different nominal Fe^{3+}/Fe^{2+} ratios at 110 ℃. Please note that the sum of the percentage values of Fe(II) species (unfilled symbols) is 100%, which is also the case for the Fe(III) species (filled symbols).

On the other hand, a considerable proportion of Fe(II) exists as free ferrous in the range of 60.1-73.0%. This trend was similar to that at 25 ℃ and 70 ℃. Furthermore, at 90 ℃, the second most abundant Fe(II) species is $FeSO_4°$, ranging from 31.3% to 19.1% with the nominal Fe^{3+}/Fe^{2+} ratios of 1:1 to 1000:1, respectively. However, at 110 ℃, $FeSO_4°$ accounts for the second largest percentage of Fe(II) (about 25.5%) only when the nominal Fe^{3+}/Fe^{2+} ratio was 1:1. Under the other three nominal Fe^{3+}/Fe^{2+} ratios, the percentage of $FeHSO_4^+$ is almost equal to that of $FeSO_4°$ (actually a little bit larger), with values in the range of 12.9%-14.1%.

Moreover, at both 90 ℃ and 110 ℃, apart from the $FeSO_4°$ and $FeSO_4^+$, the relative percentages of all other ferric and ferrous species increases with increasing nominal Fe^{3+}/Fe^{2+} ratios. Meanwhile, it can be determined that the concentration of free ferric (on the order of 10^{-4} mol kg^{-1}) slightly increases with increasing nominal Fe^{3+}/Fe^{2+} ratios, while the concentration of free ferrous decreases significantly from the order of 10^{-1} mol kg^{-1} to the order of 10^{-4} mol kg^{-1}. This trend was the same as that observed at 25 ℃ and 70 ℃.

Furthermore, under the same nominal Fe^{3+}/Fe^{2+} ratios, a temperature increase from 90 ℃ to 110 ℃ leads to an increase of the relative amounts of $FeHSO_4^{2+}$, free ferrous and $FeHSO_4^+$, and a decrease in the amounts of free ferric, $FeSO_4^+$ and $FeSO_4°$.

5.3.3 Speciation Results Calculated at 150 ℃

As reported in the literature [39-45], precipitates will be formed at 150 ℃ in acid iron sulfate solutions due to the hydrolysis of ferric depending on the acidity and the amount of metal sulfate in the system. The formation of hematite (Fe_2O_3) is favored by lower solution acidity and a relatively large amount of added divalent metal sulfate, which consequently leads to a small amount of dissolved Fe(III). The effect of the metal sulfates on the hydrolysis has been attributed to the formation of bisulfate ions through combination of the sulfate ion with hydrogen ions in

solution which will further facilitate the formation of Fe_2O_3, according to the following two reactions [42-44]:

$$SO_4^{2-} + H^+ \leftrightarrow HSO_4^- \quad (5\text{-}2)$$

$$2Fe^{3+} + 3H_2O \leftrightarrow Fe_2O_3 + 6H^+ \quad (5\text{-}3)$$

A drop in free hydrogen ion concentration in the system studied could reduce the amount of soluble ferric and based on several published results hematite is a likely precipitate in this system. Thus hematite was included in the speciation calculations at 150 ℃.

Figure 5-6 presents the calculated results of the aqueous speciation of the main ferric and ferrous species for the Fe(II)-Fe(III)-H_2SO_4 solutions with different nominal Fe^{3+}/Fe^{2+} ratios at 150 ℃. $FeSO_4^+$ remains the predominant species for Fe(III) in the aqueous solution, with its proportion ranging from about 33.7% to 49.2% at different levels of ferrous sulfate addition. As expected, a large amount of Fe(III) precipitated as Fe_2O_3, with the largest value of 61.7% obtained when the nominal Fe^{3+}/Fe^{2+} ratio was 1:1. The percentage of formed Fe_2O_3 is relatively stable under the other three nominal Fe^{3+}/Fe^{2+} ratios in the range of 44.4%-42.7%. This variation in the amount of hematite as a function of $FeSO_4$ concentrations is similar to that published in the literature with an addition of divalent metal sulfates like $ZnSO_4$ or $MgSO_4$ for a relatively low free sulfuric acid concentration [42, 43]. Free ferric and $FeHSO_4^{2+}$ still account for a minor percentage of the total Fe(III), with the free ferric representing the lowest proportion at 0.1%-0.2%.

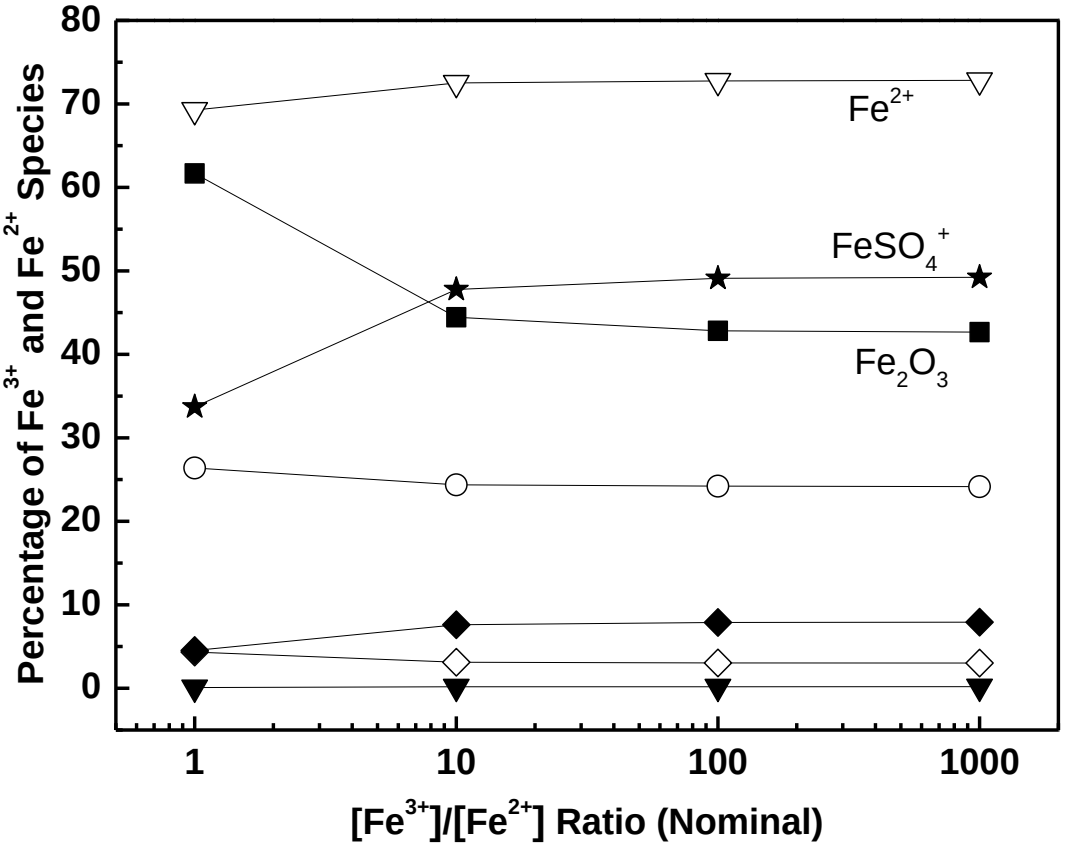

(Fe^{2+} ▽; $FeHSO_4^+$ ○; $FeSO_4$ ° ◇; Fe^{3+} ▼; $FeHSO_4^{2+}$ ◆; Fe_2O_3 ■; $FeSO_4^+$ ★)

Figure 5-6 Calculated aqueous speciation diagram of the main ferric and ferrous species in the Fe(II)-Fe(III)-H_2SO_4 solutions at $[H_2SO_4]$ = 0.31 mol/kg and $[Fe^{3+}]_{total}$ = 0.18 mol/kg with different nominal Fe^{3+}/Fe^{2+} ratios at 150 ℃. Please note that the sum of the percentage values of Fe(II) species (unfilled symbols) is 100%, which is also the case for the Fe(III) species (filled symbols).

A similar trend to that observed from 25 ℃ to 110 ℃ was found at 150 ℃ in that a large amount of Fe(II) existed in the form of free ferrous ion, in the range of 69.3-72.8%. At 150 ℃ the second most common Fe(II) species was $FeHSO_4^+$, ranging from 26.4% to 24.2% with the nominal Fe^{3+}/Fe^{2+} ratios changing from 1:1 to 1000:1. $FeSO_4$ ° accounted for the smallest

percentage of the total Fe(II). This is in contrast to the 25-90 ℃ range where $FeSO_4^\circ$ represented the second most abundant Fe(II) species. From 110-150 ℃ the relative amount of $FeHSO_4^+$ increased (except for the point with the nominal Fe^{3+}/Fe^{2+} ratio of 1:1).

At 150 ℃, besides $FeSO_4^\circ$, $FeHSO_4^+$ and Fe_2O_3, the relative percentages of all other ferric and ferrous species increase with an increase of the nominal Fe^{3+}/Fe^{2+} ratio from 1:1 to 1000:1.

It is interesting to note that for the same nominal Fe^{3+}/Fe^{2+} ratio, with the temperature increasing from 25 ℃ to 150 ℃, the free ferric concentration declines from the order of 10^{-3} mol kg^{-1} to the order of 10^{-4} mol kg^{-1}, whereas the free ferrous concentration is relatively stable with similar values of the same order of magnitude. Meanwhile, at lower pH (see results in Figure 5-8), free ferric and ferrous ions are more abundant.

5.3.4 Model Validity-Comparison with Experimental Results and Previous Work

The model can only be validated in a restricted range of conditions (as shown in Chapter 4) due to the limited availability of experimental data for this system. Nevertheless, experimental results for redox potential and ferric solubility, together with the calculated pH and ionic strength, were used to validate the model predictions presented previously.

5.3.4.1 Comparison of Redox Potential between Speciation Results and Experimental Measurements from 25 ℃ to 150 ℃

A comparison of the reversible potentials between experimental measurements performed for this work and model prediction was used to validate the thermodynamic speciation model. Please note that a detailed discussion on how to calculate the redox potential via those speciation results will be presented in Chapter 6. Figure 5-7 shows that the reversible potentials measured by experiment and predicted by the model under different nominal Fe^{3+}/Fe^{2+} ratios are in excellent agreement from 25 ℃ to 150 ℃. The difference between experimental and calculated

values was typically about ±20 mV depending on the solution composition and temperature. The comparison of experimental and calculated results suggested that the model is qualitatively and quantitatively validated. Therefore, a conclusion can be drawn that the predicted species distribution and solution concentrations are accurate for the Fe(II)-Fe(III)-H_2SO_4 solutions in the temperature and composition ranges studied here.

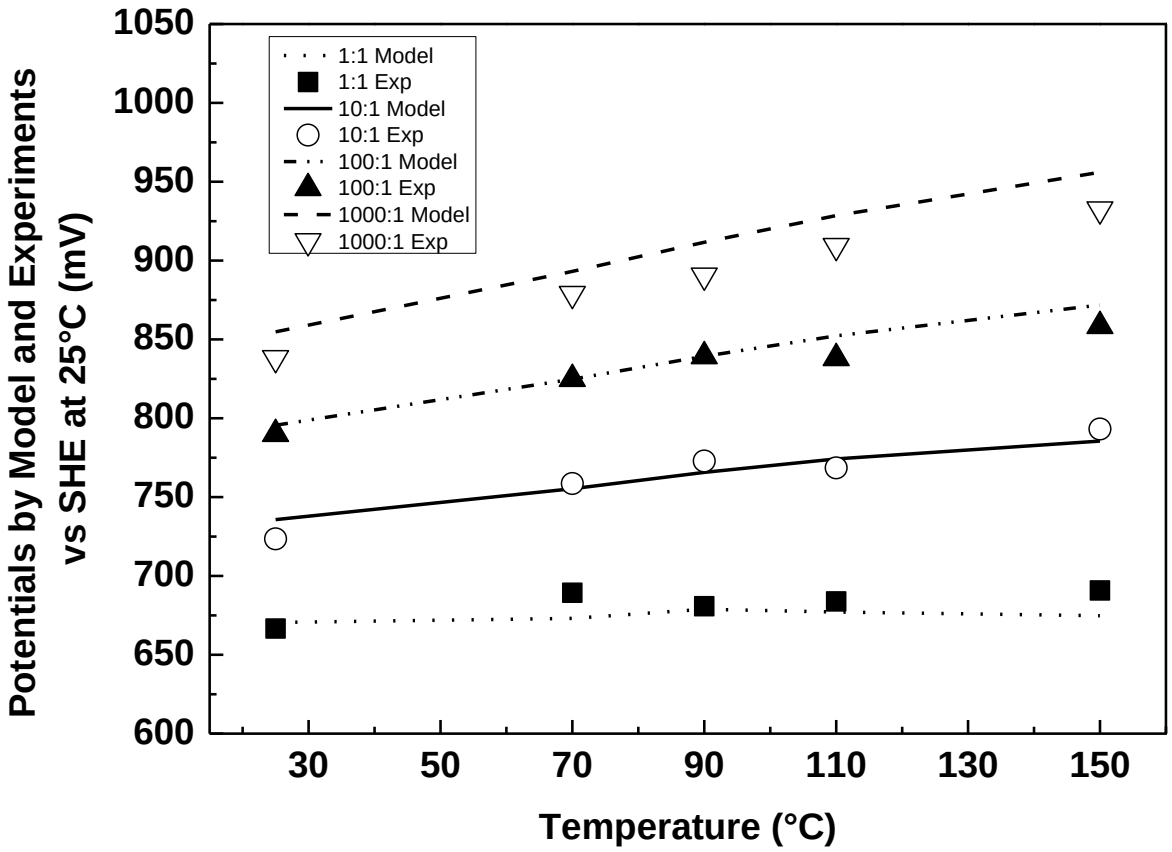

Figure 5-7 Comparison of the potentials predicted by model and measured by experiments in the Fe(II)-Fe(III)-H_2SO_4 solutions at $[H_2SO_4]$ = 0.31 mol/kg and $[Fe^{3+}]_{total}$ = 0.18 mol/kg with different nominal Fe^{3+}/Fe^{2+} ratios in the temperature range of 25 ℃-150 ℃.

Single ion activity coefficients are also part of the speciation model parameters. The ability of the model to predict the experimental data also indicates that the method for estimating activity coefficients of simple ions and complexes is valid in the present study. The B-dot model was found to be surprisingly applicable for accurate prediction of redox potential at temperatures up to 150 ℃ in the quaternary system studied here. As reported by Truesdell and Jones (1974) [140], the use of any model of single-ion activity coefficients based on experimental measurements made on single salt solutions requires the assumption that, at a given temperature, activity coefficients in simple solutions are equal to those in complex solutions of the same ionic strength. This assumption was fully justified by the reasonable prediction of solution redox potential over a wide range of different nominal Fe^{3+}/Fe^{2+} ratios and temperatures in this work, owing to the fact that relatively lower real ionic strengths were obtained compared to the higher nominal ionic strength (see the following discussion).

The following analysis (three parts) also serves as a justification for the developed model in the present work.

5.3.4.2 Comparison of Ferric Solubility between Speciation Results and Previous Work at 150 ℃

As mentioned previously, in the present acid iron sulfate solutions, the formation of hematite may occur at 150 ℃. This results in a significant decrease in the initial amount Fe(III). The model developed in this study can predict the amount of Fe_2O_3 precipitate as well as the amount of Fe(III) species present in the liquid phase (as solubility of Fe(III)). For example, for the nominal Fe^{3+}/Fe^{2+} ratio of 1000:1, from Figure 5-6, we can predict that the total dissolved amount of Fe(III) is about 0.103 mol/kg (ignoring the changes in water). The concentration of free sulfuric acid (effective/true acidity of the system) under the same conditions is

approximately 0.42 mol/kg, which is larger than the nominal amount of sulfuric acid due to the hydrolysis of free ferric.

At present, no experimental data are available for ferric solubility (introduced in the form of $Fe_2(SO_4)_3$ with equilibrium obtained by hydrolysis) in the pure quaternary H_2SO_4-$Fe_2(SO_4)_3$-$FeSO_4$-H_2O system under the highly acidic conditions employed in chalcopyrite leaching (pH typically lower than 2). Furthermore, most of the published solubility data has focused on the ternary H_2SO_4-$Fe_2(SO_4)_3$-H_2O system [39-45]. These reports have found that the extent of Fe_2O_3 precipitation is highly dependent on temperature, as well as the added divalent metal sulfates and their concentrations. For a relatively low free sulfuric acid concentration, with an increasing concentration of divalent metal sulfates (such as $ZnSO_4$, $MgSO_4$), the solubility of Fe(III) decreases and as a result a relatively large amount of hematite will form, due to the decrease in the true acidity [42, 43]. Therefore, in order to compare the model results with published experimental data, it is reasonable to assume that the behavior of the ternary H_2SO_4-$Fe_2(SO_4)_3$-H_2O system is similar to that of the quaternary H_2SO_4-$Fe_2(SO_4)_3$-$FeSO_4$-H_2O system when the concentration of ferrous sulfate is low. In the present study, with the nominal Fe^{3+}/Fe^{2+} ratio of 1000:1, the concentration of $FeSO_4$ was only about $0.18x10^{-3}$ mol/kg. As a result, such a solution could be considered to emulate a ternary H_2SO_4-$Fe_2(SO_4)_3$-H_2O system. According to the results published by Sasaki et al in 1993 [40], who studied the hydrolysis of acidic ferric sulfate solutions of various concentrations in an autoclave at 150 ℃, the solubility of ferric is 0.113 mol/kg with the concentration of free sulfuric acid of 0.42 mol/kg. Thus it is demonstrated that there is very little difference between the Fe(III) solubility obtained herein at the 1000:1 Fe^{3+}/Fe^{2+} ratio and the results of Sasaki et al. The small error between the results is likely caused by the addition of a small amount of $FeSO_4$ in the present case.

Actually, the empirical equation regressed by Reid and Papangelakis in 2006 [44] (who studied Fe_2O_3 solubility in sulfuric acid at 150℃) generates the solubility of ferric as being 0.065 mol/kg with the free sulfuric acid concentration of 0.42 mol/kg. It seems that the ferric solubility data by the current work was also on the same order of magnitude as that obtained by measurement of solubility via the Fe_2O_3 dissolution method. However, it should be noted that Umetsu et al found a solubility of 0.022 mol/kg for the same free acid concentration [41].

5.3.4.3 Analysis of Calculated pH

The calculated pH for various solution compositions are shown in Figure 5-8. In Figure 5-8, it can be observed that in general the pH of the solutions are lower than 1.1. For any given temperature, the pH first decreases as the nominal Fe^{3+}/Fe^{2+} ratio increases from 1:1 to 10:1, and it then levels off between 10:1 and 1000:1.

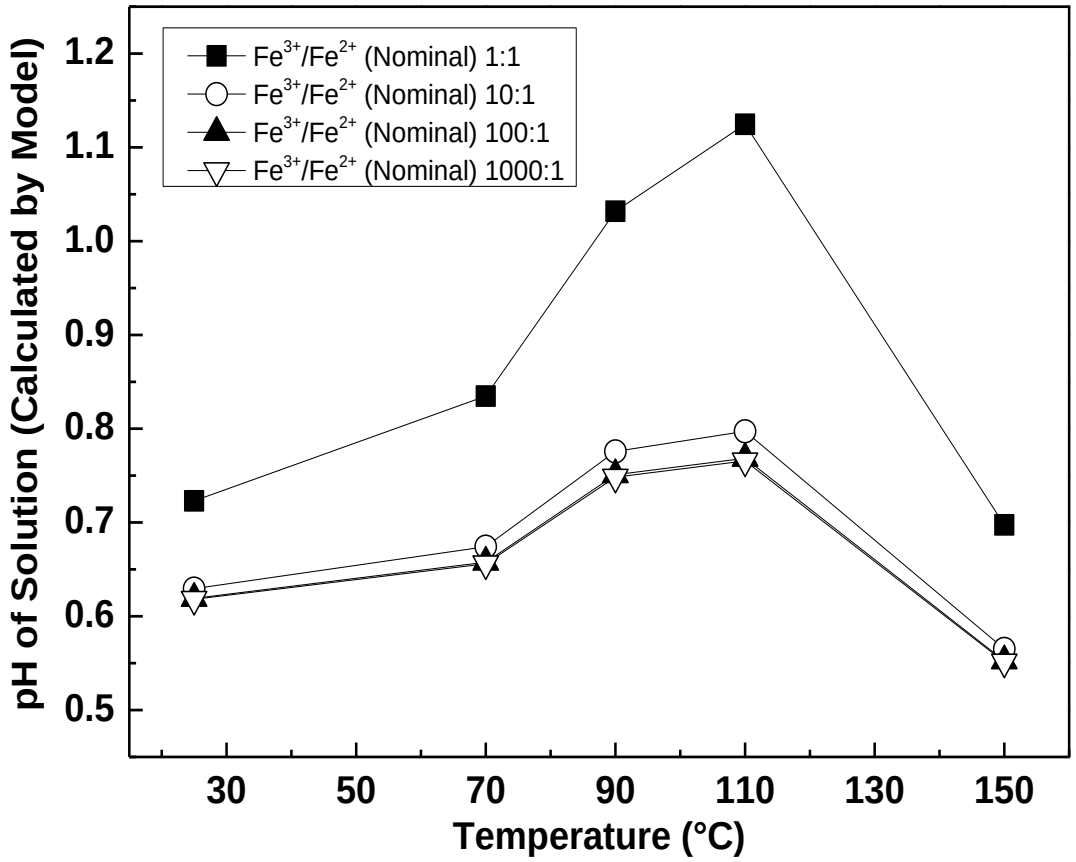

Figure 5-8 Calculated pH of the Fe(II)-Fe(III)-H_2SO_4 solutions at [H_2SO_4] = 0.31 mol/kg and $[Fe^{3+}]_{total}$ = 0.18 mol/kg with different nominal Fe^{3+}/Fe^{2+} ratios in the temperature range of 25 ℃-150 ℃.

Under the same nominal Fe^{3+}/Fe^{2+} ratio the pH increases gradually with temperature up to 110 ℃ and, as expected, a sharp drop occurs at 150 ℃, with a terminal pH value even lower than that at 25 ℃. This phenomenon can be explained by the above-mentioned Eq. (5-3):

$$2Fe^{3+} + 3H_2O \leftrightarrow Fe_2O_3 + 6H^+$$

At 150 ℃, the hydrolysis of ferric sulfate and precipitation of ferric oxide will take place and this can cause an increase in the free H^+ concentration in the solution which governs the solubility of Fe(III).

The above results justify the exclusion of hydroxide (OH^-) ions in the speciation model since their concentration is negligible in these very acidic solutions. Similarly, iron hydroxyl complexes would play a minor role in these solutions.

5.3.4.4 Analysis of Real Ionic Strength

Figure 5-9 shows the calculated real ionic strength in Fe(II)-Fe(III)-H_2SO_4 solutions, which are lower than 0.85 throughout the studied temperature range. Similar to the pH variation at a given temperature, the real ionic strength decreases first and finally levels off as the nominal Fe^{3+}/Fe^{2+} ratio approaches 1000:1.

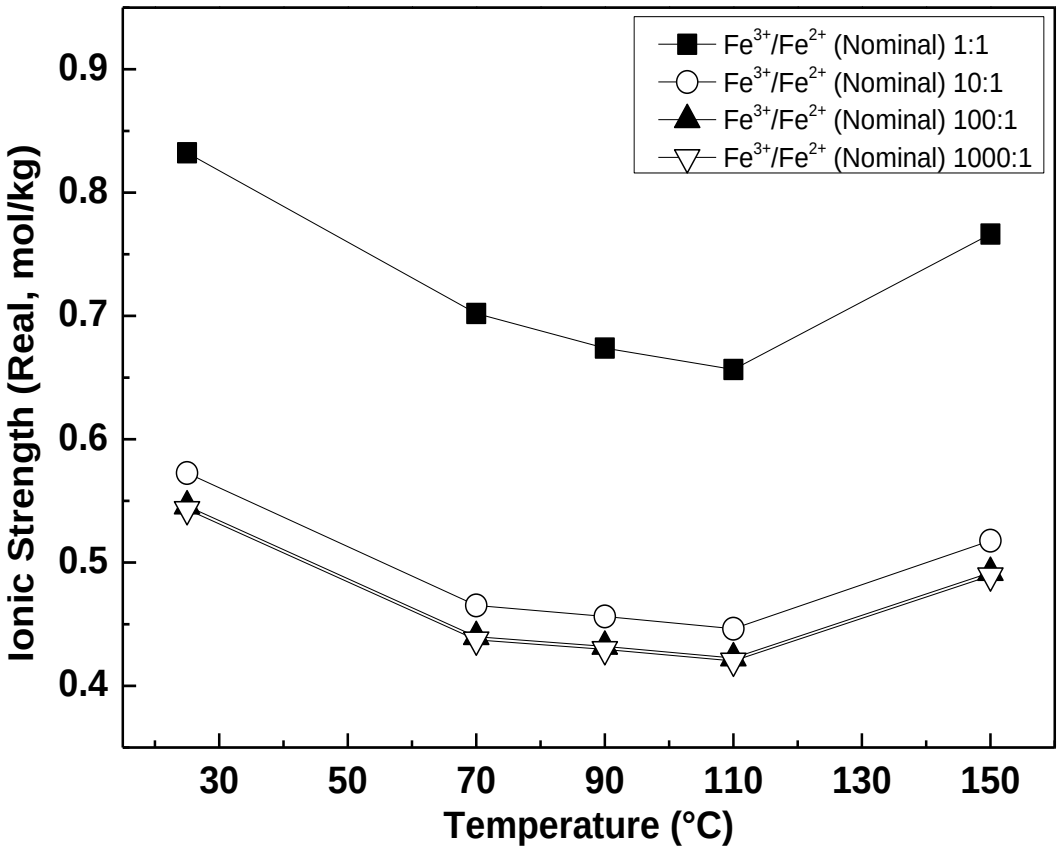

Figure 5-9 Calculated real ionic strength of the Fe(II)-Fe(III)-H_2SO_4 solutions at $[H_2SO_4]$ = 0.31 mol/kg and $[Fe^{3+}]_{total}$ = 0.18 mol/kg with different nominal Fe^{3+}/Fe^{2+} ratios in the temperature range of 25 ℃-150 ℃.

Under the same nominal Fe^{3+}/Fe^{2+} ratio, increasing the temperature from 25 ℃ to 110 ℃ was observed to result in a gradual decrease of the real ionic strength. This result may be due to ion association to form more stable species (from highly charged ions to less charged ion complexes), which will result in a decrease of the concentration of species with higher charge. In addition, despite the fact that the concentrations of ionic Fe(III) species decreases because of the formation of Fe_2O_3, an increase of ionic strength from 110 to 150 ℃ was observed for all nominal Fe^{3+}/Fe^{2+} ratios. This result may be attributed to a combination of the following two

factors: (1) the second-most abundant Fe(II) species at this temperature is $FeHSO_4^+$ and (2) there is an increase in the free H^+ concentration in the solution owing to the hydrolysis of free ferric. As a result, there is an increase in the concentration of charged ion species in the solution at 150 ℃.

The nominal ionic strengths for the four different nominal Fe^{3+}/Fe^{2+} ratios are in the range of 2.26-2.98 mol/kg. It is clear that the calculated real ionic strengths predicted by the model using the real concentration of charged species are much lower than those calculated using the nominal species concentrations in all cases. This is due to the fact that the concentrations of the species with higher charges (such as Fe^{2+}, Fe^{3+} and SO_4^{2-}) considerably diminishes due to the formation of various complexes with lower charges (such as HSO_4^-, $FeHSO_4^+$ and $FeSO_4^+$). Because the effective ionic strengths of the solutions used in this study are low enough, the use of the B-dot equation to calculate the single ion activity coefficients is reasonable.

Validation of the present model could not be extended to a wider range of composition concentrations and temperatures due to the generation of iron precipitates and the presence of additional species. Further work is required in order to expand our understanding of this quaternary system.

5.4 Summary

The speciation of the quaternary H_2SO_4-$Fe_2(SO_4)_3$-$FeSO_4$-H_2O system was studied by thermodynamic modeling under conditions most relevant to the hydrometallurgical industry. The main species involved were first identified, and then the thermodynamic data for all of the species were collected and critically assessed. These data were used to estimate the activity coefficients of species by B-dot equation, and to calculate the equilibrium constants by the Lewis formulation of the Criss-Cobble correspondence principle from 25 ℃ to 150 ℃.

Results from the calculated distribution of the main ferric and ferrous species as a function of temperature, iron and acid concentration, and the nominal Fe^{3+}/Fe^{2+} ratio reveal that most of the Fe(III) is distributed as complexes or precipitates and the free ferric ion accounts for only a minor percentage, whereas a large amount of Fe(II) exists in the form of free ferrous ion. Moreover, under the same nominal Fe^{3+}/Fe^{2+} ratio, a temperature increase in the range of 25 ℃-150 ℃ leads to a decline in the free Fe^{3+} concentration, whereas the free Fe^{2+} concentration is relatively stable. At lower pH, free ferric and ferrous ions are more abundant.

Under all of the investigated conditions, $FeSO_4^+$ is always the predominant species for Fe(III) in the aqueous solution. At 150 ℃, a large amount of Fe(III) precipitated as Fe_2O_3, with the largest value of 61.7% obtained when the nominal Fe^{3+}/Fe^{2+} ratio was 1:1. The percentage of formed Fe_2O_3 under the other three nominal Fe^{3+}/Fe^{2+} ratios is relatively stable and lower than that under nominal Fe^{3+}/Fe^{2+} ratio of 1:1, due to relatively lower amount addition of $FeSO_4$. This variation in the amount of hematite as a function of $FeSO_4$ concentrations is similar to that published in the literature with an addition of divalent metal sulfates like $ZnSO_4$ or $MgSO_4$ for a relatively low free sulfuric acid concentration.

The validity of the proposed model was confirmed by reliable prediction of measured redox potential from 25 ℃ to 150 ℃. At 150 ℃, the fact that there exists a very good agreement between the ferric solubility calculated by the present model and that measured by previous work, further justifies the validity of the model. Extensive analysis and review of the calculated pH and real ionic strength of the solution provides an additional affirmation of the validity of the present work.

In summary, this work confirms that the model developed in this study is a promising method for the study of the speciation of the quaternary H_2SO_4-$Fe_2(SO_4)_3$-$FeSO_4$-H_2O system

over a wide range of solution composition and temperature. The reliable prediction of redox potential by the speciation model is particularly valuable. Therefore, it can be expected that the findings in the present work will facilitate the research on the kinetics of the Fe^{3+}/Fe^{2+} couple in general and in particular on the surface of chalcopyrite.

6 Development of an Expression to Predict the Redox Potential of the Fe^{3+}/Fe^{2+} Couple up to 150 ℃

6.1 Introduction

Fe^{3+} is the most important and industrially relevant surrogate oxidant in many sulfide mineral leaching processes. It is often already present in hydrometallurgical leaching streams, due to the dissolution of minerals such as chalcopyrite, pyrite, and bornite. As clearly presented in the previous discussions, the redox potential of H_2SO_4-$Fe_2(SO_4)_3$-$FeSO_4$-H_2O solutions is one of the key operating parameters, which is determined by the activity ratio of free ferric to free ferrous (rather than the nominal concentration ratio) based on the Nernst equation. As a result, the speciation of the system is important in determining the redox potential (to obtain the relative amounts of free ferric and ferrous and the accompanying activity coefficients in the solution).

The model developed in Chapter 5 provides a mathematical tool capable of quantifying the concentration of free ions and complexes (and precipitates at higher temperature) as functions of temperature, acidity level, initial total amount of iron, and nominal ferric-to-ferrous ratio. In the subsequent discussion, results of this thermodynamic model will help in the interpretation of the change of redox potential with temperature for all nominal Fe^{3+}/Fe^{2+} ratios.

The present chapter aims to provide new data on the temperature dependence of the real Fe^{3+}/Fe^{2+} concentration ratio, real ratios of the activity coefficient for free ferric and free ferrous and the standard electrode potential of the Fe^{3+}/Fe^{2+} couple. These results are then used to analyze the contribution of each part to the overall redox potential of the Fe^{3+}/Fe^{2+} couple, and subsequently employed to develop a novel expression to accurately predict the redox potential of the H_2SO_4-$Fe_2(SO_4)_3$-$FeSO_4$-H_2O system. The proposed expression is determined only by the

variables of temperature and nominal Fe^{3+}/Fe^{2+} ratio. Measured redox potentials by the present author and by others in the literature agree very well with those predicted by this expression, independent of the nominal concentrations of Fe^{3+} and H_2SO_4. This information will be used in further investigations of the electrochemical reduction kinetics of the Fe^{3+}/Fe^{2+} couple on chalcopyrite as well as the mechanism of chalcopyrite leaching processes.

6.2 Speciation Results and Their Application to the Prediction of the Redox Potentials of the Fe^{3+}/Fe^{2+} Couple at 25 ℃-150 ℃

As mentioned previously, after obtaining the speciation results for the H_2SO_4-$Fe_2(SO_4)_3$-$FeSO_4$-H_2O system, what particularly interests us is the temperature dependence of the free ferric and ferrous ion concentrations and their real ratios in order to systematically study the reversible potential of the Fe^{3+}/Fe^{2+} couple.

6.2.1 Speciation Results of the Developed Model to Calculate the Redox Potential of the Fe^{3+}/Fe^{2+} Couple

The temperature dependence of the calculated real Fe^{3+}/Fe^{2+} ratio in the Fe(II)-Fe(III)-H_2SO_4 solutions under different nominal Fe^{3+}/Fe^{2+} ratios is presented in Figure 6-1. At each temperature, the calculated real Fe^{3+}/Fe^{2+} ratio is much lower than the nominal ratio, and at the same time, it is worth noting that from 25 ℃ to 150 ℃, under each given nominal Fe^{3+}/Fe^{2+} ratio, the calculated real ratios of Fe^{3+}/Fe^{2+} substantially declines with temperature. This implies that the real Fe^{3+}/Fe^{2+} ratio is markedly dependent upon temperature and the composition of the electrolyte. In fact, a plot of the logarithm of the real Fe^{3+}/Fe^{2+} ratio as a function of temperature (℃) is linear. Also, surprisingly, the four linear plots obtained under different nominal Fe^{3+}/Fe^{2+} ratios display almost the same slope but with different intercepts. Particularly, with the nominal

Fe^{3+}/Fe^{2+} ratios of 10:1, 100:1 and 1000:1, the slopes of these three linear plots were identical. Under each nominal ratio, the best fit for the temperature dependence of the real Fe^{3+}/Fe^{2+} ratio and the corresponding correlation coefficient were obtained and shown as follows:

$$\log \frac{C_{\text{ferric, real}}}{C_{\text{ferrous, real}}} = 2.67 - 1.35 \times 10^{-2} \times T(\text{K}) \;\; R^2 = 0.9607 \;\; (1{:}1) \qquad (6\text{-}1)$$

$$\log \frac{C_{\text{ferric, real}}}{C_{\text{ferrous, real}}} = 3.25 - 1.17 \times 10^{-2} \times T(\text{K}) \;\; R^2 = 0.9544 \;\; (10{:}1) \qquad (6\text{-}2)$$

$$\log \frac{C_{\text{ferric, real}}}{C_{\text{ferrous, real}}} = 4.23 - 1.17 \times 10^{-2} \times T(\text{K}) \;\; R^2 = 0.9548 \;\; (100{:}1) \qquad (6\text{-}3)$$

$$\log \frac{C_{\text{ferric, real}}}{C_{\text{ferrous, real}}} = 5.23 - 1.17 \times 10^{-2} \times T(\text{K}) \;\; R^2 = 0.9547 \;\; (1000{:}1) \qquad (6\text{-}4)$$

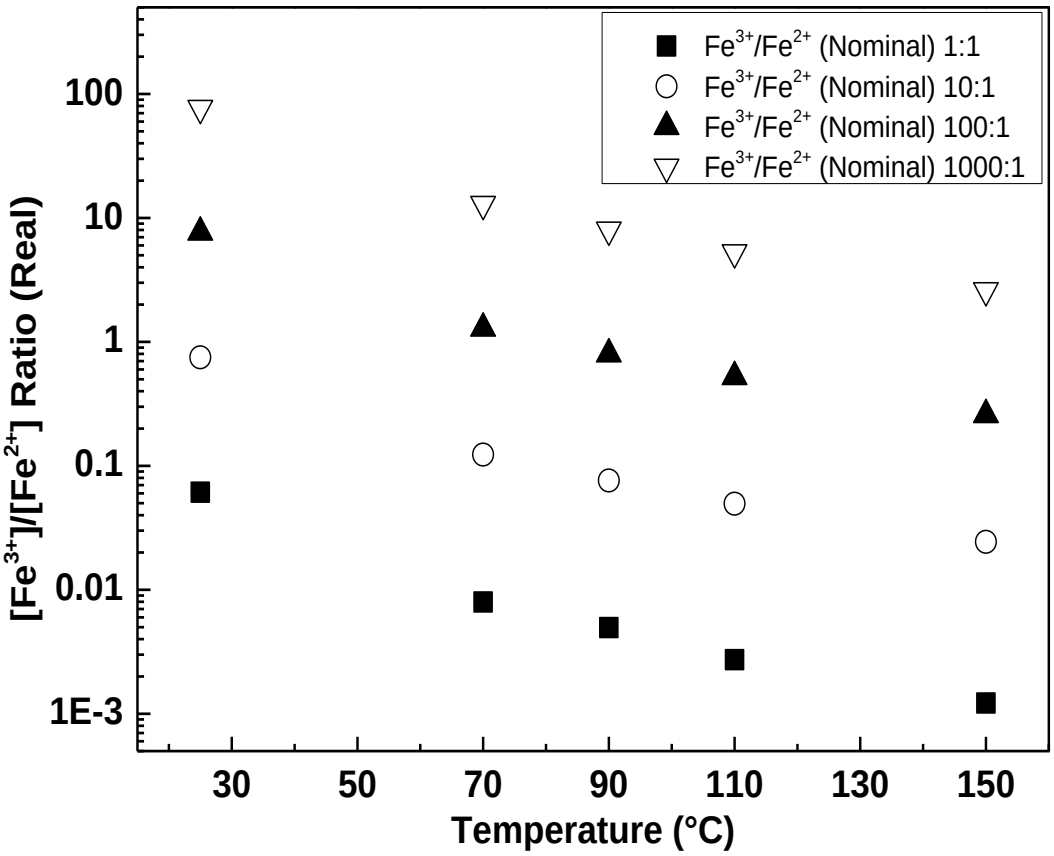

Figure 6-1 Calculated real Fe^{3+}/Fe^{2+} ratios in the Fe(II)-Fe(III)-H_2SO_4 solutions at $[H_2SO_4]$ = 0.31 mol/kg and $[Fe^{3+}]_{total}$ = 0.18 mol/kg with different nominal Fe^{3+}/Fe^{2+} ratios in the temperature range of 25 ℃-150 ℃.

Apart from the real Fe^{3+}/Fe^{2+} ratios, in order to calculate the redox potential of Fe^{3+}/Fe^{2+} couple, the standard electrode potential of the Fe^{3+}/Fe^{2+} couple (770 mV versus SHE at 25 ℃), as well as the single ion activity coefficients for free Fe^{3+} and Fe^{2+} ions, are also required to invoke the Nernst equation:

$$E = E^{o} + \frac{2.303RT}{nF} \times \log \frac{\gamma_{\text{ferric}}}{\gamma_{\text{ferrous}}} + \frac{2.303RT}{nF} \times \log \frac{C_{\text{ferric}}}{C_{\text{ferrous}}} \qquad (6\text{-}5)$$

The standard electrode potential of the Fe^{3+}/Fe^{2+} couple ($E°$, mV) at high temperatures was calculated based on thermodynamic data ($\Delta G°$) according to the above-mentioned Lewis formulation of the Criss-Cobble correspondence principle. The values are shown in Table 6-1. These calculated standard potentials for the ferric-ferrous couple agree very well with those in published literature [152-154]. It should be noted that the previously published values usually refer to the SHE at the operating temperature T (with definition of SHE as 0 at any temperature). However, in the present work all of the potentials are with respect to the SHE at 25 ℃ (the SHE potential is defined herein as a function of temperature and is 0 only at 25 ℃). This definition is preferred as the SHE is not in fact 0 at elevated temperature (a potential can be measured between a SHE at 25 ℃ and one at 100 ℃). Therefore, to compare the values presented herein to some of those presented in the previously published literature, the latter should be converted first according to Eq. (4-2). A comparison of those standard potentials is presented in Figure 6-2 and it is found that all of these data are in good agreement.

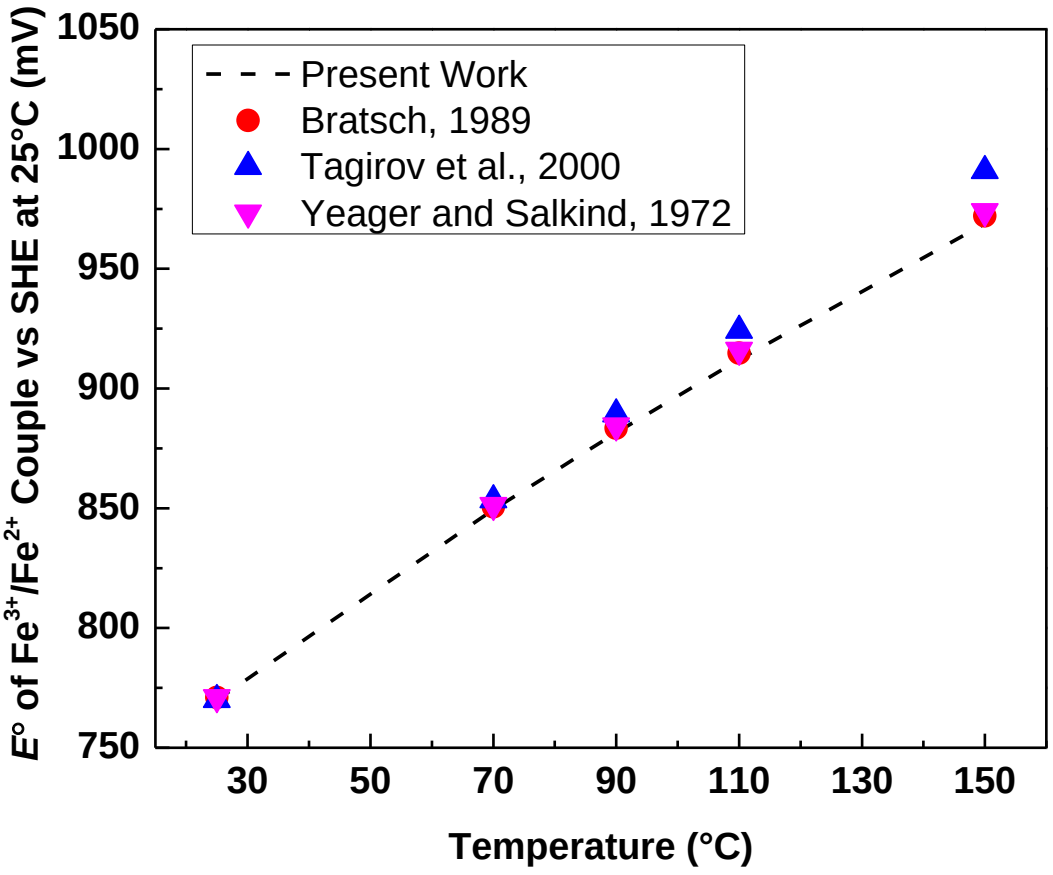

Figure 6-2 Comparison of the calculated standard electrode potentials of the Fe^{3+}/Fe^{2+} couple with those in published literature in the temperature range of 25 ℃-150 ℃.

Mathematical regression shows that the calculated standard electrode potential of the Fe^{3+}/Fe^{2+} couple varies linearly with temperature. The best fit was provided by the following relationship ($E°$ data are from Table 6-1):

$$E^o(\text{mV}) = 1.6 \times T(\text{K}) + 300.2 \qquad (6\text{-}6)$$

The correlation coefficient was 0.9967.

As to the single ion activity coefficients for species involved in the present study, they were estimated by the above-noted B-dot equation. A detailed discussion on the applicability of this model will be given later. Calculated results show that the ratios of the activity coefficient

for free ferric and free ferrous are typically only affected by temperature, and remain practically constant at each temperature under different nominal Fe^{3+}/Fe^{2+} ratios. The ratios of the activity coefficient for free ferric and ferrous ranged from 0.35 to 0.27 (each is an average of the values under four different nominal Fe^{3+}/Fe^{2+} ratios), with the temperature increasing from 25 ℃ to 150 ℃. This ratio of activity coefficients also varies linearly with temperature. The obtained activity coefficient ratios for free ferric and ferrous were included in the term $(2.303RT/nF)\times\log(\gamma_{ferric}/\gamma_{ferrous})$ where this entire expression is defined here as E_1 (mV), and which yields the potential values resulting from the single ion activity coefficients. The variation of E_1 with temperature can be estimated with the following regressed expression (The original E_1 values calculated from the model results are -27.02 mV at 25 ℃, -32.47 mV at 70 ℃, -35.55 mV at 90 ℃, -38.97 mV at 110 ℃ and -48.12 mV at 150 ℃, respectively):

$$E_1(\text{mV}) = -0.6\times10^{-3}\times[T(\text{K})]^2 + 0.3\times T(\text{K}) - 57.5 \quad (6\text{-}7)$$

The corresponding correlation coefficient was 0.9997.

All data calculated using the model results for the standard and reversible potentials of the Fe^{3+}/Fe^{2+} couple at different temperatures are shown in Table 6-1. The standard electrode potential of the Fe^{3+}/Fe^{2+} couple increased with temperature. Speciation results indicate that for a given temperature the model-calculated potentials increase considerably with the nominal Fe^{3+}/Fe^{2+} ratios. However, from 25 ℃ to 150 ℃, the potentials predicted by the model increase gradually only when the nominal Fe^{3+}/Fe^{2+} ratios are 10:1, 100:1 and 1000:1. Interestingly, the predicted potentials are relatively stable at the nominal Fe^{3+}/Fe^{2+} ratio of 1:1 and no significant change was observed as the temperature increased. The reason for this unexpected behavior at the Fe^{3+}/Fe^{2+} ratio of 1:1 lies in the fact that at each temperature, the real Fe^{3+}/Fe^{2+} ratio in the solution is much lower in such a condition, typically lower than 0.1 and on the order of 10^{-2} or

10^{-3}. Such small values will result in a large negative value for $(2.303RT/nF) \times \log (C_{ferric}/C_{ferrous})$ (this whole item is defined as E_2, mV), which is the third component of the Nernst equation. This implies that although the $E°$ increases considerably with temperature, and E_1 is relatively stable at each temperature, the calculated reversible potential for the Fe^{3+}/Fe^{2+} couple based on the sum of $E°$, E_1 and E_2 remains essentially unchanged at the 1:1 ratio condition.

Table 6-1 Standard electrode potential of Fe^{3+}/Fe^{2+} couple calculated by the Criss-Cobble method and redox potential of Fe^{3+}/Fe^{2+} couple predicted by the model in Fe(II)-Fe(III)-H_2SO_4 solutions at $[H_2SO_4]$ = 0.31 mol/kg and $[Fe^{3+}]_{total}$ = 0.18mol/kg with different nominal Fe^{3+}/Fe^{2+} ratios in the range of 25-150 ℃.

Fe^{3+}/Fe^{2+} (Nominal)	$E_{Ferric/Ferrous}$ (25°C)		$E_{Ferric/Ferrous}$ (70°C)		$E_{Ferric/Ferrous}$ (90°C)		$E_{Ferric/Ferrous}$ (110°C)		$E_{Ferric/Ferrous}$ (150°C)	
	$E°$	Model	$E°$	Model	$E°$	Model	$E°$	Model	$E°$	Model
1:1	770.0	670.5	849.5	673.1	881.6	678.9	912.2	677.1	968.8	674.8
10:1	770.0	735.7	849.5	755.3	881.6	765.7	912.2	774.2	968.8	785.5
100:1	770.0	795.6	849.5	824.8	881.6	839.3	912.2	852.3	968.8	871.8
1000:1	770.0	854.8	849.5	893.1	881.6	911.6	912.2	928.5	968.8	956.0

In addition, the very low real Fe^{3+}/Fe^{2+} ratio for the nominal 1:1 condition can be ascribed to the following two facts: (1) under the nominal Fe^{3+}/Fe^{2+} ratio of 1:1, a relatively large amount of Fe^{2+} added to the solution causes a drop in the real Fe^{3+}/Fe^{2+} ratio; (2) at the same time, a large amount of SO_4^{2-} (included with Fe^{2+}) addition also diminishes the free Fe^{3+} concentration due to ion association to form more stable Fe(III) species.

6.2.2 Development of an Expression to Predict the Redox Potential of the Fe^{3+}/Fe^{2+} Couple up to 150 ℃

At present, to the knowledge of the author there are no theoretical methods available for predicting the redox potential of the H_2SO_4-$Fe_2(SO_4)_3$-$FeSO_4$-H_2O system through a wide range of temperature and electrolyte composition. Given the variation of $E°$, E_1 and E_2 with temperature and nominal Fe^{3+}/Fe^{2+} ratio, regression of the dependence of the calculated reversible potential of the Fe^{3+}/Fe^{2+} couple was carried out, and an empirical relationship was developed. First, according to the Equations 6-2, 6-3 and 6-4, with the nominal Fe^{3+}/Fe^{2+} ratios of 10:1, 100:1 and 1000:1, the slopes of these three linear plots were identical, with the intercept difference of 1 when increasing the nominal Fe^{3+}/Fe^{2+} ratio. By taking advantage of this fact, when calculating E_2, an equation can be obtained for all three nominal Fe^{3+}/Fe^{2+} ratios:

$$E_2(\text{mV}) = -2.33\times10^{-3}\times[T(\text{K})]^2 + 0.45\times T(\text{K}) + \frac{2.303R}{nF}\times T(\text{K})\times10^3\times\log\frac{C_{\text{ferric, nominal}}}{C_{\text{ferrous, nominal}}} \quad (6\text{-}8)$$

Then, by adding all three items $E°$, E_1 and E_2, the following equation was developed by adjusting constants in order to fit all of the data points in this study:

$$E(\text{mV}) = -1\times10^{-3}\times[T(\text{K})]^2 + 0.91\times T(\text{K}) + \frac{2.303R}{nF}\times T(\text{K})\times10^3\times\log\frac{C_{\text{ferric, nominal}}}{C_{\text{ferrous, nominal}}} + 492 \quad (6\text{-}9)$$

The overall error between the calculated values from the model and the predicted values from the equation was minimized by inspection. Please note that all of the potential E(mV)

calculated by the above equation are referred to the SHE at 25 ℃. This equation can be applied to the cases under the given nominal concentrations of H_2SO_4 (0.31 mol/kg) and Fe^{3+} (0.18 mol/kg) when the nominal Fe^{3+}/Fe^{2+} ratios are 10:1, 100:1 and 1000:1 in the temperature range of 25 ℃-150 ℃, with a deviation lower than 5 mV. Its slope is the same as that of the Nernst equation. Regression of the data with the nominal Fe^{3+}/Fe^{2+} ratio of 1:1 is not included in light of the fact that the potentials calculated by the speciation model were relatively stable and independent of temperature in such a case. Nevertheless, the developed expression can still be used to evaluate the redox potential at lower temperature with the nominal Fe^{3+}/Fe^{2+} ratio of 1:1. Actually, the difference between the potentials predicted by the speciation model (as shown in Table 6-1) and calculated by the proposed expression is only about 4.5 mV at 25 ℃, and this deviation increases gradually with increasing temperature, with the largest value of 23.9 mV obtained at 150 ℃.

At 150 ℃, considering the fact that the Fe(III) existing in the form of Fe_2O_3 as a precipitate has no influence on the redox potentials of the liquid phase, a modification of Eq. (6-9) was made in order to replace the term "$C_{\text{ferric, nominal}}$" (total nominal ferric added to the autoclave) with "$C_{\text{ferric, dissolved}}$" (total ferric existing in the liquid solution after the approach to equilibrium by hydrolysis). First, the author found that there is a linear relationship between "$C_{\text{ferric, nominal}}/C_{\text{ferrous, nominal}}$" and "$C_{\text{ferric, dissolved}}/ C_{\text{ferrous, nominal}}$":

$$\frac{C_{\text{ferric, nominal}}}{C_{\text{ferrous, nominal}}} = 1.74 \times \frac{C_{\text{ferric, dissolved}}}{C_{\text{ferrous, nominal}}} + 0.32 \tag{6-10}$$

The corresponding correlation coefficient was 1. Then, by adding Eq. (6-10) into Eq. (6-9), a new equation can be obtained:

$$E(\text{mV}) = -1\times10^{-3}\times[T(\text{K})]^2 + 0.91\times T(\text{K}) + \frac{2.303R}{nF}\times T(\text{K})\times10^3\times\log\left(\frac{1.74\times C_{\text{ferric, dissolved}}}{C_{\text{ferrous, nominal}}} + 0.32\right) + 492 \tag{6-11}$$

Please note that Eq. (6-11) can be used under the conditions in the present study only at 150 ℃, and the potentials calculated by Eq. (6-11) agree very well those calculated by Eq. (6-9).

Obviously, there is some concern regarding the expression Eq. (6-9): whether it can be supported by other experimental evidence, and be used to calculate the redox potentials under different conditions such as nominal concentrations of H_2SO_4 and Fe^{3+}, nominal Fe^{3+}/Fe^{2+} ratio and temperature. This will be discussed in the following section.

6.3 Applicability of the Developed Expression-Comparison with Experimental Results by Previous Work

The applicable scope of the developed expression Eq. (6-9) was investigated based on the experimental results in the literature in terms of nominal amounts of Fe^{3+} and H_2SO_4, nominal Fe^{3+}/Fe^{2+} ratio and temperature. Figure 6-3 shows the comparison of the redox potentials in the Fe(II)-Fe(III)-H_2SO_4 solutions predicted by the developed expression Eq. (6-9) and measured by experiments from Dry and Bryson (1988) [33] at various nominal concentrations of H_2SO_4 and Fe(III)/Fe(II) with different nominal Fe^{3+}/Fe^{2+} ratios at 22 ℃ and 90 ℃. In Figure 6-3a it is demonstrated that for each nominal Fe^{3+}/Fe^{2+} ratio, the measured redox potentials are independent of the nominal concentrations of Fe^{3+} and H_2SO_4. The measured redox potentials are in good agreement with the results calculated by the expression. It should be noted that wide ranges of nominal Fe^{3+} concentration (0.01-0.99 mol/L), nominal H_2SO_4 concentration (0.102-1.021 mol/L) and nominal Fe^{3+}/Fe^{2+} ratios (from 0.01:1 to 100:1) are employed, and the nominal ionic strength of the studied solutions is in the range of 0.42-14.45 mol/L. This means that at 22 ℃, the expression is applicable over a wider range of solution composition, and there is almost no effect of nominal concentrations of Fe^{3+} and H_2SO_4 on the redox potential.

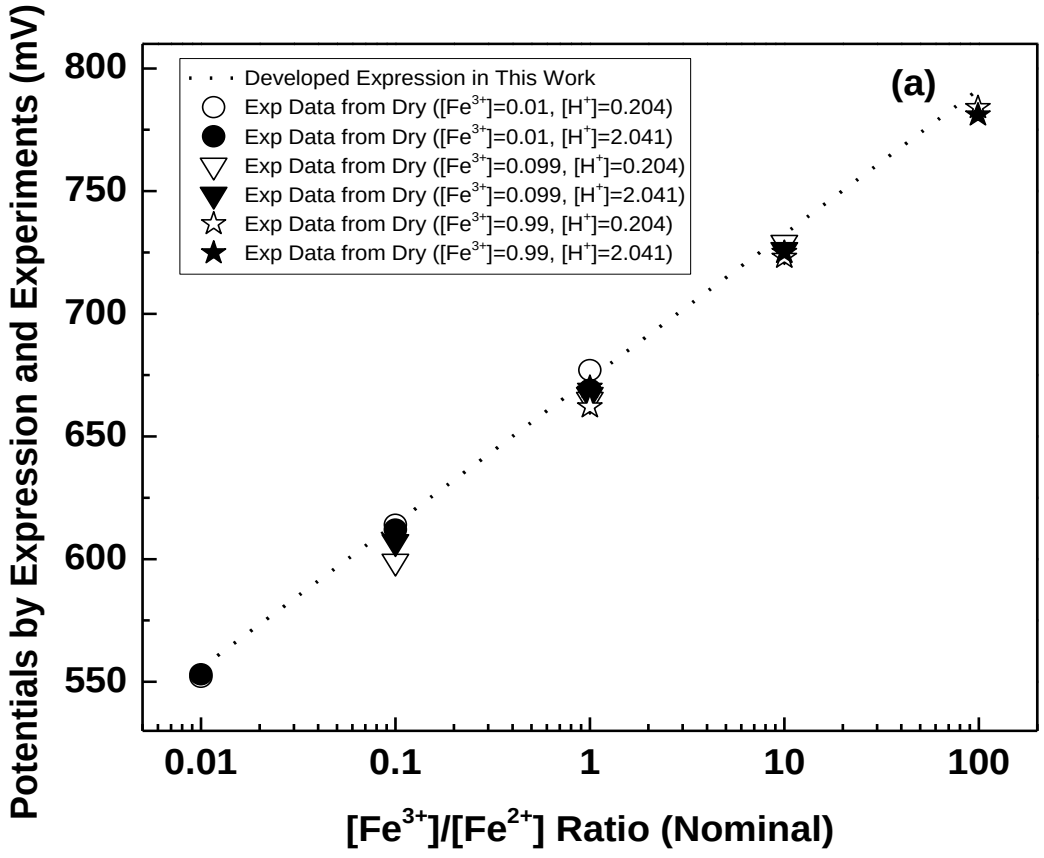

Figure 6-3 Comparison of the potentials predicted by the developed expression Eq. (6-9) in this work and measured by experiments in the Fe(II)-Fe(III)-H_2SO_4 solutions from Dry and Bryson (1988) at various nominal concentrations of H_2SO_4 and Fe(III)/Fe(II) with different nominal Fe^{3+}/Fe^{2+} ratios: (a) at 22 ℃; (b) at 90 ℃. The unit of the concentrations in the figure is mol/L. Detailed information on the nominal concentrations of Fe^{3+} and Fe^{2+} at 90 ℃ can be found in the literature.

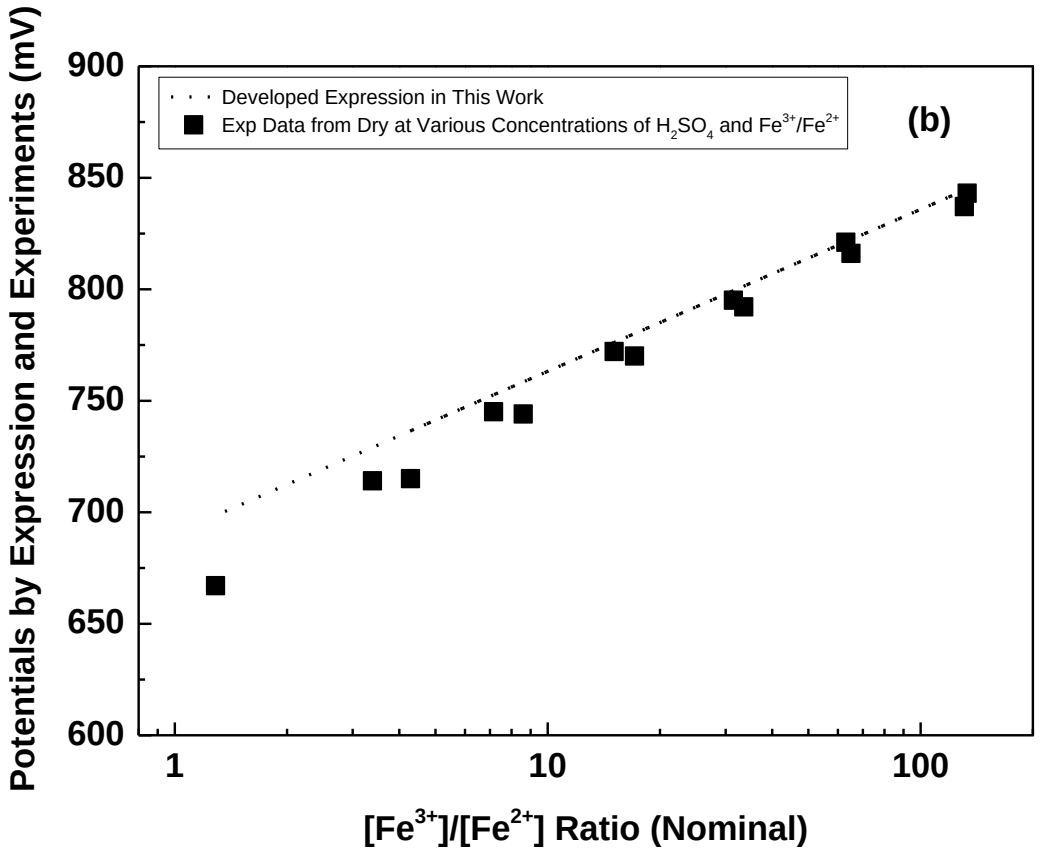

Figure 6-3 Continued.

Furthermore, in Figure 6-3b, at 90 ℃, it is interesting to observe that when the nominal Fe^{3+}/Fe^{2+} ratios are around or larger than 10:1 (the values of the two points around 10:1 in Figure 6-3b are 7.2 and 8.6), the measured redox potentials agree very well with that predicted by the expression, unrelated to the nominal concentrations of Fe^{3+} and H_2SO_4. As the nominal Fe^{3+}/Fe^{2+} ratios decrease (for example, around 3.4 and 4.3), an acceptable deviation of the measured redox potentials from that calculated by the expression occurs. However, when the nominal Fe^{3+}/Fe^{2+} ratio approaches 1:1, a larger deviation was found and this trend is similar to the findings in this work. It should be noted that the nominal concentrations of Fe^{3+}, Fe^{2+} and H_2SO_4 used in the work of Dry and Bryson are discrete values at 90 ℃ in the range of 1.223-1.866 mol/L, 0.013-

0.951 mol/L and 0.643-0.889 mol/L, respectively, and the nominal ionic strength typically ranged from 15.08 mol/L to 15.94 mol/L.

From the above analysis, it seems that the redox potential depends significantly on the nominal Fe^{3+}/Fe^{2+} ratio and temperature, but is almost unaffected by the nominal concentration of Fe^{3+}, Fe^{2+} and H_2SO_4. The developed expression Eq. (6-9) can even be applied over a wider range of nominal Fe^{3+}/Fe^{2+} ratio at lower temperature. To confirm this and to obtain more detailed information, the effect of nominal amounts of Fe^{3+}, Fe^{2+}, H_2SO_4 and the nominal Fe^{3+}/Fe^{2+} ratio on the redox potential was investigated at room temperature based on measured data published in the literature [53, 69, 155]. In Figure 6-4, it is shown that at each given nominal Fe^{3+}/Fe^{2+} ratio, there is almost no difference for the redox potentials between the measured results by three different authors and that calculated by the expression Eq. (6-9) presented herein. At the same time, it is worth noting that the measured redox potentials at the 1:1 ratio from three different sources are nearly identical to each other. Also, it should be emphasized that a wider range of nominal Fe^{3+}/Fe^{2+} ratio (from 0.01:1 to 2000:1) is used and the solution composition was different in the studies used for Figure 6-4.

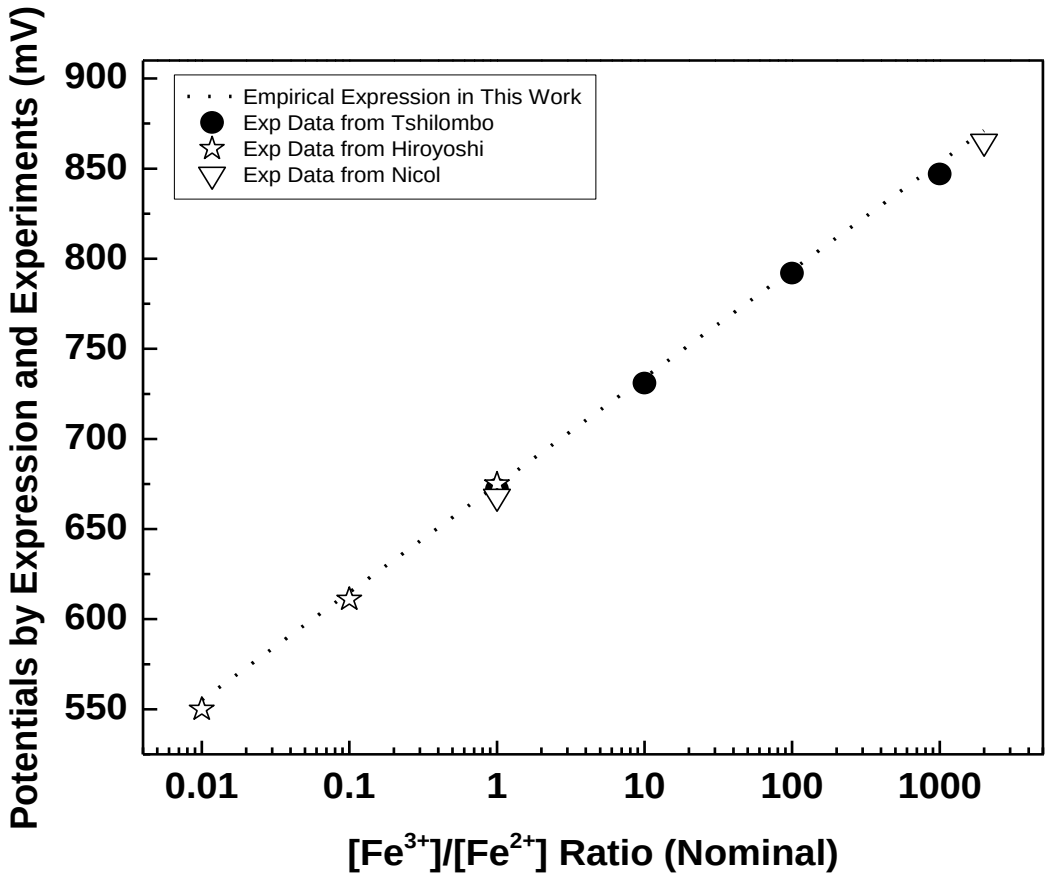

Figure 6-4 Comparison of the potentials predicted by the developed expression Eq. (6-9) in this work and measured by experiments in the Fe(II)-Fe(III)-H_2SO_4 solutions from Hiroyoshi et al. (2001), Tshilombo (2004) and Nicol and Lázaro (2002) at various nominal concentrations of H_2SO_4 and Fe(III)/Fe(II) with different nominal Fe^{3+}/Fe^{2+} ratios at room temperature.

(Hiroyoshi: $[H_2SO_4]$ = 0.1 mol/L and $[Fe^{3+}]_{total}$ = 0.01 mol/L; Tshilombo: $[iron]_{total}$ = 5 g/L and pH = 1.4; Nicol and Lázaro: pH = 1.5, 10 g/L Fe^{3+} and 5 mg/L Fe^{2+} at 2000:1 ratio, 5 g/L Fe^{3+} and 5 g/L Fe^{2+} at 1:1 ratio)

The above analyses of the experimental results from the literature strongly support the proposed expression Eq. (6-9) in this work. It appears that the redox potential could be easily and accurately determined based on the variables of temperature and nominal Fe^{3+}/Fe^{2+} ratio, and there is almost no change in redox potential caused by the nominal concentrations of H_2SO_4 and Fe^{3+}. Moreover, the developed expression Eq. (6-9) is probably applicable to more general cases at or around room temperature (or maybe slightly higher temperature), in spite of the fact that a deviation occurs at higher temperatures (for example at 90 ℃) under lower nominal ratios. These results are particularly valuable and of interest: at any given temperature, the redox potential of quaternary H_2SO_4-$Fe_2(SO_4)_3$-$FeSO_4$-H_2O system is solely determined by the nominal Fe^{3+}/Fe^{2+} ratio and a temperature dependence of the same slope as the Nernst equation. This expression avoids the complicated calculations of the standard electrode potential and the activity coefficient.

6.4 Summary

Based on the model developed in Chapter 5, the temperature dependence of the real Fe^{3+}/Fe^{2+} ratios and their activity coefficient ratios were obtained. The calculated real Fe^{3+}/Fe^{2+} ratio is much lower than the nominal ratio, and from 25 ℃ to 150 ℃, under each given nominal Fe^{3+}/Fe^{2+} ratio, the calculated real ratio of Fe^{3+}/Fe^{2+} substantially declines with temperature. The activity coefficient ratios are typically only affected by temperature, and remain practically constant at each temperature under different nominal Fe^{3+}/Fe^{2+} ratios. These results, together with the calculated standard electrode potential of the Fe^{3+}/Fe^{2+} couple, were employed to systematically study the redox potential of the Fe^{3+}/Fe^{2+} couple. For a given temperature, the model-calculated potentials increase considerably with the nominal Fe^{3+}/Fe^{2+} ratio. However, from 25 ℃ to 150 ℃, the potentials predicted by the model increase gradually only when the

nominal Fe^{3+}/Fe^{2+} ratios are 10:1, 100:1 and 1000:1 (with its values in the range of ~736–956 mV), while at the nominal Fe^{3+}/Fe^{2+} ratio of 1:1 they are relatively stable (typically between ~671 and 679 mV) and no significant change was observed as the temperature increased. The speciation model explains the change of redox potential with temperature for all nominal Fe^{3+}/Fe^{2+} ratios.

An expression (Eq. 6-9, reproduced below) determined only by the variables of temperature and nominal Fe^{3+}/Fe^{2+} ratio was developed to predict the redox potential of the Fe^{3+}/Fe^{2+} couple. Measured redox potentials in the literature agree very well with those predicted by the developed expression, independent of the nominal concentrations of Fe^{3+} and H_2SO_4. Moreover, the expression is probably applicable to more general cases at or around room temperature. Future work will be required to determine the broader range of applicability of this equation.

$$E(\mathrm{mV}) = -1\times10^{-3}\times[T(\mathrm{K})]^2 + 0.91\times T(\mathrm{K}) + \frac{2.303R}{nF}\times T(\mathrm{K})\times10^{3}\times\log\frac{C_{\text{ferric, nominal}}}{C_{\text{ferrous, nominal}}} + 492$$

7 Reduction Kinetics of Ferric Ion on Chalcopyrite from 25 ℃ to 150 ℃

7.1 Introduction

The results obtained in the previous Chapters open the way to investigate the reduction behavior of ferric ion on chalcopyrite, and provide an opportunity for a comprehensive study and comparison of its reduction kinetics at different temperatures relevant to industrial chalcopyrite leaching processes.

The objective of this Chapter is to systematically study the kinetics of ferric reduction in the quaternary H_2SO_4-$Fe_2(SO_4)_3$-$FeSO_4$-H_2O system on chalcopyrite by electrochemical measurements. This investigation aims to obtain the temperature dependence of fundamental electrochemical kinetic parameters, such as exchange current density, transfer coefficient and rate constant. This study yields detailed information about the ferric ion reduction processes involved in industrially significant leaching conditions relevant to the previously mentioned processes at different temperatures from 25 to 150 ℃.

Since in acidic iron sulfate solution, the concentrations of ferric and ferrous ions are limited by the formation of charged cations and anions, as well as neutral species, herein they are first obtained as a function of electrolyte composition and temperature by the developed speciation model (details can be found in **Section 7.2.1**). This information is then used to apply thermodynamic and chemical kinetic principles, i.e., to invoke the Nernst equation and other basic electrochemical kinetic equations (Butler-Volmer equation and its extensions). Then, the reduction kinetics of ferric on chalcopyrite are investigated by cathodic potentiodynamic polarization at temperatures relevant to existing industrial processes and thus the temperature

dependence of the exchange current density, transfer coefficient and rate constant are determined and discussed.

7.2 Results and Discussion

7.2.1 Determination of the Concentrations of Free Ferric and Ferrous Ions in H_2SO_4-$Fe_2(SO_4)_3$-$FeSO_4$-H_2O System by the Speciation Model between 25 ℃ and 150 ℃

According to the published literature, the iron sulfates present in sulfuric acid solution are distributed as soluble species including simple metal ions, neutral or charged complexes, as well as precipitates such as Fe_2O_3 formed at high temperatures [33-45]. Therefore, a speciation model is required to quantify the concentrations of the main species involved in acidic iron sulfate solutions. These results can then be employed to study the reduction kinetics of ferric ions on chalcopyrite (the concentration of free ferric ions is required when invoking basic electrochemical kinetic equations). Further, this information can be used to calculate the exchange current density by extrapolating the cathodic linear Tafel line to the reversible potential of the Fe^{3+}/Fe^{2+} couple (concentrations of free ferric and ferrous ions are required when invoking the Nernst equation).

However, most existing relevant speciation studies of the quaternary acidic iron sulfate system are limited to lower concentrations and/or temperatures [33-38]. As a result, in Chapter 5, a thermodynamic model was developed and shown to reliably simulate the speciation of the quaternary H_2SO_4-$Fe_2(SO_4)_3$-$FeSO_4$-H_2O system through a wide range of solution compositions and temperatures (25 ℃-150 ℃). The main species involved were identified, and the thermodynamic data for all of the species were collected and critically assessed. These data were used to estimate the activity coefficients of species with the B-dot equation [137-139], and to calculate the equilibrium constants by the Lewis formulation of the Criss-Cobble correspondence

principle [144, 145, 149] from 25 to 150 ℃. Results from the calculated distribution of the main ferric and ferrous species in H_2SO_4 solutions reveal that most of the Fe(III) is distributed as complexes or precipitates and the free Fe^{3+} accounts for only a minor percentage, whereas a large amount of Fe(II) exists in the form of free Fe^{2+}. Moreover, under the same nominal Fe^{3+}/Fe^{2+} ratio, a temperature increase in the range of 25-150 ℃ leads to a decline in the free Fe^{3+} concentration due to the ion association to form more stable species, whereas the free Fe^{2+} concentration is relatively stable with similar values of the same order of magnitude. The proposed model was validated by the experimental data in the present work and results published by other authors. Detailed information on the speciation model can be found in Chapter 5 and 6.

Table 7-1 presents the obtained concentrations of free Fe^{3+} and Fe^{2+} in the above-mentioned aqueous Fe(II)-Fe(III)-H_2SO_4 solutions in the range of 25-150 ℃ according to the developed speciation model. These results will be subsequently used in the following discussion, in order to investigate the electrochemical reduction kinetics of the Fe^{3+}/Fe^{2+} couple on chalcopyrite as well as mechanistic analysis in industrial chalcopyrite leaching processes.

Table 7-1 The calculated concentrations of free Fe^{3+} and Fe^{2+} ions in aqueous Fe(II)-Fe(III)-H_2SO_4 solutions in the range of 25-150 ℃ according to the developed speciation model (Unit: mol/kg).

Fe^{3+}/Fe^{2+} (Nominal)	Free Iron at 25 ℃		Free Iron at 70 ℃		Free Iron at 90 ℃		Free Iron at 110 ℃		Free Iron at 150 ℃	
	C_{ferric}	$C_{ferrous}$	C_{ferric}	$C_{ferrous}$	C_{ferric}	$C_{ferrous}$	C_{ferric}	$C_{ferrous}$	C_{ferric}	$C_{ferrous}$
1:1	6.75E-03	1.10E-01	9.44E-04	1.18E-01	5.33E-04	1.08E-01	3.01E-04	1.10E-01	1.51E-04	1.24E-01
10:1	8.92E-03	1.19E-02	1.61E-03	1.31E-02	9.62E-04	1.26E-02	6.40E-04	1.29E-02	3.17E-04	1.30E-02
100:1	9.19E-03	1.20E-03	1.70E-03	1.32E-03	1.02E-03	1.28E-03	6.84E-04	1.31E-03	3.36E-04	1.30E-03
1000:1	9.22E-03	1.20E-04	1.71E-03	1.32E-04	1.02E-03	1.28E-04	6.88E-04	1.31E-04	3.39E-04	1.30E-04

7.2.2 CPC Results at 25 ℃

Figure 7-1 shows the CPC and corresponding OCP results at 25 ℃. It can be observed that the OCP values are quite stable under each nominal Fe^{3+}/Fe^{2+} ratio. OCP slightly shifted towards positive values when increasing the nominal Fe^{3+}/Fe^{2+} ratio. The shape of the polarization plots for different nominal Fe^{3+}/Fe^{2+} ratios are similar, indicating identical processes in the systems. All of the plots exhibit reproducible well-defined linear Tafel regions. The reduction reaches a well-defined limiting current density at approximately E = 100 mV versus SHE. Addition of ferrous by varying the nominal Fe^{3+}/Fe^{2+} ratio from 1000:1 to 1:1 has no apparent effect on the Tafel plots. In addition, it can be found that the polarization curves cross each other (e.g. the curve at 1:1 nominal Fe^{3+}/Fe^{2+} ratio crosses over the curves at the three other nominal Fe^{3+}/Fe^{2+} ratios). This is probably caused by the different free iron concentrations and starting OCP values at the early stages of the experiment, as well as the fact that the measured Tafel slopes are essentially unchanged. Specifically, when a chalcopyrite electrode was immerged in the acidic iron sulfate solution, the starting OCP values were different depending on the solution composition (e.g. the OCP value at 1:1 nominal Fe^{3+}/Fe^{2+} ratio is lower than that at the nominal Fe^{3+}/Fe^{2+} ratio of 10:1). Meanwhile, the free ferric ion concentrations are similar (see the results in Table 7-1). This means that the ferric ion reduction behavior should also be in a similar range of the E-Log i figure. Finally, the Tafel slopes of those plots are essentially unchanged. A combination of the above three factors resulted in such a cross-over behavior for the polarization plots. This phenomenon appears for all temperatures used in the present study, as shown in the following sections.

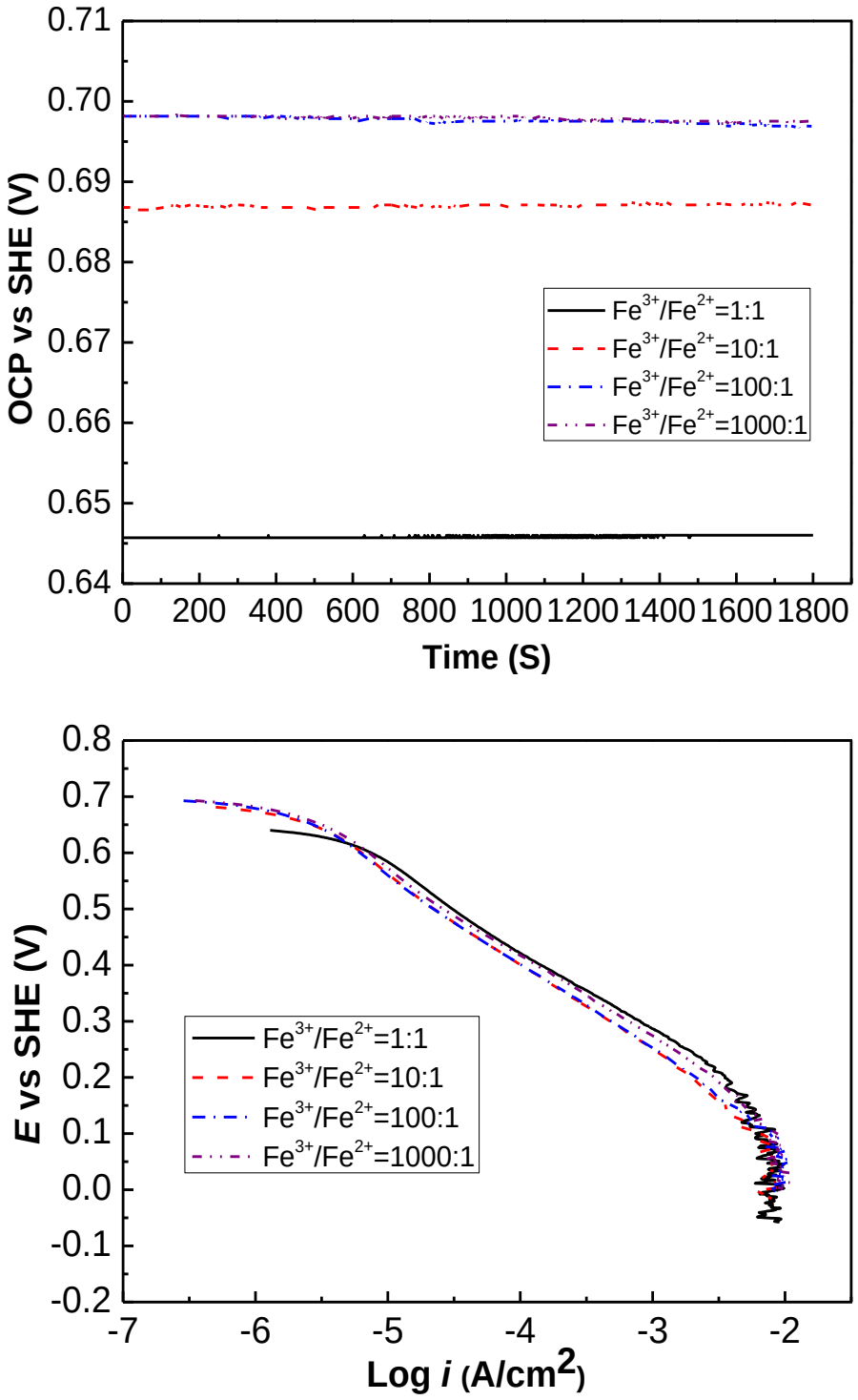

Figure 7-1 Cathodic potentiodynamic polarization curves and corresponding OCP in deaerated aqueous Fe(II)-Fe(III)-H_2SO_4 solutions at $[H_2SO_4]$ = 0.31 mol/kg and $[Fe^{3+}]_{total}$ = 0.18 mol/kg on chalcopyrite with different nominal Fe^{3+}/Fe^{2+} ratios at 25 ℃.

According to the results obtained by the above-mentioned speciation model, it is clearly shown in Table 7-2 that the real Fe^{3+}/Fe^{2+} ratio in the Fe(II)-Fe(III)-H_2SO_4 solutions under different nominal Fe^{3+}/Fe^{2+} ratios is much lower than the nominal ratio at 25 ℃. By further invoking the Nernst equation (the standard electrode potentials for the Fe^{3+}/Fe^{2+} couple were also calculated by the Lewis formulation of the Criss-Cobble correspondence principle), the reversible potential of the Fe^{3+}/Fe^{2+} couple (E_C) can be calculated and the results are also presented in Table 7-2.

Table 7-2 CPC results at 25 ℃.

Fe^{3+}/Fe^{2+} (Nominal)	Fe^{3+}/Fe^{2+} (Real)	Tafel Slope (V/decade)	Transfer Coefficient	E_M		E_C	
				E_M (V)	i_M (A/cm^2)	E_C (V)	i_0 (A/cm^2)
1:1	6.13E-02	0.154	0.38	0.6457	3.51E-06	0.6705	2.43E-06
10:1	0.75	0.163	0.36	0.6868	1.65E-06	0.7357	8.27E-07
100:1	7.67	0.162	0.37	0.6982	1.37E-06	0.7956	3.41E-07
1000:1	76.9	0.156	0.38	0.6982	1.48E-06	0.8548	1.46E-07

Based on the obtained cathodic linear Tafel line and the reversible potential of the Fe^{3+}/Fe^{2+} couple, the transfer coefficients and exchange current densities could be calculated at 25 ℃. As indicated in Table 7-2, no significant change in the cathodic Tafel slopes for the reduction of ferric ions on the $CuFeS_2$ surface was observed and the slopes ranged between 0.154 and 0.163 V/decade. The measured Tafel slopes, according to Eq. (7-1), yield the values for α in the range of 0.36-0.38. The average values of the transfer coefficient calculated from the

cathodic Tafel slopes obtained from CPC are lower than 0.5, which is probably related to the semi-conducting behavior of chalcopyrite and/or the passive film that forms thereon.

Usually, the Tafel slope is considered to be proportional to temperature and transfer coefficient according to the following expression:

$$b = \frac{2.303RT}{\alpha nF} \tag{7-1}$$

where b is the Tafel slope (V/decade), n is the number of electrons transferred in the rate determining step (n may be taken as unity because the rate determining processes mostly involve single charge transfer steps) [24], F is the Faraday constant (C/mol), α is the transfer coefficient, R is the universal gas constant (J/mol•K) and T is the temperature (K).

With the increase of nominal Fe^{3+}/Fe^{2+} ratio from 1:1 to 1000:1, the obtained exchange current densities (i_0) declined from 2.43×10^{-6} A/cm^2 to 1.46×10^{-7} A/cm^2. The reason for this behavior may be attributed to a combination of the following two factors: (1) the calculated reversible potentials are higher as the nominal Fe^{3+}/Fe^{2+} ratio is increased and (2) at the same time the cathodic Tafel plots remain essentially unchanged under different nominal Fe^{3+}/Fe^{2+} ratios. Actually, i_0 is related to the concentration of free Fe^{2+} in the solution and increases with a higher concentration of Fe^{2+}. This trend, i.e. the effect of increasing Fe^{2+} concentration, prevails for all temperatures used in the present study, as shown in the following sections. Please note that in the present study, the total amount of Fe(III) is constant, and hence the total amount of Fe(II) decreases when increasing the nominal Fe^{3+}/Fe^{2+} ratio.

The obtained mixed potential (E_M, obtained from Figure 7-1) and mixed current density (i_M) are also shown and summarized in Table 7-2. Please note that the i_M was calculated by extrapolating the cathodic linear Tafel line to the corresponding mixed potential. Typically, the i_M values are on the order of 10^{-6} A/cm^2 at 25 ℃. The E_M decreases with an increase of iron(II)

concentration. It is interesting to observe that the mixed potential is approximately equal to the cathodic reversible potential only when the nominal Fe^{3+}/Fe^{2+} ratio approaches 1:1. This trend is similar to that observed by Nicol and Lázaro in 2002, who demonstrated that the potential measured in the bulk of the solution can only be approximated to that at the surface of the minerals under conditions of relatively high concentrations of iron(II) [69].

The development of corrosion pits on the anodic sites of the chalcopyrite electrode surface under oxidizing conditions could be observed. Hence, the surface of a chalcopyrite specimen before and after electrochemical treatment was examined by OM, to see whether corrosion pits were formed or enlarged. It is suggested in Figure 7-2 that, as expected, numerous small pits appeared after finishing the electrochemical experiment. The kinetic and mechanistic analysis of the anodic oxidation processes (including the generated products) is complicated and is beyond the scope of the present study.

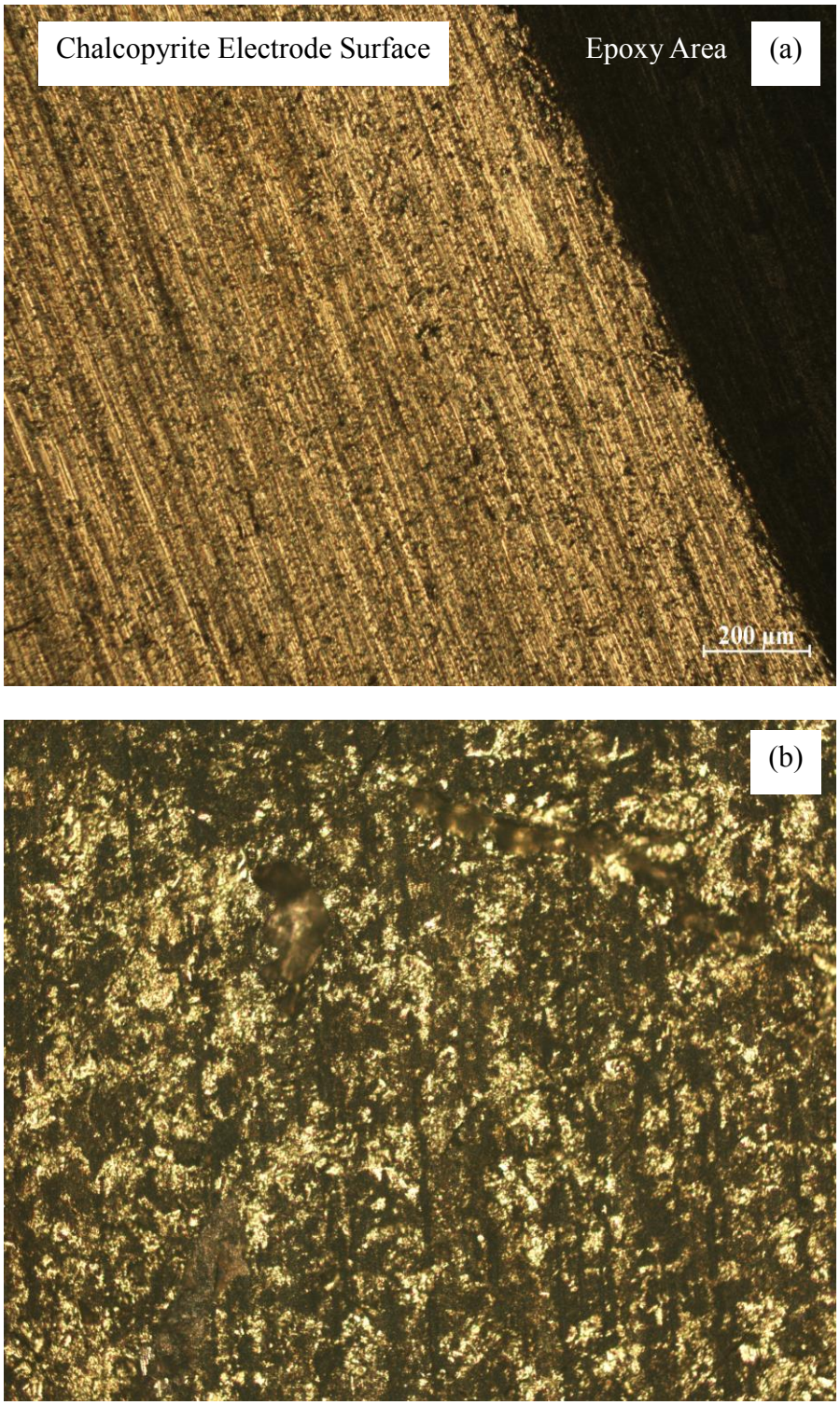

Figure 7-2 OM analysis results of the prepared chalcopyrite electrode surface before (a) and after electrochemical test (b) in the electrolyte with nominal Fe^{3+}/Fe^{2+} ratio of 1000:1 at 25 ℃.

7.2.3 CPC Results at 70 ℃

The results of OCP and CPC measurement in Fe(II)-Fe(III)-H_2SO_4 solutions with different nominal Fe^{3+}/Fe^{2+} ratios at 70 ℃ are presented in Figure 7-3. The OCP values are relatively stable and no obvious deviation was found under each nominal Fe^{3+}/Fe^{2+} ratio. The polarization plots for different nominal Fe^{3+}/Fe^{2+} ratios almost overlap with each other, and increasing the nominal Fe^{3+}/Fe^{2+} ratio has little or no effect on the polarization curve. This trend is similar to that at 25 ℃. The reduction process approaches a limiting current density at approximately E = 180 mV versus SHE.

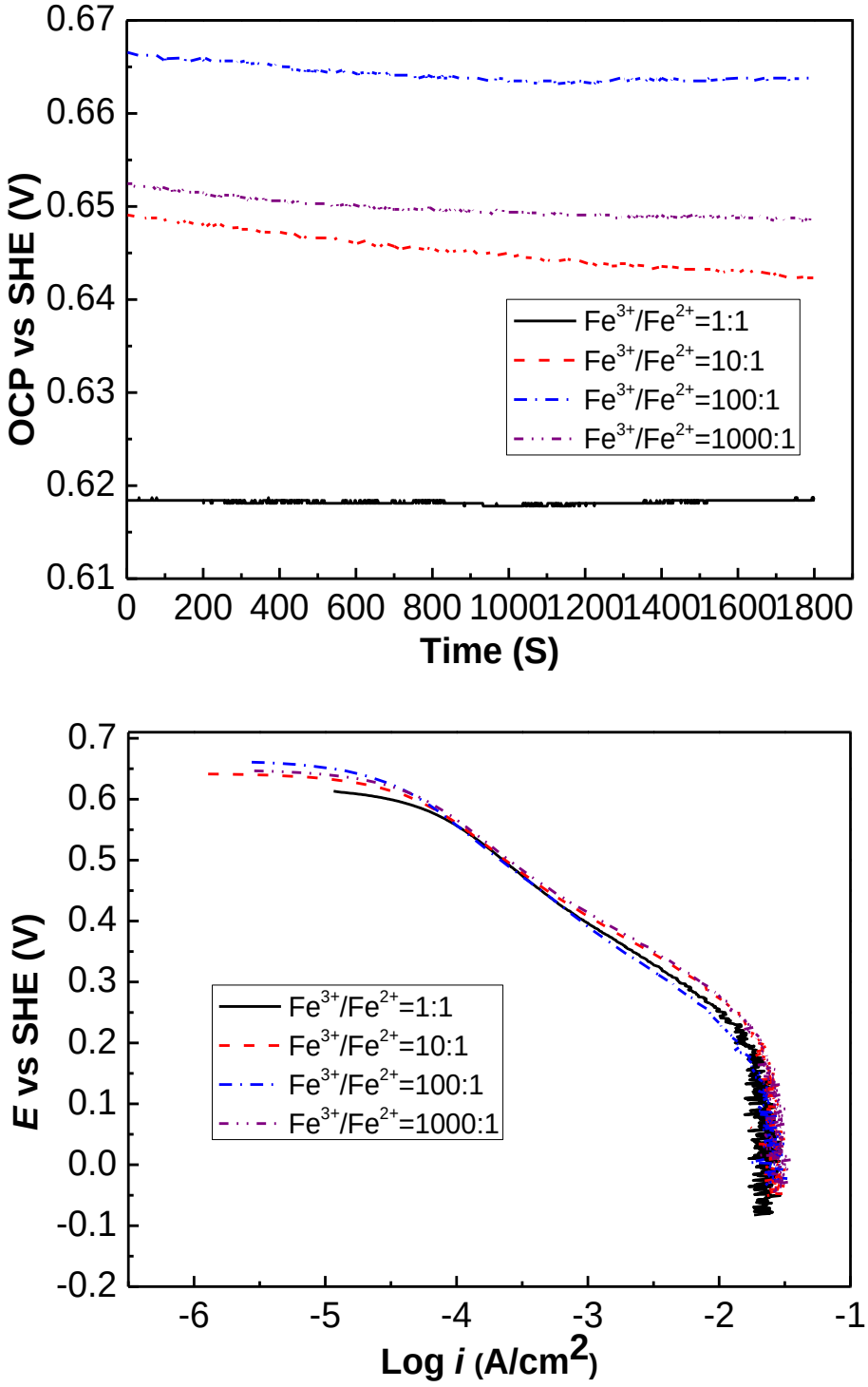

Figure 7-3 Cathodic potentiodynamic polarization curves and corresponding OCP in deaerated aqueous Fe(II)-Fe(III)-H_2SO_4 solutions at $[H_2SO_4]$ = 0.31 mol/kg and $[Fe^{3+}]_{total}$ = 0.18 mol/kg on chalcopyrite with different nominal Fe^{3+}/Fe^{2+} ratios at 70 ℃.

Table 7-3 lists the nominal and real Fe^{3+}/Fe^{2+} ratio in aqueous Fe(II)-Fe(III)-H_2SO_4 solution at 70 ℃. It can be seen that the real Fe^{3+}/Fe^{2+} ratio is still much lower than the nominal ratio, and it is worth noting that the real Fe^{3+}/Fe^{2+} ratio at 70 ℃ is even smaller than that at 25 ℃.

Table 7-3 CPC results at 70 ℃.

Fe^{3+}/Fe^{2+} (Nominal)	Fe^{3+}/Fe^{2+} (Real)	Tafel Slope (V/decade)	Transfer Coefficient	E_M		E_C	
				E_M (V)	i_M (A/cm^2)	E_C (V)	i_0 (A/cm^2)
1:1	7.98E-03	0.156	0.44	0.6184	3.86E-05	0.6731	1.72E-05
10:1	0.123	0.151	0.45	0.6491	2.46E-05	0.7553	4.88E-06
100:1	1.29	0.165	0.41	0.6666	2.13E-05	0.8248	2.33E-06
1000:1	12.9	0.154	0.44	0.6525	2.62E-05	0.8931	7.13E-07

The transfer coefficients and exchange current densities were also calculated at 70 ℃. Table 7-3 shows that there is no significant change in the cathodic Tafel slopes for ferric reduction and the slopes varied between 0.151 and 0.165 V/decade. The measured Tafel slopes are similar to those obtained at 25 ℃, and give the values for α in the range of 0.41-0.45 according to Eq. (7-1). When increasing the nominal Fe^{3+}/Fe^{2+} ratio from 1:1 to 1000:1, the exchange current densities decreased from $1.72\text{x}10^{-5}$ A/cm^2 to $7.13\text{x}10^{-7}$ A/cm^2. This tendency is the same as that observed at 25 ℃. At 70 ℃, there is a decrease in the measured E_M in comparison with that at 25 ℃ under the same nominal Fe^{3+}/Fe^{2+} ratio, and at the same time the Tafel slopes are relatively stable, which subsequently leads to an increased i_M. In general, the i_M values are on the order of 10^{-5} A/cm^2. In addition, under the same nominal Fe^{3+}/Fe^{2+} ratio,

increasing the temperature from 25 ℃ to 70 ℃ gives rise to an increase of the i_M and i_0 for the Fe^{3+}/Fe^{2+} couple on chalcopyrite, by almost one order of magnitude.

7.2.4 CPC Results at 90 ℃

Figure 7-4 presents the CPC and corresponding OCP results at 90 ℃. It is shown again that the OCP values are quite stable under each nominal Fe^{3+}/Fe^{2+} ratio, and are larger when increasing the nominal Fe^{3+}/Fe^{2+} ratio. The polarization plots for different nominal Fe^{3+}/Fe^{2+} ratios display similar behavior, apart from the fact that there is deviation at the very beginning of scanning due to the different OCP values. A limiting current density is obtained at approximately E = 210 mV versus SHE. The addition of ferrous ion when changing the nominal Fe^{3+}/Fe^{2+} ratio from 1000:1 to 1:1 has no obvious influence on the Tafel plots.

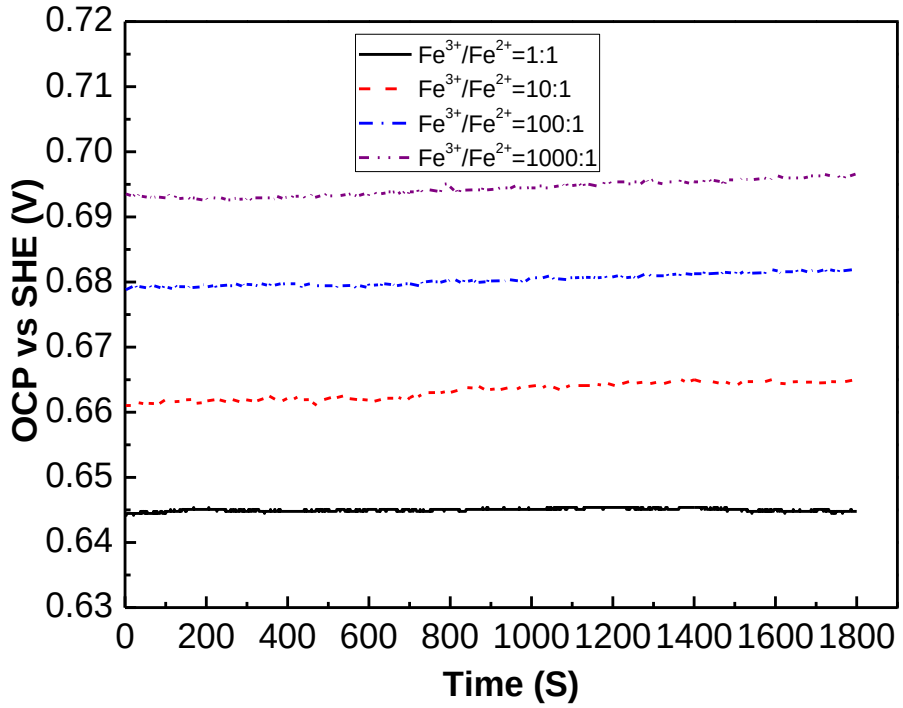

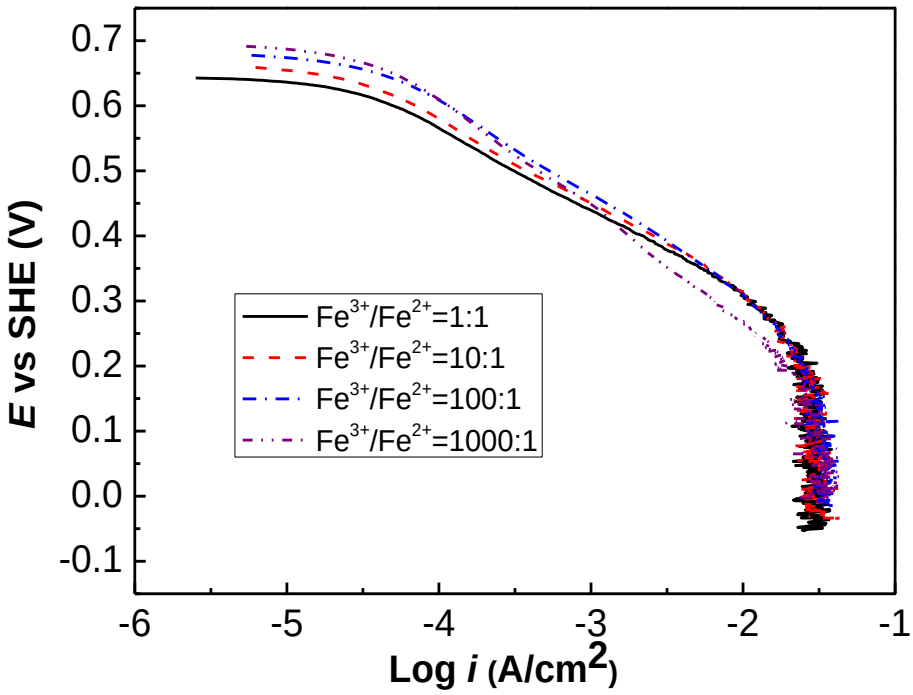

Figure 7-4 Cathodic potentiodynamic polarization curves and corresponding OCP in deaerated aqueous Fe(II)-Fe(III)-H_2SO_4 solutions at [H_2SO_4] = 0.31 mol/kg and [Fe^{3+}]$_{total}$ = 0.18 mol/kg on chalcopyrite with different nominal Fe^{3+}/Fe^{2+} ratios at 90 ℃.

All of the CPC results at 90 ℃ are included in Table 7-4. It is seen in Table 7-4 that the calculated real Fe^{3+}/Fe^{2+} ratios at 90 ℃ are even smaller, compared with those obtained at 25 ℃ and 70 ℃ under the same nominal Fe^{3+}/Fe^{2+} ratio. A slight decrease in the cathodic Tafel slopes for the reduction of ferric ions on the $CuFeS_2$ surface was observed compared to those obtained at 25 ℃ and 70 ℃, especially when the nominal Fe^{3+}/Fe^{2+} ratio is 1:1, 10:1 and 100:1. The slopes ranged between 0.123 and 0.159 V/decade, and were further employed to calculate the transfer coefficients, with values being in the range of 0.45-0.58.

Table 7-4 CPC results at 90 ℃.

Fe^{3+}/Fe^{2+} (Nominal)	Fe^{3+}/Fe^{2+} (Real)	Tafel Slope (V/decade)	Transfer Coefficient	E_M		E_C	
				E_M (V)	i_M (A/cm^2)	E_C (V)	i_0 (A/cm^2)
1:1	4.96E-03	0.123	0.58	0.6448	2.11E-05	0.6789	1.11E-05
10:1	0.08	0.125	0.58	0.6650	1.85E-05	0.7657	2.88E-06
100:1	0.80	0.139	0.52	0.6819	2.66E-05	0.8393	1.96E-06
1000:1	8.01	0.159	0.45	0.6966	2.67E-05	0.9116	1.19E-06

As to the E_M and i_M, it was found that when increasing the temperature from 70 ℃ to 90 ℃, there is a slight increase in E_M under the same nominal Fe^{3+}/Fe^{2+} ratio, whereas the i_M data are relatively stable with similar values of the same order of magnitude (10^{-5} A/cm^2). As expected, the i_0 increases by increasing the concentration of ferrous. Furthermore, although the i_0 at 70 ℃ and 90 ℃ are still on the same order, the temperature increase results in a small decline in i_0. The

reason for this unexpected behavior can be ascribed to the following two facts: (1) the temperature increase causes an increase in the reversible potentials of the Fe^{3+}/Fe^{2+} couple; (2) the Tafel slopes diminished a little in contrast to those measured at 70 ℃.

7.2.5 CPC Results at 110 ℃

Currently, most of the proposed leaching processes for chalcopyrite are operated under pressure, primarily because fast leaching kinetics can be achieved at the elevated temperatures employed in an autoclave. However, although in the past several decades a lot of effort has been expended to understand the mechanisms involved in the leaching system and the key parameters that limit the leaching kinetics, except for very few reported results [46, 109, 110], the majority are limited to temperatures below 90 ℃. According to recent reviews of high temperature and high pressure (HTHP) electrochemical studies [111, 112], although in recent years significant developments have been made, HTHP electrochemistry remains a relatively unexplored field of research and the relative lack of experimental data is ascribed to the various technical obstacles. As to HTHP mineral electrochemistry, very few reports are available [113]. In the following sections, the reduction kinetics of ferric on chalcopyrite will be discussed at 110 ℃ and 150 ℃.

Figure 7-5 presents the CPC and corresponding OCP results at 110 ℃. It can be observed that the OCP values are relatively stable and no obvious deviation was found under each nominal Fe^{3+}/Fe^{2+} ratio. A very similar tendency in the polarization plots for different nominal Fe^{3+}/Fe^{2+} ratios was observed: there is a relatively smaller slope existing in the Tafel region, despite the fact that the OCP values of the 100:1 and 1000:1 nominal Fe^{3+}/Fe^{2+} ratios are a little larger than those of the 10:1 and 1:1 nominal Fe^{3+}/Fe^{2+} ratios. As the current increases, the current becomes independent of the applied potential, indicating that the reaction becomes mass transfer

controlled. The reduction reaches a limiting current density at approximately E = 230 mV versus SHE.

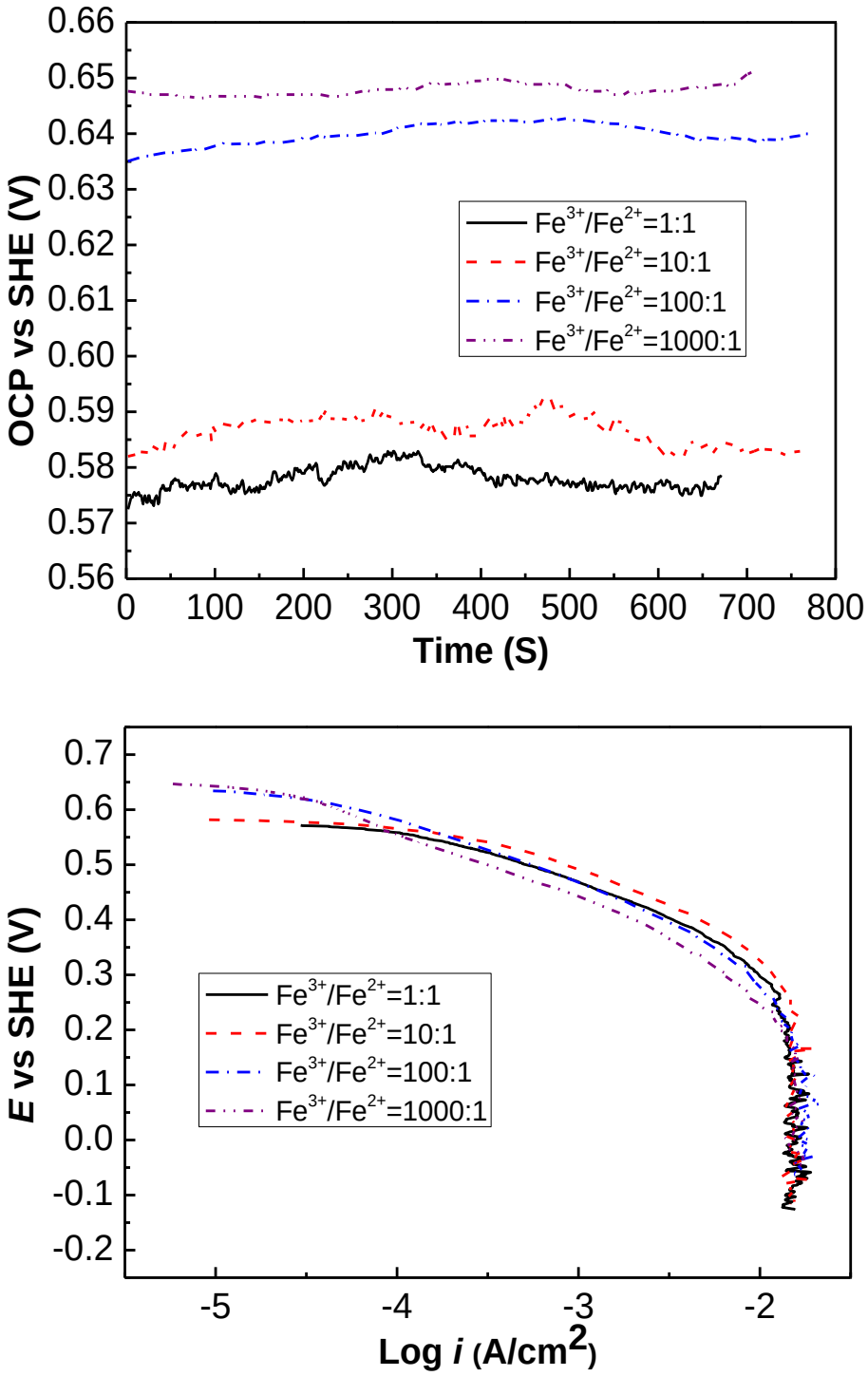

Figure 7-5 Cathodic potentiodynamic polarization curves and corresponding OCP in deaerated aqueous Fe(II)-Fe(III)-H_2SO_4 solutions at [H_2SO_4] = 0.31 mol/kg and [Fe^{3+}]$_{total}$ = 0.18 mol/kg on chalcopyrite with different nominal Fe^{3+}/Fe^{2+} ratios at 110 ℃.

In Table 7-5, it is worth noting that a continuous drop in the calculated real Fe^{3+}/Fe^{2+} ratio is found at 110 ℃, compared with that obtained at or below 90 ℃ under the same nominal Fe^{3+}/Fe^{2+} ratio. In addition, it may be mentioned that the Tafel slopes of the polarization plots under different nominal Fe^{3+}/Fe^{2+} ratios are very similar and relatively smaller than those obtained at lower temperatures. The cathodic Tafel slopes for ferric reduction varied in the range of 0.117-0.129 V/decade, which can subsequently be used to calculate α with values in the range of 0.59-0.65.

Table 7-5 CPC results at 110 ℃.

Fe^{3+}/Fe^{2+} (Nominal)	Fe^{3+}/Fe^{2+} (Real)	Tafel Slope (V/decade)	Transfer Coefficient	E_M		E_C	
				E_M (V)	i_M (A/cm^2)	E_C (V)	i_0 (A/cm^2)
1:1	2.73E-03	0.120	0.64	0.5786	1.16E-04	0.6771	1.74E-05
10:1	0.05	0.129	0.59	0.5829	1.92E-04	0.7742	6.31E-06
100:1	0.52	0.119	0.64	0.6400	3.56E-05	0.8523	5.91E-07
1000:1	5.26	0.117	0.65	0.6510	1.58E-05	0.9285	6.74E-08

Under the same nominal Fe^{3+}/Fe^{2+} ratio, the measured E_M is lower than that obtained at lower temperatures, while the i_M is larger due to the increased kinetics at elevated temperatures. Similarly, with the nominal Fe^{3+}/Fe^{2+} ratios of 1:1 and 10:1, the i_0 at 110 ℃ also begins to increase, in spite of the fact that larger reversible potentials of the Fe^{3+}/Fe^{2+} couple and smaller Tafel slopes are obtained in contrast to those measured at 70 ℃. However, at the 100:1 and 1000:1 ratios, a drop in the i_0 was found again, which probably results from the relatively higher

reversible potentials of the Fe^{3+}/Fe^{2+} couple under such high temperatures and nominal Fe^{3+}/Fe^{2+} ratios.

7.2.6 CPC Results at 150 ℃

Figure 7-6 shows the CPC and corresponding OCP measurement results at 150 ℃. Under each nominal Fe^{3+}/Fe^{2+} ratio, it appears that there is a very slight variation in the OCP values. Due to the fast kinetics at such a temperature, the time for OCP measurements was shorter compared to that of the previous experiments in order to avoid significant changes on the electrode surface associated with long term exposure to the electrolyte. As shown in Figure 7-7, at 150 ℃, about 1-hour of immersion of the chalcopyrite electrode in the electrolyte will result in significant corrosion on the surface. The pits are substantially enlarged compared to those formed at 25 ℃. Hence, for the tests at 150 ℃, the time for OCP test was shortened to about 7 minutes. The overall shape of the polarization curves is generally the same for different nominal Fe^{3+}/Fe^{2+} ratios, and these polarization plots exhibit linear Tafel regions. The reduction reaches a limiting current density at approximately E = 250 mV versus SHE.

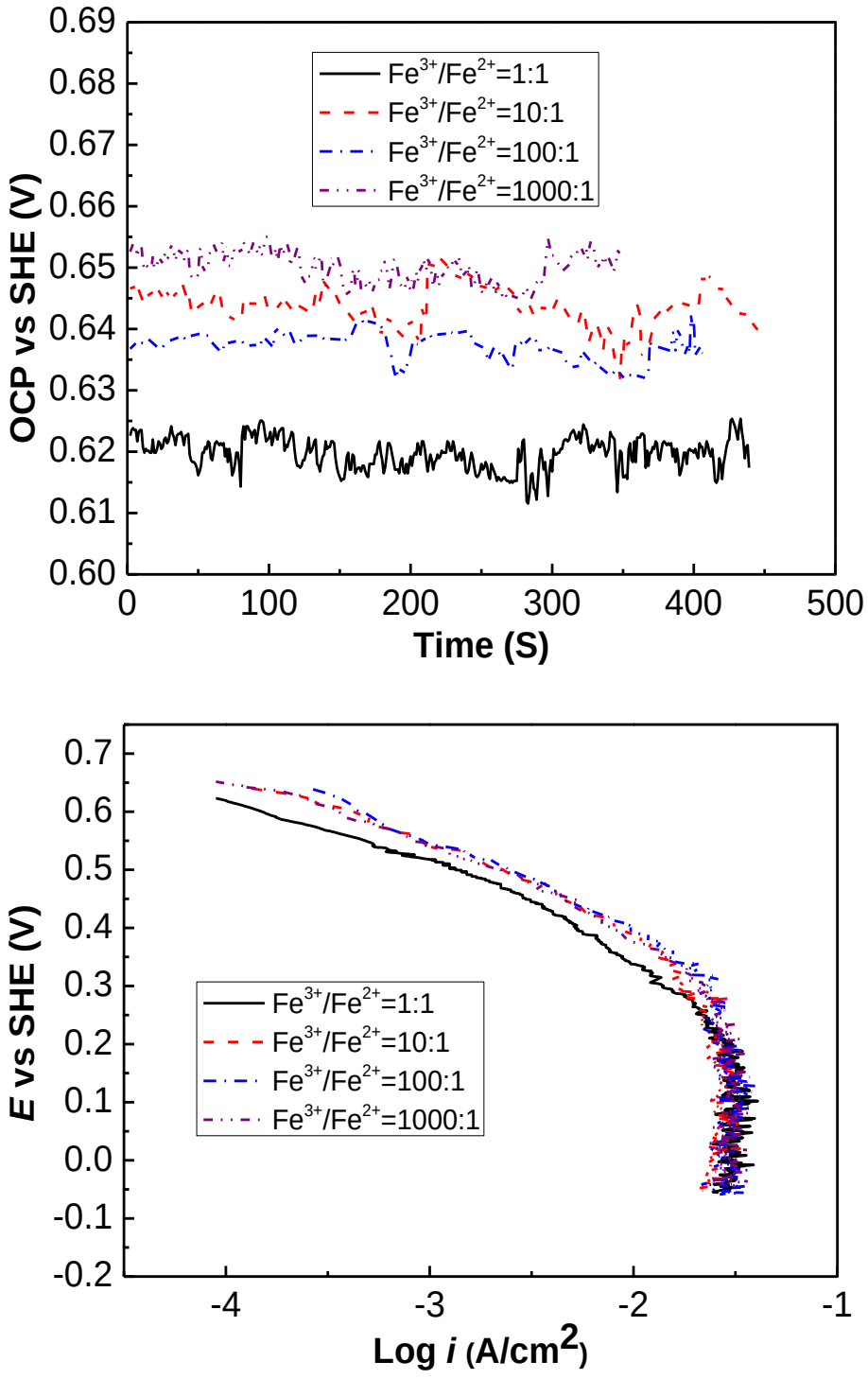

Figure 7-6 Cathodic potentiodynamic polarization curves and corresponding OCP in deaerated aqueous Fe(II)-Fe(III)-H_2SO_4 solutions at [H_2SO_4] = 0.31 mol/kg and [Fe^{3+}]$_{total}$ = 0.18 mol/kg on chalcopyrite with different nominal Fe^{3+}/Fe^{2+} ratios at 150 ℃.

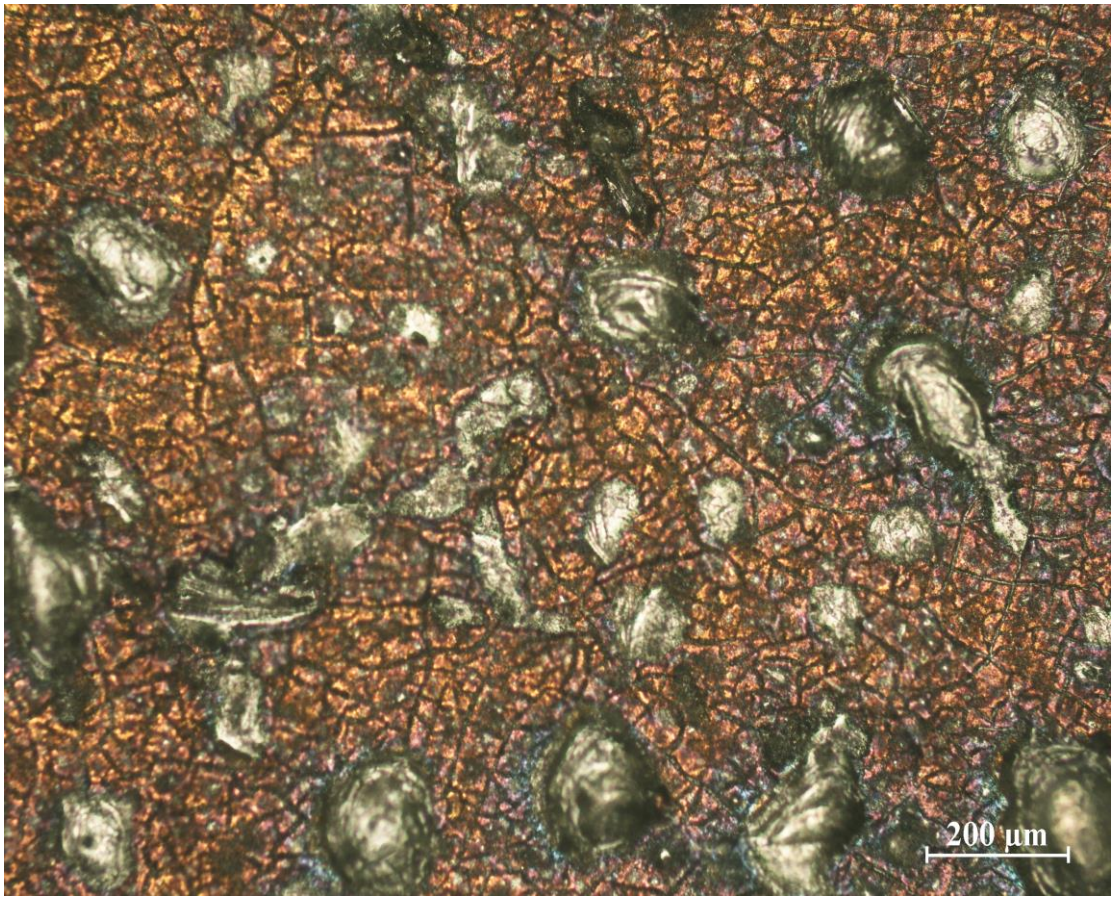

Figure 7-7 OM analysis results of the prepared chalcopyrite electrode surface after about 1 hour exposure to the electrolyte with nominal Fe^{3+}/Fe^{2+} ratio of 1:1 at 150 ℃.

In Table 7-6, it should be noted that a similar trend to that observed from 25 to 110 ℃ was found at 150 ℃ in that the calculated real Fe^{3+}/Fe^{2+} ratio is much smaller than the nominal Fe^{3+}/Fe^{2+} ratio. For any given nominal Fe^{3+}/Fe^{2+} ratio, the smallest value of the calculated real Fe^{3+}/Fe^{2+} ratio was observed at 150 ℃, due to ion association. The Tafel slopes under different nominal Fe^{3+}/Fe^{2+} ratios are in the range of 0.114-0.136 V/decade. The calculated value of α ranged from 0.62 to 0.74.

Table 7-6 CPC results at 150 ℃.

Fe^{3+}/Fe^{2+} (Nominal)	Fe^{3+}/Fe^{2+} (Real)	Tafel Slope (V/decade)	Transfer Coefficient	E_M		E_C	
				E_M (V)	i_M (A/cm^2)	E_C (V)	i_0 (A/cm^2)
1:1	1.22E-03	0.114	0.74	0.6226	1.08E-04	0.6748	3.76E-05
10:1	0.02	0.136	0.62	0.6398	1.99E-04	0.7855	1.68E-05
100:1	0.26	0.136	0.62	0.6368	2.23E-04	0.8718	4.14E-06
1000:1	2.60	0.126	0.67	0.6526	1.32E-04	0.9560	5.07E-07

Under all of the nominal Fe^{3+}/Fe^{2+} ratios, the measured E_M is relatively stable. At 150 ℃, as expected, the highest i_M values are obtained and are on the order of 10^{-4} A/cm^2 due to the fast kinetics achieved at this temperature. In addition, it should be emphasized that the largest values of i_0 were also observed with the nominal Fe^{3+}/Fe^{2+} ratios of 1:1 and 100:1, despite the fact that largest reversible potentials of the Fe^{3+}/Fe^{2+} couple and relatively smaller Tafel slopes are obtained in comparison to lower temperatures. At the 1000:1 ratio, the value of i_0 is of the same order of magnitude as that obtained at 25 ℃, 70 ℃ and 90 ℃. Given the fact that the reversible potentials at 150 ℃ are so high and that the Tafel slopes are relatively invariant with temperature, the similarity in the values of i_0 indicates that the increased kinetics at 150 ℃ play a dominant role in determining i_0.

Based on the above analyses, it is interesting to note that at each temperature the exchange current densities increase with an increasing amount of ferrous (i.e. when decreasing the nominal Fe^{3+}/Fe^{2+} ratios). In addition, a substantial increase in i_M from the order of 10^{-6} A/cm^2 to the

order of 10^{-4} A/cm^2 is found when increasing the temperature from 25 to 150 ℃, i.e. an increase of approximately two orders of magnitude.

7.2.7 Comparison with i_0 of the Fe^{3+}/Fe^{2+} Couple on Other Electrodes and the Application of i_0 to Calculate the Rate Constants at 25 ℃-150 ℃

As mentioned in the Introduction, after obtaining the reduction kinetics of ferric on chalcopyrite at different temperatures, what particularly interests us is the temperature dependence of the exchange current density, transfer coefficient and rate constant. In this and the following section, this temperature dependence is discussed.

7.2.7.1 Comparison with i_0 of the Fe^{3+}/Fe^{2+} Couple on Other Electrodes

The obtained exchange current densities for the Fe^{3+}/Fe^{2+} couple on chalcopyrite were compared with those obtained on other electrodes [103-105]. All of the results are presented in Table 7-7. The reaction rate of the Fe^{3+}/Fe^{2+} couple is quite fast on the surface of oxide free metals such as platinum and was reported to have an exchange current density of 1.5×10^{-2} A/cm^2. A distinct decrease by several orders of magnitude in the exchange current densities of the Fe^{3+}/Fe^{2+} couple on Ni, Fe, Ti, Fe-Cr alloy and 304 stainless steel (with passive oxide films) was observed and the values are on the order of 10^{-5}-10^{-8} A/cm^2. Such small exchange current densities found for the Fe^{3+}/Fe^{2+} reaction on passive electrodes are probably a consequence of the semiconductor characteristics of the passive film [103]. In the case of chalcopyrite, the results are consistent with the exchange current densities of the Fe^{3+}/Fe^{2+} couple on the above-noted passive electrodes. The exchange current densities are substantially less than those on platinum, on the order of 10^{-7}-10^{-5} A/cm^2 in a wide range of 25 ℃-150 ℃, almost certainly due to the formation of the passive film. In general, at the same nominal Fe^{3+}/Fe^{2+} ratio, increasing the

temperature from 25 to 150 ℃ was observed to give rise to an increase in i_0, especially when a larger amount of free ferrous existed in the solution.

Table 7-7 Comparison of exchange current densities Fe^{3+}/Fe^{2+} couple on various electrodes.

Electrode	Solution	Ferric	Ferrous	Temperature	i_0 (A/cm^2)
Pt	H_2SO_4	0.05M	0.05M	25℃	$1.5x10^{-2}$
Fe	H_2SO_4+Na_2SO_4	0.30M	0.03M	40℃	$1x10^{-5}$
Ni	H_2SO_4+$MgSO_4$	0.05M	0.05M	30℃	$7.5x10^{-5}$
Ti	H_2SO_4+ $MgSO_4$	0.05M	0.05M	20℃	$2.6x10^{-7}$
Fe-Cr Alloy	H_2SO_4+ $MgSO_4$	0.05M	0.05M	30℃	$1x10^{-6}$
304 Stainless Steel	Ferric-ferrous Sulfate	0.356M	$2.52x10^{-3}$M	25℃	$4.5x10^{-8}$
Chalcopyrite	H_2SO_4	0.179M	$1.79x10^{-4}$-0.179M	25℃	$1.46x10^{-7}$-$2.43x10^{-6}$
Chalcopyrite	H_2SO_4	0.179M	$1.79x10^{-4}$-0.179M	70℃	$7.13x10^{-7}$-$1.72x10^{-5}$
Chalcopyrite	H_2SO_4	0.179M	$1.79x10^{-4}$-0.179M	90℃	$1.19x10^{-6}$-$1.11x10^{-5}$
Chalcopyrite	H_2SO_4	0.179M	$1.79x10^{-4}$-0.179M	110℃	$6.74x10^{-8}$-$1.74x10^{-5}$
Chalcopyrite	H_2SO_4	0.179M	$1.79x10^{-4}$-0.179M	150℃	$5.07x10^{-7}$-$3.76x10^{-5}$

7.2.7.2 Calculation of Rate Constants

Based on the obtained exchange current densities, the rate constant for ferric reduction, k_c, was calculated with the following equation [24]:

$$i_0 = z_C F k_C C_{Ferric} \exp(-\frac{\alpha n F E_C}{RT}) \quad (7\text{-}2)$$

where i_0 is the exchange current density (A/cm^2), Z_C is the number of electrons involved in the cathodic reaction, F is Faraday constant (C/mol), k_c is the rate constant of ferric reduction (cm/s), C_{Ferric} is the bulk concentration of ferric ion in the solution (mol/L), α is the transfer coefficient, n is the number of electrons transferred in the rate determining step for the cathodic reaction, E_C is the reversible potential of the Fe^{3+}/Fe^{2+} couple, R is the universal gas constant (J/mol•K) and T is the temperature (K).

The bulk concentrations of free Fe^{3+} in aqueous Fe(II)-Fe(III)-H_2SO_4 solutions in the range of 25-150 ℃ are shown in Table 7-1 and used to calculate the rate constant in the present study. Please note that for the dilute aqueous solutions used in the present study, the C (molarity mol/L) can be approximately calculated by using the m (molality mol/kg) multiplied by the corresponding solution density. Because of the unavailability of the data on the density of the solutions in this work over such a large range of temperatures, and considering the fact that the water density does not vary significantly under the temperatures of interest (the solution density should be a little higher than that of pure water), for the sake of simplicity and maintaining internal consistency the author assumed a solution density of unity in the following calculations. All of the calculated rate constants by the above equation from the previous kinetic data are demonstrated in Figure 7-8a. Each point represents an average of the values under four different Fe^{3+}/Fe^{2+} ratios.

According to Eq. (7-2), the calculated average rate constants are 0.049 cm/s at 25 ℃, and 2.80 cm/s at 70 ℃ for nominal Fe^{3+}/Fe^{2+} ratios ranging from 1:1 to 1000:1, as shown in Figure 7-8a. A further increase in temperature leads to larger rate constants, with the largest value (almost 900 cm/s) obtained at 150 ℃. It is evident that the kinetics of the ferric reduction reaction on chalcopyrite increase as the temperature is enhanced.

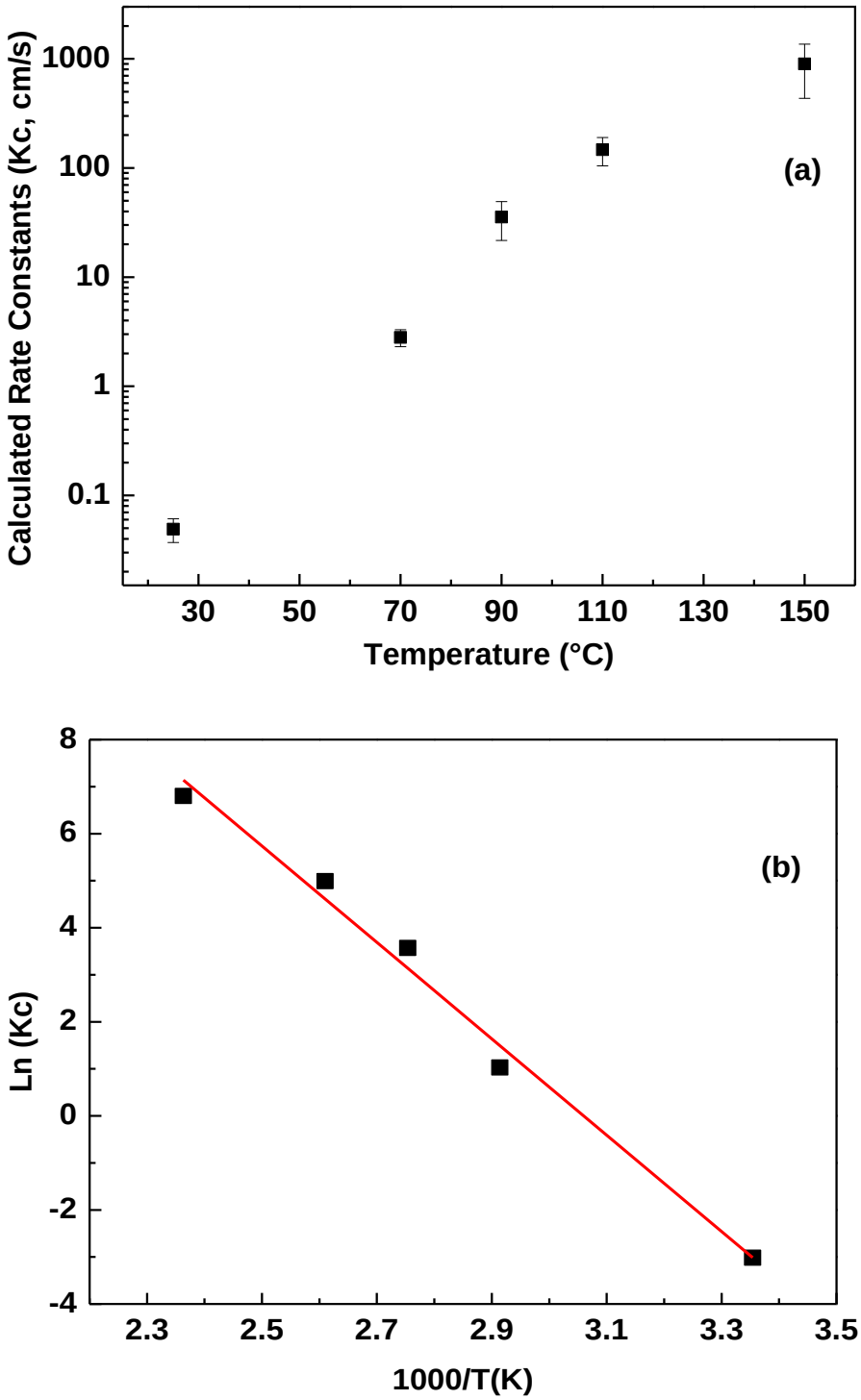

Figure 7-8 (a) Calculated rate constants (k_C) of ferric ion reduction on chalcopyrite as a function of temperature in the range of 25-150 ℃ according to Equation 7-2; (b) ln k_C versus 1/T, displays the linear Arrhenius behavior.

To further understand the temperature-dependent behavior of the rate constants, the natural logarithm of k_c as a function of the inverse of absolute temperature ($1/T$), $\ln k_c$ versus $1/T$, as seen in Figure 7-8b, was plotted on the basis of the Arrhenius equation [119]:

$$k_C = Ae^{-\frac{E_a}{RT}} \tag{7-3}$$

In Eq. (7-3), k_c is the rate constant of ferric reduction (cm/s), A is a frequency factor, E_a is the activation energy, R is the gas constant and T is the absolute temperature.

If the rate constant follows the Arrhenius behavior given by Eq. (7-3), the plot of $\ln k_c$ versus $1/T$ should be linear. Results in Figure 7-8b indicate that the temperature-dependent behavior of the rate constant is consistent with Arrhenius behavior. The best fit was provided by the following relationship:

$$\ln k_C = -10245 \times \frac{1}{T(\mathrm{K})} + 31.349 \tag{7-4}$$

The correlation coefficient was 0.9887.

The fit to the Arrhenius equation gives values for the parameters A and E_a. The activation energy for the ferric reduction reaction was calculated to be 85 ± 1 kJ mol^{-1} in the temperature range of 25-150 ℃. The magnitude of this activation energy indicates that the ferric reduction reaction on chalcopyrite in the region of potentials in which chalcopyrite dissolves is under activation control (kinetic control). This is in agreement with the findings previously indicated by the measured cathodic polarization plots.

7.2.8 Temperature Dependence of Tafel Slopes and Transfer Coefficients for Ferric Ion Reduction

As indicated in Tables 7-2 to 7-6, it seems that the Tafel slope b is essentially independent of temperature over the range of 25 to 150 ℃, and consequently the transfer coefficient

calculated with Eq. (7-1) increases with temperature rather than being constant. In this section, a more detailed analysis of the effect of temperature on the Tafel slope and transfer coefficient in the Fe(II)-Fe(III)-H_2SO_4 solutions under different nominal Fe^{3+}/Fe^{2+} ratios will be discussed and presented. All of the obtained results are presented in Figure 7-9 and Figure 7-10.

7.2.8.1 Variation of Tafel Slopes with Temperature

Traditionally, in Eq. (7-1), the transfer coefficient α, is a function of the symmetry factor β and the stoichiometric number v. For a simple one-electron one-step reaction, $\alpha = \beta$. In the classical treatment of electrode kinetics the symmetry factor β (or α for more complex multiple-step reactions) is considered to be independent of both temperature and potential. Therefore, for a given rate-determining step, the Tafel slope is expected to be directly proportional to temperature. However, according to experimental studies in various systems, the temperature dependence of the Tafel slopes can deviate from the direct proportionality of the classical Eq. (7-1) if α is a constant, and hence a temperature-dependent symmetry factor has been suggested. The systems that deviate from the constant α were reviewed by Conway [156], and a detailed analysis related to this subject is found in the published report of Bockris and Gochev [157]. The most widely studied systems are the hydrogen evolution reaction [158, 159] and the oxygen evolution and reduction reaction [114, 160].

Conway suggested that a linear relation exists between the Tafel slope and temperature rather than a direct proportionality [158]. He developed the following empirical formula:

$$b = \frac{RT}{\beta F} + C \tag{7-5}$$

where b is the Tafel slope (V/decade), F is the Faraday constant (C/mol), β is the symmetry factor, C is a constant, R is the universal gas constant (J/mol•K) and T is the temperature (K).

An alternative relation between the Tafel slope and symmetry factor was also suggested as follows:

$$b = \frac{RT}{\beta' F} \qquad \beta' = \frac{RT}{RT + \beta FC} \tag{7-6}$$

where β', an apparent symmetry factor, should be temperature-dependent.

In limiting cases, b is almost independent of T, and therefore β should be linearly temperature dependent ($\beta = \gamma T + \delta$). For such cases, the following form was proposed:

$$b = \frac{RT}{(\gamma T + \delta)F} \tag{7-7}$$

where γ and δ are constants.

The measured Tafel slopes observed as a function of temperature in the Fe(II)-Fe(III)-H_2SO_4 solutions under different nominal Fe^{3+}/Fe^{2+} ratios is given in Figure 7-9. The dashed line in this figure corresponds to the conventionally expected b-T dependence, i.e., if the apparent transfer coefficient, α, was independent of temperature and equal to 0.5. Although the conditions for the experiments vary widely, it seems that the measured Tafel slopes are relatively independent of temperature and solution composition, and remain within the range of 0.114-0.165 V/decade. From 90 to 150 ℃ the Tafel slopes are in general a little lower than those observed at 25 ℃ and 70 ℃. This phenomenon of lower Tafel slopes at higher temperature requires further study for clarification, but is probably the result of simultaneous changes in the fundamental nature on the surface of $CuFeS_2$ and in the symmetry of the potential energy barrier for the rate-determining step at elevated temperatures. Please note that all of the Tafel plots were linear over at least one order of magnitude of current density.

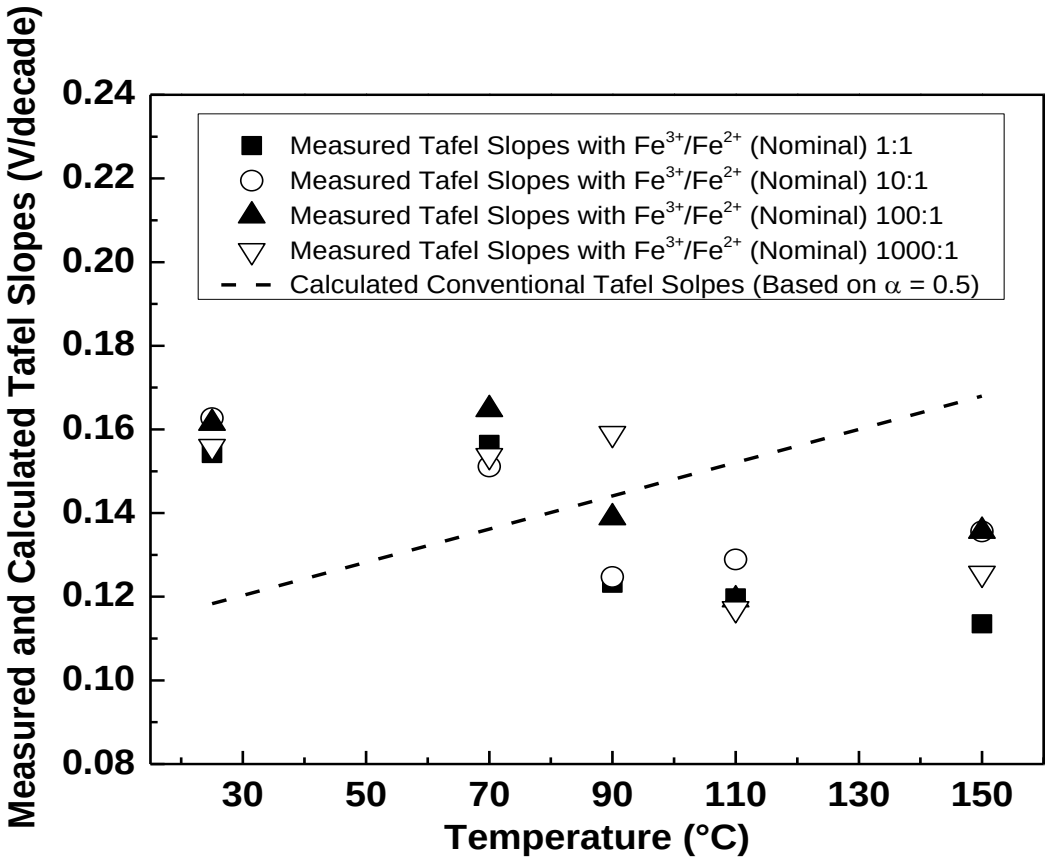

Figure 7-9 Comparison of the measured Tafel slopes and the calculated conventional theoretical values (based on α=0.5) in deaerated aqueous Fe(II)-Fe(III)-H_2SO_4 solutions under different nominal Fe^{3+}/Fe^{2+} ratios in the temperature range of 25 ℃-150 ℃.

In fact, based on the conventional theoretical α value of 0.5, according to Eq. (7-1), it should be expected that the calculated Tafel slopes increase linearly with temperature. However, as clearly demonstrated in Figure 7-9, the difference between the measured Tafel slope and that predicted from Eq. (7-1) is not small, and thus this rule does not apply to the results in the present study. A detailed study is required to explain this phenomenon, but this is probably caused by the result of changes in the fundamental nature of the surface of $CuFeS_2$ and/or in the symmetry of the potential energy barrier for the rate-determining step at different temperatures.

Therefore, from the above analysis, it is obvious that contrary to the view commonly held, the Tafel slopes do not follow the conventional temperature dependence.

7.2.8.2 Variation of Transfer Coefficients with Temperature

The apparent transfer coefficients in the present work were calculated from the measured Tafel slopes by Eq. (7-1). A comparison of transfer coefficients between the values calculated in this work and the conventional assumption (α=0.5) in the temperature range of 25 ℃-150 ℃ is plotted in Figure 7-10. Please recall that in the present study α does not have a single value, and the conventional assumption of α=0.5 is only employed for comparison with the values obtained in this work. At each temperature, the obtained transfer coefficient is an average of the values under four different nominal Fe^{3+}/Fe^{2+} ratios. It can be clearly observed that from 25 to 150 ℃, the transfer coefficient increases with temperature rather than being independent of temperature. Given the variation of α with temperature, regression was carried out and an expression was developed as follows:

$$\alpha = 0.0025 \times T(\mathrm{K}) - 0.3941 \tag{7-8}$$

The corresponding correlation coefficient was 0.923. The obtained value of the temperature coefficient of α ($\partial\alpha/\partial T$=2.5x$10^{-3}$ K^{-1}) is in reasonable agreement with that (approximately 1.5x10^{-3} K^{-1}) needed to account for a *b* that is independent of temperature [157].

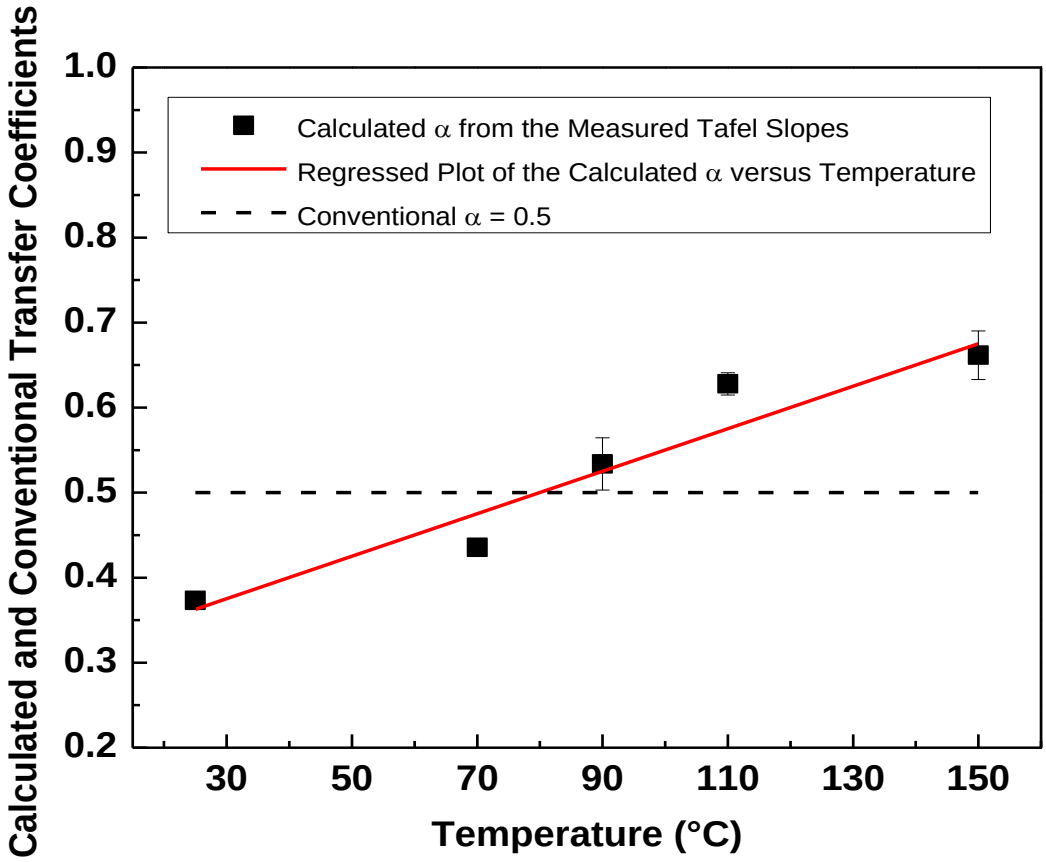

Figure 7-10 Comparison of the calculated transfer coefficients based on the measured Tafel slopes in this work and the conventional value (α=0.5) under different nominal Fe^{3+}/Fe^{2+} ratios in the temperature range of 25 ℃-150 ℃.

From the above equation, it seems that over the temperature range investigated, the transfer coefficient for ferric reduction on chalcopyrite increases linearly with the absolute temperature rather than being a constant. A larger value of α can result in a lower free energy of activation. This result is consistent with the previous conclusion that faster kinetics for ferric reduction on chalcopyrite could be achieved at elevated temperatures, as mentioned in **Section 7.2.7.2**.

The above-noted unexpected temperature independence for the Tafel slope, as well as the anomalous temperature-dependent transfer coefficient, are not unique to the ferric reduction

reaction on chalcopyrite and have been observed previously in other systems [114, 158-162]. These studies were carried out over a wide range of temperatures. For example, Clouser et al [114] investigated the temperature dependence of the Tafel slope and apparent transfer coefficient for oxygen reduction on platinum in H_3PO_4. The observed Tafel slopes were essentially independent of temperature over the 25-250 ℃ range, and were quite different from the values expected from theory. The apparent transfer coefficient for oxygen reduction has been found to be approximately proportional to temperature rather than independent of temperature. A similar anomalous temperature dependence of Tafel slopes and transfer coefficients was also observed for oxygen evolution and reduction on a Pt electrode in dilute aqueous H_2SO_4 and $HClO_4$ solutions in the temperature range of 20-325 ℃ [160].

Various possible factors which may give rise to such behavior and phenomena have been proposed and discussed, including potential dependent adsorption of solution phase species, restructuring of the solution in the compact layer, proton and electron tunneling, a shift in rate-determining step, changes in the symmetry of the potential energy barrier, penetration of the electric field into the electrode phase, insufficient correction for ohmic losses, and impurity effects [114, 157, 158]. Further measurements over a wide range of conditions will be required to confirm the temperature dependency of α and to further study the reason for these observations.

7.3 Summary

The kinetics of ferric reduction on chalcopyrite were systematically investigated by electrochemical measurements in aqueous H_2SO_4-$Fe_2(SO_4)_3$-$FeSO_4$-H_2O solution from 25 to 150 ℃. Since ferric and ferrous ions readily complex in acidic iron sulfate solution to form cations and anions, as well as neutral species, the concentrations of free ferric and ferrous ions were first obtained as a function of electrolyte composition and temperature by a speciation

model developed previously. This information was then employed to analyze the obtained experimental data, by invoking the Nernst equation and other basic electrochemical kinetic equations in order to investigate the electrochemical reduction kinetics of the Fe^{3+}/Fe^{2+} couple on chalcopyrite as well as mechanistic analysis in industrial chalcopyrite leaching processes.

With potentiodynamic polarization, the temperature dependence of the exchange current density, transfer coefficient and rate constant were determined and discussed. Results reveal that, from 25 to 150 ℃, all of the polarization plots exhibit reproducible well-defined linear Tafel regions. The exchange current densities of the Fe^{3+}/Fe^{2+} couple obtained by extrapolating the cathodic linear Tafel line to the reversible potential are on the order of 10^{-7}-10^{-5} A/cm^2 in the range of 25-150 ℃, substantially less than that on platinum due to the formation of a passive film. In general, at the same nominal Fe^{3+}/Fe^{2+} ratio, increasing the temperature from 25 to 150 ℃ was observed to give rise to an increase in i_0, especially when a larger amount of free ferrous existed in the solution. In addition, at each temperature, i_0 increases by increasing the concentration of ferrous in the solution.

Based on the obtained exchange current densities, the rate constant for ferric reduction was calculated, and its values increase with temperature from 0.049 cm/s at 25 ℃ to almost 900 cm/s at 150 ℃. Further analysis indicates that the rate constant follows Arrhenius behavior and the activation energy for the ferric ion reduction reaction was calculated to be 85 ± 1 kJ mol^{-1} in the temperature range of 25-150 ℃. The temperature increase from 25 to 150 ℃ also caused a substantial increase in i_M, from the order of 10^{-6} A/cm^2 at 25 ℃ to the order of 10^{-4} A/cm^2 at 150 ℃.

Analysis of the measured Tafel slopes as a function of temperature in the Fe(II)-Fe(III)-H_2SO_4 solutions under different nominal Fe^{3+}/Fe^{2+} ratios indicates that the Tafel slopes are

essentially independent of temperature and the solution composition over the range of 25 to 150 ℃, and remain within the range of 0.114-0.165 V/decade. Consequently, the apparent transfer coefficients calculated from the measured Tafel slopes, increase linearly with respect to temperature rather than being a constant from 25 to 150 ℃. The obtained value of the temperature coefficient of α ($2.5x10^{-3}$ K^{-1}) is in reasonable agreement with that (in the region of $1.5x10^{-3}$ K^{-1}) needed to account for a b independent of temperature. The unexpected temperature independence for the Tafel slope, as well as the anomalous temperature-dependent transfer coefficient, are not unique to the ferric reduction reaction on chalcopyrite, and have been observed previously in various systems.

8 Influence of Ferric Ion Reduction Reaction on Chalcopyrite Leaching Behavior from 25 ℃ to 150 ℃

8.1 Introduction

The mixed potential theory involved two half-cell reactions provides a unique advantage of having a greater insight into the mechanism of the dissolution process. In the present Chapter, based on the previously obtained reversible potentials of the Fe^{3+}/Fe^{2+} couple and the mixed potentials measured under oxidizing conditions, as well as the calculated reversible potentials of possible anodic reactions, the mechanism involved in the chalcopyrite leaching system will be analyzed by mixed potential theory, to obtain detailed information about the electrochemical reactions involved, and hence determine to what extent the cathodic ferric ion reduction reaction can affect the overall leaching process.

The concept of mixed potential (E_M) has been widely used to explain the kinetics observed in hydrometallurgical processes [23, 24, 46-50, 163]. Only the mixed potential measured on a mineral surface is representative of the dissolution process. The difference between the mixed potential and the relevant reversible potential, the over-potential (η_C and η_A), represents the driving force for each half-reaction. In the present study, OCP is a mixed potential between the reversible potential of the cathodic reduction of ferric (E_C) and the reversible potential of the anodic oxidation of chalcopyrite (E_A). A comparison of the calculated reversible potentials and measured mixed potentials was used to analyze the control scenario. The mixed potential of a chalcopyrite electrode in a leaching environment may be used as an indicator of the control mechanism of the leaching reaction. Figure 8-1 is a schematic diagram of the mixed potential theory for the oxidative dissolution of chalcopyrite by ferric ion. The present section aims at a

more detailed analysis of the observed trend of the involved potentials versus temperature in the leaching process.

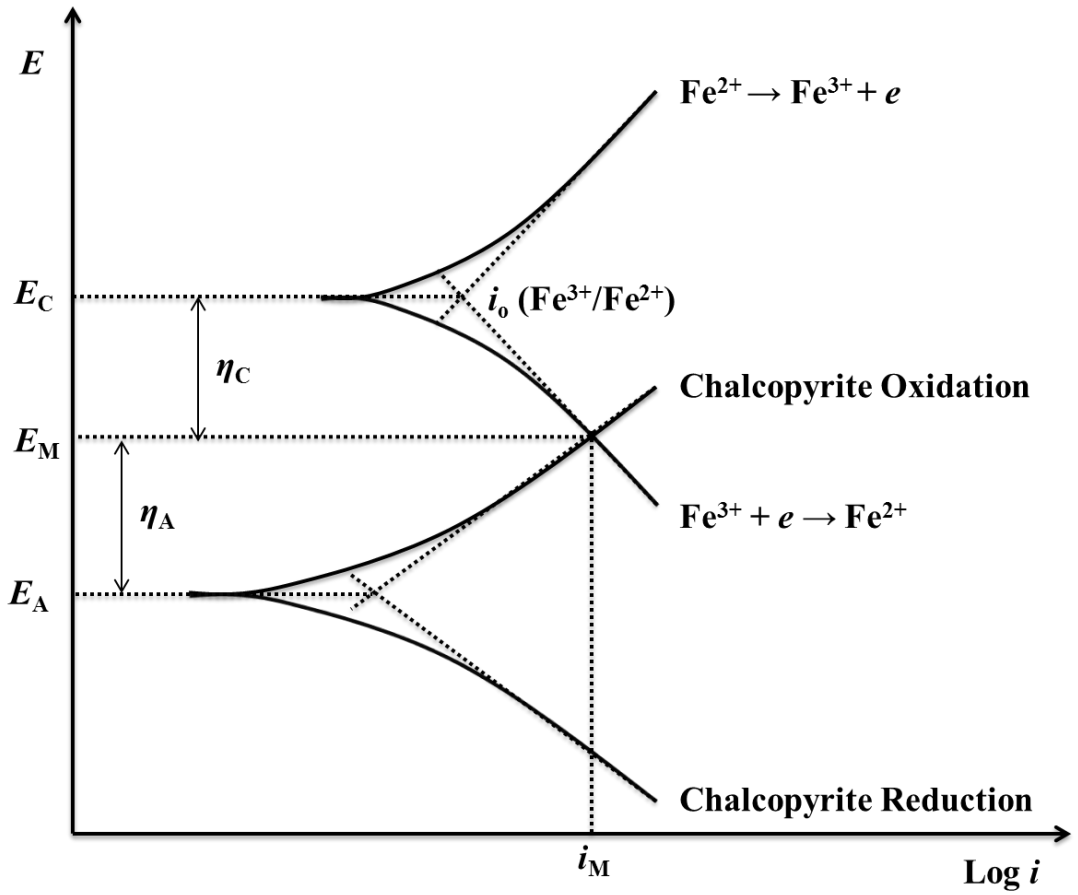

Figure 8-1 Schematic diagram of the mixed potential theory for the oxidative dissolution of chalcopyrite by ferric ion.

8.2 Results and Discussion

8.2.1 Calculated E_C and Measured E_M Potentials

The calculated E_C and measured E_M potentials in the Fe(II)-Fe(III)-H_2SO_4 solutions under different nominal Fe^{3+}/Fe^{2+} ratios in the temperature range of 25–150 ℃ are given in Tables 7-2

to 7-6. In order to employ mixed potential theory, however, the reversible potential of the anodic oxidation reaction for chalcopyrite (E_A) is also required and this will be calculated and provided as follows.

8.2.2 Calculation of Reversible Potential of Anodic Oxidation Reactions of Chalcopyrite from 25 ℃ to 150 ℃

In the past decades, although great international efforts have been devoted to understanding the mechanisms of chalcopyrite leaching, no unanimous theory is available to account for its slow kinetics in most leaching environments. Nevertheless, there is consensus that the formation of a passivating layer on the chalcopyrite surface slows the dissolution kinetics. These studies, and the proposed possible anodic oxidation reactions, were summarized and reviewed by several authors [155, 164-166].

Relying on the limited availability of the relevant thermodynamic data for the products generated by the anodic oxidation reaction, herein five typically cited and possible anodic oxidation reactions for chalcopyrite have been considered and their reversible potentials were calculated. Table 8-1 lists the selected possible anodic oxidation reactions for chalcopyrite in aqueous Fe(II)-Fe(III)-H_2SO_4 solutions [18, 54, 165]. Please note that, for the oxidation of chalcopyrite in acidic iron sulfate solution, Reaction 1 and Reaction 2 are the well-accepted forms, and it is frequently assumed that Reaction 1 is the predominant one. To calculate the reversible potential for these anodic oxidation reactions (E_A), the standard electrode potentials of the anodic oxidation reaction of chalcopyrite ($E_A°$), as well as the single ion activity for ionic species, were first obtained.

When calculating $E_A°$, the standard Gibbs free energies of ionic species at high temperatures were estimated by the above-mentioned Lewis formulation of the Criss-Cobble

correspondence principle based on thermodynamic data available at room temperature. For solid and liquid species, this can be achieved with knowledge of the standard Gibbs free energy of formation at 298.15 K and the heat capacity. The heat capacity parameters (Kelley equation coefficients) of those species were taken from HSC 7.1 [143], and ΔG° at higher temperature were calculated by the Kelley equation. The thermodynamic data at 298.15 K (ΔG° and S°) were taken from the literature [129, 166]. All of the thermodynamic data used in the calculation are shown in Table 8-2, and data of H^+, SO_4^{2-}, Fe^{2+} and H_2O were already shown in Chapter 5.

Table 8-1 Calculated standard electrode potentials for the possible anodic oxidation reactions of chalcopyrite in aqueous Fe(II)-Fe(III)-H_2SO_4 solutions in the range of 25-150 ℃.

Anodic Oxidation Reactions of Chalcopyrite	E_A° (V)				
	25°C	70°C	90°C	110°C	150°C
$CuFeS_2 \rightarrow Cu^{2+} + Fe^{2+} + 2S^0 + 4e$ (1)	0.439	0.467	0.476	0.484	0.489
$CuFeS_2 + 8H_2O \rightarrow Cu^{2+} + Fe^{2+} + 16H^+ + 2SO_4^{2-} + 16e$ (2)	0.374	0.397	0.405	0.413	0.425
$CuFeS_2 \rightarrow CuS + Fe^{2+} + S^0 + 2e$ (3)	0.263	0.290	0.299	0.307	0.313
$CuFeS_2 \rightarrow 0.75CuS + 0.25Cu^{2+} + Fe^{2+} + 1.25S^0 + 2.5e$ (4)	0.333	0.361	0.370	0.378	0.383
$CuFeS_2 \rightarrow 0.5Cu_2S + Fe^{2+} + 1.5S^0 + 2e$ (5)	0.311	0.337	0.345	0.352	0.352

Table 8-2 Thermodynamic data at 25 ℃ and Kelley equation coefficients of the solids involved in the anodic chalcopyrite oxidation reactions in the range of 25-150 ℃.

Species	$\Delta G°$ (kJ/mol)	$S°$ (J/mol K)	C_p (J/mol K)			
			A	B	C	D
Cu^{2+}	65.7	-97.2				
S (100-368.3 K)	0.00	31.8	7.835	79.793	-0.207	-97.893
S (368.3-388.36 K)			968.639	-3355.340	-223.772	3368.169
S (388.36-428.15 K)			-8691.858	28083.985	2467.293	-25321.119
$CuFeS_2$ (298.15-830 K)	-195.1	124.9	86.985	53.555	-5.607	0
CuS (298.15-1000 K)	-53.2	66.96	43.671	20.136	-2.102	-0.005
Cu_2S (298.15-376.00 K)	-87.6	118.8	53.438	76.459	-0.117	2.456
Cu_2S (376.00-717.00 K)			112.140	-30.973	-0.046	0.147

a. The heat capacity parameters (Kelley equation coefficients) of S, $CuFeS_2$, CuS and Cu_2S used to calculate the equilibrium constants were taken from HSC 7.1 .

b. Kelley equation: $C_p(T) = A + B*10^{-3}*T + C*10^{5}*T^{-2} + D*10^{-6}*T^{2}$ (J/mol*K).

All of the calculated $E_A°$ of the five reactions at different temperatures are shown in Table 8-1. $E_A°$ of the five reactions increases with temperature. Interestingly, the calculated $E_A°$ for Reaction 1 (100% S^0 formation) is larger than that of Reaction 2 (100% SO_4^{2-} formation), and hence Reaction 2 is thermodynamically more favorable.

As to the single ion activities for Fe^{2+}, H^+ and SO_4^{2-} involved in the present study, they were obtained by the above-mentioned speciation model under different conditions. When

involving the activity of Cu^{2+}, a value of $a_{Cu2+} = 10^{-5}$ was assumed. This value is reasonable because at the very beginning of leaching (on the scale of the measurement time used herein), the activity of Cu^{2+} produced by the oxidation of $CuFeS_2$ should be very small. $a_{Cu2+} = 10^{-3}$ was also used to compare the calculated reversible potentials. Cu^{2+} is not included in Reaction 3 and Reaction 5, so their potentials are not affected by the change of Cu^{2+} activity. For Reaction 1, changing the Cu^{2+} activity from 10^{-5} to 10^{-3} results in an increase of the calculated reversible potential of no more than 45 mV (typically within the range of 30-40mV); for Reaction 2 and Reaction 4, such an increase only leads to an increase in the calculated potentials of no more than 17 mV. Actually, even increasing the Cu^{2+} activity from 10^{-3} to 1, the reversible potentials for Reaction 1 (smaller than 60 mV), Reaction 2 and Reaction 4 (smaller than 25 mV) under all of the solution conditions in the present study did not increase to any appreciable extent. Therefore, it appears that the Cu^{2+} activity does not exert an important influence on E_A, and the above assumption employed to estimate the reversible potentials of anodic oxidation reactions is acceptable and applicable.

By using the above methods, E_A of the five possible anodic oxidation reactions of chalcopyrite were calculated. A detailed discussion on the obtained results will be given in the following section.

8.2.3 Analysis of Leaching Process by Mixed Potential Theory

Figure 8-2 and Figure 8-3 present all of the measured mixed potentials and calculated theoretical cathodic and anodic reversible potentials in the Fe(II)-Fe(III)-H_2SO_4 solutions for the present study over the temperature range of 25℃-150℃ under different nominal Fe^{3+}/Fe^{2+} ratios. It is observed that the measured mixed potentials lie between the cathodic and anodic reversible potentials. As shown previously, even though there is Fe^{2+} being produced by the reduction of

Fe^{3+} and oxidation of $CuFeS_2$, the concentration change is not high enough to exert a significant influence on the mixed potential during the measurement time of the experiment. Typically, it is important to observe that all of the measured mixed potentials are generally within the range of 0.64 ± 0.06 V under all of the conditions employed in the present study. At each temperature, in general, there is an obvious drop in the measured E_M when a large amount of ferrous exists in the electrolyte, which agrees with the previous finding at 90 ℃ reported by Jones [46].

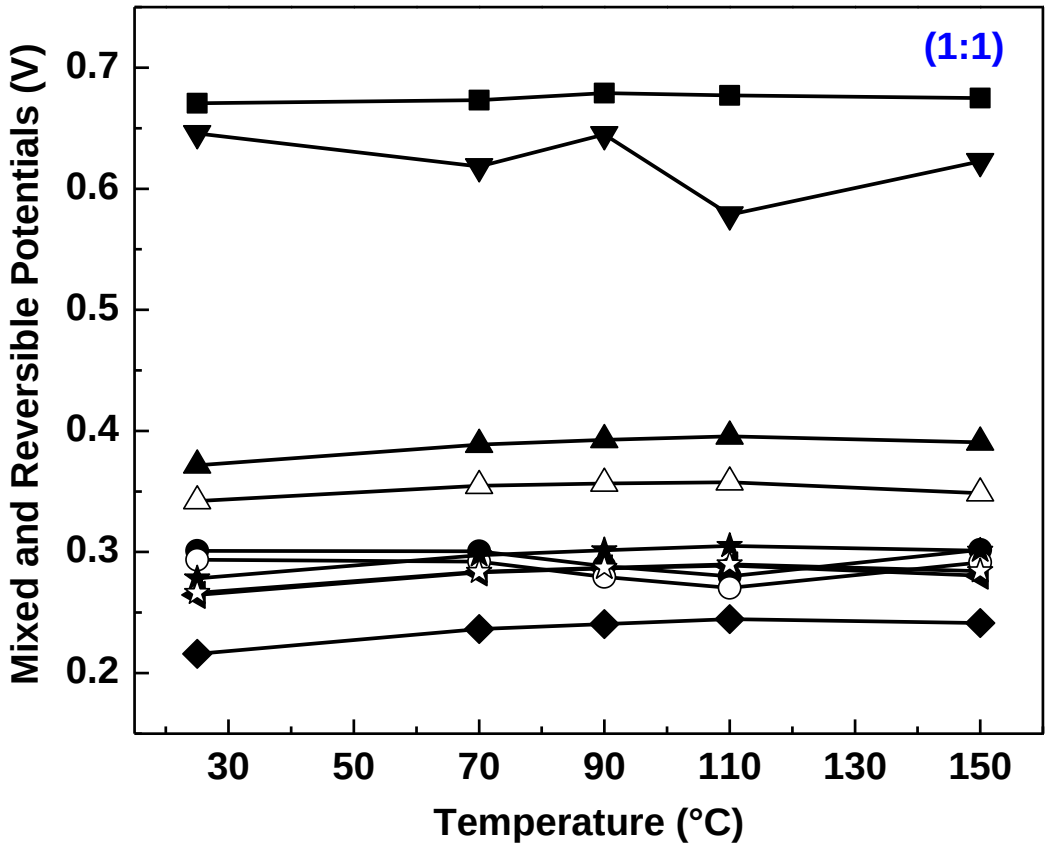

Figure 8-2 Measured mixed potentials and calculated theoretical cathodic and anodic reversible potentials in the Fe(II)-Fe(III)-H_2SO_4 solutions at [H_2SO_4] = 0.31 mol/kg and [Fe^{3+}]$_{total}$ = 0.18 mol/kg in the temperature range of 25 ℃-150 ℃ with nominal Fe^{3+}/Fe^{2+} ratio of 1:1.

(cathodic reversible potential E_C ■; mixed potential E_M ▼; reversible potential of anodic reaction 1 assuming $a_{Cu2+} = 10^{-3}$ ▲; reversible potential of anodic reaction 1 assuming $a_{Cu2+} = 10^{-5}$ △; reversible potential of anodic reaction 3 ◆; reversible potential of anodic reaction 5 ◄; reversible potential of anodic reaction 2 assuming $a_{Cu2+} = 10^{-3}$ ●; reversible potential of anodic reaction 2 assuming $a_{Cu2+} = 10^{-5}$ ○; reversible potential of anodic reaction 4 assuming $a_{Cu2+} = 10^{-3}$ ★; reversible potential of anodic reaction 4 assuming $a_{Cu2+} = 10^{-5}$ ☆.)

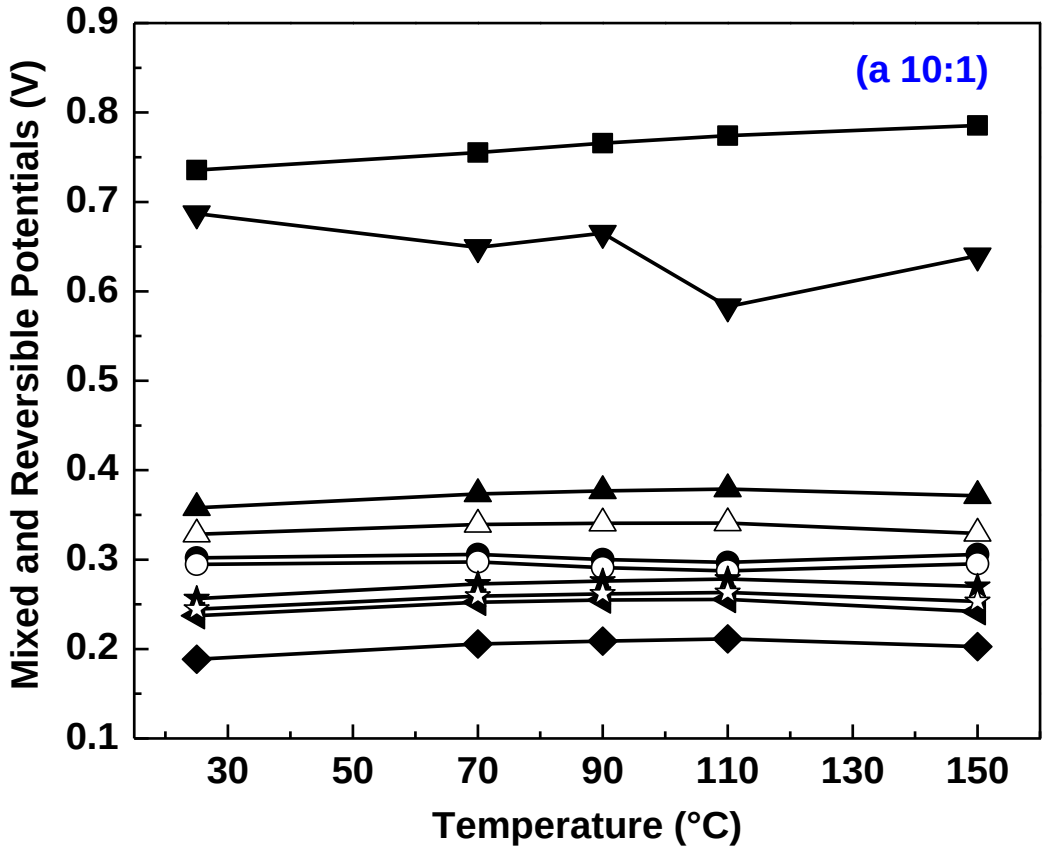

Figure 8-3 Measured mixed potentials and calculated theoretical cathodic and anodic reversible potentials in the Fe(II)-Fe(III)-H_2SO_4 solutions at $[H_2SO_4]$ = 0.31 mol/kg and $[Fe^{3+}]_{total}$ = 0.18 mol/kg in the temperature range of 25 ℃-150 ℃ under higher nominal Fe^{3+}/Fe^{2+} ratios: (a) 10:1; (b) 100:1; (c) 1000:1. The symbols used in these Figures are the same as those shown in Figure 8-2.

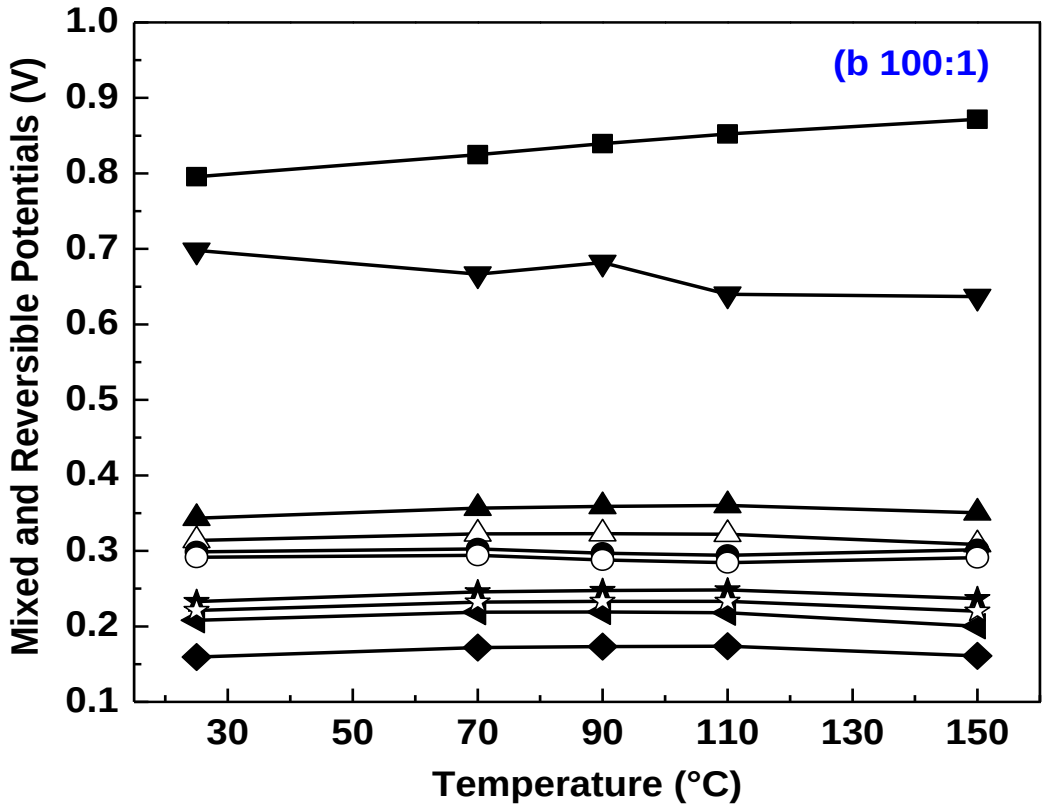

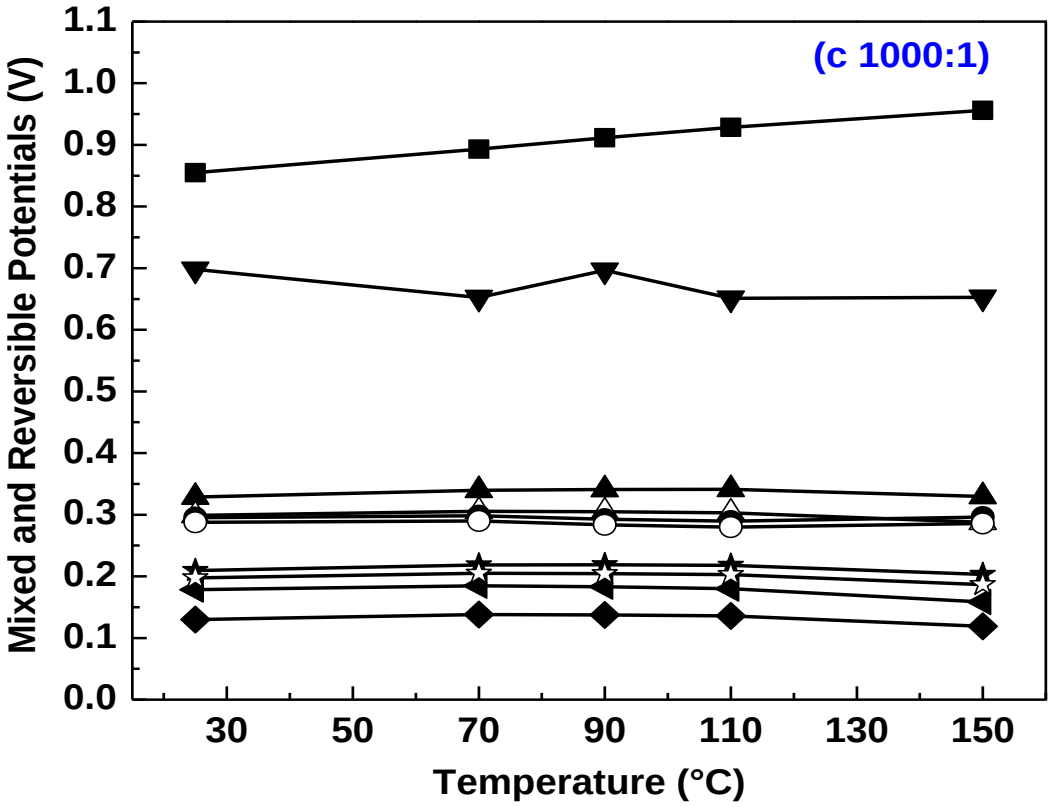

Figure 8-3 Continued.

As discussed previously, the reaction rate of the Fe^{3+}/Fe^{2+} couple is quite fast on the surface of platinum, and the reaction can be considered reversible or highly quasi-reversible. However, the measured E_M of chalcopyrite indicates that, in acidic iron sulfate solutions, the Fe^{3+}/Fe^{2+} couple is much less reversible on the chalcopyrite surface, especially at higher nominal Fe^{3+}/Fe^{2+} ratio and temperature (in such a case the cathodic over-potential η_C is so large that the back reaction involving Fe^{2+} is negligible). As to the anodic dissolution reaction of chalcopyrite, the measured E_M during ferric sulfate leaching is typically 200-300 mV (or even lager) higher than those calculated E_A, and therefore there appears to be a significant degree of anodic polarization. These results are also in agreement with those published by Jones [46], who calculated the Nernst potentials of the anodic and cathodic reactions with some simple assumptions (for example without considering ferrous or ferric complexes in sulfate solutions) and examined the leaching of chalcopyrite in ferric sulfate solution by mixed potential theory at 90 ℃.

It should be noted that in the region of the mixed potential (at mixed potential the rate of the oxidation reaction is balanced by that of the reduction reaction), the rates of the reverse processes can be ignored. As reported by Nicol [163], this is generally valid for the oxidation of minerals which tend to be highly irreversible systems, but is not always valid for the oxidant (as with iron (III) in his paper). This concept is fully justified by the above analysis of the chalcopyrite leaching in acidic iron sulfate solution. In the present study, E_M is approximately equal to E_C only when the nominal Fe^{3+}/Fe^{2+} ratio is 1:1 (the solution contains appreciable amounts of ferrous) and the temperature is low (25 ℃). This means that, at the mixed potential, the contribution of the anodic current due to the oxidation of chalcopyrite is small, compared to

that of the oxidation of ferrous. The mixed potential in such a case is therefore determined by the characteristics of the Fe^{3+}/Fe^{2+} couple, and not by the anodic characteristics of chalcopyrite (so-called Type III situation from Nicol's paper). However, when further increasing the nominal Fe^{3+}/Fe^{2+} ratio and temperature, the contribution of the partial anodic current from the oxidation of ferrous is almost negligible and hence the E_M is much lower than E_C. Thus, in such a case, only the anodic characteristics of chalcopyrite and the cathodic characteristics of Fe^{3+} are significant in the region of the mixed potential (so-called Type I situation from Nicol's paper). It should be mentioned that in Nicol's paper, an intermediate situation (labeled Type II) is the one for which all of the three half-reactions must be taken into account. From the above results, it appears that under the investigated conditions, Type I leaching plays a more common role in the oxidation of chalcopyrite by acidic iron sulfate solution, while Type III leaching applies only at low temperature with low nominal Fe^{3+}/Fe^{2+} ratios. In fact, Type I leaching was also observed for chalcopyrite in sulfate solution with oxygen as the oxidant by Yu et al. [167], and in chloride solution with ferric as the oxidant by Majima et al [168], as reported in Nicol's paper. Type I leaching for sphalerite dissolution in acidic iron sulfate electrolyte at 78 ℃ was also reported by Crundwell [55]. A detailed discussion on the Type I and Type III leaching model (along with schematic diagram) can be found in the literature [163, 165].

Comparison of E_M and E_C over a wide range of temperature in Figure 8-2 and Figure 8-3 indicates that the mixed potential (a kinetic quantity) is always different from the cathodic reversible potential (a thermodynamic quantity). It is also noteworthy that no significant increase in E_M on chalcopyrite was achieved, even at very high nominal Fe^{3+}/Fe^{2+} ratios and temperatures where the Nernst equation would predict a substantial increase in E_C. This raises some concerns about the use of higher concentrations of iron (III) and higher nominal Fe^{3+}/Fe^{2+} ratios in the

industrial hydrometallurgical leaching processes. Actually, it has been reported that chalcopyrite's leaching rate is strongly affected by ferric ion concentration only at concentrations less than 0.01 or 0.1 M, and at higher concentrations the effect is negligible [12, 54]. Given the importance of the ferric concentration and the nominal Fe^{3+}/Fe^{2+} ratio in commercial leaching processes, additional investigation would be required to determine the optimum parameters.

An electrochemical reaction may be said to be under anodic, cathodic or mixed control, depending on the relative polarization degrees of the anodic and cathodic reactions. It can be clearly seen in Figure 8-2 that η_C is always smaller than η_A, no matter which of the possible anodic oxidation reactions is chosen and no matter the conditions used in the present work. Hence, with the nominal Fe^{3+}/Fe^{2+} ratio being 1:1, the degree of cathodic polarization is quite small and the leaching reaction could be said to be under anodic control, because the anodic reaction is highly polarized. However, as indicated in Figure 8-3a, Figure 8-3b and Figure 8-3c, when further increasing the nominal Fe^{3+}/Fe^{2+} ratio and temperature, the effect of the cathodic ferric reduction reaction on the overall leaching process is progressively enhanced, even at lower temperatures. For the 1000:1 nominal Fe^{3+}/Fe^{2+} ratio, at 110 ℃ and 150 ℃, η_C is almost equal to η_A when employing Reaction 1 or Reaction 2, which means that the leaching of chalcopyrite in ferric sulfate solution is under mixed control, both by the ferric reduction reaction and the anodic chalcopyrite oxidation reaction. In such a case, both anodic and cathodic reactions are quite irreversible, according to the relative position of the mixed potential and the calculated Nernst potentials of the anodic and cathodic reactions. Thus, based on the above analysis, a conclusion can be drawn that the control scenario is influenced by both the solution composition and temperature for chalcopyrite oxidation in acidic iron sulfate leaching solution, and the importance of the cathodic Fe^{3+}/Fe^{2+} processes to determine the leaching kinetics in the coupled

system is progressively enhanced when increasing the nominal Fe^{3+}/Fe^{2+} ratio and temperature (not just by the anodic oxidation reaction).

In addition, from Figure 8-2 and Figure 8-3, it can be seen that the ferric reduction reaction at potentials near the mixed potential is always in the kinetic-controlled region for the Fe^{3+}/Fe^{2+} couple. This result is in agreement with the previous finding that a relatively large activation energy was obtained for the ferric reduction reaction, as mentioned in **Section 7.2.7.2**.

As mentioned previously, compared with Reaction 1, Reaction 2 is thermodynamically more favorable, due to the relatively smaller E_A. In addition, in Figure 8-2 and Figure 8-3, it is interesting to note that the E_A of Reaction 1 approaches that of Reaction 2 under higher nominal Fe^{3+}/Fe^{2+} ratios and elevated temperatures. This implies that in such a case, Reaction 1 becomes progressively more favorable (Please note that because of its the relatively smaller E_A Reaction 2 is still thermodynamically more favorable).

In this section, although the present study provided some useful conclusions of the mechanism in chalcopyrite leaching systems, it should be emphasized that some of these conclusions depend on the accuracy of the selection of the anodic reactions and the corresponding E_A calculation. Detailed research on the anodic reactions would be required in order to substantiate these results and expand our understanding of this leaching system.

8.3 Summary

In this Chapter, a comparison between the calculated reversible potentials of the cathodic and possible anodic reactions and measured mixed potentials was used to analyze the control scenario.

Typically, the measured mixed potentials lie between the cathodic and anodic reversible potentials and are within the range of 0.64 ± 0.06 V under all of the conditions employed in the

present study. At each temperature, in general, there is an obvious drop in the measured E_M when a large amount of ferrous exists in the electrolyte. The measured E_M indicates that, in acidic iron sulfate solutions, the Fe^{3+}/Fe^{2+} couple is much less reversible on the chalcopyrite surface, especially at higher nominal Fe^{3+}/Fe^{2+} ratio and temperature. In the region of the mixed potential, Type I leaching prevails in the oxidation of chalcopyrite by acidic iron sulfate solution, while Type III leaching applies only at low temperature with lower nominal Fe^{3+}/Fe^{2+} ratios.

Analysis by mixed potential theory indicates that in the acidic iron sulfate leaching system the control scenario highly depends on both the solution composition and temperature, and the effect of cathodic ferric reduction reaction on the overall leaching process is progressively enhanced when increasing the nominal Fe^{3+}/Fe^{2+} ratio and temperature. The leaching reaction is under anodic control when the nominal Fe^{3+}/Fe^{2+} ratio is around 1:1, whereas at higher nominal Fe^{3+}/Fe^{2+} ratio and temperature the reaction is under mixed control, both by the ferric reduction reaction and the anodic oxidation reaction. In such a case, both anodic and cathodic reactions are quite irreversible.

9 Conclusions, Industrial Applications and Recommendations

A thermodynamic model has been developed and shown to reliably simulate the speciation of the quaternary H_2SO_4-$Fe_2(SO_4)_3$-$FeSO_4$-H_2O system under conditions most relevant to the hydrometallurgical industry. The model results are further employed to predict the redox potential of the Fe^{3+}/Fe^{2+} couple in acidic iron sulfate solutions, investigate the reduction kinetics of the Fe^{3+}/Fe^{2+} couple on the surface of chalcopyrite, and carry out a mechanistic analysis relevant to industrial leaching processes for chalcopyrite.

9.1 Conclusions

- Results from the calculated distribution of the main ferric and ferrous species as a function of temperature, iron and acid concentration, and the nominal Fe^{3+}/Fe^{2+} ratio reveal that most of the Fe(III) is distributed as complexes or precipitates and the free ferric ion accounts for only a minor percentage, whereas a large amount of Fe(II) exists in the form of free ferrous ion. Moreover, under the same nominal Fe^{3+}/Fe^{2+} ratio, a temperature increase within the range of 25 ℃-150 ℃ leads to a decline in the free Fe^{3+} concentration, whereas the free Fe^{2+} concentration is relatively stable. Under all of the investigated conditions, $FeSO_4^+$ is always the predominant species for Fe(III) in the aqueous solution. At 150 ℃, a large amount of Fe(III) precipitated as Fe_2O_3, with the largest value of 61.7% obtained when the nominal Fe^{3+}/Fe^{2+} ratio was 1:1. The percentage of formed Fe_2O_3 under higher nominal Fe^{3+}/Fe^{2+} ratios is relatively stable and lower than that under nominal Fe^{3+}/Fe^{2+} ratio of 1:1, due to relatively lower amount addition of $FeSO_4$. The validity of the proposed model was confirmed by reliable prediction of measured redox potential from 25 ℃ to 150 ℃, and of ferric solubility at

150 ℃. Extensive analysis and review of the calculated pH and real ionic strength of the solution provides an additional affirmation of the validity of the present work.

- Based on the model results, the temperature dependence of the real Fe^{3+}/Fe^{2+} ratios and their activity coefficient ratios were obtained. The calculated real Fe^{3+}/Fe^{2+} ratio is much lower than the nominal ratio, and from 25 ℃ to 150 ℃, under each given nominal Fe^{3+}/Fe^{2+} ratio, the calculated real ratio of Fe^{3+}/Fe^{2+} substantially declines with temperature. The activity coefficient ratios are typically only affected by temperature, and remain practically constant at each temperature under different nominal Fe^{3+}/Fe^{2+} ratios. These results, together with the calculated standard electrode potential of the Fe^{3+}/Fe^{2+} couple, were employed to systematically study the redox potential of the Fe^{3+}/Fe^{2+} couple. Results indicate that for a given temperature the model-calculated potentials increase considerably with the nominal Fe^{3+}/Fe^{2+} ratio. However, from 25 ℃ to 150 ℃, the potentials predicted by the model increase gradually only when the nominal Fe^{3+}/Fe^{2+} ratios are 10:1, 100:1 and 1000:1 (with its values in the range of ~736–956 mV), while at the nominal Fe^{3+}/Fe^{2+} ratio of 1:1 they are relatively stable (typically between ~671 and 679 mV) and no significant change was observed as the temperature increased. The speciation model explains the change of redox potential with temperature for all nominal Fe^{3+}/Fe^{2+} ratios.
- An expression Eq. (6-9) determined only by the variables of temperature and nominal Fe^{3+}/Fe^{2+} ratio was developed to predict the redox potential of the Fe^{3+}/Fe^{2+} couple. Measured redox potentials in the literature agree very well with those predicted by the developed expression, independent of the nominal concentrations of Fe^{3+} and H_2SO_4.

Moreover, the expression is probably applicable to more general cases at or around room temperature.

- By using cathodic potentiodynamic polarization, the temperature dependence of the exchange current density, transfer coefficient and rate constant were determined and discussed. Results reveal that, from 25 to 150 ℃, all of the polarization plots exhibit reproducible well-defined linear Tafel regions. The exchange current densities of the Fe^{3+}/Fe^{2+} couple obtained by extrapolating the cathodic linear Tafel line to the reversible potential are on the order of 10^{-7}-10^{-5} A/cm^2 in the range of 25-150 ℃, substantially less than that on platinum due to the formation of a passive film. In general, at the same nominal Fe^{3+}/Fe^{2+} ratio, increasing the temperature from 25 to 150 ℃ was observed to give rise to an increase in i_0, especially when a larger amount of free ferrous existed in the solution. Based on the obtained exchange current densities, the rate constant for ferric reduction was calculated, and its values increase with temperature from 0.049 cm/s at 25 ℃ to almost 900 cm/s at 150 ℃. Further analysis indicates that the rate constant follows Arrhenius behavior and the activation energy for the ferric ion reduction reaction was calculated to be 85 ± 1 kJ mol^{-1} in the temperature range of 25-150 ℃. The temperature increase from 25 to 150 ℃ also caused a substantial increase in i_M, from the order of 10^{-6} A/cm^2 at 25 ℃ to the order of 10^{-4} A/cm^2 at 150 ℃.
- Analysis of the measured Tafel slopes as a function of temperature in the Fe(II)-Fe(III)-H_2SO_4 solutions under different nominal Fe^{3+}/Fe^{2+} ratios indicates that the Tafel slopes are essentially independent of temperature and the solution composition over the range of 25 to 150 ℃, and remain within the range of 0.114-0.165 V/decade. Consequently, the apparent transfer coefficients calculated from the measured Tafel slopes, increase linearly

with respect to temperature rather than being a constant from 25 to 150 ℃. The obtained value of the temperature coefficient of α (2.5×10^{-3} K^{-1}) is in reasonable agreement with that (in the region of 1.5×10^{-3} K^{-1}) needed to account for a *b* independent of temperature.

- Typically, the measured mixed potentials lie between the cathodic and anodic reversible potentials and are within the range of 0.64 ± 0.06 V under all of the conditions employed in the present study. At each temperature, in general, there is an obvious drop in the measured E_M when a large amount of ferrous exists in the electrolyte. The measured E_M indicates that, in acidic iron sulfate solutions, the Fe^{3+}/Fe^{2+} couple is much less reversible on the chalcopyrite surface, especially at higher nominal Fe^{3+}/Fe^{2+} ratio and temperature. In the region of the mixed potential, Type I leaching prevails in the oxidation of chalcopyrite by acidic iron sulfate solution, while Type III leaching applies only at low temperature with lower nominal Fe^{3+}/Fe^{2+} ratios.
- Analysis by mixed potential theory indicates that in the acidic iron sulfate leaching system the control scenario highly depends on both the solution composition and temperature, and the effect of cathodic ferric reduction reaction on the overall leaching process is progressively enhanced when increasing the nominal Fe^{3+}/Fe^{2+} ratio and temperature. The leaching reaction is under anodic control when the nominal Fe^{3+}/Fe^{2+} ratio is around 1:1, whereas at higher nominal Fe^{3+}/Fe^{2+} ratio and temperature the reaction is under mixed control, both by the ferric reduction reaction and the anodic oxidation reaction. In such a case, both anodic and cathodic reactions are quite irreversible.

9.2 Industrial Applications

- At 150 ℃, a relatively large amount of Fe(III) precipitated as Fe_2O_3 when the nominal Fe^{3+}/Fe^{2+} ratio was 1:1 as compared to the amount precipitated at higher nominal Fe^{3+}/Fe^{2+} ratios. This is due to the larger amount of $FeSO_4$ present at the 1:1 condition. Hence, under industrial conditions, such as those processes operated at 150 ℃ (Dynatec, AAC/UBC and CESL), it would be advantageous to maintain larger concentrations of $FeSO_4$ in order to promote Fe_2O_3 precipitation. There is also supporting evidence (not yet published) from co-workers in the Asselin group that larger amounts of ferrous ion promote the precipitation of hematite and reduce super-saturation. This has important implications for iron control in such processes.
- According to the equation developed in this work (Eq. 6-9, reproduced below), the redox potential of the quaternary H_2SO_4-$Fe_2(SO_4)_3$-$FeSO_4$-H_2O system is solely determined by the variables of the nominal Fe^{3+}/Fe^{2+} ratio and temperature. This implies that whenever two of these variables are known, the third can be calculated. For example, if the redox potential is measured at a given temperature, the nominal Fe^{3+}/Fe^{2+} ratio can then be calculated. By further measuring the total iron in the solution, the nominal Fe(II) and Fe(III) amounts can be obtained. Hence, this equation is quite useful for understanding and studying leach chemistry. Moreover, the expression is probably applicable to more general cases at lower temperatures. This is of particular interest in the industrial processes operated at lower temperatures, such as Nenatech, Galvanox, and heap leaching of copper sulfides. Even if oxygen is included in the system, the kinetics of reduction of oxygen are sufficiently slow (as well documented in many literature studies) and ferric

reduction is always dominant. Hence the measured redox potential is dominated by the Fe^{3+}/Fe^{2+} couple.

$$E(\mathrm{mV}) = -1\times10^{-3}\times[T(\mathrm{K})]^2 + 0.91\times T(\mathrm{K}) + \frac{2.303R}{nF}\times T(\mathrm{K})\times10^{3}\times\log\frac{C_{\text{ferric, nominal}}}{C_{\text{ferrous, nominal}}} + 492$$

Very importantly, this expression also avoids the complicated calculations of the standard electrode potential and the activity coefficient.

- The present study reveals that in the acidic iron sulfate leaching system the leaching reaction is under anodic control when the nominal Fe^{3+}/Fe^{2+} ratio is around 1:1. At higher nominal Fe^{3+}/Fe^{2+} ratios and temperatures the reaction is under mixed control, both by the ferric reduction reaction and the anodic oxidation reaction. In addition, published results of the previously mentioned industrial processes show that the nominal Fe^{3+}/Fe^{2+} ratios in the leaching solution are typically lower than 7:1 at the initial stages. This implies that the leaching reaction is under anodic control for those processes. Admittedly, during a long term leaching reaction, the nominal Fe^{3+}/Fe^{2+} ratio in the leaching solution changes. Moreover, it has also been reported that lower nominal Fe^{3+}/Fe^{2+} ratios (with a corresponding lower redox potential) can enhance the leaching rate, as discussed in **Section 2.1.1.2**. As a result, the operating parameters, such as nominal Fe^{3+} concentration, nominal Fe^{3+}/Fe^{2+} ratio, and oxygen supply could be optimized. Hence, when designing or improving such industrial leaching processes, more attention should be paid to the control mechanism so as to increase the leaching rate according to these theoretical aspects. For example, for chalcopyrite heap leaching, by measuring the iron concentration and obtaining the nominal Fe^{3+}/Fe^{2+} ratios in the leaching solution, the control mechanism can be known according to the kinetic findings in this work. As an example, under lower nominal Fe^{3+}/Fe^{2+} ratios, the leaching reaction is usually under anodic

control and the only way to increase the leaching rate is to increase the kinetics of the anodic reaction. Thus under these conditions increases in Fe^{3+} concentration, nominal Fe^{3+}/Fe^{2+} ratio will not substantially change the leaching rate.

9.3 Recommendations

This work forms a baseline to improve the understanding on the chalcopyrite leaching mechanisms in acidic iron sulfate solutions. The following investigations are recommended in order to enable a deeper understanding of the leaching system:

- The developed model was validated in a restricted range of conditions (conditions by the author and by others shown in the present study) due to the limited availability of experimental data. When extending to a wider range of solution composition and temperature, due to the generation of iron precipitates and the presence of additional species, further work will be required to expand our understanding of the quaternary system. The influence of other ions such as Cu^{2+}, Cl^{-} on the speciation results and the calculation of redox potential also require further detailed study.
- According to the developed expression, Eq. (6-9), at any given temperature, the redox potential of the quaternary H_2SO_4-$Fe_2(SO_4)_3$-$FeSO_4$-H_2O system is solely determined by the nominal Fe^{3+}/Fe^{2+} ratio. This result is particularly valuable and of interest: it is highly useful for understanding leach chemistry and calculating nominal Fe^{3+}/Fe^{2+} ratio based on measured redox potential. Future work should be done to determine the range of applicability of this equation.
- Long-term behavior of the leaching process is also important as it may be different from its short-term electrochemical response. Therefore, long term open circuit potential tests, together with polarization resistance and electrochemical impedance spectroscopy tests

(these two techniques were selected because they do not polarize the sample significantly from the open circuit potential; therefore, it would be reasonable to assume these tests would not affect the overall trend of the long term open circuit potential test) at specific intervals can be applied to provide data on the evolution of the chalcopyrite/solution interface in acidic iron sulfate leaching system, and hence to learn the influence of the Fe^{3+}/Fe^{2+} couple on the long-term electrochemical behavior of the leaching process at different temperatures.

- Results over a wide range of temperature indicate that no significant increase in the mixed potential on chalcopyrite was achieved, even at very high nominal Fe^{3+}/Fe^{2+} ratios and temperatures where the Nernst equation would predict a substantial increase in theoretical cathodic reversible potential. Given the importance of the ferric concentration and the nominal Fe^{3+}/Fe^{2+} ratio in commercial leaching processes, additional investigation will be required to determine the optimum parameters in different leaching systems.

References

1. Schlesinger ME, King MJ, Sole KC, Davenport WG. Extractive Metallurgy of Copper, fifth edition. Amsterdam: Elsevier Ltd., 2011.
2. Wang S. Copper leaching from chalcopyrite concentrates. Journal of Metals, 2005, 57(7), 48-51.
3. Córdoba EM, Muñoz JA, Blázquez ML, González F, Ballester A. Leaching of chalcopyrite with ferric ion. Part I: general aspects. Hydrometallurgy, 2008, 93 (3-4), 81-87.
4. Corrans IJ, Angove JE. Activation of a mineral species. US5232491A, 1993.
5. Hourn MM, Turner DW, Holzberger IR. Atmospheric mineral leaching process. US5993635A, 1999.
6. Collins MJ, Kofluk DK. Hydrometallurgical process for the extraction of copper from sulphidic concentrates. US5730776A, 1998.
7. Dempsey P, Dreisinger DB. Process for the extraction of copper. US6503293B1, 2003.
8. King JA. Hydrometallurgical process for copper-containing materials. US5698170A, 1997.
9. Jones DL. Chloride assisted hydrometallurgical extraction of metal. US5874055A, 1999.
10. Dixon DG, Tshilombo AF. Leaching process for copper concentrates. US2005/0269208A1, 2005.
11. Peters E. Leaching of sulfides (Chapter 26). In: Somasundaran P. (Eds.), Advances in Mineral Processing. SME/AIME, Littleton, CO, 1986, pp. 445-462.
12. Hirato T, Majima H, Awakura Y. The leaching of chalcopyrite with ferric sulfate. Metallurgical Transactions B-Process Metallurgy, 1987, 18(3), 489-496.
13. Córdoba EM, Muñoz JA, Blázquez ML, González F, Ballester A. Leaching of chalcopyrite with ferric ion. Part II: Effect of redox potential. Hydrometallurgy, 2008, 93(3-4), 88-96.

14. Córdoba EM, Muñoz JA, Blázquez ML, González F, Ballester A. Passivation of chalcopyrite during its chemical leaching with ferric ion at 68°C. Minerals Engineering, 2009, 22(3), 229-235.
15. Warren GW, Wadsworth ME, El-raghy SM. Passive and transpassive anodic behavior of chalcopyrite in acid solutions. Metallurgical Transactions B-Process Metallurgy, 1982, 13(4), 571-579.
16. Ghahremaninezhad A, Asselin E, Dixon DG. Electrochemical evaluation of the surface of chalcopyrite during dissolution in sulfuric acid solution. Electrochimica Acta, 2010, 55(18), 5041-5056.
17. Hiroyoshi N, Kuroiwa S, Miki H, Tsunekawa M, Hirajima T. Synergistic effect of cupric and ferrous ions on active-passive behavior in anodic dissolution of chalcopyrite in sulfuric acid solutions. Hydrometallurgy, 2004, 74(1-2), 103-116.
18. Biegler T, Horne MD. The electrochemistry of surface oxidation of chalcopyrite. Journal of the Electrochemical Society, 1985, 132(6), 1363-1369.
19. Arce EM, González I. A comparative study of electrochemical behavior of chalcopyrite, chalcocite and bornite in sulfuric acid solution. International Journal of Mineral Processing, 2002, 67(1-4), 17-28.
20. Biegler T, Swift DA. The electrolytic reduction of chalcopyrite in acid solution. Journal of Applied Electrochemistry, 1976, 6(3), 229-235.
21. Biegler T. Reduction kinetics of a chalcopyrite electrode surface. Journal of Electroanalytical Chemistry, 1977, 85(1), 101-106.

22. Nava D, Gonz á lez I, Leinen D, Ramos-Barrado JR. Surface characterization by X-ray photoelectron spectroscopy and cyclic voltammetry of products formed during the potentiostatic reduction of chalcopyrite. Electrochimica Acta, 2008, 53(14), 4889-4899.

23. Paramguru, RK. Electrochemical aspects in some of the hydrometallurgical processes. Mineral Processing and Extractive Metallurgy Review, 2002, 23(2), 65-100.

24. Paramguru RK, Ray HS. Use of polarization data for the study of initial dissolution behavior of semiconducting minerals. Mineral Processing and Extractive Metallurgy Review, 1996, 16(2), 63-87.

25. Parker AJ, Paul RL, Power GP. Electrochemistry of the oxidative leaching of copper from chalcopyrite. Journal of Electroanalytical Chemistry, 1981, 118(10), 305-316.

26. McMillan RS, Mackinnon DJ, Dutrizac JE. Anodic dissolution of n-type and p-type chalcopyrite. Journal of Applied Electrochemistry, 1982, 12(6), 743-757.

27. Tshilombo AF, Petersen J, Dixon DG. The influence of applied potentials and temperature on the electrochemical response of chalcopyrite during bacterial leaching. Minerals Engineering, 2002, 15(11), 809-813.

28. Dixon DG, Mayne DD, Baxter KG. Galvanox^{TM}-a novel galvanically-assisted atmospheric leaching technology for copper concentrations. Canadian Metallurgical Quarterly, 2008, 47(3), 327-336.

29. Kametani H, Aoki A. Effect of suspension potential on the oxidation rate of copper concentrate in a sulfuric acid solution. Metallurgical Transactions B-Process Metallurgy, 1985, 16(4), 695-705.

30. Hiroyoshi N, Arai M, Miki H, Tsunekawa M, Hirajima T. A new reaction model for the catalytic effect of silver ions on chalcopyrite leaching in sulfuric acid solutions. Hydrometallurgy, 2002, 63(3), 257-267.
31. Hiroyoshi N, Kitagawa H, Tsunekawa M. Effect of solution composition on the optimum redox potential for chalcopyrite leaching in sulfuric acid solutions. Hydrometallurgy, 2008, 91(1-4), 144-149.
32. Vilcáez J, Yamada R, Inoue C. Effect of pH reduction and ferric ion addition on the leaching of chalcopyrite at thermophilic temperatures. Hydrometallurgy, 2009, 96(1-2), 62-71.
33. Dry MJ, Bryson AW. Prediction of redox potential in concentrated iron sulphate solutions. Hydrometallurgy, 1988, 21(1), 59-72.
34. Stipp SL. Speciation in the Fe(II)-Fe(III)-SO_4-H_2O system at 25 ℃ and low pH: sensitivity of an equilibrium model to uncertainties. Environmental Science & Technology, 1990, 24(5), 699–706.
35. Casas JM, Crisóstomo G, Cifuentes L. Speciation of the Fe(II)-Fe(III)-H_2SO_4-H_2O system at 25 and 50 ℃. Hydrometallurgy, 2005, 80(4), 254-264.
36. Cifuentes L, Casas JM, Simpson J. Temperature dependence of the speciation of copper and iron in acidic electrolytes. Chemical Engineering Research and Design, 2006, 84(A10), 965-969.
37. Sapieszko RS, Patel RC, Matljevlc E. Ferric hydrous oxide sols. 2. Thermodynamics of aqueous hydroxo and sulfato ferric complexes. Journal of Physical Chemistry, 1977, 81(11), 1061-1068.

38. Filippou D, Demopoulos GP, Papangelakis VG. Hydrogen-ion activities and species distribution in mixed-metal sulfate aqueous system. AIChE Journal, 1995, 41(1), 171-184.

39. Posnjak E, Merwin HE. The system, Fe_2O_3-SO_3-H_2O. Journal of the American Chemical Society, 1922, 44 (9), 1965-1994.

40. Sasaki K, Ootsuka K, Tozawa K. Equilibrium diagram in the system, Fe_2O_3-SO_3-H_2O, at elevated Temperatures-Hydrometallurgical studies on hydrolysis of the ferric sulphate solutions at elevated temperatures (2nd Report). Shigen-to-Sozai, 1993, 109(11), 871-879.

41. Umetsu Y, Tozawa K, SasakiK. The hydrolysis of ferric sulphate solutions at elevated temperatures. Canadian Metallurgical Quarterly, 1977, 16(1), 111-117.

42. Papangelakis VG, Blakey BC, Liao H. Hematite solubility in sulphate process solutions. In: Monhemius AJ, editor. Hydrometallurgy ’94. Cambridge, England: Springer, Netherlands, 1994:159-175.

43. Tozawa K, Sasaki K. Effect of coexisting sulphates on precipitation of ferric oxide from ferric sulphate solutions at elevated temperatures. In: Dutrizac JE, Monhemius AJ, editors. Iron Control in Hydrometallurgy. Toronto ON: Ellis Horwood Limited, Chichester, England, 1986:454-476.

44. Reid M, Papangelakis VG. New data on hematite solubility in sulphuric acid solutions from 130 to 270 ℃. In: Dutrizac JE, Riveros PA, editors. Iron Control Technologies. Proceedings of the Third International Symposium on Iron Control in Hydrometallurgy. Montreal, QC: CIM, Montreal, QC, 2006:673-686.

45. Liu H, Papangelakis VG, Alam MS, Singh G. Solubility of hematite in H_2SO_4 solutions at 230-270 ℃. Canadian Metallurgical Quarterly, 2003, 42(2), 199-207.

46. Jones DL. The leaching of chalcopyrite. Ph.D. Thesis, the University of British Columbia, Vancouver, Canada, 1974.

47. Li J, Zhong TK, Wadsworth ME. Application of mixed potential theory in hydrometallurgy. Hydrometallurgy, 1992, 29(1-3), 47-60.

48. Power GP, Ritchie IM. Mixed potential measurements in the elucidation of corrosion mechanisms-I introductory theory. Electrochimica Acta, 1981, 26(8), 1073-1078.

49. Power GP, Staunton WP, Ritchie IM. Mixed potential measurements in the elucidation of corrosion mechanisms-II some measurements. Electrochimica Acta, 1982, 27(1), 165-169.

50. Zembura Z. Relationship between metallic corrosion and limiting current using the rotating disk method. Corrosion Science, 1968, 8(9), 703-713.

51. Hiroyoshi N, Hirota M, Hirajima T, Tsunekawa M. A case of ferrous sulfate addition enhancing chalcopyrite leaching. Hydrometallurgy, 1997, 47(1), 37-45.

52. Hiroyoshi N, Miki H, Hirajima T, Tsunekawa M. A model for ferrous-promoted chalcopyrite leaching. Hydrometallurgy, 2000, 57(1), 31-38.

53. Hiroyoshi N, Miki H, Hirajima T, Tsunekawa M. Enhancement of chalcopyrite leaching by ferrous ions in acidic ferric sulfate solutions. Hydrometallurgy, 2001, 60(3), 185-197.

54. Dutrizac JE, MacDonald RJC, Ingraham TR. The kinetics of dissolution of synthetic chalcopyrite in aqueous acidified ferric sulphate solutions. Transactions of the Metallurgical Society of AIME, 1969, 245(5), 955-959.

55. Crundwell FK. Kinetics and mechanism of the oxidative dissolution of a zinc sulphide concentrate in ferric sulphate solution. Hydrometallurgy, 1987, 19(2), 227-242.

56. Peters E. Direct leaching of sulfides: chemistry and applications. Metallurgical Transactions B-Process Metallurgy, 1976, 7(4), 505-517.

57. Antonijević MM, Bogdanović GD. Investigation of the leaching of chalcopyritic ore in acidic solutions. Hydrometallurgy, 2004, 73(3-4), 245-256.

58. Munoz PB, Miller JD, Wadsworth ME. Reaction mechanism for the acid ferric sulfate leaching of chalcopyrite. Metallurgical Transactions B-Process Metallurgy, 1979, 10(2), 149-158.

59. Parker GK, Hope GA, Woods R. Gold-enhanced Raman observation of chalcopyrite leaching. Colloids and Surfaces A-Physicochemical and Engineering Aspects, 2008, 325(3), 132-140.

60. Viramontes-Gamboa G, Rivera-Vasquez BF, Dixon DG. The active-to-passive transition of chalcopyrite. ECS Transactions, 2006, 2(3), 165-175.

61. Viramontes-Gamboa G, Rivera-Vasquez BF, Dixon DG. The active-passive behavior of chalcopyrite comparative study between electrochemical and leaching responses. Journal of the Electrochemical Society, 2007, 154(6), C299-C311.

62. Sequeira CAC, Santos DMF. Transient film formation on chalcopyrite in acidic solutions. Journal of Applied Electrochemistry, 2010, 40(1), 123-131.

63. Lázaro I, Martínez-Medina N, Rodríguez I, Arce E, González I. The use of carbon paste electrodes with non-conducting binder for the study of minerals: Chalcopyrite. Hydrometallurgy, 1995, 38(3), 277-287.

64. Elsherief AE. The influence of cathodic reduction, Fe^{2+} and Cu^{2+} ions on the electrochemical dissolution of chalcopyrite in acidic solution. Minerals Engineering, 2002, 15(4), 215-223.

65. Nava D, González I. Electrochemical characterization of chemical species formed during the electrochemical treatment of chalcopyrite in sulfuric acid. Electrochimica Acta, 2006, 51(25), 5295-5303.

66. Biegler T, Swift DA. Anodic electrochemistry of chalcopyrite. Journal of Applied Electrochemistry, 1979, 9(5), 545-554.

67. Holliday RI, Richmond WR. An electrochemical study of the oxidation of chalcopyrite in acidic solution. Journal of Electroanalytical Chemistry, 1990, 288(1-2), 83-98.

68. Lazaro I, Nicol MJ. A rotating ring-disk study of the initial stages of the anodic dissolution of chalcopyrite in acidic solutions. Journal of Applied Electrochemistry, 2006, 36(4), 425-431.

69. Nicol MJ, La´zaro I. The role of E_H measurements in the interpretation of the kinetics and mechanisms of the oxidation and leaching of sulphide minerals. Hydrometallurgy, 2002, 63(1), 15-22.

70. Córdoba EM, Muñoz JA, Blázquez ML, González F, Ballester A. Leaching of chalcopyrite with ferric ion. Part III: Effect of redox potential on the silver-catalyzed process. Hydrometallurgy, 2008, 93(3-4), 97-105.

71. Córdoba EM, Muñoz JA, Blázquez ML, González F, Ballester A. Comparative kinetic study of the silver-catalyzed chalcopyrite leaching at 35 and 68°C. International Journal of Mineral Processing, 2009, 92(3-4), 137-143.

72. Misra M, Fuerstenau MC. Chalcopyrite leaching at moderate temperature and ambient pressure in the presence of nanosize silica. Minerals Engineering, 2005, 18(3), 293-297.

73. Madhuchhanda M, Devi NB, Rao KS, Rath PC, Paramguru RK. Galvanic interaction between sulfide minerals and pyrolusite. Journal of Solid State Electrochemistry, 2000, 4(4), 189-198.

74. Liu QY, Li HP, Zhou L. Study of galvanic interactions between pyrite and chalcopyrite in a flowing system: implications for the environment. Environmental Geology, 2007, 52(1), 11-18.

75. Fuentes-Aceituno JC, Lapidus GT, Doyle FM. A kinetic study of the electro-assisted reduction of chalcopyrite. Hydrometallurgy, 2008, 92(1-2), 26-33.

76. Antonijević MM, Janković ZD, Dimitrijevií MD. Kinetics of chalcopyrite dissolution by hydrogen peroxide in sulphuric acid. Hydrometallurgy, 2004, 71(3-4), 329-334.

77. Olubambi PA, Potgieter JH. Investigations on the mechanisms of sulfuric acid leaching of chalcopyrite in the presence of hydrogen peroxide. Mineral Processing & Extractive Metallurgy Review, 2009, 30(4), 327-345.

78. Lu ZY, Jeffrey MI, Lawson F. The effect of chloride ions on the dissolution of chalcopyrite in acidic solutions. Hydrometallurgy, 2000, 56(2), 189-202.

79. Lu ZY, Jeffrey MI, Lawson F. An electrochemical study of the effect of chloride ions on the dissolution of chalcopyrite in acidic solutions. Hydrometallurgy, 2000, 56(2), 145-155.

80. Carneiro MFC. The role of sodium chloride on surface properties of chalcopyrite leached with ferric sulphate. Hydrometallurgy, 2007, 87(3-4), 73-82.

81. Al-Harahsheh M, Kingman S, Al-Harahsheh A. Ferric chloride leaching of chalcopyrite: Synergetic effect of $CuCl_2$. Hydrometallurgy, 2008, 91(1-4), 89-97.

82. Hirato T, Majima H, Awakura Y. The leaching of chalcopyrite with cupric chloride. Metallurgical Transactions B-Process Metallurgy, 1987, 18(1), 31-39.

83. Lundström M, Aromaa J, Forsén O, Hyvärinen O, Barker MH. Cathodic reactions of Cu^{2+} in cupric chloride solution. Hydrometallurgy, 2007, 85(1), 9-16.

84. O'malley ML, Liddell KC. Leaching of $CuFeS_2$ by aqueous $FeCl_3$, HCl, and NaCl: Effects of solution composition and limited oxidant. Metallurgical Transactions B-Process Metallurgy, 1987, 18(3), 505-510.

85. Warren GW, Wadsworth ME. The electrochemical oxidation of chalcopyrite in ammoniacal solutions. Metallurgical Transactions B-Process Metallurgy, 1984, 15(2), 289-297.

86. Tiwari BL, Kolbe J, Hayden HW. Leaching of high-solids, attritor-ground chalcopyrite concentrate by in situ generated ferric sulfate solution. Metallurgical Transactions B-Process Metallurgy, 1980, 11(1), 89-93.

87. Vaughan DJ, England KER, Kelsall GH, Yin Q. Electrochemical oxidation of chalcopyrite ($CuFeS_2$) and the related metal-enriched derivatives $Cu_4Fe_5S_8$, $Cu_9Fe_9S_{16}$, and $Cu_9Fe_8S_{16}$. American Mineralogist, 1995, 80(7-8), 725-731.

88. Farquhar ML, Wincott PL, Wogelius RA, Vaughan DJ. Electrochemical oxidation of the chalcopyrite surface: an XPS and AFM study in solution at pH 4. Applied Surface Science, 2003, 218(1-4), 34-43.

89. Velásquez P, Gómez H, Ramos-Barrado JR, Leinen D. Voltammetry and XPS analysis of a chalcopyrite $CuFeS_2$ electrode. Colloids and Surfaces A-Physicochemical and Engineering Aspects, 1998, 140(1-3), 369-375.

90. Velásquez P, Gómez H, Leinen D, Ramos-Barrado JR. Electrochemical impedance spectroscopy analysis of chalcopyrite $CuFeS_2$ electrodes. Colloids and Surfaces A-Physicochemical and Engineering Aspects, 1998, 140(1-3), 177-182.

91. Velásquez P, Leinen D, Pascual J, Ramos-Barrado JR, Grez P, Gómez H, Schrebler R, Del Río R, Córdova R. A chemical, morphological, and electrochemical (XPS, SEM/EDX, CV, and EIS) analysis of electrochemically modified electrode surfaces of natural chalcopyrite ($CuFeS_2$) and pyrite (FeS_2) in alkaline solutions. Journal of Physical Chemistry B, 2005, 109 (11), 4977–4988.

92. Yin Q, Vaughan DJ, England KER, Kelsall GH, Brandon NP. Surface oxidation of chalcopyrite ($CuFeS_2$) in alkaline solutions. Journal of the Electrochemical Society, 2000, 147(8), 2945-2951.

93. Liu QY, Li HP. A comparison of the electrochemical behaviors of pyrite and chalcopyrite in a NaCl solution at room temperature and under differential stress. Minerals Engineering, 2010, 23(9), 691-697.

94. Padilla R, Vega D, Ruiz MC. Pressure leaching of sulfidized chalcopyrite in sulfuric acid-oxygen media. Hydrometallurgy, 2007, 86(1-2), 80-88.

95. Padilla R, Pavez P, Ruiz MC. Kinetics of copper dissolution from sulfidized chalcopyrite at high pressures in H_2SO_4-O_2. Hydrometallurgy, 2008, 91(1-4), 113-120.

96. Padilla R, Rodríguez G, Ruiz MC. Copper and arsenic dissolution from chalcopyrite-enargite concentrate by sulfidation and pressure leaching in H_2SO_4-O_2. Hydrometallurgy, 2010, 100(3-4), 152-156.

97. Biegler T, Rand DAJ, Woods R. Oxygen reduction on sulphide minerals Part I. Kinetics and mechamism at rotated pyrite. Electroanalytical Chemistry and Interfacial Electrochemistry, 1975, 60(2), 151-162.

98. Biegler T. Oxygen reduction on sulphide minerals Part II relation between ativity and semiconducting properties of pyrite electrodes. Journal of Electroanalytical Chemistry, 1976, 70(3), 265-275.

99. Holmes PR, Crundwell FK. The kinetics of the oxidation of pyrite by ferric ions and dissolved oxygen: An electrochemical study. Geochimica et Cosmochimica Acta, 2000, 64(2), 263-274.

100. Rimstidt JD, Vaughan DJ. Pyrite oxidation: A state-of-the-art assessment of the reaction mechanism. Geochimica et Cosmochimica Acta, 2003, 67(5), 873-880.

101. Liu R, Wolfe AL, Dzombak DA, Horwitz CP, Stewart BW, Capo RC. Electrochemical study of hydrothermal and sedimentary pyrite dissolution. Applied Geochemistry, 2008, 23(9), 2724-2734.

102. Lin HK, Say WC. Study of pyrite oxidation by cyclic voltammetric, impedance spectroscopic and potential step techniques. Journal of Applied Electrochemistry, 1999, 29(8), 987-994.

103. Makrides AC. Kinetics of redox reactions on passive electrodes. Journal of the Electrochemical Society, 1964, 111(4), 392-400.

104. Makrides AC. Kinetics of the Fe+++/Fe++ Reaction on Fe-Cr Alloys. Journal of the Electrochemical Society, 1964, 111(4), 400-407.

105. Stern M. Electrochemical polarization II. ferrous-ferric electrode kinetics on stainless steel. Journal of the Electrochemical Society, 1957, 104(9), 559-563.

106. Dutrizac JE, MacDonald RJC. The effect of some impurities on the rate of chalcopyrite dissolution. Canadian Metallurgical Quarterly, 1973, 12(4), 409-420.

107. Thomas G, Ingraham TR, MacDonald RJC. Kinetics of dissolution of synthetic digenite and chalcocite in aqueous acidic ferric sulphate solutions. Canadian Metallurgical Quarterly, 1967, 6(3), 281-292.

108. Ghahremaninezhad A, Dixon DG, Asselin E. Kinetics of the ferric–ferrous couple on anodically passivated chalcopyrite ($CuFeS_2$) electrodes. Hydrometallurgy, 2012, 125-126, 42-49.

109. Jones DL, Peters E. Electrochemical experiments with chalcopyrite electrodes in aqueous solutions up to 200°C. International Corrosion Conference Series, NACE-4 (High Temperature High Pressure Electrochemistry in Aqueous Solutions), 1976, 443-458.

110. Lázaro I, Jeffrey MI. A rotating disc electrochemical dual autoclave for the study of electrochemistry and leaching at high temperature and pressure. ECS Transactions, 2006, 2(3), 243-252.

111. Wildgoose GC, Giovanelli D, Lawrence NS, Compton RG. High-temperature electrochemistry-a review. Electroanalysis, 2004, 16(6), 421-433.

112. Giovanelli D, Lawrence NS, Compton RG. Electrochemistry at high pressures-a review. Electroanalysis, 2004, 16(10), 789-810.

113. Jayasekera S, Marinovich Y, Avraamides J, Bailey SI. Pressure leaching of reduced ilmenite-electrochemical aspects. Hydrometallurgy, 1995, 39(1-3), 183-199.

114. Clouser SJ, Huang JC, Yeager E. Temperature dependence of the Tafel slope for oxygen reduction on platinum in concentrated phosphoric acid. Journal of Applied Electrochemistry, 1993, 23(6), 597-605.

115. Liu JQ, Nicol MJ. Thermodynamics and kinetics of the dissolution of gold under pressure oxidation conditions in the presence of chloride. Canadian Metallurgical Quarterly, 2002, 41(4), 409-415.

116. Tanaka N, Tamamushi R. Kinetic parameters of electrode reactions. Electrochimica Acta, 1964, 9(7), 963-989.

117. Angell DH, Dickinson T. The kinetics of the ferrous/ferric and ferro/ferricyanide reactions at platinum and gold electrodes: Part I. Kinetics at bare-metal surfaces. Journal of Electroanalytical Chemistry, 1972, 35(1), 55-72.

118. Bochmann HG, Vielstich W. On the reaction rate of the Fe^{2+}/Fe^{3+} redox couple in sulfate solution. Electrochimica Acta, 1988, 33(6), 805-809.

119. Bard AJ, Faulkner LR. *Electrochemical Methods-Fundamentals and Applications*, second ed. John Wiley & Sons, Inc., New York, 2001.

120. Zoski CG. Handbook of Electrochemistry, first ed. In: Swain GM. Solid Electrode Materials: Pretreatment and Activation. Elsevier B.V., Amsterdam, 2007, pp. 111-153.

121. Dutrizac JE. The physical chemistry of iron precipitation in the zinc industry. In: Cigan JM, Mackey TS, O'Keefe TJ (Eds.). Lead-Zinc-Tin'80. AIME, New York, 1980, pp. 532-564.

122. Bayoumi FM, Ghanem WA, Ateya BG. Electrochemical behavior of Cr-Mo steel alloy in high temperature aqueous sodium chloride solution. International Journal of Electrochemical Science, 2006, 1(5), 258-267.

123. Huang JB, Wu XQ, Han EH. Influence of pH on electrochemical properties of passive films formed on Alloy 690 in high temperature aqueous environments. Corrosion Science, 2009, 51(12), 2976-2982.

124. Olmedo AM, Villegas M, Alvarez MG. Corrosion behaviour of Alloy 800 in high temperature aqueous solutions: Electrochemical studies. Journal of Nuclear Materials, 1996, 229(2), 102-114.

125. Bosch RW, Bogaerts WF, Zheng JH. Simple and robust external reference electrodes for high-temperature electrochemical measurements. Corrosion, 2003, 59(2), 162-171.

126. Macdonald DD, Scott AC, Wentrcek P. External reference electrodes for use in high temperature aqueous systems. Journal of the Electrochemical Society, 1979, 126(6), 908-911.

127. Macdonald DD, Scott AC, Wentrcek P. Silver-silver chloride thermocells and thermal liquid junction potentials for potassium chloride solutions at elevated temperatures. Journal of the Electrochemical Society, 1979, 126(9), 1618-1624.

128. Scholz F. Electroanalytical methods-guide to experiments and applications, second ed. In: Kahlert H. Reference Electrodes. Springer, New York, 2010, pp. 291-308.

129. Bard AJ, Parsons R, Jordan J. Standard Potentials in Aqueous Solution. Marcel Dekker, Inc., New York, 1985.

130. Rao YK. Stoichiometry and Thermodynamics of Metallurgical Processes. Cambridge University Press, New York, 1985.

131. Harper HW. Calculation of liquid junction potentials. Journal of Physical Chemistry, 1985, 89(9), 1659-1664.

132. Tromans D, Silva JC. Behavior of copper in acidic sulfate solution: Comparison with acidic chloride. Corrosion, 1997, 53(3), 171-178.

133. Nickchi T, Alfantazi A. Construction and characterization of a solution-filled external pressure balanced reference electrode. Corrosion Science, 2012, 63, 174–181.

134. Casas JM, Papangelakis VG, Liu H. Performance of three chemical models on the high-temperature aqueous $Al_2(SO_4)_3$-$MgSO_4$-H_2SO_4-H_2O system. Industrial & Engineering Chemistry Research, 2005, 44(9), 2931-2941.

135. Liu H, Papangelakis VG. Chemical modeling of high temperature aqueous processes. Hydrometallurgy, 2005, 79(1-2), 48-61.

136. Liu H, Papangelakis VG. Thermodynamic equilibrium of the O_2-$ZnSO_4$-H_2SO_4-H_2O system from 25 to 250 ℃. Fluid Phase Equilibria, 2005, 234(1-2), 122-130.

137. Helgeson HC. Thermodynamics of hydrothermal systems at elevated temperatures and pressures. American Journal of Science, 1969, 267(7), 729-804.

138. Helgeson HC, Kirkham DH. Theoretical prediction of the thermodynamic behavior of aqueous electrolytes at high pressures and temperatures: II. Debye-Hückel parameters for activity coefficients and relative partial molal properties. American Journal of Science, 1974, 274(10), 1199-1261.

139. Wolery TJ. EQ3NR, a computer program for geochemical aqueous speciation-solubility calculations: theoretical manual, user's guide, and related documentation (Version 7.0). Lawrence Livermore National Laboratory, UCRL-MA-110662 PT III, 1992.

140. Truesdell AH, Jones BF. WATEQ, a computer program for calculating chemical equilibria of natural waters. Journal of Research of the U. S. Geological Survey, 1974, 2(2), 233-248.

141. Kielland J. Individual activity coefficients of ions in aqueous solutions. Journal of the American Chemical Society, 1937, 59(9), 1675-1678.

142. Wolery TJ. EQ3/6 Software Package, Version 7.2b, Lawrence Livermore National Laboratory, Livermore, CA. USA, 1996

143. Roine A. HSC Chemistry Software (version 7.1). Outotec Research Oy, Finland, www.outotec.com, 2011.

144. Criss CM, Cobble JW. The thermodynamic properties of high temperature aqueous solutions. IV. Entropies of the ions up to 200 °and the correspondence principle. Journal of the American Chemical Society, 1964, 86(24), 5385-5390.

145. Criss CM, Cobble JW. The thermodynamic properties of high temperature aqueous solutions. V. The calculation of ionic heat capacities up to 200 °. Entropies and heat capacities above up to 200 °. Journal of the American Chemical Society, 1964, 86(24), 5390-5393.

146. Helgeson HC, Kirkham DH, Flowers GC. Theoretical prediction of the thermodynamic behavior of aqueous electrolytes at high pressures and temperatures: IV. Calculation of activity coefficients, osmotic coefficients, and apparent molal and standard and relative partial molal properties to 600 ℃ and 5KB. American Journal of Science, 1981, 281(10), 1249-1516.

147. Tanger JC, Helgeson HC. Calculation of the thermodynamic and transport properties of aqueous species at high pressures and temperatures: revised equations of state for the standard partial molal properties of ions and electrolytes. American Journal of Science, 1988, 288(1), 19-98.

148. Connick RE, Powell RE. The entropy of aqueous oxy-anions. Journal of Chemical Physics, 1953, 21(12), 2206-2207.

149. Lewis D. Studies of redox equilibria at elevated temperatures I: The estimation of equilibrium constants and standard potentials for aqueous systems up to 374 ℃. Arkiv för Kemi, 1970, 32, 385-404.

150. Brent RP. Algorithms for Minimization without Derivatives. Prentice-Hall, Englewood Cliffs, New Jersey, 1973.

151. Sahoo PK, Tripathy S, Equeenuddin SM, Panigrahi MK. Geochemical characteristics of coal mine discharge vis-à-vis behavior of rare earth elements at Jaintia Hills coalfield, northeastern India. Journal of Geochemical Exploration, 2012, 112, 235-243.

152. Yeager E, Salkind AJ. Techniques of Electrochemistry (Volume 1). New York: John Wiley & Sons, Inc., 1972.

153. Bratsch SG. Standard electrode potentials and temperature coefficients in water at 298.15 K. Journal of Physical and Chemical Reference Data, 1989, 18(1), 1-21.

154. Tagirov BR, Diakonov II, Devina OA, Zotov AV. Standard ferric–ferrous potential and stability of $FeCl^{2+}$ to 90 ℃. Thermodynamic properties of Fe^{3+}(aq) and ferric-chloride species. Chemical Geology, 2000, 162(3–4), 193–219.

155. Tshilombo AF. Mechanism and kinetics of chalcopyrite passivation and depassivation during ferric and microbial leaching. Ph.D. Thesis. University of British Columbia, Vancouver, Canada, 2004.

156. Conway BE, Chapter 2, In: B. E. Conway, J. O'M. Bockris, R. White (Eds.), Modern Aspects of Electrochemistry Vol. 16, Plenum, New York, 1986, p. 103

157. Bockris JO'M, Gochev A. Temperature dependence of the symmetry factor in electrode kinetics. Journal of Physical Chemistry, 1986, 90(21), 5232-5239.

158. Conway BE, MacKinnon DJ, Tilak BV. Significance of electrochemical brϕnsted factors. Kinetic studies over a wide range of temperatures. Transactions of the Faraday Society, 1970, 66, 1203-1226.

159. Vračar LM, Dražić DM. Anomalous temperature dependence of the hydrogen evolution reaction on iron. Journal of Electroanalytical Chemistry, 1989, 265(1-2), 171-178.

160. Kriksunov LB, Bunakova LV, Zabusova SE, Krishtalik LI. Anodic oxygen evolution reaction at high temperatures in acid solutions at platinum. Electrochimica Acta, 1994, 39(1), 137-142.

161. Zinola CF, Castro Luna AM, Arvia AJ. Temperature dependence of kinetics parameters related to oxygen electroreduction in acid solutions on platinum electrodes. Electrochimica Acta, 1994, 39(13), 1951-1959.

162. Solorza-Feria O, Durón S. Temperature effects for oxygen reduction on Ru-nanoparticles in acid solution. International Journal of Hydrogen Energy, 2002, 27(4), 451-455.

163. Nicol MJ. The role of electrochemistry in hydrometallurgy. In: J.B. Hiskey, G.W. Warren (Eds.), Hydrometallurgy: Fundamentals, Technology and Innovation, Salt Lake City, Utah, The Minerals, Metals and Materials Society of AIME, 1993, p. 43.

164. Lai JC. Fundamental study of the controlled-potential leaching of chalcopyrite. Master Thesis, University of British Columbia, Vancouver, Canada, 2003.

165. Lázaro-Báez MI. Electrochemistry of the leaching of chalcopyrite. Ph.D. Thesis, Murdoch University, Western Australia, Australia, 2001.

166. Abed N. A fundamental study of the reductive leaching of chalcopyrite using metallic iron. Master Thesis, University of British Columbia, Vancouver, Canada, 1999.

167. Yu PH, Hansen CK, Wadsworth ME. A kinetic study of the leaching of chalcopyrite at elevated temperatures. In: Evans DJI, Shoemaker RS (Eds.), International Symposium on Hydrometallurgy, New York, AIME, 1973, p. 375.

168. Majima H, Awakura Y, Hirato T, Tanaka T. The leaching of chalcopyrite in ferric chloride and ferric sulfate solutions. Canadian Metallurgical Quarterly, 1985, 24(4), 283-291.

Appendices

Appendix A High Temperature Electrochemical Apparatus

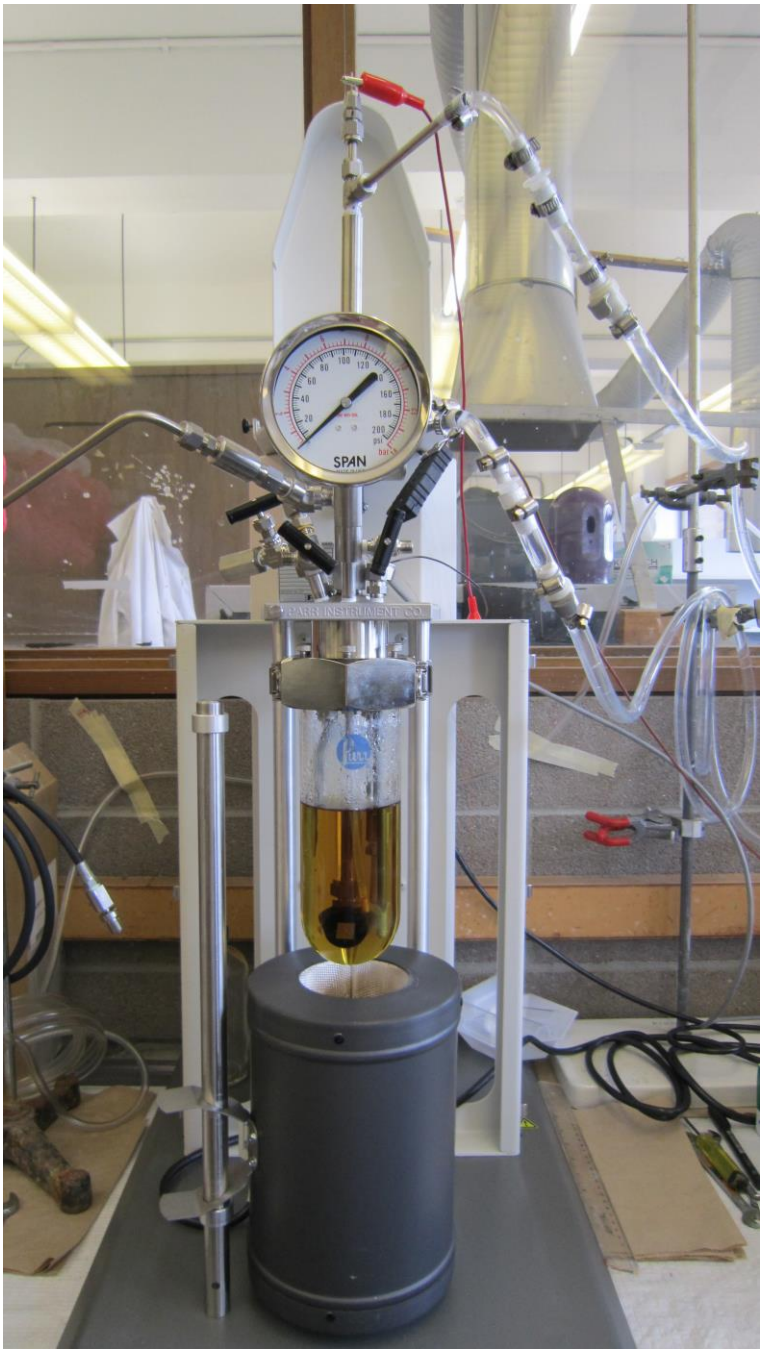

Figure A-1 High temperature high pressure autoclave.

Figure A-2 Inside of the glass reactor for high temperature high pressure autoclave.

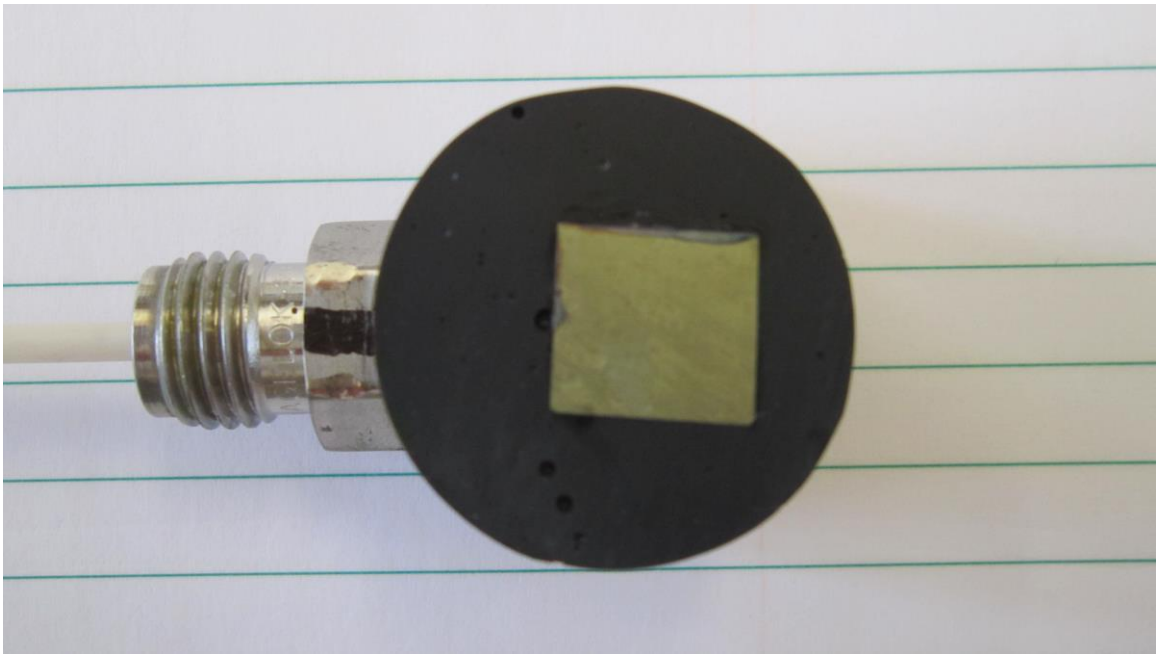

Figure A-3 Disassembled chalcopyrite working electrode used in the autoclave.

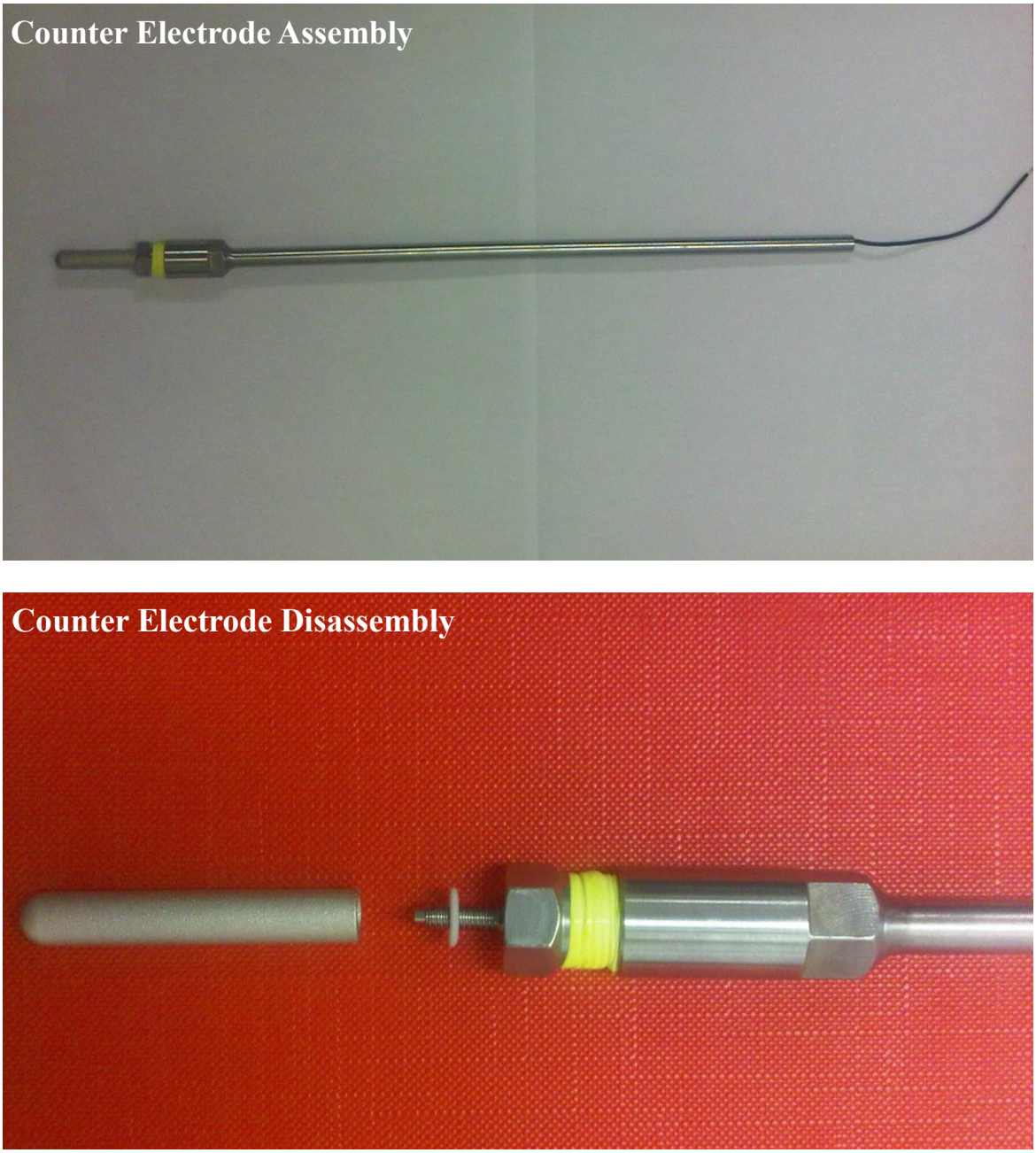

Figure A-4 (a) Assembly and (b) disassembly of the Pt-Nb electrode from Cortest Inc. served as counter electrode for high temperature high pressure electrochemical test in the autoclave.

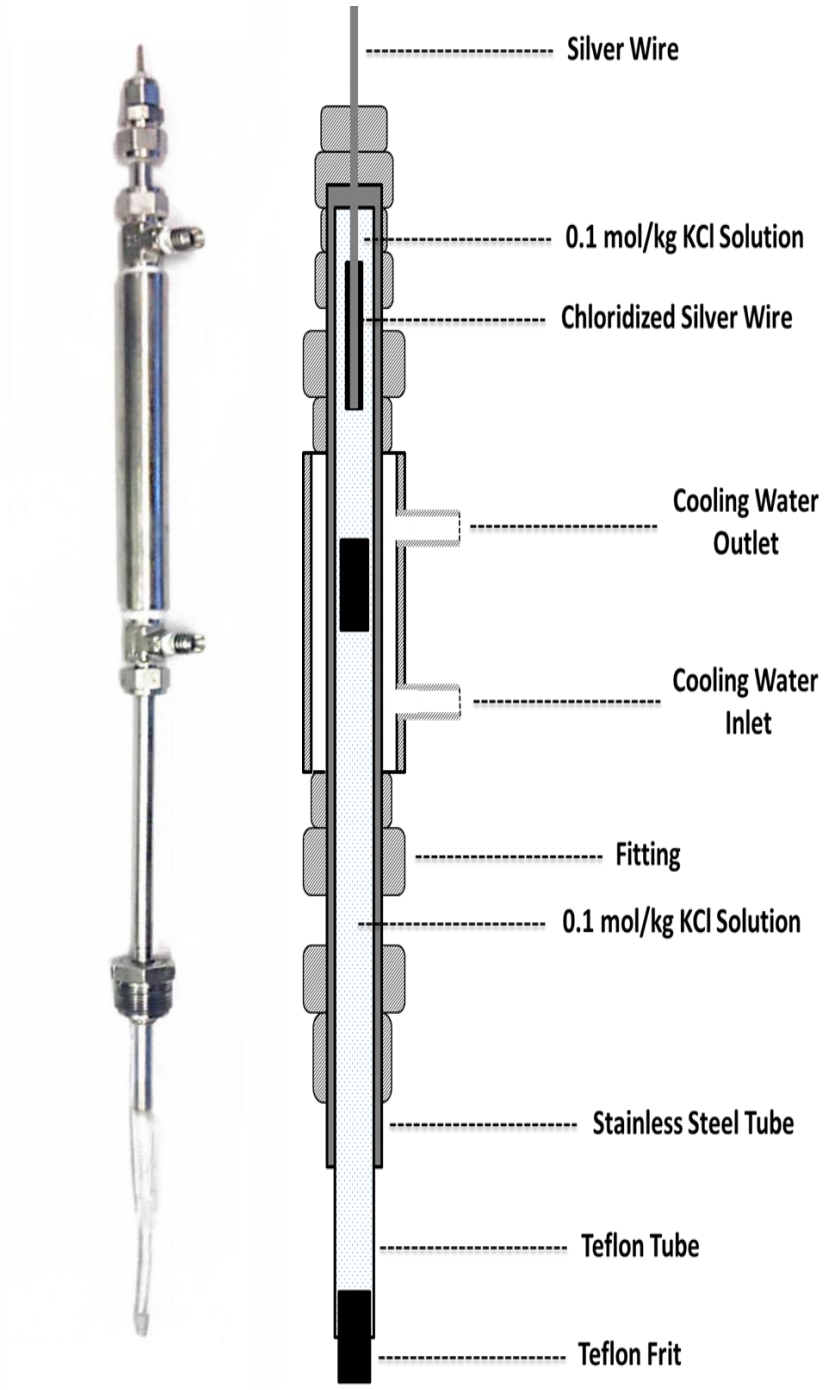

Figure A-5 High temperature external pressure balanced reference electrode (EPBRE).

Appendix B Fortran Code by Brent's Method Employed in the Present Work for the Speciation Study

As an example, the code shown in the following pages were used to carry out the speciation study at 150 ℃, which is the most complicated one as we need to first make a judgement whether the precipitate (Fe_2O_3) is formed or not. As discussed previously in Chapter 5, the species involved in the model vary depending on temperature. Hence, for the calculation at lower temperatures the code needs to be adjusted accordingly. For example, at 90 ℃ and 110 ℃, the part for judging the precipitate formation should be removed; at 25 ℃ and 70 ℃, information on $Fe(SO_4)_2^-$ should be added to the code. The calculated concentrations of all species in aqueous Fe(II)-Fe(III)-H_2SO_4 solutions in the range of 25-150 ℃ according to the developed speciation model with nominal Fe^{3+}/Fe^{2+} ratio of 10:1 was also shown in Table B-1 as an example.

The equations involved in the code are shown as follows:

(1) The 7 chemical equilibrium equations according to the reactions shown in Table 5-2. For any equilibrium reaction at a given temperature:

$$K_T = \prod a_i^{v_i} \tag{B-1}$$

$$a_i = \gamma_i \times c_i \tag{B-2}$$

$$I = \frac{1}{2}\sum_{j=1}^{n} z_i^2 \times c_i \tag{B-3}$$

Where K_T represents the equilibrium constant of the formation reactions shown in Table 5-2, a_i is the activity of the species *i*, v_i is the stoichiometric coefficient of the species *i* (positive for products and negative for reactants) in the formation reactions, γ_i is the activity coefficient of the

species *i* calculated by the B-dot equation, c_i is the molal concentration of the species *i*, *j* is the number of ionic species involved in the model, *I* (mol kg^{-1}) is the effective (or real/true) ionic strength of the solution and z_i is the ionic charge of species *i*.

(2) The component mass balance equations in terms of Fe^{2+}, Fe^{3+} and SO_4^{2-} (three in total):

$$\left[\mathrm{Fe(II)}\right]_{\mathrm{total}} = c_{Fe^{2+}} + c_{FeHSO_4^{+}} + c_{FeSO_4^{o}} \quad \text{(B-4)}$$

$$\left[\mathrm{Fe(III)}\right]_{\mathrm{total}} = c_{Fe^{3+}} + c_{FeHSO_4^{2+}} + c_{Fe(SO_4)_2^{-}} + c_{FeSO_4^{+}} + 2\times c_{Fe_2O_3} \quad \text{(B-5)}$$

$$\left[SO_4^{2-}\right]_{\mathrm{total}} = c_{SO_4^{2-}} + c_{HSO_4^{-}} + c_{FeHSO_4^{+}} + c_{FeSO_4^{o}} + c_{FeHSO_4^{2+}} + 2\times c_{Fe(SO_4)_2^{-}} + c_{FeSO_4^{+}} \quad \text{(B-6)}$$

(3) The electroneutrality equation:

$$c_{H^+} - 2\times c_{SO_4^{2-}} - c_{HSO_4^{-}} + 2\times c_{Fe^{2+}} + c_{FeHSO_4^{+}} + 3\times c_{Fe^{3+}} + 2\times c_{FeHSO_4^{2+}} - c_{Fe(SO_4)_2^{-}} + c_{FeSO_4^{+}} = 0 \quad \text{(B-7)}$$

Table B-1 Calculated concentrations of all species in aqueous Fe(II)-Fe(III)-H_2SO_4 solutions from 25-150 ℃ using the newly developed speciation model with nominal Fe^{3+}/Fe^{2+} ratio of 10:1 (Unit: mol/kg). In the cell or autoclave, $[Fe(III)]_{total}$ = 0.18 mol/kg and $[Fe(II)]_{total}$ = 0.018 mol/kg, respectively.

Species	at 25 ℃		at 70 ℃		at 90 ℃		at 110 ℃		at 150 ℃	
	γ_i	c_i	γ_i	c_i	γ_i	c_i	γ_i	c_i	γ_i	c_i
H^+	0.8347	0.2812	0.8339	0.2539	0.8277	0.2025	0.8197	0.1946	0.7882	0.3452
SO_4^{2-}	0.1842	0.0573	0.1799	0.0152	0.1690	0.0110	0.1572	0.0055	0.1166	0.0009
HSO_4^-	0.7218	0.3277	0.7216	0.3505	0.7125	0.3981	0.7014	0.4035	0.6553	0.4875
Fe^{2+}	0.2631	0.0119	0.2557	0.0131	0.2434	0.0126	0.2297	0.0129	0.1836	0.0130
$FeHSO_4^+$	0.7031	0.0001	0.7032	0.0009	0.6937	0.0017	0.6822	0.0025	0.6337	0.0044
$FeSO_4°$	1.0000	0.0059	1.0000	0.0039	1.0000	0.0036	1.0000	0.0025	1.0000	0.0006
Fe^{3+}	0.0924	0.0089	0.0859	0.0016	0.0787	0.0010	0.0711	0.0006	0.0494	0.0003
$FeHSO_4^{2+}$	0.2045	0.0030	0.1993	0.0067	0.1880	0.0097	0.1757	0.0113	0.1333	0.0136
$Fe(SO_4)_2^-$	0.7031	0.0313	0.7032	0.0445	-	-	-	-	-	-
$FeSO_4^+$	0.7031	0.1357	0.7032	0.1262	0.6937	0.1683	0.6822	0.1670	0.6337	0.0855
Fe_2O_3	-	-	-	-	-	-	-	-	-	0.0397
$[Fe(II)]_{total}$ by Model	-	0.018	-	0.018	-	0.018	-	0.018	-	0.018
$[Fe(III)]_{total}$ by Model	-	0.18	-	0.18	-	0.18	-	0.18	-	0.18

```
C     **********

C      THIS PROGRAM SOLVES the NONLINEAR
C     EQUATIONS
C

C     **********
      INTEGER I,INT,INFO,LWA,N,NFCALL,NFEV,NWRITE,kk
      DOUBLE PRECISION FNORM1,FNORM2,H,TEMP,TOL
      DOUBLE PRECISION X(10),FVEC(10),WA(130),gam(9),qi
      DOUBLE PRECISION DFLOAT,x7,x11
      EXTERNAL BVP
      COMMON /REFNUM/ NFCALL
            open(2,file='a150-1-1.dat',status='unknown',form='formatted')
C
C                              LOGICAL      OUTPUT      UNIT      IS      ASSUMED      TO      BE      NUMBER      6.
00000230
      DATA NWRITE /6/
C
c      DFLOAT(INT) = INT
      LWA = 200
      TOL = 1.D-30
      N = 8
C
C     STARTING VALUES.
C
      H = 1.D0/DFLOAT(N+1)
      DO 10 I = 1, N
            X(I) = 0.1
c        TEMP = DFLOAT(I)*H
c        X(I) = TEMP*(TEMP - 1.D0)

   10    CONTINUE
C
C     INITIAL MAX-NORM OF THE RESIDUALS.
C
      CALL BVP(N,X,FVEC,110)
            FNORM1 = 0.D0
      DO 20 I = 1, N
c        CALL BVP(N,X,FVEC,I)
        FNORM1 = DMAX1(FNORM1,DABS(FVEC(I)))
   20    CONTINUE
C
      NFCALL = 0
      CALL BRENT1(BVP,N,X,FVEC,TOL,INFO,WA,LWA)
      NFEV = NFCALL/N
C
C     FINAL MAX-NORM OF THE RESIDUALS.
```

```
C
      FNORM2 = 0.D0
            CALL BVP(N,X,FVEC,1)
      DO 30 I = 1, N
c        CALL BVP(N,X,FVEC,I)
         FNORM2 = DMAX1(FNORM2,DABS(FVEC(I)))
   30    CONTINUE
C
      WRITE (NWRITE,1000) N,FNORM1,FNORM2,NFEV,INFO,(X(I),I=1,N)

            kk=150
            if(kk.eq.130)then
            x7=x(1)**3/(10**2.72)
            end if

            qi=0.765
c     qi=0.5*(x(1)+4*x(2)+x(3)+4*x(4)+x(5)+9*x7+4*x(7)+x(8))
            qi=dsqrt(qi)

            if(kk.eq.150)then
            gam(1)=-0.6855*qi/(1.+9.*0.3525*qi)+0.0470
            gam(2)=-4.*0.6855*qi/(1.+4.*0.3525*qi)+0.0470
            gam(3)=-1.*0.6855*qi/(1.+4.5*0.3525*qi)+0.0470
            gam(4)=-4.*0.6855*qi/(1.+6.*0.3525*qi)+0.0470
      gam(5)=-1.*0.6855*qi/(1.+4.*0.3525*qi)+0.0470
            gam(6)=0
            gam(7)=-9.*0.6855*qi/(1.+9.*0.3525*qi)+0.0470
            gam(8)=-4.*0.6855*qi/(1.+4.5*0.3525*qi)+0.0470
            gam(9)=-1.*0.6855*qi/(1.+4.*0.3525*qi)+0.0470
            end if

            if(kk.eq.150)then
            x7=(10**gam(1))**3*x(1)**3/(10**3.11)/10**gam(7)
            end if

            x11=(0.179-x7-x(7)-x(8))*0.5



c           write(*,*)x7,(0.179-x7-x(7)-x(8))*0.5
c           write(*,*)x(1)-2.*x(2)-x(3)+2.*x(4)+x(5)+3.*x7+2.*x(7)+x(8)
            WRITE (2,1000) N,FNORM1,FNORM2,NFEV,INFO,(X(I),I=1,N)
c           do i=1,6

            write(2,*)'c(1)=', x(1)
            write(2,*)'c(2)=', x(2)
            write(2,*)'c(3)=', x(3)
            write(2,*)'c(4)=', x(4)
            write(2,*)'c(5)=', x(5)
            write(2,*)'c(6)=', x(6)
```

```
      write(2,*)'c(7)=', x7
      write(2,*)'c(8)=', x(7)
      write(2,*)'c(10)=', x(8)
      write(2,*)'c(11)=', x11

      write(2,*)'gam(1)=', gam(1)
      write(2,*)'gam(2)=', gam(2)
      write(2,*)'gam(3)=', gam(3)
      write(2,*)'gam(4)=', gam(4)
      write(2,*)'gam(5)=', gam(5)
      write(2,*)'gam(6)=', gam(6)
      write(2,*)'gam(7)=', gam(7)
      write(2,*)'gam(8)=', gam(8)
      write(2,*)'gam(10)=', gam(9)




      a1=dlog10(x(3))-dlog10(x(1))-dlog10(x(2))-4.05+
     *gam(3)-gam(1)-gam(2)
     a2=dlog10(x(5))-dlog10(x(4))-dlog10(x(1))-dlog10(x(2))-4.61+
     *gam(5)-gam(4)-gam(1)-gam(2)
     a3=dlog10(x(6))-dlog10(x(4))-dlog10(x(2))-3.35+
     *gam(6)-gam(4)-gam(2)
     a4=dlog10(x(7))-dlog10(x7)-dlog10(x(1))-dlog10(x(2))-6.61+
     *gam(8)-gam(7)-gam(1)-gam(2)
     a5=dlog10(x(8))-dlog10(x(2))-dlog10(x7)-7.52+
     *gam(9)-gam(2)-gam(7)
      a6=x(1)-2.*x(2)-x(3)+2.*x(4)+x(5)+3.*x7+2.*x(7)+x(8)
c     fvec(6)=x(1)+x(3)+x(5)+x(8)-0.612
     a7=x(4)+x(5)+x(6)-0.179
c      fvec(8)=dlog10(x(1))-dlog10(x7)-2.72
c     fvec(8)=x(7)+x(9)+x(8)-0.179
     a8=x(2)+x(3)+x(6)+x(5)+x(8)+x(7)-0.7535

      qi=0.5*(x(1)+4*x(2)+x(3)+4*x(4)+x(5)+9*x7+4*x(7)+x(8))
      qi=dsqrt(qi)

      write(*,*)a1,a2,a3,a4,a5,a6,a7,a8,qi**2

      write(2,*)'I', qi**2

     STOP
 1000 FORMAT (5X,10H DIMENSION,I5,5X //
    1     5X,34H INITIAL MAX-NORM OF THE RESIDUALS,D15.7 //
    2     5X,34H FINAL MAX-NORM OF THE RESIDUALS  ,D15.7 //
    3     5X,33H NUMBER OF FUNCTION EVALUATIONS  ,I10 //
    4     5X,15H EXIT PARAMETER ,18X,I10 //
    5     5X,27H FINAL APPROXIMATE SOLUTION  // (5X,5D15.7))
C
```

```
C    LAST CARD OF SAMPLE PROGRAM.
C
      END
      SUBROUTINE BVP(N,X,FVEC,IFLAG)
      INTEGER N,IFLAG,jj,kk
      DOUBLE PRECISION X(N),FVEC(N)
C     **********
C
C     SUBROUTINE BVP DEFINES THE BOUNDARY VALUE PROBLEM.
C
C     **********
      INTEGER INT,NFCALL
      DOUBLE PRECISION H,TEMP,TEMP1,TEMP2,gam(9),qi
      DOUBLE PRECISION DFLOAT,x7
      COMMON /REFNUM/ NFCALL

            do jj=1,n
            if(x(jj).lt.1.e-7)then
            x(jj)=1.e-6
            end if
            end do



            kk=150
c           write(*,*)10**2.72

      qi=0.765
            qi=dsqrt(qi)
            gam(1)=-0.6855*qi/(1.+9.*0.3525*qi)+0.0470
            gam(2)=-4.*0.6855*qi/(1.+4.*0.3525*qi)+0.0470
            gam(3)=-1.*0.6855*qi/(1.+4.5*0.3525*qi)+0.0470
            gam(4)=-4.*0.6855*qi/(1.+6.*0.3525*qi)+0.0470
      gam(5)=-1.*0.6855*qi/(1.+4.*0.3525*qi)+0.0470
            gam(6)=0
            gam(7)=-9.*0.6855*qi/(1.+9.*0.3525*qi)+0.0470
            gam(8)=-4.*0.6855*qi/(1.+4.5*0.3525*qi)+0.0470
            gam(9)=-1.*0.6855*qi/(1.+4.*0.3525*qi)+0.0470
c           if(kk.eq.150)then
            x7=(10**gam(1))**3*x(1)**3/(10**3.11)/10**gam(7)
c           end if

c     qi=0.5*(x(1)+4*x(2)+x(3)+4*x(4)+x(5)+9*x7+4*x(7)+x(8))
c           qi=dsqrt(qi)



            if(kk.eq.150)then
```

```
            fvec(1)=dlog10(x(3))-dlog10(x(1))-dlog10(x(2))-4.05+
     *gam(3)-gam(1)-gam(2)
      fvec(2)=dlog10(x(5))-dlog10(x(4))-dlog10(x(1))-dlog10(x(2))-4.61+
     *gam(5)-gam(4)-gam(1)-gam(2)
      fvec(3)=dlog10(x(6))-dlog10(x(4))-dlog10(x(2))-3.35+
     *gam(6)-gam(4)-gam(2)
      fvec(4)=dlog10(x(7))-dlog10(x7)-dlog10(x(1))-dlog10(x(2))-6.61+
     *gam(8)-gam(7)-gam(1)-gam(2)
      fvec(5)=dlog10(x(8))-dlog10(x(2))-dlog10(x7)-7.52+
     *gam(9)-gam(2)-gam(7)
            fvec(6)=x(1)-2.*x(2)-x(3)+2.*x(4)+x(5)+3.*x7+2.*x(7)+x(8)
c     fvec(6)=x(1)+x(3)+x(5)+x(8)-0.612
      fvec(7)=x(4)+x(5)+x(6)-0.179
c           fvec(8)=dlog10(x(1))-dlog10(x7)-2.72
c     fvec(8)=x(7)+x(9)+x(8)-0.179
      fvec(8)=x(2)+x(3)+x(6)+x(5)+x(8)+x(7)-0.7535
      end if




      RETURN
C
C     LAST CARD OF SUBROUTINE BVP.
C
      END
      SUBROUTINE BRENT1(FCN,N,X,FVEC,TOL,INFO,WA,LWA)
      INTEGER N,INFO,LWA
      DOUBLE PRECISION TOL
      DOUBLE PRECISION X(N),FVEC(N),WA(LWA)
      EXTERNAL FCN
C     **********
C
C     SUBROUTINE BRENT1
C
C     THE PURPOSE OF THIS SUBROUTINE IS TO FIND A ZERO OF
C     A SYSTEM OF N NONLINEAR EQUATIONS IN N VARIABLES BY A
C     METHOD DUE TO R. BRENT. THIS IS DONE BY USING THE
C     MORE GENERAL NONLINEAR EQUATION SOLVER BRENTM.
C
C     THE SUBROUTINE STATEMENT IS
C
C       SUBROUTINE BRENT1(FCN,N,X,FVEC,TOL,INFO,WA,LWA)
C
C     WHERE
C
C       FCN IS THE NAME OF THE USER-SUPPLIED SUBROUTINE WHICH
C         CALCULATES COMPONENTS OF THE FUNCTION. FCN SHOULD BE
C         DECLARED IN AN EXTERNAL STATEMENT IN THE USER CALLING
```

```
C       PROGRAM, AND SHOULD BE WRITTEN AS FOLLOWS.
C
C       SUBROUTINE FCN(N,X,FVEC,IFLAG)
C       INTEGER N,IFLAG
C       DOUBLE PRECISION X(N),FVEC(N)
C       ----------
C       CALCULATE THE IFLAG-TH COMPONENT OF THE FUNCTION
C       AND RETURN THIS VALUE IN FVEC(IFLAG).
C       ----------
C       RETURN
C       END
C
C       THE VALUE OF IFLAG SHOULD NOT BE CHANGED BY FCN UNLESS
C       THE USER WANTS TO TERMINATE EXECUTION OF BRENT1.
C       IN THIS CASE SET IFLAG TO A NEGATIVE INTEGER.
C
C     N IS A POSITIVE INTEGER INPUT VARIABLE SET TO THE NUMBER
C       OF EQUATIONS AND VARIABLES.
C
C     X IS AN ARRAY OF LENGTH N. ON INPUT IT MUST CONTAIN
C       AN INITIAL ESTIMATE OF THE SOLUTION VECTOR. ON OUTPUT X
C       CONTAINS THE FINAL ESTIMATE OF THE SOLUTION VECTOR.
C
C     FVEC IS AN ARRAY OF LENGTH N. ON OUTPUT IT CONTAINS
C       THE FINAL RESIDUALS.
C
C     TOL IS A NONNEGATIVE INPUT VARIABLE. THE ALGORITHM CONVERGES
C       IF EITHER ALL THE RESIDUALS ARE AT MOST TOL IN MAGNITUDE,
C       OR IF THE ALGORITHM ESTIMATES THAT THE RELATIVE ERROR
C       BETWEEN X AND THE SOLUTION IS AT MOST TOL.
C
C     INFO IS AN INTEGER OUTPUT VARIABLE SET AS FOLLOWS. IF
C       THE USER HAS TERMINATED EXECUTION, INFO WILL BE SET TO
C       THE (NEGATIVE) VALUE OF IFLAG. SEE DESCRIPTION OF FCN.
C       OTHERWISE
C
C       INFO = 0   IMPROPER INPUT PARAMETERS.
C
C       INFO = 1   ALL RESIDUALS ARE AT MOST TOL IN MAGNITUDE.
C
C       INFO = 2   ALGORITHM ESTIMATES THAT THE RELATIVE ERROR
C                  BETWEEN X AND THE SOLUTION IS AT MOST TOL.
C
C       INFO = 3   CONDITIONS FOR INFO = 1 AND INFO = 2 BOTH HOLD.
C
C       INFO = 4   NUMBER OF FUNCTION EVALUATIONS HAS REACHED OR
C                  EXCEEDED 50*(N+3).
C
C       INFO = 5   APPROXIMATE JACOBIAN MATRIX IS SINGULAR.
C
```

```
C       INFO = 6   ITERATION IS NOT MAKING GOOD PROGRESS.
C
C       INFO = 7   ITERATION IS DIVERGING.
C
C       INFO = 8   ITERATION IS CONVERGING, BUT TOL IS TOO
C                  SMALL, OR THE CONVERGENCE IS VERY SLOW
C                  DUE TO A JACOBIAN SINGULAR NEAR THE OUTPUT
C                  X OR DUE TO BADLY SCALED VARIABLES.
C
C     WA IS A WORK ARRAY OF LENGTH LWA.
C
C     LWA IS A POSITIVE INTEGER INPUT VARIABLE NOT LESS THAN
C       N*(N+3).
C
C    SUBPROGRAMS REQUIRED
C
C     USER-SUPPLIED ..... FCN, BRENTM
C
C     FORTRAN-SUPPLIED ... DLOG
C
C    **********
      INTEGER I,IVAR,MAXFEV,MOPT,NFEV
      DOUBLE PRECISION EMAX,FTOL,TEMP,XTOL,ZERO
      DOUBLE PRECISION DFLOAT
      DATA ZERO /0.D0/
      DFLOAT(IVAR) = IVAR
      INFO = 0
C
C    CHECK THE INPUT PARAMETERS FOR ERRORS.
C
      IF (N .LE. 0 .OR. TOL .LT. ZERO .OR. LWA .LT. N*(N+3)) GO TO 30
C
C    DETERMINE AN OPTIMAL VALUE FOR MOPT.
C
      EMAX = ZERO
      DO 10 I = 1, N
        TEMP = DLOG(DFLOAT(I+1))/DFLOAT(N+2*I+1)
        IF (TEMP .LT. EMAX) GO TO 20
        MOPT = I
        EMAX = TEMP
   10   CONTINUE
   20 CONTINUE
C
C    CALL BRENTM.
C
      MAXFEV = 50*(N + 3)
      FTOL = TOL
      XTOL = TOL
      CALL BRENTM(FCN,N,X,FVEC,FTOL,XTOL,MAXFEV,MOPT,
     1          INFO,NFEV,WA(3*N+1),N,WA(1),WA(N+1),WA(2*N+1))
```

```
   30 CONTINUE
      RETURN
C
C     LAST CARD OF SUBROUTINE BRENT1.
C
      END
      SUBROUTINE BRENTM(FCN,N,X,FVEC,FTOL,XTOL,MAXFEV,MOPT,
     1                  INFO,NFEV,Q,LDQ,SIGMA,WA1,WA2)
      INTEGER N,MAXFEV,MOPT,INFO,NFEV,LDQ
      DOUBLE PRECISION FTOL,XTOL
      DOUBLE PRECISION X(N),FVEC(N),Q(LDQ,N),SIGMA(N),WA1(N),WA2(N)
C     **********
C
C     SUBROUTINE BRENTM
C
C     THE PURPOSE OF THIS SUBROUTINE IS TO FIND A ZERO TO
C     A SYSTEM OF N NONLINEAR EQUATIONS IN N VARIABLES BY A
C     METHOD DUE TO R. BRENT.
C
C     THE SUBROUTINE STATEMENT IS
C
C       SUBROUTINE BRENTM(FCN,N,X,FVEC,FTOL,XTOL,MAXFEV,MOPT,
C                         INFO,NFEV,Q,LDQ,SIGMA,WA1,WA2)
C
C     WHERE
C
C       FCN IS THE NAME OF THE USER-SUPPLIED SUBROUTINE WHICH
C         CALCULATES COMPONENTS OF THE FUNCTION. FCN SHOULD BE
C         DECLARED IN AN EXTERNAL STATEMENT IN THE USER CALLING
C         PROGRAM, AND SHOULD BE WRITTEN AS FOLLOWS.
C
C         SUBROUTINE FCN(N,X,FVEC,IFLAG)
C         INTEGER N,IFLAG
C         DOUBLE PRECISION X(N),FVEC(N)
C         ----------
C         CALCULATE THE IFLAG-TH COMPONENT OF THE FUNCTION
C         AND RETURN THIS VALUE IN FVEC(IFLAG).
C         ----------
C         RETURN
C         END
C
C         THE VALUE OF IFLAG SHOULD NOT BE CHANGED BY FCN UNLESS
C         THE USER WANTS TO TERMINATE EXECUTION OF BRENTM.
C         IN THIS CASE SET IFLAG TO A NEGATIVE INTEGER.
C
C       N IS A POSITIVE INTEGER INPUT VARIABLE SET TO THE NUMBER OF
C         EQUATIONS AND VARIABLES.
C
C       X IS AN ARRAY OF LENGTH N. ON INPUT IT MUST CONTAIN
C         AN ESTIMATE TO THE SOLUTION OF THE SYSTEM OF EQUATIONS.
```

```
C       ON OUTPUT X CONTAINS THE FINAL ESTIMATE TO THE SOLUTION
C       OF THE SYSTEM OF EQUATIONS.
C
C     FVEC IS AN ARRAY OF LENGTH N. ON OUTPUT IT CONTAINS
C       THE FINAL RESIDUALS.
C
C     FTOL IS A NONNEGATIVE INPUT VARIABLE. CONVERGENCE
C       OCCURS IF ALL RESIDUALS ARE AT MOST FTOL IN MAGNITUDE.
C
C     XTOL IS A NONNEGATIVE INPUT VARIABLE. CONVERGENCE
C       OCCURS IF THE RELATIVE ERROR BETWEEN TWO SUCCESSIVE
C       ITERATES IS AT MOST XTOL.
C
C     MAXFEV IS A POSITIVE INTEGER INPUT VARIABLE. TERMINATION
C       OCCURS IF THE NUMBER OF FUNCTION EVALUATIONS IS AT
C       LEAST MAXFEV BY THE END OF AN ITERATION. IN BRENTM,
C       A FUNCTION EVALUATION CORRESPONDS TO N CALLS TO FCN.
C
C     MOPT IS A POSITIVE INTEGER INPUT VARIABLE. MOPT SPECIFIES
C       THE NUMBER OF TIMES THAT THE APPROXIMATE JACOBIAN IS
C       USED DURING EACH ITERATION WHICH EMPLOYS ITERATIVE
C       REFINEMENT. IF MOPT IS 1, NO ITERATIVE REFINEMENT WILL
C       BE DONE. MAXIMUM EFFICIENCY IS USUALLY OBTAINED IF
C       MOPT MAXIMIZES LOG(K+1)/(N+2*K+1) FOR K = 1,...,N.
C
C     INFO IS AN INTEGER OUTPUT VARIABLE SET AS FOLLOWS. IF
C       THE USER HAS TERMINATED EXECUTION, INFO WILL BE SET TO
C       THE (NEGATIVE) VALUE OF IFLAG. SEE DESCRIPTION OF FCN.
C       OTHERWISE
C
C       INFO = 0   IMPROPER INPUT PARAMETERS.
C
C       INFO = 1   ALL RESIDUALS ARE AT MOST FTOL IN MAGNITUDE.
C
C       INFO = 2   RELATIVE ERROR BETWEEN TWO SUCCESSIVE ITERATES
C                  IS AT MOST XTOL.
C
C       INFO = 3   CONDITIONS FOR INFO = 1 AND INFO = 2 BOTH HOLD.
C
C       INFO = 4   NUMBER OF FUNCTION EVALUATIONS HAS REACHED OR
C                  EXCEEDED MAXFEV.
C
C       INFO = 5   APPROXIMATE JACOBIAN MATRIX IS SINGULAR.
C
C       INFO = 6   ITERATION IS NOT MAKING GOOD PROGRESS.
C
C       INFO = 7   ITERATION IS DIVERGING.
C
C       INFO = 8   ITERATION IS CONVERGING, BUT XTOL IS TOO
C                  SMALL, OR THE CONVERGENCE IS VERY SLOW
```

```
C                DUE TO A JACOBIAN SINGULAR NEAR THE OUTPUT
C                X OR DUE TO BADLY SCALED VARIABLES.
C
C     NFEV IS AN INTEGER OUTPUT VARIABLE SET TO THE NUMBER OF
C       FUNCTION EVALUATIONS USED IN PRODUCING X. IN BRENTM,
C       A FUNCTION EVALUATION CORRESPONDS TO N CALLS TO FCN.
C
C     Q IS AN N BY N ARRAY. IF JAC DENOTES THE APPROXIMATE
C       JACOBIAN, THEN ON OUTPUT Q IS (A MULTIPLE OF) AN
C       ORTHOGONAL MATRIX SUCH THAT JAC*Q IS A LOWER TRIANGULAR
C       MATRIX. ONLY THE DIAGONAL ELEMENTS OF JAC*Q NEED
C       TO BE STORED, AND THESE CAN BE FOUND IN SIGMA.
C
C     LDQ IS A POSITIVE INTEGER INPUT VARIABLE NOT LESS THAN N
C       WHICH SPECIFIES THE LEADING DIMENSION OF THE ARRAY Q.
C
C     SIGMA IS A LINEAR ARRAY OF LENGTH N. ON OUTPUT SIGMA
C       CONTAINS THE DIAGONAL ELEMENTS OF THE MATRIX JAC*Q.
C       SEE DESCRIPTION OF Q.
C
C     WA1 AND WA2 ARE LINEAR WORK ARRAYS OF LENGTH N.
C
C    SUBPROGRAMS REQUIRED
C
C     USER-SUPPLIED ..... FCN
C
C     FORTRAN-SUPPLIED ... DABS,DMAX1,DSQRT,DSIGN
C
C    **********
      INTEGER I,IFLAG,J,K,M,NFCALL,NIER6,NIER7,NIER8,NSING
      LOGICAL CONV
      DOUBLE PRECISION DELTA,DIFIT,DIFIT1,EPS,EPSMCH,ETA,FKY,FKZ,
     1      FNORM,FNORM1,H,P05,SCALE,SKNORM,TEMP,XNORM,ZERO
      DATA ZERO,P05,SCALE /0.D0,5.D-2,1.D1/
C
C    WARNING.
C
C    THIS IS AN IBM CODE. TO RUN THIS CODE ON OTHER MACHINES IT
C    IS NECESSARY TO CHANGE THE VALUE OF THE MACHINE PRECISION
C    EPSMCH. THE MACHINE PRECISION IS THE SMALLEST FLOATING
C    POINT NUMBER EPSMCH SUCH THAT
C
C        1 + EPSMCH .GT. 1
C
C    IN WORKING PRECISION. IF IN DOUBT ABOUT THE VALUE OF
C    EPSMCH, THEN THE FOLLOWING PROGRAM SEGMENT DETERMINES
C    EPSMCH ON MOST MACHINES.
C
C    EPSMCH = 0.5D0
C 1 CONTINUE
```

```
C     IF (1.D0+EPSMCH .EQ. 1.D0) GO TO 2
C     EPSMCH = 0.5D0*EPSMCH
C     GO TO 1
C   2 CONTINUE
C     EPSMCH = 2.D0*EPSMCH
C
C     THE IBM DOUBLE PRECISION EPSMCH.
C
      EPSMCH = 16.D0**(-13)
C
      INFO = 0
      IFLAG = 0
      NFEV = 0
      NFCALL = 0
C
C     CHECK THE INPUT PARAMETERS FOR ERRORS.
C
      IF (N .LE. 0 .OR. FTOL .LT. ZERO .OR. XTOL .LT. ZERO .OR.
     1    MAXFEV .LE. 0 .OR. MOPT .LE. 0 .OR. LDQ .LT. N) GO TO 220
C
C     INITIALIZE SOME OF THE VARIABLES.
C
      NIER6 = -1
      NIER7 = -1
      NIER8 = 0
      FNORM = ZERO
      DIFIT = ZERO
      XNORM = ZERO
      DO 10 I = 1, N
        XNORM = DMAX1(XNORM,DABS(X(I)))
   10   CONTINUE
      EPS = DSQRT(EPSMCH)
      DELTA = SCALE*XNORM
      IF (XNORM .EQ. ZERO) DELTA = SCALE
C
C     ENTER THE PRINCIPAL ITERATION.
C
   20 CONTINUE
C
C     TO PRINT THE ITERATES, PLACE WRITE STATEMENTS
C     FOR THE VECTOR X HERE.
C
      NSING = N
      FNORM1 = FNORM
      DIFIT1 = DIFIT
      FNORM = ZERO
C
C     COMPUTE THE STEP H FOR THE DIVIDED DIFFERENCE WHICH
C     APPROXIMATES THE K-TH ROW OF THE JACOBIAN MATRIX.
C
```

```
      H = EPS*XNORM
      IF (H .EQ. ZERO) H = EPS
      DO 40 J = 1, N
        DO 30 I = 1, N
          Q(I,J) = ZERO
   30     CONTINUE
        Q(J,J) = H
        WA1(J) = X(J)
   40   CONTINUE
C
C     ENTER A SUBITERATION.
C
      DO 150 K = 1, N
        IFLAG = K
        CALL FCN(N,WA1,FVEC,IFLAG)
        FKY = FVEC(K)
        NFCALL = NFCALL + 1
        NFEV = NFCALL/N
        IF (IFLAG .LT. 0) GO TO 230
        FNORM = DMAX1(FNORM,DABS(FKY))
C
C       COMPUTE THE K-TH ROW OF THE JACOBIAN MATRIX.
C
        DO 60 J = K, N
          DO 50 I = 1, N
            WA2(I) = WA1(I) + Q(I,J)
   50       CONTINUE
          CALL FCN(N,WA2,FVEC,IFLAG)
          FKZ = FVEC(K)
          NFCALL = NFCALL + 1
          NFEV = NFCALL/N
          IF (IFLAG .LT. 0) GO TO 230
          SIGMA(J) = FKZ - FKY
   60     CONTINUE
        FVEC(K) = FKY
C
C       COMPUTE THE HOUSEHOLDER TRANSFORMATION TO REDUCE THE K-TH ROW
C       OF THE JACOBIAN MATRIX TO A MULTIPLE OF THE K-TH UNIT VECTOR.
C
        ETA = ZERO
        DO 70 I = K, N
          ETA = DMAX1(ETA,DABS(SIGMA(I)))
   70     CONTINUE
        IF (ETA .EQ. ZERO) GO TO 150
        NSING = NSING - 1
        SKNORM = ZERO
        DO 80 I = K, N
          SIGMA(I) = SIGMA(I)/ETA
          SKNORM = SKNORM + SIGMA(I)**2
   80     CONTINUE
```

```
      SKNORM = DSQRT(SKNORM)
      IF (SIGMA(K) .LT. ZERO) SKNORM = -SKNORM
      SIGMA(K) = SIGMA(K) + SKNORM
C
C       APPLY THE TRANSFORMATION AND COMPUTE THE MATRIX Q.
C
      DO 90 I = 1, N
        WA2(I) = ZERO
   90   CONTINUE
      DO 110 J = K, N
        TEMP = SIGMA(J)
        DO 100 I = 1, N
          WA2(I) = WA2(I) + TEMP*Q(I,J)
  100     CONTINUE
  110   CONTINUE
      DO 130 J = K, N
        TEMP = SIGMA(J)/(SKNORM*SIGMA(K))
        DO 120 I = 1, N
          Q(I,J) = Q(I,J) - TEMP*WA2(I)
  120     CONTINUE
  130   CONTINUE
C
C       COMPUTE THE SUBITERATE.
C
      SIGMA(K) = SKNORM*ETA
      TEMP = FKY/SIGMA(K)
      IF (H*DABS(TEMP) .GT. DELTA) TEMP = DSIGN(DELTA/H,TEMP)
      DO 140 I = 1, N
        WA1(I) = WA1(I) + TEMP*Q(I,K)
  140   CONTINUE
  150 CONTINUE
C
C     COMPUTE THE NORMS OF THE ITERATE AND CORRECTION VECTOR.
C
    XNORM = ZERO
    DIFIT = ZERO
    DO 160 I = 1, N
      XNORM = DMAX1(XNORM,DABS(WA1(I)))
      DIFIT = DMAX1(DIFIT,DABS(X(I)-WA1(I)))
      X(I) = WA1(I)
  160 CONTINUE
C
C     UPDATE THE BOUND ON THE CORRECTION VECTOR.
C
    DELTA = DMAX1(DELTA,SCALE*XNORM)
C
C     DETERMINE THE PROGRESS OF THE ITERATION.
C
    CONV = (FNORM .LT. FNORM1 .AND. DIFIT .LT. DIFIT1 .AND.
   1       NSING .EQ. 0)
```

```
      NIER6 = NIER6 + 1
      NIER7 = NIER7 + 1
      NIER8 = NIER8 + 1
      IF (CONV) NIER6 = 0
      IF (FNORM .LT. FNORM1 .OR. DIFIT .LT. DIFIT1) NIER7 = 0
      IF (DIFIT .GT. EPS*XNORM) NIER8 = 0
C
C     TESTS FOR CONVERGENCE.
C
      IF (FNORM .LE. FTOL) INFO = 1
      IF (DIFIT .LE. XTOL*XNORM .AND. CONV) INFO = 2
      IF (FNORM .LE. FTOL .AND. INFO .EQ. 2) INFO = 3
      IF (INFO .NE. 0) GO TO 230
C
C     TESTS FOR TERMINATION.
C
      IF (NFEV .GE. MAXFEV) INFO = 4
      IF (NSING .EQ. N) INFO = 5
      IF (NIER6 .EQ. 5) INFO = 6
      IF (NIER7 .EQ. 3) INFO = 7
      IF (NIER8 .EQ. 4) INFO = 8
      IF (INFO .NE. 0) GO TO 230
C
C     ITERATIVE REFINEMENT IS USED IF THE ITERATION IS CONVERGING.
C
      IF (.NOT. CONV .OR. DIFIT .GT. P05*XNORM .OR. MOPT .EQ. 1)
     1   GO TO 220
C
C     START ITERATIVE REFINEMENT.
C
      DO 210 M = 2, MOPT
        FNORM1 = FNORM
        FNORM = ZERO
        DO 190 K = 1, N
          IFLAG = K
          CALL FCN(N,WA1,FVEC,IFLAG)
          FKY = FVEC(K)
          NFCALL = NFCALL + 1
          NFEV = NFCALL/N
          IF (IFLAG .LT. 0) GO TO 230
          FNORM = DMAX1(FNORM,DABS(FKY))
C
C         ITERATIVE REFINEMENT IS TERMINATED IF IT DOES NOT
C         GIVE A REDUCTION OF THE RESIDUALS.
C
          IF (FNORM .LT. FNORM1) GO TO 170
          FNORM = FNORM1
          GO TO 220
  170     CONTINUE
          TEMP = FKY/SIGMA(K)
```

```
         DO 180 I = 1, N
           WA1(I) = WA1(I) + TEMP*Q(I,K)
 180       CONTINUE
 190     CONTINUE
C
C       COMPUTE THE NORMS OF THE ITERATE AND CORRECTION VECTOR.
C
       XNORM = ZERO
       DIFIT = ZERO
       DO 200 I = 1, N
         XNORM = DMAX1(XNORM,DABS(WA1(I)))
         DIFIT = DMAX1(DIFIT,DABS(X(I)-WA1(I)))
         X(I) = WA1(I)
 200     CONTINUE
C
C       STOPPING CRITERIA FOR ITERATIVE REFINEMENT.
C
       IF (FNORM .LE. FTOL) INFO = 1
       IF (DIFIT .LE. XTOL*XNORM) INFO = 2
       IF (FNORM .LE. FTOL .AND. INFO .EQ. 2) INFO = 3
       IF (NFEV .GE. MAXFEV .AND. INFO .EQ. 0) INFO = 4
       IF (INFO .NE. 0) GO TO 230
 210   CONTINUE
 220 CONTINUE
C
C     END OF THE ITERATIVE REFINEMENT.
C
     GO TO 20
C
C     TERMINATION, EITHER NORMAL OR USER IMPOSED.
C
 230 CONTINUE
     IF (IFLAG .LT. 0) INFO = IFLAG
     RETURN
C
C     LAST CARD OF SUBROUTINE BRENTM.
C
     END
```